THREE-DIMENSIONAL SOIL VAPOUR EXTRACTION MODELING

A Thesis

Presented to

The Faculty of Graduate Studies

of

The University of Guelph

by

LIAN ZHAO

In partial fulfilment of requirements

for the degree of

Doctor of Philosophy

May, 2007

Your file Votre référence
ISBN: 978-0-494-33630-4
Our file Notre référence
ISBN: 978-0-494-33630-4

THREE-DIMENSIONAL SOIL VAPOUR EXTRACTION MODELING

ABSTRACT

Lian Zhao
University of Guelph, 2007

Advisor:
Professor Richard G. Zytner, PhD, P. Eng

Soil vapour extraction (SVE) is a widely accepted and cost-effective technique used to remediate unsaturated soils contaminated with volatile organic compounds (VOCs). In order to improve SVE design, it is necessary to develop a comprehensive mathematical model that incorporates multiphase flow and multicomponent transport with nonequilibrium mass transfer. The model must include key controlling parameters such as relative permeability, dispersion coefficients, phase densities and interphase mass transfer.

Research has been completed on comprehensive three-dimensional SVE models entitled 3D-SVE-L/F. Use of these models allows quantitative evaluation of the SVE tailing effect, a current obstacle for SVE technology. The numerical solutions of the 3D-SVE-L/F models are obtained using FEMLAB, a commercial multi-physics modeling software developed by COMSOL Inc.; 3D-SVE-L/F have been calibrated against known data from lab-scale and field-scale SVE operations. The numerical simulation study indicates that 3D-SVE-L/F models can simulate SVE tailing effects. Accordingly, the pressure field and the distribution of the concentration of contaminant in the soil gas phase as well as the saturation reasonably are predicted.

The completed multivariable sensitivity analysis of the calibrated 3D-SVE-L/F models under a 95% confidence interval manifests that empirical mass transfer parameters consisting of the NAPL to vapour mass transfer coefficient are the most sensitive, followed by air-phase permeability. Dispersivity is the least sensitive. Comparison of the mass transfer coefficients between lab and field has shown that the field conditions are more resistant to mass transfer, consistent with high water content, more complex soil properties, and site heterogeneity.

A challenge facing SVE designs is estimating the length of SVE treatment time using a 3D-SVE model; a concept referring to a critical time index (CTI) was developed to predict the closure time for stopping an SVE operation. Applying CTI to an SVE operation may save operational time and cost. Additionally, the 3D model developed in this study can be used to assist in field-scale SVE design.

ACKNOWLEDGEMENTS

Many people with immense talent and valuable friendship have assisted me during the unforgettable journey to pursue my PhD degree. I would like to sincerely thank them all here to express my appreciation and give them the respect they deserve.

Thesis advisor committee members have contributed their academic insights, precious time and kind patience to my work. At first, I express my sincere thanks to my advisor, Professor Richard G. Zytner. My achievements documented in this dissertation originated from his blue print for soil remediation areas, and I have enjoyed this research project very much. No technical skill is more worthwhile than that of knowing how to select an exciting and challenging research project. Professor Zytner has always been extremely prompt in giving me feedback about my work. In particular, the structures of his academic pyramid which provided the theoretical and experimental foundations for the relevant studies in soil remediation have been extremely helpful for me. He was an excellent example as an academic advisor. Especially, I appreciate very much the financial support provided by Professor Zytner during the four years of my PhD program.

I give heartfelt thanks for the honesty and the faith Professor Gary Parkin has shown. His constant support and encouragement indeed stimulated me to focus on solving the tough academic research problems and to leave all negative issues behind. His academic instructions have motivated me to pursue my research goals. His creative teaching of soil physics and the relevant research on multiphase flow and

transport of contaminants in porous media have been established as a methodology. I cannot cite these in the references of this dissertation, but they will remain in my mind forever.

Since February 2004, Professor Edward McBean has been a member of my advisory committee. He especially gave me valuable suggestions about statistical methods on the multivariable regression sensitivity analysis. Moreover, many of his published works have helped me greatly. I have taken benefit from the harmony of Professor McBean's academic insight and enthusiasm.

Dr. Doug Joy is a member of my advisory committee. I appreciated his wonderful teaching in the groundwater modeling course. His resourceful questions on the key challenging topics in the relevant areas led me to make a valuable contribution to SVE modeling and allowed my thesis to be defensible. In particular, Dr. Joy challenged me greatly, and pinpointed my presentation of this thesis. Deliberating the proposed questions and comments has boosted significantly my confidence.

The revised advisory committee helped me to face the challenges! So completing my PhD represents not only my own personal achievements but also the achievements of an academic and professional community. Foremost, experiencing the PhD program at the University of Guelph is worthwhile for my life because I will have opportunity to work on empowerment of my hardworking value with persistence and aspiration.

Throughout the course of my PhD study, Professor Ralph G. Brown has played an important role as a graduate coordinator. I would also like to thank administrative

staff Susan Lewis, Lucy Cremasco and Stephanie Wilson, and the computer technical and network administrators, John Whiteside and Rose Cochrane, who always kindly helped me with routine issues in the School of Engineering at the University of Guelph. I truly enjoyed the academic community.

Also, special thanks go to Dr. Isobel Heathcote, the dean of graduate program services. Dr. Heathcote always can give promptly the most satisfactory solutions for many problems, I believe.

Some of my best friends include: Yu Li (P. Eng), ; Dr. Jeanne Huang, Victor (Haisheng) Wu, the most helpful vice president of GES; Jin Zeng, Jinlong Zang, Jian Gao, Baihua, Jin Li, Xiaojun Bao, Yi Li, Guangfa Lu, Windy Wang, Dr. Andy Zhu and Dr. Fengshen Fan, all of whom have given me fantastic memories. Their friendships have helped me work in an atmosphere which allowed me to leave the stress behind me. We spent a lot time having parties and congratulating each other for seemingly small achievements, but these are the symbols of happy student life. Also I deeply thank Eyad Brakat and Thair Patro for their friendship. I am grateful to Mr. Chu Ying Li, Dr. Linan Zhang and Mr. Wu Guangxing for their support during the final defence, and we are working together no matter where we live, in China or in Canada.

I am also indebted to Professor Zhou Daqian at the University of Daqing Petroleum. I am grateful to DanianYe academician who has taught me a powerful methodology to success. Professor Zhang Nianxian in the Institute of Geology and Geophysics in the Chinese Academy of Sciences. I benefited from their praiseworthy

advice in academic research work as my mentors. I would like to thank Professor Changjiu Li and his family at the Institute of Northeast China Electric Power Engineering; they have always been proud to be my best friends.

I greatly thank my fabulous husband Lin Qi and our wonderful son Tom; they have enriched my life tremendously. I am grateful to my parents for encouraging me all the time. They are most supportive and influential persons in my life. My parents have raised two generations of me and Tom with profound Chinese culture and firm beliefs as well as faith. I also greatly thank my husband's family for their love. My close relatives have given the greatest lovely caring and incentive in my life. In a word, my big family is the Great Wall against which I can put my ladder to strongly lean. I also feel great about my two younger brothers Zhao Yan, Zhao Mingyuan and they have made outstanding contributions in their management and technical occupations with commitment, competence and confidence. My cousins have contributed their unquenchable encouragement, understanding and love on me.

I would like to express my thank to Ms. Julia Zhukui for her empathy and the shared insights into the personal characteristics and awareness. She has learned these from the prophets. Gratefully I have been filled with admiration for her broad exploration on the happiness and wisdom.

My research assistantship funding was provided by the NSERC Strategic Grant Program. Also, Canada Female Doctoral Grant; the Dean's scholarship and special award form Graduate Services Program in the University of Guelph, OSAP, University of Guelph Access Bursary and Child Bursary, Richard and Sophia

Hungerford Graduate Travel Grants financial supports are gratefully acknowledged. Further thanks are extended to Conestoga Rovers and Associates, the industrial partner for the project, for the data and technical support on the SVE field operation. The technical writer Beth Murison, and Editor Lenore Latta have been very helpful.

Inadvertently missing anyone, I am expressing my sense of gratitude to you.

Lian Zhao

May, 2007

TABLE OF CONTENTS

APPENDIX

LIST OF TABLES

LIST OF FIGURES

NOMENCLATURE

The symbols and abbreviations used in this thesis are summarized in this section. Throughout this dissertation, SI units are applied to the physical amount unless the prescript units are non-SI. The general subscripts and superscripts are used in the formulation of variables for easy identification of each term. Double subscript in the mass transfer rate means the process goes from one phase to another.

English alphabet and abbreviations

a — empirical mass transfer parameter, T^{-1}

A — specific surface area, L^{-1}

b — empirical mass transfer parameter, dimensionless

c — empirical mass transfer parameter, T^{-1}

$(C_{g,i})_{exp}$ — i-th value of concentrations of offgas from the experimental data, mol/L^3

$(C_{g,i})_{mod}$ — i-th value of predicted concentrations of offgas from the model, mol/L^3

$C_{g,k}$ — concentration of component k in vapour phase, mol/L^3

$C_{a,k}$ — concentration of component k in aqueous phase, mol/L^3

$C_{n,k}$ — concentration of component k in NAPL phase, mol/L^3

$C_{\beta,k}$ — concentration of component k in phase β, mol/L^3

C_s — concentration of sorbed contaminant in soil phase, $M_{compound}/M_{soil}$

$\overline{C}$ — concentration of contaminant source, M/L^3

$\overline{C_\beta}$ — concentration induced by mass transfer into β phase, mol/L^3

Cal_i — i-th calculated value

$\hat{C}_g$ — average value of concentration of offgas, mol/L^3

CTI — critical time index

d — empirical mass transfer parameter, dimensionless

D_g — dispersion coefficient in gas phase, L^2/T

D_{ij} — dispersion coefficient tensor, L^2/T

$D_{\beta m}$ — molecular diffusion coefficient in β phase, L^2/T

e — error of linear multivariable method

E — elapsed time weighted relative slope of breakthrough curve, T^{-2}

E — rate of interphase mass transfer, M/L^{3}T

E_n^a — mass transfer of NAPL species from NAPL to aqueous phase, M/L^3 T

E_n^g — mass transfer of NAPL species from NAPL to gas phase, M/L^3 T

phase, M/L^3 T

$E_{n/a}^s$ — adsorption mass transfer of NAPL species from aqueous to solid phase,

M/L^3 T

f_{oc} — mass fraction of organic carbon,%

f_{cs} — mass fraction of organic carbon considering the total petroleum hydrocarbon,

g — gravitational acceleration constant, L/T^2

h — hydraulic head or soil water potential head, L

h_0 — reference pressure head, L

h_p — soil water potential head for unsaturated condition, L

H — dimensionless Henry's law constant

H_w — height of the screened well through contamination region, L

J — mass flux including the advective and dispersive flux, M/L^2T

J_a — advective flux, M/L^2T

J_{dis} — dispersive flux, M/L^2T

k_{ag} — mass transfer coefficient of aqueous phase to vapour phase, T^{-1}

k_{as} — mass transfer coefficient of aqueous phase to solid phase, T^{-1}

k_{na} — mass transfer coefficient of NAPL phase to aqueous phase, T^{-1}

k_{ng} — mass transfer coefficient of NAPL phase to vapour phase, T^{-1}

$k_g a_m$ — lumped mass transfer coefficient, T^{-1}

$k_g a_m$ — mass transfer empirical constant, T^{-1}

k_g — overall mass transfer coefficient, L/T

$k_{\alpha,\beta}$ — mass transfer coefficient from α phase to β phase, T^{-1}

k_0 — overall mass transfer coefficient, T^{-1}

k_{ij} — intrinsic permeability tensor, L^2

k_r — relative permeability

$k_{r\beta}$ — relative permeability of β phase

K_d — distribution coefficient, L^3/M_{soil}

K_{oc} — organic carbon partition coefficient

K_{ow} — octanol water distribution coefficient

m — van Genuchten empirical parameter

M — molecular weight of a chemical component, M/M

M_a — molecular weight of pure air, g/mol

M_k — molecular weight of component k, g/mol

n — van Genuchten empirical parameter

N — number of the sampled points in predicted and experimental data used to calibrate the model

i — i-th sampled point for experimental and predicted data

Nc — total number of contaminant

Obs_i — i-th observed value

p_β — pressure of β phase, M/LT^2

p_c — capillary pressure, M/LT^2

p_{atm} — atmospheric pressure, Pa

p_g — pressure of gas phase, Pa

p_W — venting absolute pressures on the venting well, Pa

Q — sink/source, M/L^3T

Q_s — volumetric flux of water per unit volume, T^{-1}

Q_w — flow rate of venting well, L^3/T

q — Darcy's velocity, L/T

q_a — Darcy's velocity of aqueous phase, L/T

q_d — density related Darcy's velocity, L/T

q_g — Darcy's velocity of gas phase, L/T

q_n — Darcy's velocity of NAPL phase, L/T

r_w — radius of venting well, L

r_I — radius of influence of venting well, L

R — retardation coefficient

R — relative slope of the modeled breakthrough curve, T^{-1}

R — universal gas constant, 8.3145, J/mol K°

s — standard error of estimate

S — degree of saturation of a fluid phase

S_a — degree of saturation of aqueous phase

S_g — degree of saturation of gas phase

S_n — degree of saturation of NAPL phase

S_r — degree of residual saturation of aqueous phase

S_s — specific storage term, L^{-1}

S_t — total degree of saturation of wetting phase

T — absolute temperature, K°

t — time variable, T

t_α — considered confidence interval from student distribution.

$\text{var}(\sigma)_{\alpha,i}$ — variance for the estimate of $\widehat{\alpha}_i$

$x_{\beta,k}$ — molar fraction of a component k in multicomponent mixture in β phase

$x^e_{\beta,k}$ — equilibrium mass fraction of a component k in β phase

z — elevation head, L

x, y, z — direction in a Cartesian coordinate system

Greek Symbols

$\hat{\alpha}_i$ — estimate of coefficient of linear regression equation

α_i — possible maximum and minimum values by considering the standard errors

α_0 — constant in linear multivariable regression equation

α_j — linear regression coefficients of the variable *j*.

α_L — longitudinal dispersivity, L

α_{TH} — transverse dispersivity horizontal, L

α_{TV} — transverse dispersivity vertical, L

β_c — coefficient of expansivity from change of solute concentration, L^3/M

β_h — coefficient of expansivity from change of hydraulic head, M/L^3

δ_n — standardized variable

δ_n^T — transfer matrix of δ_n.

$\eta(b)$ — empirical expression dependent on the soil type and soil structure

ε — air-filled porosity in porous medium, L^3/L^3

φ — porosity of porous medium

ρ — density of fluid, M/L^3

ρ_0 — density of air, M/L^3

ρ_b — bulk density of soil, M_{soil}/L^3

ρ_n — density of NAPL phase, M/L^3

ρ_g — density of vapour phase, M/L^3

ρ_a — density of aqueous phase, M/L^3

ρ_w — referenced density of water at zero chemical concentration, M/L^3

ρ^* — density of either injection water or withdrawn water, M/L^3

ρ_s — density of pure chemical, M/L^3

ρ_v^k — density of pure of vapour of component k, M/L3

θ — volumetric content of moisture, L^3/L^3

θ_g — gas phase content in porous media, L^3/L^3

θ_e — effective liquid content in the soil, L^3/L^3

θ_a — liquid content in the soil, L^3/L^3

θ_r — irreducible liquid content in the soil, L^3/L^{3shi}

λ — Brooks Corey constitutive relation empirical parameter

γ — rate of mass transfer of component, $M/L^3/T$

γ_g — compression coefficient of air, LT^2/M

μ — dynamic viscosity of fluid, M/LT

φ — porosity of porous medium

τ — tortuosity of porous medium

υ — Darcy velocity, L/T

ζ — mass transfer empirical constant, dimensionless

Units

Length, L

Area, L^2

Volume, L^3

Linear velocity, LT^{-1}

Time, T

Mass, M

Molar mass, mol

Dimensionless Number

Sh — Sherwood number

Pe — Peclet number

Re — Reynolds number

Sc — dimensionless parameter

Subscripts and superscripts:

α , β — any fluid phase

k — *k*-th component in β phase, refers to *g* for gas phase , *a* for aqueous phase , *s* for solid phase.

Abbreviations and acronyms

BTEX refers to Benzene, Toluene, Ethylbenzene and Xylene;

1D-SVE-L refers to one-dimensional soil vapour extraction model in lab-scale in homogenous porous medium;

3D-SVE-L refers to three-dimensional soil vapour extraction model in lab-scale in homogenous porous medium;

3D-SVE-F refers to three-dimensional soil vapour extraction model in field-scale in homogenous porous medium;

3D-SVE-L/F refers to both three-dimensional lab-scale and field-scale models;

NSSRD refers to normalized sum of squared residual difference.

RMS refers to the root mean of squared residual errors

CHAPTER 1
INTRODUCTION

Soil vapour extraction (SVE) is a widely accepted and cost-effective in-situ technique that is frequently used to remediate unsaturated soils contaminated with volatile organic compounds (VOCs) and semi-volatile organic compounds (SVOCs) (USEPA, 2004). A number of design methods, standards and guidelines for the operation of an SVE system have been published (USEPA, 2002, 2004; USACE, 2001a, 2001b) since the first SVE operation was exercised by Texas Research Institute in 1984 (Rathfelder et al., 1995).

Modeling of field settings with respect to tailing effects has drawn the attention of many experts because the remediation practices over past decades have manifested that the ideal cleanup degree cannot be reached (Chien et al., 2004; Barnes and White, 2006). It has been broadly experienced that tailing effects cause SVE remediation deficiency based on a large number of experimental and numerical investigations in lab-scale and field-scale. Many researchers have reported a wide variety of operational practices in the lab and field that influence the cleanup of sites. But there has been scant information on the comprehensive behaviour for a specific SVE system design. In this chapter, the scope and the objectives of the complicated 3D SVE modeling research, the significance of the 3D modeling methodology, as well as the major contributions of this research work are briefly addressed.

1.1 The Scope of 3D SVE Modeling Studies

SVE is one of the most successful remediation technologies for underground storage tank sites and is compatible with other soil and groundwater remediation technologies (Ball and Wolf, 1990; Sun et al., 1996; Sun and Yeh, 1998). Although thousands of SVE operations have been completed, and complicated mathematical models have been developed, simple and empirical designs based on "rules of thumb" are still being used. The reason is due to ambiguous modeling intentions and the inability of models to simulate real world SVE situations. The complexity of SVE performance and nonideal situations is due to the presence of tailing effects. Unfortunately, there have been limited reports on SVE modeling that can handle tailing effects properly, minimizing their impact on the prediction and monitoring of field-scale remediation operations.

Two aspects of the primary concerns that relate to the cost-effectiveness of SVE remediation operations are closure time and ultimate degree of cleanup over the entire site. Empirically, the stopping time has been defined as the time when the vapour concentration is reduced to about 0.1 % of the initial concentration of contaminants (Wilson, 1995; Ng and Mei, 1996). But this concept for closure time cannot principally represent the maximum cost-effective capability of SVE operation to clean up a site. Even though significant development has been made in SVE remediation technologies (Sawyer and Kamakoti, 1998; Schulenberg and Reeves, 2002), including theoretical studies on the physical and chemical processes existing in SVE (Schaefer et al., 1999; Abriola et al., 1999), there is still limited

understanding of the controlling processes in field settings (Lingineni and Dhir, 1997). The optimized SVE closure time should occur at the start of the tailing stage.

One of the challenges with SVE remediation is the occurrence of tailing effects that curtails the effectiveness of SVE, since tailing effects can last days, months, or even years. Continued use of SVE technology during the tailing stage is not cost-effective. Accordingly, it is important to research the causes of tailing and predict the performance of the tailing stage, so that other more effective remediation methods like bioventing can be used to reach final cleanup targets. Identifying characteristic performances of SVE by forecasting the progress of tailing stages and determining the pertinent criteria to assess closure time is a challenging task (Zhao and Zytner, 2004, 2005).

In order to better understand the SVE tailing process and predict closure time, a comprehensive mathematical model is required. This model needs to capture significant complexities including soil/contaminant interaction relationships by dealing with coupled multiphase flow and multicomponent transport, and nonequilibrium mass transfer through the underlying assumptions. Doing so allows to analyze and predict the SVE performance at field scale because this model increases the possibility and range of the realistic settings that may be captured and numerically simulated.

Mathematical modeling has become an important tool in the development of soil vapour extraction technology to better understand the remediation processes and enhance its application (Carey, 1995; Barnes, 2003). Developing a comprehensive 3D model and improving the numerical simulation is an effective way to predict

quantitatively the long tailing processes and performance of lab-scale and field-scale SVE (Zhao and Zytner, 2004, 2005). The scope of 3D SVE modeling studies in this context will cover a complete methodology and development of the simulator. The proposed conceptual and mathematical models simulate multiphase flow and multicomponent transport of contaminants in the subsurface under nonequilibrium transient mass transfer conditions for both lab- and field-scale tests. The details include developing the conceptual model for the most general SVE processes and the corresponding mathematical model with the simplifying assumptions, implementing the numerical simulation, calibrating the model, conducting sensitivity analysis, predicting closure time and the final cleanup degree, and developing the protocol of design by the modeled results.

1.2 Objectives of Research

Modeling practices have provided considerable insights into the processes governing SVE system design and evaluation of system performance because of the complexities and expense of conducting experiments either in the field or in the lab (USEPA, 2002). Modeling has become one of the critical remediation operation design elements because modeling results reflect how the designed SVE operation system will respond (Adeel et al., 2001). The most direct objective of developing 3D models has been to advance the prediction capability as a planning tool for the design and operation of an SVE system (Rathfelder et al., 1991). However, since SVE technology arose, very limited studies have been done to focus on this goal.

The improved understanding of SVE processes has been the expectation since SVE emerged; furthermore, model advances will be meaningful to obtain sound information on the performances of an SVE system due to the ability of a model to:

- identify the key governing processes which significantly affect the performance of SVE; and
- enhance the understanding of SVE processes, especially the dominant mechanism for SVE long tailing effects.

The goal of this research is to develop a comprehensive three-dimensional soil vapour extraction model using FEMLAB with an accurate prediction capability for field settings. The overall approach is manifested in the practical realities of operating a soil vapour extraction system. The objectives of the research toward this goal are summarized as follows:

- develop a three-dimensional model, which incorporates a coupled multiphase flow, multicomponent transport, nonequilibrium transient mass transfer, captures the entire site geometry including SVE system configurations and specific operation conditions; and
- predict spatial and temporal progress of the SVE operation and suggest the operational cleanup level and closure time according to the behaviour of the quantitatively simulated tailing stages.

1.3 Framework of Modeling

The approach to developing a complex 3D field-scale SVE model requires the following:

- envisioning the generalized SVE operation into a conceptual model,
- formulating the conceptual model into a mathematical model,
- solving the mathematical model by a chosen numerical method by combining SVE system configurations and operation conditions,
- predicting the expected response with realism and accuracy,
- calibrating the model against known data from similar settings, and
- predicting the closure time and cleanup degree.

A multivariable regression method is then used to carry out the sensitivity analysis of the calibrated 3D SVE model to identify the key controlling parameters. Further, the calibrated model can be used to simulate other similar SVE settings.

The solution of the numerical model of an SVE system is a function of the location of SVE wells, well spacing, screened length, surface sealing status, controlled operation conditions, and the properties of soils and contaminants and their interaction. Developing such a complex three-dimensional model introduces additional complexities compared with one- or two-dimensional modeling with respect to the following:

- need for sufficient data and more site-specific information, for example, data on the site characterization and realistic remediation operation monitoring data;

- increased number of factors that describe heterogeneous characteristics and parameters of physico-chemical processes involved in SVE;
- complicated mathematical formulations for some parameters related to the dimensionality, such as spatial derivatives, Darcy's velocity and dispersion coefficient tensor; and
- advanced requirements for applicable computer resources and programming load for numerical simulation of the coupled highly nonlinear partial differential equations.

In order to develop the proposed three-dimensional model, the research takes into account the following aspects of:

- comprehensive modeling methodology to target the current obstacle of tailing effects on SVE technology;
- empirical and theoretical methods and formulation to quantify the physical and chemical processes possibly simulated in SVE remediation;
- data and parameters obtained from experiments in lab and field; and
- use of the powerful modeling software packages FEMLAB and MATLAB.

1.4 The Significance and Feasibility of 3D Modeling

During the past three decades, there has been general agreement on SVE remediation technology and related mathematical modeling exercises. Some critical common viewpoints are as follows:

- design of optimal, cost-effective installations tends to be highly site-specific (Johnson et al., 1990a, b; Wilson, 1995);
- modeling studies may successfully fit experimental results in the lab (Harper, 1999; Harper et al., 2003; Gidda, 2003) for the concentration of offgas and in the few field studies (Farhan et al., 2001);
- modeling of migration and remediation of the subsurface contaminants sometimes is necessary to aid decision making (Schnoor, 1996);
- modeling in one dimension and two dimensions with excessive simplifying assumptions for dynamics of flow limits the application of the models in field situations (Sepehr and Samani, 1998; Lingineni and Dhir, 1997); and
- mathematical modeling is the most cost-effective tool for predicting the response of an SVE design (Wilson, 1995).

The significance and feasibility of three-dimensional modeling are obvious. A large number of long-term investigations and experience in exploring the SVE system design tools and models have demonstrated the need to develop the three-dimensional SVE models (Baehr, 1987; Baehr et al., 1989; Zhao and Zytner, 2005). Three-dimensional models may produce a markedly improved remediation design relative to the design based on a one- or two-dimensional model. First, modeling in three dimensions may use the maximum information available from the actual spatially variable characteristics of the subsurface site. Predictions may be improved by using detailed soil mapping processes and conducting experiments with contaminated soil. Secondly, due to the inclusion of SVE configurations and operation conditions, modified multiphase, multicomponent, nonequilibrium three-dimensional models

would be possible and more realistic than local equilibrium, one- or two-dimensional models. Thirdly, a large number of previous theoretical and practical study results in the laboratory and the field have provided a sound foundation for the modeling and simulation of three-dimensional field-scale settings. Fourthly, three-dimensional models can provide a more accurate representation of field settings, despite the fact that more significant data requirements and a large computational effort for numerical simulation is necessary. Additionally, air and groundwater contamination modeling also requires information on the contaminant concentrations of the source from soil as the input (Nair et al., 1990). Therefore, the monitored outcomes from a three-dimensional model, which describes SVE remediation, are also helpful for the compatible soil and groundwater contamination investigations and other remediation issues.

1.5 Contributions to the SVE Area

Based on data available on the two lab-scale and field-scale SVE settings and the reasonable simplifying assumptions, the 3D-SVE-L/F models are calibrated and the according studies on lab-scale and field-scale SVE performance by the calibrated model are carried out. The major achievements in the present work are summarized below.

1. Developed a comprehensive 3D SVE mathematical model that couples multiphase flow and multicomponent transport with nonequilibrium mass transfer. Other 3D models reported in the literature do not have this essential capability (compared details of the typical 3D models see Section 2.5). There

has been very limited work to intentionally target the specific features of tailing effects mathematically in terms of a realistic SVE setting. In terms of the work of Harper (1999) and Gidda (2003), both confirmed numerically and experimentally that the tailing effect was simulated in a one-dimensional domain. Their achievements have built a sound foundation for future studies regarding tailing performance under field settings. Of the few existing three-dimensional airflow models, many are modified from groundwater flow models, with limited capabilities for including nonequilibrium mass transfer for SVE, and predicting response on a specific system configuration.

2. Used a general and powerful commercial package named FEMLAB to resolve the systems of highly nonlinear partial differential equations. Numerical simulation with FEMLAB is able to completely and quantitatively describe the performance of SVE in three dimensions and to examine with realism and accuracy of the simulated parameters such as pressure distribution, impact of variations in parameters and various operation conditions on the performance of SVE. Meanwhile, the combination of FEMLAB and MATLAB generates considerable capacities of pre-processing, computation and post-processing function for the modeled results. The 3D-SVE-L/F models were calibrated against both known lab-scale and field-scale data, and the corresponding mass transfer coefficients were obtained.
3. Used multivariable sensitivity analysis of the complex 3D SVE model to evaluate the role of parameters. There has been a conventional method for conducting sensitivity analysis for a hydrological model, but multivariable

regression sensitivity analysis was used to characteristically quantify the impact of the different parameters in the developed complex model.

4. Proposed the criteria of the closure time for SVE remediation. It was essential to work out a characteristic criterion, which indicates the time when SVE remediation is no longer cost-effective, and then properly stop SVE operation. The evaluation criteria for the characteristics of the tailing stage were developed using lab data and then refined with field data. The critical time index (*CTI*) was determined.

Predicting the performances of SVE remediation by modeling needs a model platform with significant complexity to capture the dominant physico-chemical processes and operational conditions with site settings in three dimensions, further based on the platform for the calibration, verification and validation of typical SVE remediation so that the various performances of SVE may be effectively compared and evaluated.

The background knowledge of SVE modeling, the complete methodology, and modeling results numerically simulated with FEMLAB will be elaborated on in this dissertation. The contents are organized into the following seven chapters. Chapter 2 is a critical review of literature. Chapter 3 introduces testing FEMLAB with a soil physics case, groundwater flow and transport of contaminants, and density-driven flow and transport in a variable-saturated zone, as well as a modified one-dimensional quaternary component transport nonequilibrium mass transfer SVE model. Chapter 4 gives the essential theories and pertinent properties of a typical SVE system, and the detailed processes regarding developing the conceptual model

and the corresponding mathematical model. Chapter 5 demonstrates the numerical simulations and calibrations of the 3D-SVE-L/F models; also the behaviours of the 3D-SVE-L/F models, the predicted performance of SVE operation and the impact of variations in parameters are illustrated. Chapter 6 addresses the sensitivity analysis and the prediction of closure time. Ultimately, the protocol of designing an SVE system by three-dimensional modeling also is outlined. Chapter 7 highlights the conclusions and recommendations for further work.

CHAPTER 2
LITERATURE REVIEW

In this chapter, the representative achievements and the important findings about the SVE mathematical models and applications are presented and critically discussed. A critical review of the latest case studies, models, and the methodology as well as the developed progress for essential techniques provides sound background knowledge prior to modeling the three-dimensional multiphase flow and multi-component transport with nonequilibrium mass transfer processes. Also, this information provides an understanding of the conceptual model of SVE field remediation operation and indicates the need to develop a powerful mathematical model.

Following a brief discussion, this review is divided into five relevant subtopics to characterize the current existing SVE modeling studies relating to the objectives of this research topic: 1) mathematical modeling of SVE technology and application of models in SVE practice, 2) the closure time, 3) coupled multiphase flow and multicomponent transport modeling, 4) interphase mass transfer, and 5) computer codes.

2.1 Background

Since SVE technology first emerged in the early 1980s, many literature reviews, research reports, operation manuals, standards, guidelines and mathematical

models have been published (DiGiulio, 1992; Jordan et al., 1995; USEPA, 2002, 2004, Wise et al. 2000). These documents concentrated on the various subtopic domains to constitute almost all aspects of SVE research and experiments in the lab and field, as well as SVE remediation operations (USEPA, 2002; Harper, 1999; Gidda, 2003). Significant knowledge of SVE modeling, focusing on individual or limited combined processes accompanying the simplified assumptions, has been built up, such as experimental and numerical investigations in lab scale (Abriola et al., 1999; Hoeg et al., 2004) and in pilot studies (DiGiulio and Varaham, 2001). Largely, the completed models in 1990s insufficiently incorporated the non-steady gas phase transport processes; therefore, few models may provide any prediction of the performance of the SVE system (Jennings and Patil, 2002).

Although many guidelines are available for the design of a field-scale SVE remediation system, there are few clues as to how the response for various system configurations can be approached quantitatively. The existing approaches for SVE design are mainly based on experience or simplified analytical approximation with the limited simulations (Pedersen and Curtis, 1991; Johnson et al., 1990a, b; USEPA, 2004). SVE system designs have advanced from experimental assessment, analytical approximation, and simplified simulations to optimization design (Sun and Yeh, 1998; Barnes and White, 2006). However, these methods have limited capability for predicting the performance of the system. The process simulation models, which predict the response of systems, are often an integral part of an SVE optimization design package (Sun and Yeh, 1998), but the accuracy of SVE process simulation was doubtful because a relatively simple equilibrium model was used. Obviously, the

realism and accuracy of SVE simulation to predict the removal of contaminants greatly affects the optimization schemes, and ultimately affects the estimation of the cost of SVE operation. Similar concerns are also present for the risk assessment of SVE remediation where the consequences of risk evaluation models depend on the predicted concentration of contaminants.

Developing the three-dimensional model and introducing nonequilibrium mass transfer is an inevitable course to quantitatively predict the performance of a field SVE operation. A field-scale SVE model should capture the main physical and chemical processes that occur in SVE remediation, and SVE system configurations. Doing so will not only allow the prediction of the closure time of the operation, but also allow comparison of optional remediation schemes. Because of their limited complexity, many of the existing models and software cannot be used to extensively deal with the complex system of governing equations, which mathematically describe SVE operations.

2.2 Modeling of SVE Processes and Application of Models

2.2.1 Early Models and Applications

Considering the purpose of this study and the complexities of the various current models, the expected modeling procedure in an SVE field operation may be categorized into three stages: 1) preliminary screening, 2) estimation of SVE system closure time, and 3) design of new SVE system configurations and plan with further

research tools. The mathematical models presented in the literature describe how the SVE processes have varied greatly in the level of complexity since the earliest modeling work (Rathfelder et al., 1995, 2000). Mirsal (2004) proposed the generic advanced ideology for modeling by which the model is used to solve problems or find the answer for which a solution or answer, directly under the prevailing conditions, is not feasible, or is difficult. Obviously, significant discrepancies exist in the capacities of SVE models available, making it difficult to implement the fundamental functions which may predict the response of the various SVE system configurations.

Uses of a groundwater model for the design of soil vapour extraction operations are basic applications of the early air flow models based on the similarity of the groundwater flow by pumping and the flow of air by venting in SVE (Coffin and Glasgow, 1992). The simplest models with analytical solutions were applied to evaluate gas flow and intended to aid the SVE design by delineating the influence zone of a venting well (USEPA, 2002). At present the SVE system design by modeling method is still superficial, and largely can be utilized only on the preliminary screening of the candidate sites for SVE remediation (Mohr and Merz, 1995; Baehr and Hult, 1991) by using air flow models which are modified in terms of groundwater flow models.

The fundamental components considered with respect to an SVE system design consist of the number of wells, location of wells, spacing of wells, combination of venting and air injection or passive wells, sealing area of the surface, depth to well screen, and operation conditions (Chen and Gosselin, 1998). However, there have not been many model simulations which could completely capture the

wells' situation except the work done by El-Beshry et al. (2001) using VENT3D, an equilibrium mass transfer model developed by Benson et al. (1993). Benson et al. (1993) extended the equilibrium gas phase flow and transport model built by Johnson et al. (1990a, b) to a three-dimensional spatially heterogeneous soil and multi-component contaminant mixture.

Johnson et al. (1990a, b) incorporated the first comprehensive application of fluid hydraulics to unsaturated zone vapour flow testing and SVE system design. Massman (1989) showed that when the maximum pressure difference between any two points is less than 0.5 atmospheres, the effects of gas compressibility can be neglected. Thus, the utilization of groundwater flow models was regarded as suitable for gas flow. An analytical flow model using this approach has been developed for one-dimensional transient flow (Massman, 1989). Johnson et al. (1990a, b) used simple analytical tools in conjunction with typical advection and diffusion transport rates from SVE systems to suggest that near-saturated vapour concentrations from NAPL volatilization occur over relatively short gas phase travel distances.

Joss and Baehr (1995) coupled analytical two- and three-dimensional steady-state air flow simulators with an advection-dominated transport model. There has been no calibration conducted for these models since these models were completed. The simulated outputs by these models represented only roughly the decreased tendency of concentration of offgas without predictive capability as SVE operation proceeds.

Most previous SVE models referred to homogeneous vapour phase as only one mobile phase (Johnson et al., 1990a, b; Mohr and Merz, 1995). Early vapour flow

models based on density-dependent flow of groundwater were based on the equivalent air head (h^*) formulation in Equation (2.1), which was proposed by Frind (1982) and Mendoza and Frind (1990a).

$$h^* = \frac{p_g}{\rho_0 g} + z \tag{2.1}$$

Where:

p_g = pressure of gas phase, M/LT^2

ρ_0 = density of uncontaminated soil gas, M/L^3

g = gravitational acceleration, L/T^2

z = elevation head, L

The governing equation of 2Dgas phase flow is expressed as:

$$\frac{\partial}{\partial x}\left[k_{xx}k_r \frac{\rho_0 g}{\mu}\frac{\partial h^*}{\partial x}\right] + \frac{\partial}{\partial z}\left[k_{zz}k_r \frac{\rho_0 g}{\mu}\left(\frac{\partial h^*}{\partial z} + \rho_r\right)\right] = S_s \frac{\partial h^*}{\partial t} \tag{2.2}$$

$$\rho_r = \frac{\rho_g}{\rho_0} - 1 \tag{2.3}$$

Where:

μ = dynamic viscosity, Pa·s

k_{xx} and k_{zz} = permeability along principal coordinates, L^2

k_r = relative permeability

S_s = specific storage term, L^{-1}

ρ_r = the relative density of gas phase.

ρ_g = density of the contaminated soil gas mixtures, M/L^3

The relative permeability of gas phase in the matrix k_r can be expressed by (Brooks and Corey, 1964):

$$k_r = (1-\theta_e)^2\left(1-\theta_e^{(2+\lambda)/\lambda}\right) \tag{2.4}$$

$$\theta_e = \frac{\theta_g - \theta_r}{\varphi - \theta_r} \tag{2.5}$$

Where:

φ = total porosity, L^3/L^3

θ_e = effective liquid content in the soil, L^3/L^3

θ_g = gas phase content in porous media, L^3/L^3

θ_r = irreducible liquid content in the soil, L^3/L^3

Assuming the porous medium is rigid, the specific storage term S_s in Equation (2.2) is expressed by Mendoza and Frind (1990) as Equation (2.6):

$$S_s = \theta_g \rho_0 g \gamma \tag{2.6}$$

Where:

γ = compression coefficient of air, LT^2/M

Croisé and Kaleris (1992) used substitution of variables to modify the U.S. Geological Survey modular three-dimensional finite-difference flow model (MODFLOW). And more detailed studies were reported on the advancement of gas phase flow (Falta et al., 1989, 1992a, b; Mendoza and Frind, 1990a; Shikaze et al., 1994).

The migration of the gas phase of a DNAPL's plume induced by volatilization of the gas phase caused early investigations on behaviour of density-driven gas flow (Reeves and Abriola, 1994) as expressed by Equation (2.6). Shikaze et al. (1994) developed a 2D air water flow and transport model with equilibrium mass transfer in fractured and porous media, using the specific storage parameter in flow equation defined by Mendoza and Frind (1990) in Equation (2.6). Meanwhile, the transport equations were expressed as:

$$\frac{\partial}{\partial x_i}\left(\theta_g D_{ij}\frac{\partial C}{\partial x_j}\right) - q_i\frac{\partial}{\partial x_i}(\theta_g C) = R\theta_g\frac{\partial C}{\partial t} \quad (i, j = x, z) \tag{2.7}$$

$$R = 1 + \frac{\theta_a}{\theta_g H} + \frac{\rho_b}{\theta_g}\frac{K_d}{H} \tag{2.8}$$

Where:

D_{ij} = mechanical dispersion coefficient, L^2/T

C = concentration of contaminant, mol/L^3

R = retardation coefficient

H = dimensionless Henry's constant

K_d = distribution coefficient, L^3/M

q_i = Darcy's velocity, L/T

θ_a = aqueous phase content

Sleep and Sykes (1989) developed a two-dimensional, two component, and two phase flow with a linear driving force expression of rate-limited mass transfer. The multiphase flow equations of water and gas phase were decoupled by assuming a mutually independent relationship between the gas phase and water phase. Eventually the gas phase equation was formulated by Equation (2.2). Gas phase was simplified to a constant density equivalent to air density.

This gas flow equation was used to design the spacing of wells and screen length through a contaminated vadose zone and sealing area on the surface (Gamlie and Abdul, 1993). A numerical model based on saturated/unsaturated flow was employed by Gamlie and Abdul (1993) to generate transient flow fields. Moreover, the authors expected that the future study of gas flow regime should focus on:

- developing a three-dimensional model, analyzing and optimizing the SVE

configuration of injection and venting;

- solving the contaminant transport equation; and
- exploring the relationship between the removal of contaminant and closure time.

Another type of representative coupled gas flow and transport model is Armstrong's work (1998). Combining the continuity equation for flow of vapour, ideal gas law, and Darcy's law, and neglecting the mass transfer in the flow equation through variably saturated porous media may be denoted by Equation (2.9) and (2.10) (Armstrong, 1998; Wagner, 1998). This model consists of a nonequilibrium model that solves a set of partial differential equations for two-dimensional gas flow and advective-dispersive vapour transport in variably saturated porous media with a finite-difference approach.

$$\frac{\partial(\theta_g \rho_g)}{\partial t} = -\nabla(\rho_g q_g) \tag{2.9}$$

Where:

q_g = Darcy flux of vapour phase L/T.

$$\frac{\partial}{\partial x}\left(\theta_g D_{xx} \frac{\partial C}{\partial x}\right) + \frac{\partial}{\partial y}\left(\theta_g D_{yy} \frac{\partial C}{\partial y}\right) - \theta_g q_x \frac{\partial C}{\partial x} - \theta_g q_y \frac{\partial C}{\partial y} + k_\alpha (C_{eq} - C) = R \frac{\partial}{\partial t}(\theta_g C) \tag{2.10}$$

Where:

C_{eq} = equilibrium vapour concentration at the liquid-vapour interface, mol/L^3

k_α = overall mass transfer coefficient of volatilization of residual liquids, T^{-1}

The above-mentioned model considered gas phase flow and transport as well as mass transfer, but does not have the capacity to update NAPL content. The fact is that the residual saturation varies during SVE operation, and must be accounted for. Additionally, the method of handling the gas phase flow is feasible, but neglecting

the mass transfer which occurs in other concurrent phases is inappropriate for predictive SVE modeling, especially for tailing, because mass transfer processes are the dominant mechanism for tailing stage.

Using Equation (2.2), Cho (1993) developed a three-dimensional air flow computer model to simulate the soil-air pressure distribution at steady state and specific discharge vectors during soil venting with multiple wells in unsaturated soil. Although Cho (1993) obtained accurate, calibrated pressure and velocity fields in a three-dimensional model for a multiple well SVE system, the author postulated that the analytical solution of this flow equation might be linked to the transport equation to produce the predictive model by gas concentration. However, later advancement of SVE modeling method manifested that this expectation cannot further create the accurate simulated results for SVE tailing effects.

Conclusively, the numerical simulation for single phase air flow and transport has been used to produce a better SVE design of the layout of wells with varying operating parameters and observing the results of simulations. An air flow model mainly is used to delineate the air flow pattern under different operation parameters and to select and optimize well placement and well screening. But the consequences of application of air flow models have not further been extended to modeling transport and mass transfer processes and then predicting the closure time of SVE remediation operations. More advanced modeling should incorporate contaminant transport and mass transfer processes in multiphase systems. Emphasis should be on the heterogeneity of porous media, profiles of pressure around venting wells and mass transfer characteristics. More complex models will be introduced in Section 2.3.

2.2.2 Prediction of Closure Time

The major limitation of the current procedure to evaluate SVE is that it does not yield accurate estimates of the time necessary for the appropriate restoration of a contaminated site to reach the cleanup target (Armstrong et al., 1994; Zhao and Zytner, 2005). One reason is that the simple models have not captured the crucial processes. Many dominant and measurable mechanisms have been studied to improve the prediction capability of models and applications in field SVE remediation designs (Sawyer and Kamakoti, 1998). In principle, modeling the pilot-scale test would normally be done to verify both flow and chemical transport aspects of the SVE design (Rossabi, 1997; USEPA, 2002).

Predicting the closure time has always been difficult and complicated for SVE remediation operation (Chai and Miura, 2004; Nobre and Nobre, 2004); the closure time is an important criterion to evaluate properly the efficiency of SVE because the operation time on the site closely relates to the life-cycle cost of SVE (Wilson, 1995; Barness and White, 2006). Johnson et al. (1990b) explained the three aspects of standard index which might be considered to estimate when the SVE system can be turned off: cumulative amount removed, extraction well vapour concentration and composition, soil gas concentration and composition. However, these indexes cannot determine if the progress of SVE operation has been maximized. Kaleris and Croise (1997) utilized dimensionless parameters to estimate the cleanup time, but in principle, still used one-dimensional advective-dispersion transport to obtain the most direct relation among parameters of SVE and the removal rate of contaminants. They

treated the rate-limited mass transfer between the pore water and the solid phase, and formulated the relationship between the cleanup time and the concentration of offgas.

Kaleris and Croise (1999) estimated the cleanup time for the SVE operations using a mixed petroleum reservoir model with local equilibrium mass transfer. Later, this numerical model was modified and dealt with the advection–dispersion differential equations with Darcian isothermal air flow, local equilibrium contaminant mass transfer between gas phase and soil water, and first-order kinetics mass transfer between soil water and solid phase (Kaleris, 2002).

Wilson (1995) reported on a generic method to determine the closure time of an SVE operation based on a simple equilibrium or nonequilibrium model to predict the time at which the removal rate of 0.1% was reached (Hinsenveld and van den Brink, 1990). Figure 2-1 sketches the typical modeled breakthrough curves. These predicted results cannot represent the ubiquitous presence of the tailing effects because the equilibrium and nonequilibrium models have no capacity to identify the characteristics of tailing effects. Figure 2-1 also demonstrated the difference in predicted cleanup time between the equilibrium and nonequilibrium models. The closure time for the nonequilibrium case is about five times as long as that for the equilibrium case (Wilson, 1995). However, despite using the nonequilibrium mass transfer model and the removal rate of 0.1% has been reached, whether the tailing may start at this time or tendency of no cost-effective remediation may proceed has not been indicated. Pedersen and Curtis (1991) noted that the purpose of the SVE design process is to construct an SVE system that removes the greatest amount of contaminants from the site in the most efficient, timely and economical manner.

Based on the trend shown in Figure 2-1, apparently, the closure time quantitative evaluation is not yet available.

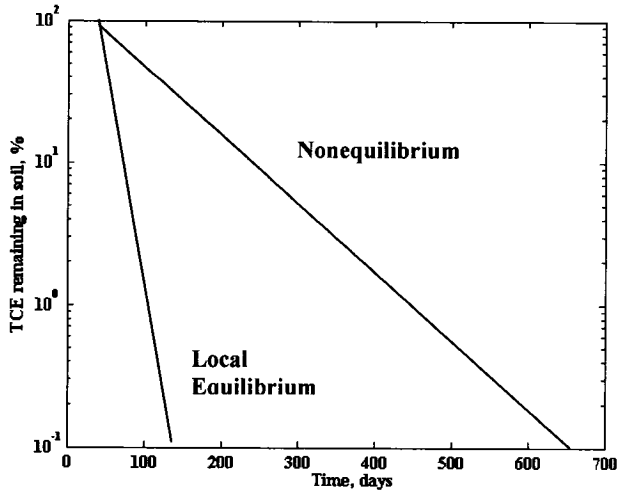

Figure 2-1 Comparison of TCE Removal Time for Local Equilibrium and Nonequilibrium Cases at a Radius of Influence of 10 m (Cited from Wilson, 1995).

2.3 Multiphase Flow and Multicomponent Transport

Over the past few years, multiphase flow and transport phenomena in porous media have become increasingly important (Chien et al., 2004). Intensive research in vadose zone modeling has taken place in the field of environmental engineering, including analyzing distribution contaminants in the subsurface and remediation of the site (Thomson and Johnson, 2000; van Geel and Sykes, 1994a, b). SVE operation is a typical multiphase flow process under the following situations in the vadose zone:

- NAPL migration if NAPL contaminant source is still located in-situ;
- moisture movement resulting from the fluctuation of groundwater table;
- gas phase venting process.

Although three fluid phases (air-water-NAPL) are present at most SVE remediation sites, very few models have been reported in the literature that can simulate the coupled multiphase flow, multicomponent transport, and interphase mass exchange (Rathfelder et al., 2000). In this section, advancement of fundamental multiphase flow theory and the applied status in soil and groundwater NAPL contamination issues are reviewed.

2.3.1 Advancement of Multiphase Flow Theory

A comprehensive review on multiphase systems in soil and groundwater contamination, mathematical simulations and the experiments of interest have been outlined by Farquhar et al. (1990), Bear and Bachamat (1990), Corapcioglu (1991), Weber and DiGiano (1996), and van Genuchten et al. (1999). Some authors reviewed the multiphase flow and transport of contaminants in porous media (Allen el al., 1988; Adenekan et al., 1993). In particular, Miller et al. (1998) have given an extensive overview on the advancement, remaining challenges and approaches of interest. Both flow and contaminant transport in the vadose zone have complex issues that do not exist in the saturated zone. Historically, the theory of vadose zone flow emerged by the extension of the concepts used in saturated zone flow that have been developed since the early 1900s. The earliest application of multiphase flow theory was demonstrated in the 1930s based on Richards equation (Jury and Horton, 2004), which illustrates flow of moisture in soil and other porous media. In the 1960s, petroleum engineering simulations became well developed (Peaceman et al., 1977),

and the classic constitutive relationships between the capillary pressure and the saturation of a fluid phase and between relative permeability and saturation were established (Brook and Corey, 1964, 1966). The governing equations for the earliest three-phase flow models with constitutive relationships have come from petroleum engineering simulations (Faust, 1985). In hydrology, by the 1980s, much research had been done as groundwater contamination issues became an increasing concern to the public (Zheng and Bennett, 2002). A number of overviews on the multiphase flow and transport of contaminants in groundwater contaminated by NAPLs (Abriola et al., 1999; Miller et al., 1998) were presented. The more complex issues of coupled flow and transport in the vadose zone have become of increasing concern since the 1990s (Frind, 1990; Ying and Zheng, 1999; Lenhard et al., 2004). The most pertinent capability to deal with SVE simulations should capture the coupled multiphase flow and multicomponent transport with nonequilibrium mass transfer.

Multiphase flow modeling studies in contaminant hydrology are largely based on the modeling theory derived from petroleum reservoir simulation (Peaceman, 1977; Brush, 1994). The basic governing equations and the derivation have been addressed very clearly (Bear, 1972; Abriola and Pinder, 1985; Bear and Bachmat, 1990). Adeel et al. (2001) reviewed advancements in multiphase flow and transport of contaminants in soil and groundwater, and the typically used software. In particular, they addressed the difference between petroleum engineering and environmental engineering modeling and the limitations to exploring environmental case studies. The complicated properties of soil and contaminants in the subsurface have made the SVE system design empirical and site-specific (Hutzler et al., 1989);

also, the history of environmental sites is relatively short compared to petroleum reservoirs with a million year historical genesis, in that there is a limited amount of repeatable data available for remediation and modeling studies for various contaminated sites, unlike for petroleum reservoirs.

Most three-phase flow models in porous media assume the air phase to be passively connected to air with respect to uniform atmosphere pressure (Abriola and Pinder, 1985; Faust, 1985; Parker and Lenhard, 1987). They dealt with the interphase mass transfer as equilibrium partitioning. It is extremely difficult to keep all three phases active when undertaking numerical simulation because of the highly nonlinear governing equation system.

The earliest interest in gas phase advection and dispersion transport depended on the findings from the investigation of volatilization of DNAPL and smear zones produced with the gas phase along the NAPL plume (Sleep and Sykes, 1989; Thomson et al., 1997). Some of the investigations on multiphase flow neglected density-driven gas advection (Abriola et al, 1987; Lenhard et al., 1995). Few models demonstrate gas phase flow behaviours of SVE using hypothetical mass transfer coefficients (Armstrong et al., 1994) without the calibration against known data from realistic SVE settings (Jang, 2005).

Successful SVE practices have induced greatly the continued interest in studies of gas phase flow and transport in a multiphase system (Brusseau and Rao, 1989; Brusseau, 1991; Campagnolo and Akgerman, 1995). Many of the models described in these reviews are worthwhile references for simulating the typical processes occurring in SVE even though they do not include complex 3D

mathematical models, complete parameterization and rigorous 3D numerical simulation.

2.3.2 Complex SVE Models

This section will elucidate the application and advancement of the multiphase flow and multicomponent transport theory in SVE modeling studies. There have been some multiphase flow and multicomponent transport mathematical models dealing with SVE processes incorporating interface mass transfer documented in the literature (Sleep and Sykes, 1989, 1993; Lingineni and Dhir, 1992; Abriola et al., 1997, 1999; Rathfelder et al., 2000). Sleep and Sykes (1993) clearly pointed out that before their work, all models that handled multiphase flow and multicomponent transport had neglected gas phase advection.

Sleep and Sykes (1989) introduced ideas of multiphase flow and multicomponent transport into SVE settings without mass transfer involved in flow equations and completed numerical simulation for a hypothetical SVE case. Sleep and Sykes (1993) proposed a compositional simulator to analyze groundwater contamination and remediation action. The proposed model dealt with water, gas and NAPL three-phase flow and an arbitrary number of species transport considering equilibrium interphase mass transfer partitioning. Advection of all three fluid phases with diffusion in the water and air phases were involved. All solutions were calibrated against a one-dimensional and three-dimensional analytical solution assuming three-phase flow and single solute transport. Rathfelder et al. (2000) reported a two-dimensional aqueous and gas phase two-phase flow SVE model.

There was no information on the adjustable parameters which may be tuned to complete calibration, and no index was reported to evaluate the goodness of the calibration. Only the qualitative analysis and the reasonability of the numerical solutions with respect to the hypothetical SVE case with cyclohexane contamination were summarized without the calibration conducted for a field 3D SVE scenario. There have been no reports to address the predictive capability of the model or the comparable consequences to forecast the performance of real SVE operations related to tailing effects.

2.4 Computer Codes Applied in SVE Modeling Studies

In general, even the simplified versions of the flow and transport equations arising from a simplified conceptual model are too complicated to be solved analytically (Wheeler, 1988). The availability of solutions to a system of governing equations always is a significant concern and obstacle for a modeler. Choosing an appropriate computer code is essential for successful modeling. There are computer codes of personal software and commercial specialized software which can be chosen to implement the SVE modeling studies. The computer codes developed by individual researchers are constrained strictly under specific governing equations with limited flexibility available. Therefore it is difficult to modify them to perform a more complex modeling study.

Abriola et al. (1999) reviewed the modeling framework and considered that there are three types of models which demonstrate SVE processes:

- Air flow models;
- Steady-state air flow and organic transport models with equilibrium and nonequilibrium interphase mass transfer; and
- Multiphase flow, multicomponent transport with interphase mass transfer limitations.

Correspondingly, the solutions to these flow and transport governing equations can be obtained by the following methods and relevant numerical schemes:

- Analytical and semi-analytical methods (Huang and Goltz, 1999)

Several models have dealt with the flow of gas phase by analytical pressure solution under different conditions (Falta, 1993; Kaleris and Croise, 1997, 1999), but a very limited analytical solution for chemical transport equation can be obtained.

- Finite-difference numerical method in one dimension and/or two dimensions (Sleep and Sykes, 1989, 1993; Sepher and Samani, 1993; El-Beshry, 2001; Yoon et al., 2002; Harper, 1999) or three dimensions (Benson et al., 1993)
- Finite element numerical method in one dimension and/or two dimensions (Huyakorn et al., 1983, 1994; Carey, 1995; Armstrong et al., 1994; Wagner, 1998; Rathfelder et al., 2000; Gidda, 2003).

There is substantial commercial or open source computer software available. In fact, Jenninga and Patil (2002) listed and briefly summarized about 30 models developed in the 1990s alone; however, transport models do no prevail among these models. What follows is a summary of a variety of commercial models currently available.

MISER is a 2D SVE/BV simulator developed by Abriola et al. (1999) and Rathfeldar et al. (2000). MISER deals with only one organic contaminant component (toluene) and uses a linear driving force for rate-limited mass transfer. It is a coupled aqueous and gas two-phase flow and transport finite element simulator in field scale. Intermodel calibrations were carried out, but there have not been calibrations against known data from real SVE operations and system configurations. There has been no literature, which reported the predicted tailing effects or field SVE settings by MISER simulator.

RESSQ is a 2D contaminant transport semi-analytical model for advection and adsorption in homogeneous, isotropic, confined and unconfined aquifers of uniform thickness where regional flow occurs. RESSQ is suitable for determining capture zones of wells in steady uniform groundwater flow and SVE gas flow conditions (http://www.ejge.com/1996/Ppr9602/cont2dan.htm). Beckett and Huntley (1994) found that an underestimated cleanup time and overestimated radial cleanup effectiveness occurred using VENTING and RESSQ software packages because they should be used only under confined flow conditions.

VapourT is a finite element model that simulates incompressible soil-gas flow and vapour transport processes. VapourT has the capability to model VOC transport by diffusion, dispersion and advection in gas and aqueous phases; it can simulate density-driven gas phase flow, as well as VOC gas-aqueous phase partitioning. A detailed description of VapourT was provided in Mendoza (1989), Mendoza and Frind (1990). As well, VapourT was used to estimate the closure time for field SVE operations (Barnes, 2003; Barness and White, 2006). But it is difficult to couple the

rate-limited mass transfer with VapourT because VapourT simply dealt with equilibrium mass transfer by the fixed model governing equations.

NUFT is a general purpose finite-difference computer code and may be used to simulate soil vapour extraction. However, detailed information has been not reported on its commercial applicability, and the results of its application in SVE scenarios are lacking (Dortch et al., 2001).

The USEPA (2002) has reported several three-dimensional models for personal computer application for soil vapour extraction, but these models have been used only to simulate air flow and design the SVE system by screening the candidacy of a site and arranging the layout of wells. When utilizing these models, one can roughly predict pressure distribution and air flow streamlines without the coupled vapour transport processes. One of these is the model MAGNAS, which was written in Fortran 77 and is based on Huyakorn and Panday's work (1994). MODFLOW is a three-dimensional finite-difference groundwater model; connected to GMS (Groundwater Modeling System) (Dorth et al., 2001), it is often used in SVE simulation (Sawyer and Kamakoti, 1998) assuming the single gas phase flow, whereas water and NAPL phases are immobile. AIR3D was used to estimate the unsaturated zone permeability from field data obtained from horizontal well SVE tests (USEPA, 2002). AIR3D is an adaptation of the groundwater flow code MODFLOW to simulate three-dimensional air flows in a heterogeneous, anisotropic unsaturated zone where air flow is induced through dry wells or trenches, as in vapour extraction remediation (USEPA, 2002). An SVE simulation-optimization model, which incorporates MODFLOW and AIR3D was utilized to design the

number of extraction wells, and location and pumping rates of the wells in a study by Sawyer and Kamakoti (1998).

UTCHEM and SIMUSCOPP are the specialized petroleum engineering simulators, which were tested to model SVE processes and enhanced groundwater remediation simulation (Delshad et al., 1998). Although the UTCHEM compositional simulator, which has been included in (GMS) and opened to the public, was developed to accommodate the multiphase flow and multicomponent transport with chemical reaction and to handle an unsaturated system, it is not well suited to simulate soil vapour extraction (Dorth et al., 2001) due to its specialization in petroleum reservoir settings. Similarly, Thiez (1996) applied a simulator entitled SIMUSCOPP to design SVE remediation pilot tests. SIMUSCOPP is a software package modified from a petroleum reservoir compositional simulator, and may simulate three-phase flow, nonequilibrium mass transfer and multicomponent categorized by the organic carbon groups of the target contaminants. However, there have been no further reports on its applicability and availability.

GAS2D and GAS3D are numerical two- and three-dimensional models developed by Sepehr and Samani (1993) to simulate gas flow conditions under vadose zone conditions. The model has been validated and used to assess the gas pressure distribution and anticipated gas flow rates from vapour extraction wells under different boundary conditions, soil moisture contents and heterogeneous and anisotropic conditions. This model has been used extensively to evaluate and design vapour extraction systems for different projects. The development and testing of a 3D gas flow model "GAS3D" for the design of soil venting systems has been described,

and the simulated pressure around a vapour extraction well by the developed GAS3D model was verified and validated by comparing the results of the finite-difference solution to actual field measurements and the results of an analytical solution under homogeneous and isotropic conditions without transport of contaminants (Sepehr and Samani, 1993).

STOMP was developed by Pacific Northwest National Laboratory's Hydrology Group. STOMP is a multipurpose engineering simulator for investigating remediation technologies for the cleanup of organic compounds within soil and groundwater. The simulator numerically solves flow and transport through variably saturated geologic media by a finite-difference scheme. STOMP has been used to simulate multiphase, compositional NAPL, and nonisothermal conditions involving nonvolatile three-phase systems. Saturations computed from STOMP were calibrated against experimental data for one-dimensional, nonvolatile three-phase flow systems (Lenhard et al., 1995). It was also tested against simulation results from a published numerical code MOFAT-2D, and against nonhysteretic and hysteretic relationships between capillary pressure and saturation data from three-phase flow experiments. STOMP may accurately predict multiphase flow behaviours at a site when the model parameters are correctly calibrated to the site under the appropriate site characterization (White et al., 1995). However, STOMP does not have significant flexibility to allow researchers to incorporate rate-limited mass transfer coefficients into individual phase and the improved capillary pressure-saturation-relative permeability constitutive relations (van Geel and Roy, 2002), even in an updated STOMP version (2006, at website: http://stomp.pnl.gov).

At present time, two commercially available 3-D vapour flow and transport models are VENT3D developed and marketed by David A. Benson in 1993 and SVE-3D (at website http://scientificsoftwaregroup.com, accessed on January, 2006) by Scientific Software Group. Both of these models are compared against the model developed in this study (3D-SVE-F) in the summary presented at the end of this chapter.

Most of the above-mentioned models performed the 3D gas flow simulation based on groundwater flow models. Even though some compositional simulators are available to simulate multiphase flow and transport processes, the existing codes have limited flexibility for modification to meet the high requirements of complicated models (Karapanagioti et al., 2003). The development of computer software and hardware, including the numerical schemes, are certain to continue; therefore, any three-dimensional time-variant comprehensive models with limited information available are likely to be tentative. There have been very few coupled multiphase flow and multicomponent transport compositional simulators that can demonstrate the performance of actual SVE operation. Furthermore, predicting closure time and the cleanup target of a real SVE operation also remains a challenge.

2.5 Rate-Limited Mass Transfer

The issue of mass transfer involved in multiphase systems has become an active research field in enhanced recovery petroleum engineering (Aziz et al., 1979), and groundwater and soil contamination and remediation operations (Kaleris, 2002;

Benitez, 2002; Zhao and Zytner, 2005). Because of the immeasurable mass transfer rate, the mass transfer coefficients may be obtained only by fitting modeled results to known experimental data. Studies in field and laboratory settings have indicated that the rate-limited interphase mass transfer is crucial for predicting realistic performance of field SVE. Many investigators applied mass transfer coefficients developed in terms of a dimensionless parameter group from a simple experimental setup (Powers et al., 1992; Rathfelder et al., 1991; Harper, 1999; Gidda, 2003).

In this section, the classic multiphase mass transfer theory, the characteristics of mass transfer processes involved in SVE operation, and a myriad of typical results of laboratory column experimental and numerical investigations are reviewed briefly.

2.5.1 Mass Transfer Processes in SVE Operation

Laboratory and controlled field experiments represent evidence for rate-limited mass transfer during venting (Gierke et al., 1992; Hayden et al., 1994). Various relevant mechanisms have been proposed to account for the phenomena observed as mass transfer rate limitations, including film transfer limitations, intra-aggregate diffusion processes (Powers et al., 1992), gas flow by-passing low permeability zones (Gomez et al., 1991), zones of high aqueous phase saturations and rate-limited desorption from the soil matrix (Brusseau and Rao, 1989). Eventually, a study on rate-limited mass transfer during SVE operation completely depends on modeling results because of the unavailability of measured mass transfer coefficients (Anwar et al., 2000).

The logical question is whether the mass transfer parameters obtained from calibrating any model against lab-scale SVE experiments may be extrapolated to real field-scale situations or not. Accuracy of predictions for mass transfer coefficients depend on the level of complexity to which the model was developed and the similarity of experimental results and model outputs as well as the accuracy and stability of the numerical simulation.

Mass transfer processes occurring in SVE remedial operations are extremely complex; furthermore, it is still intensely challenging to decide how to represent them with the calibrated mathematical models and how to explain the diverse or various realistic situations that occur in the laboratory and field. Lucid comprehension of the mass transfer-controlled mechanisms has central importance for improving the predictive capability of an SVE mathematical model in order to assist the design of SVE configurations and predict the corresponding response. Subsequently, the destination of modeling studies logically should focus on how the mass transfer modification may control the SVE long tailing effect in three-dimensional realistic site settings. Ultimately, the characteristics of mass transfer coefficients related to the performance of SVE operation will be demonstrated, and the magnitudes of mass transfer obtained by the calibration against known data will be extrapolated to similar site settings.

Many studies have been conducted to reveal the typical mass transfer processes, such as volatilization of residual NAPLs (Ng and Mei, 1999), dissolved NAPL in the water phase (Armstrong et al., 1994; Fischer et al., 1996, 1998), and desorption of contaminants from soil particles. Powers et al. (1992) exhaustively

reviewed the interphase mass transfer processes of various contiguous phase pairs. The likely mass transfer-controlled processes emerging in SVE originate from NAPLs across NAPL-water and air-NAPL interface mass transfer. NAPLs in contaminated soil may exist as a pure NAPL phase, dissolved in an aqueous phase, volatilized into an air phase and adsorbed in a soil particle phase (Kim, 1994).

Ideally, all volatile organic compounds should produce the phase change into the air phase during SVE operation. However, SVE remedial experiences have shown the situation to be not always ideal due to limitations of rate of mass transfer (Hayden et al., 1994, 1997). One reason for non-ideal behaviour is the controlling mechanisms of mass transfer limitations resulting from soil heterogeneity with diffusion through low permeability layers (non-advective layers) to high permeability layers (advective layers) (Johnson, 1990a, b; Hoffman et al., 1999; Ho and Udell, 1992). Some physico-chemical processes are so fast at reaching local equilibrium or transient equilibrium that mass transfer limitations are neglected. The nonuniform contaminant distribution in soil and contaminant molecular diffusion in pore water mass transfer resistances are also mass transfer limitations, especially for high dispersivity and high pore water content. These complex scenarios are difficult to simulate (Yang et al., 1999; Schaefer et al., 1999). The development of long-term, broad and intensive studies on various mass transfer limitations has promoted the elaborate work toward the realization of SVE field operation settings in models.

Introducing isolated NAPL-gas phase, NAPL-aqueous, aqueous-gas phase mass transfer (Yang et al., 1999; Huang and Goltz, 1999; Yoon et al., 2002) and the rate of mass transfer between different phases have been reported (Wilkins et al.,

1995; Rathfelder et al., 2000) even though specifying the rate of mass transfer of various phase pairs is a difficult task due to demanding a more complex model.

Currently, many models developed based on the lab-scale experimental scenarios have uncertainly proven connection to field-scale applications and modeling consequences. It is doubtful whether the consequences from lab-scale limited simulations may be extrapolated to field-scale SVE domains to predict, for instance, the tailing effect in which residual vapour concentration decreases gradually over a long period of time. The laboratory results have not been directed to assist field-scale SVE design, although they have provided significant information on the dominant physical and chemical mechanisms involved in SVE operations. As such, it is difficult to extrapolate laboratory results to real field SVE applications (Harper, 1999; Harper et al., 2003; Gidda, 2003) when one considers historical experience, operation parameters, field performance, and unanticipated subsurface conditions.

As reported, almost all modeling studies pertaining to the mass transfer calibration against one-dimensional column experimental data have been conducted using one- dimensional SVE numerical models (Falta, 1993; Yoon, 2002; Harper, 1999; Harper et. al., 2003; Gidda, 2003). Few studies related to experimental and numerical investigation of SVE systems at the lab-scale in two dimensions (Fisher, 1996; Rathfelder et al., 2000; Hoeg et al., 2004) have been conducted, and they are without any calibration and sensitivity analysis. Moreover, these developed models in multiphase experimental and numerical investigations are unable to simulate the variation of NAPL and aqueous phase saturation. The mathematical representation of the mass transfer between the contiguous phases in a multiphase system is the crucial

key in flow and transport modeling. Ultimately, there have rarely been models that depict the special tailing effects of SVE because of the inappropriate capability and limited complexity of these models to match tailing effects. Limited modeling studies which stressed the availability of calibration and further verification against the known SVE settings have been published. In three-dimensional SVE modeling work, there is the challenge of how to adjust model outputs to match the diverse performance of field SVE in order to identify optimal SVE design.

2.5.2 Mass Transfer Rate and Mass Transfer Coefficients

In order to mathematically incorporate mass transfer processes in a coupled flow and transport model, it is necessary to formulate mass transfer flux into the continuity equation. The investigations for interphase mass transfer are grounded on the molecular diffusion principle, thus Fick's diffusion law is used principally (Sherwood et al., 1975). Since the best known theory on the gas molecular diffusion process is that it works in a similar format to liquid molecular diffusion, interface mass transfer by convection is described by replacing the diffusion coefficient by the mass transfer coefficient (Rolle, 2000; Benitez, 2002). Accordingly, mass transfer flux is denoted by Equation 2.11.

Mass net flux = (mass transfer coefficient) * (concentration difference) (2.11)

The mass transfer processes are handled by two ways. The first one is deal with only one dominant NAPL to gas phase mass transfer process as nonequilibrium with the lumped mass transfer coefficient, but equilibrium mass transfer is assumed between other phase pairs (Harper, 1999). Another way is to deal with each phase

pair as nonequilibrium processes with different mass transfer coefficients. The mathematical expressions of transient mass transfer coefficients and the empirical constants involved have been discussed in the literature (Hoffman et al., 1993; Wilkins et al., 1995; Harper, 1999; Gidda, 2003).

Mass transfer coefficients may be constant or a function of the NAPL saturation or concentration of contaminants in the aqueous phase (Gidda, 2003), depending on the competitive significance of these phase pairs. The variable mass transfer coefficient also can be formulated linearly or exponentially as a function of saturation of NAPL phase. A transient mass transfer coefficient may better fit the experimental data (Armstrong et al., 1994; Harper, 1999; Yoon et al., 2002).

Mass transfer limitations are highly site-specific. The mass transfer limitations using laboratory column venting experiments for the recovery of entrapped NAPLs with a variety of media, fluids, and scales have been documented in the literature (Abriola et al., 1999; USEPA, 2002). The main framework used to model the mass transfer-controlled SVE processes include:

- exploring lumped interphase mass transfer coefficients for typical soil media and organic contaminants, such as glass beads, silt loam soil, sandy soil, etc., and different fluids;
- quantifying interphase mass transfer rates;
- setting up the mathematical models to capture the advection, dispersion and mass transfer processes in SVE operation under the specific site conditions.

In order to combine the rate of mass transfer into the advection-dispersion transport equation as a source or sink term, the interfacial specific surface area "α" is

multiplied on both sides of Equation (2.12). The first-order mass transfer expression can be incorporated into a transport model formulated as Equation (2.13) (Sherwood et al., 1975). However, due to the complexity of the porous media and NAPL morphography, it is difficult to measure the specific interfacial surface areas.

$$JA = \frac{\partial \overline{C}_\beta}{\partial t} = k_0 (C_{\beta,l} - C_{\beta,g}) \tag{2.12}$$

Where:

J = flux of mass transfer, mol/TL^2

$\overline{C_\beta}$ = concentration induced by mass transfer into β phase, mol/L^3

A = specific surface area of interface, L^{-1}

k_0 = lumped mass transfer coefficient, T^{-1}

$C_{\beta,l}$ = concentration in liquid phase of interface of β phase, mol/L^3

$C_{\beta,g}$ = concentration of gas phase of interface of β phase, mol/L^3

The general form of the first-order driving kinetics expression for the rate of mass transfer in SVE processes is denoted by (Abriola et al., 1999; Rathfelder et al., 2000):

$$\gamma_{\alpha\beta,k} = \varphi S_\beta k_{\alpha\beta} (x^e_{\beta,k} - x_{\beta,k}) \rho_\beta \tag{2.13}$$

Where:

ρ_β = density of phase β, M/L^3

$\gamma_{\alpha\beta,k}$ = rate of mass transfer of component k from phase α to phase β, M/L^{3}T

$k_{\alpha\beta}$ = mass transfer coefficient from α to β phase, T^{-1}

$x_{\beta,k}$ = molar fraction of component k

$x^e_{\beta,k}$ = equilibrium molar fraction of component k

Based on the rate of mass transfer expressed in Equation (2.12) or (2.13), the general governing equation for gas to aqueous phase mass transfer only that predicts SVE in one-dimensional settings considering nonequilibrium mass transfer limitations for the gas phase is written as (Armstrong et al., 1994):

$$\theta_g \frac{\partial C_g}{\partial t} = \theta_g D_{ij} \frac{\partial}{\partial x_i}\left(\frac{\partial C_g}{\partial x_j}\right) - q_g \theta_g \frac{\partial C_g}{\partial x_i} + \theta_a k_{ag}(C_g - HC_a) \qquad (2.14)$$

Where:

C_g = concentration of gas phase, mol/L^3

C_a = concentration of aqueous phase, mol/L^3

θ_a = aqueous phase content, L^3/L^3

H = Henry's constant dimensionless

k_{ag} = constant mass transfer coefficient between aqueous and vapour phase, T^{-1}

For different mass transfer processes involved in SVE operations, mass transfer coefficients are specific. A linear-driving-force model is adequate to describe the interphase mass transfer process during NAPL volatilization or dissolution in porous media (Bradford et al., 2000; Faisal et al., 2003; Power et al., 1992, 1994). Variable mass transfer coefficients may fit experimental results better than do fixed rates (Rao, 1980; Wilkins et al., 1995; Fisher et al., 1996; Harper, 1999; Van der Ham and Brouwers, 1998; Yoon et al., 2002). This feature explains why many models cannot be fitted to all of the stages of experimental data by a fixed value of the single mass transfer coefficient, but the decreasing mass transfer coefficient with time may

be appropriate. Thus the lumped mass transfer coefficients may be expressed as a function of the fraction of NAPL present.

Harper (1999) introduced the overall volumetric mass transfer coefficient represented in Equation (2.15), which is treated as a variable and modeled as a linear function of the NAPL volumetric fraction with two adjustable empirical parameters. This linear expression of mass transfer coefficient illustrates a limited accuracy in fitting experimental results. The improved model for Harper's (1999) one-dimensional model and the numerical solutions will be discussed in Section 3.2.

$$k_g\alpha = k_g\alpha_{\min} + m(\frac{\theta_n}{\theta_{n,i}}) \tag{2.15}$$

Where:

$k_g\alpha$ = overall air-NAPL volumetric mass transfer coefficient, T^{-1}

$k_g\alpha_{\min}$ and m = mass transfer empirical parameters, T^{-1}

$\theta_{n,i}$ = volumetric initial NAPL content, L^3/L^3

θ_n = volumetric NAPL content, L^3/L^3

van der Ham and Brouwers (1998) defined the reduction of the NAPL-gas interfacial area between the NAPL-gas phases in terms of the volumetric saturation of NAPL, and developed the exponential expression in Equation (2.16). Yoon et al. (2002) and Gidda (2003) applied a similar format of mass transfer coefficients between NAPL to gas phase in a one-dimensional SVE transport model.

$$k_{go} = (k_{go})_i(\frac{S_n}{S_{n,i}})^{\zeta} \tag{2.16}$$

Where:

k_{go} = lumped mass transfer coefficient, T^{-1}

$(k_{go})_i$ = initial NAPL-gas lumped mass transfer coefficient, T^{-1}

ζ = mass transfer empirical constant, dimensionless

S_n = saturation of NAPL

$S_{n,i}$ = initial saturation of NAPL.

Updating the mass transfer coefficients relating to the saturation of the NAPL phase over time is the more advanced modification by which the change in the time-dependent rate of mass transfer is expressed. The unknown mass transfer coefficient makes the calibration of the mathematical model more complex (Armstrong et al., 1994; Faisal et al., 2003). But most mass transfer coefficients reported in the literature are considered as a constant in all stages of SVE operations. Rathfelder et al. (2000) extensively and exhaustively reviewed the constant lumped mass transfer coefficients reported in literature with regards to dissolution, absorption and volatilization physico-chemical processes present during an SVE operation. Poulsen et al. (1996, 1998, 1999), Sleep and Sykes (1989), Rathfelder et al. (1991) and Wilkins et al. (1995) reported the empirical range of the lumped mass transfer coefficient. Rate-limited mass transfer coefficients of NAPL to gas ranged from 0.1 to 13000 day^{-1}. However, these results have not been tested against any known SVE experiment in lab or field SVE operations.

Mass transfer coefficients strongly depend on the seepage velocity and mean grain size of the porous material and other properties of the porous medium, contaminant and flow rate (Wilkins, 1995; Yoon et al., 2002). Based upon one-dimensional column experimental data, the empirical correlation for the lumped mass transfer coefficients has been reported. A dimensional analysis is usually adopted to

correct the lumped mass transfer coefficients in specific experimental systems by the following several dimensionless numbers (Powers et al., 1994; Wilkins et al., 1995; Miller et al., 1990; Chao et al., 1998), which are given in Equation 2.17 through 2.20.

$$Sh_0 = k_{ag}(d_{50})^2 / D_g \tag{2.17}$$

Where:

Sh_0 = dimensionless parameter, also called Sherwood number

K_{ag} = mass transfer coefficient of aqueous to vapour phase, T^{-1}

d_{50} = soil mean grain size, L

D_g = dispersion coefficient of gas phase, L^2/T

$$Pe = \upsilon_g d_{50} / D_g \tag{2.18}$$

Where:

P_e = Peclet number, dimensionless parameter

$$\text{Re} = \frac{\rho_0 \upsilon_g d_{50}}{\mu} \tag{2.19}$$

Where:

Re = Reynolds number, dimensionless parameter

v_g = Darcy's velocity of gas phase, L/T

μ = dynamic viscosity of gas phase, cp

$$Sc = \frac{\mu}{D_m \rho} \tag{2.20}$$

Where:

Sc = Schimdt number, dimensionless parameter

D_m = molecular diffusion coefficient in free air phase, L^2/T

The Reynolds number (Re) describes the hydrodynamic property of fluid and the Schimdt number (Sc) reflects the properties of diffusion. Many investigations of

the relationships among Sh_0, Sc and Re and Pe have been reported for various soils and VOCs under different air flow rates of lab-scale experimental conditions (Wilkins et al., 1995; Faisal et al., 2003). The strongest correlation for the NAPL saturation used by Szatkowski and Imhoff (1995), and Faisal et al. (2003) is given as:

$$Sh_0 = B_0 \theta_n^{B_1} Pe^{B_2} \tag{2.21}$$

This can be rewritten in log-linearized form as

$$\log Sh_0 = \log B_0 + B_1 \log \theta_n + B_2 \log Pe \tag{2.22}$$

Where:

B = adjustable constants

Currently, no evidence has been reported to demonstrate how the calculated mass transfer coefficients were to be used to model the relevant designated SVE system or calibrated effectively against known data obtained from actual SVE settings. So to date there have been very few 3D models which may capture the mass transfer characteristics and demonstrate the long tailing effects even though mass transfer studies on developing powerful and rigorous model simulations have been aimed at improving the SVE field design (Sun and Yeh, 1998; Barnes and McWhorter, 2000a, b).

A myriad of research results have indicated that mass transfer mainly governs the overall transport processes that occur in the interface between the two contiguous fluid phases, as is evident with the emerging SVE behaviour of early stage fast removal of contaminant followed by long tailing (Faisal et al., 2003); the rate-limited mass transfer causes a non-ideal long-term tailing process in SVE (Huang and Goltz, 1999). The rate-limited mass transfer and heterogeneity of porous media are two

reasons to cause the long non-ideal tailing performance in SVE operations (USEPA, 2002). Tailing can result in extremely long remediation times and requires the extraction of a large amount of soil gas while removing only a small quantity of contaminants (Kim, 1994).

Most modeling research on multiphase flow and transport has considered the equilibrium mass transfer processes between contiguous phases (Nair et al., 1990; Rathefelder et al., 1991). Clearly, the equilibrium models failed to capture the significant features of experimental results in lab and field due to the exclusion of the rate-limited mass transfer considerations. The advanced methodology to study rate-limited mass transfer is to combine the experiments in lab or field with the calibrated three-dimensional comprehensive mathematical modeling.

Owing to the development of the commercial computer software packages for numerical simulation and the increased investigation for SVE experiments in lab and field, the following aspects which deal with mass transfer limitations by SVE models are involved:

- multicomponent mass transfer processes and mass transfer coefficient expressions;
- sensitivity analysis for the controlling parameters for the calibrated rigorous mathematical model, such as mass transfer coefficients, permeability and dispersivity;
- extrapolation to the 3D settings of the currently existing typical mass transfer limitations and the possible size range of their mass transfer coefficients;

- estimation of the cleanup time in terms of a complex three-dimensional model;
- establishing the rate-limited mass transfer in the coupled multiphase flow and multicomponent contaminant transport governing equations.

Although three fluid phases (air-water-NAPL) are present at most SVE remediation sites, few models have been developed that can simulate the coupled multiphase flow, multicomponent transport, and three fluid phases and a solid phase rate-limited interphase mass exchange in three dimensions (USEPA, 2002).

2.6 Summary

The available models and relevant research have shown how further efforts should be directed to conduct comprehensive three-dimensional SVE modeling studies. The essential step is to undertake model simulation that includes practical SVE design and demonstrate the performance of SVE operation quantitatively. A complex multiphase flow and transport model should be developed for three-dimensional SVE settings, and then calibrated against experimental data to better understand the processes and to provide a prediction and design tool for SVE remediation operation (Chien et al., 2004).

To the best of the author's knowledge as conveyed in this literature review, it is a challenge to develop a comprehensive SVE model which consists of accurate nonequilibrium transient mass transfer rate, coupled multiphase flow and multi-component transport processes with average lab and field SVE settings. The reviewed findings of the processes and settings in SVE modeling studies are summarized

briefly in Tables 2-1 through 2-3. Tables 2-1 and 2-2 provide a concise summary to examine the level of complexity of the previously constructed SVE models related to the simulated SVE settings, mass transfer processes and the relevant mass transfer coefficients, the calibration experience, sensitivity analysis and numerical simulation methods. Table 2-2 summarizes the application of the variable mass transfer coefficients incorporated in various models.

At present, an important achievement in SVE modeling studies is to introduce the transient mass transfer rate by using a variable expression for formulating the mass transfer coefficient expression associated with NAPL saturation. To date, the essential elements in tracking the tailing stage are simply applied one-dimensionally in experimental settings and numerical models.

Using the proposed three-dimensional SVE model developed in this study, a comprehensive comparison with respect to various technical aspects of other models is illustrated in Table 2-3. The models are described briefly in the following section.

- VENT3D is a 3D finite difference code for vapour flow and transport of a multicomponent mixture (Benson et al. 1993; Barnes and White, 2006);
- SVE-3D is the most advanced model on the market as remarked by the developer Scientific Software Group (2006);
- 3D-SVE-F by the author of this thesis; and
- other typical SVE models (Sleep and Sykes, 1989, 1993; Rathfelder et al., 2000).

Table 2-3 suggests that the 3D-SVE-F model has a technical strategy for conquering the prediction of field-scale tailing effects in SVE operations.

The early nonequilibrium modeling studies have successfully shown that the rate-limited mass transfer is crucial for quantitative demonstrations of the performance of SVE remediation. However, these models simulated the progress of SVE operations just up to the removal rate of 99.9% by means of the breakthrough curve of offgas concentration versus time, neglecting the likely higher removal rate operation because of the lack of knowledge of the performance of the tailing stage. The accurate behaviours of SVE tailing effects are related directly to the determination of the closure time and the ultimate degree to which the contaminated site is cleaned up.

The methodology in the present study will be implemented to track the progress of SVE tailing effects in terms of the simulated results and stop SVE cost-effectively at the start of the tailing stage by developing a closure time index. Accurate prediction of the closure time and properly switching SVE to another cost-effective remediation strategy to meet the cleanup target of the site is a reasonable strategy.

Table 2-1 Some Coupled Multiphase Flow and Transport SVE Model*

Cases	Size of domain (m^2) & Dimensions	Duration of simulated time (Days)	Dispersivity (m)	Mass transfer with constant mass transfer coefficients	Sensitivity analysis	Numerical schemes
Armstrong et al., 1994	2D 0.5m by 0.1m	4	0.01/0.001	NAPL to air Aqueous to air Aqueous to sorbed	No	Finite element
Rathfelder** et al., 1991	1D, 2D 300m by 10m	90	0.001	NAPL to air NAPL to aqueous Aqueous to air Aqueous to sorbed	Yes	Finite difference
Rathfelder** et al., 2000	2D 15m by 6m	50	1.0	NAPL to air NAPL to aqueous Aqueous to air Aqueous to sorbed	No	Finite element
Sleep and Sykes, 1989	2D 80m by 10m	600	0	NAPL to air	No	Finite element

Notes: * The constant mass transfer coefficients of all cases are applied without calibrations and dealt with a single component transport process;

** In these cases, the radii of venting wells were considered to be equal to 0.5 m.

Table 2-2 Summary of Models Dealing with Transient Mass Transfer Coefficient*

Cases	Velocity (m/sec)	Mass transfer Coefficient expressions**	Dispersivity (m)	Calibrations	Numerical schemes
Van der Ham & Brouwers, 1998	No data	Exponent	No	Yes	Analytical solution
Harper et al., 2003	0.0023	Linear	No	Yes	Finite element
Yoon, 2002	0.001	Exponent	No	No	Finite difference
Gidda, 2003	0.001	Exponent	0.05~0.1	Yes	Finite element

Notes:

* All models simulated a one-dimensional column experiments without conducting sensitivity analysis, and dealt with single component transport, except Harper's work dealt with quaternary components. Mass transfer coefficient expression consists of single adjustable empirical parameter in Van der ham and Brouwers' works; all the others handle two adjustable empirical parameters;

** Mass transfer coefficient is a function of the saturation of NAPL phase.

Table 2-3 The Complete Comparisons of VENT3D, 3D-SVE-F and Other Models

Models	3D-SVE-F	SVE-3D	VENT3D	Other models
Developer	Lian Zhao, 2007	Scientific Software Inc., 2005	Benson et al., 1993	Sleep and Sykes, 1989, Abriola et al., 1997 Rathefelder et al., 2000, Thomson et al., 1997,
Numerical scheme	Finite element FEMLAB	Finite element	Finite difference	Finite difference or finite element
User Adaptation	√	X	X	X
Heterogeneous permeability	√	√	√	Limited
Multicomponent	√	√	√	√
Phases	4 phases, single gas active phase flow	4 phases, three phase flow	Gas phase only	Aqueous and gas phase flow
Mass Transfer	Nonequilibrium Transient mass transfer coefficients	Nonequilibrium, constant mass transfer coefficients First-order biodegradation	Equilibrium	Nonequlibrium Constant mass transfer coefficients
Special features	Predict closure time and degree of final cleanup	Estimate number of SVE wells, well's spacing, and cleanup time under complex conditions	Third-order transport algorithm	Model dependent
Calibrations Adjustable parameters	√ Mass transfer empirical parameters	No	Initial concentration	√ Intermodel, analytical solution

CHAPTER 3

NUMERICAL SIMULATION WITH FEMLAB

The developed 3D mathematical model in this study was solved numerically through the computation functions of FEMLAB. FEMLAB is a multiphysics modeling software developed by COMSOL Inc. (FEMLAB, 2006) that uses the finite element method. The use of FEMLAB improves computational issues such as the numerical approximation method, solution algorithm and computer load. These are ongoing challenges for multiphase flow and multicomponent transport modeling studies (Miller et al., 1998). As the preceeding discussion on computer codes in Section 2.4 showed, specialized commercial software has limited the flexibility to be modified in order to incorporate user-specified complex processes. FEMLAB as a general powerful finite element method modeling software has overcome the aspects of the above-mentioned shortages which limited the numerical simulation for complex processes.

In this chapter, an overview of FEMLAB modeling software is briefly addressed. Various typical applications in the unsaturated and saturated zone modeling were simulated to define FEMLAB's limits. These tested models include the flow and transport of contaminants in saturated and unsaturated zones, soil moisture flow, and a one-dimensional multiphase SVE transport model. The outcomes of the FEMLAB models for individual cases and the resultant calibration against the available data are presented. Besides determining that FEMLAB is

capable to resolve the relevant hydrological modeling issues, the techniques learned from these test cases in this chapter were applied to the three-dimensional SVE model developed for this study. The power and robustness of FEMLAB makes it possible to implement the complex mathematical modeling of SVE in this study. Specifically, the numerical simulations performed by FEMLAB allow users to deal with large amounts of diverse spatial and temporal data related to field-scale models, and output the numerical solution in a wide variety of visualization and animation functions. These could not be done easily before.

3.1 Overview of Modeling Software

MATLAB and FEMLAB are powerful science and engineering calculation interactive software tools. FEMLAB is commercial modeling software based on the finite element method using the MATLAB platform. FEMLAB can solve a system of highly nonlinear partial differential equations (PDEs) under complex geometries and deal with the interacting phenomena of the simulated processes. FEMLAB incorporates the latest finite element numerical simulation method regarding multiple options for the types and sizes of finite element mesh, discretization of spatial and time domains, iterative solver and preconditioner in order to meet the needs of various complex modeling settings. Using FEMLAB allows users to obtain an accurate, stable and convergent solution to the highly nonlinear governing equations that describe the three-dimensional SVE system (Zhao and Zytner, 2004, 2005).

The prerequisite for modeling complex cross-coupled flow and transport processes is the rigorous treatment of the nonlinear equations. In particular, FEMLAB generates the flexible forms to handle nonlinear coefficients, sources/sinks and the characteristic initial and boundary conditions by defining the relevant expressional functions. These dependent functions or any primary unknown variables are part of a complex model's governing equation system. Appendix A outlines how FEMLAB can be used to solve any modeling situation through the following steps:

- initialization of a mathematical model;
- setting up the model;
- inputing constants and expressions;
- solving the PDE;
- calibrating against known data; and
- post-processing for the results of numerical simulation.

3.2 One-Dimensional SVE Transport Model

In order to test applicability of FEMLAB, the first modeling exercise undertaken is based on a modified Harper's (1999) model, which is a one-dimensional multiphase quaternary component transport nonequilibrium mass transfer SVE case entitled 1D-SVE-L model. All input parameters used by Harper (1999) were applied to the model. Specifically, the contaminant mixture has quaternary components consisting of hexane, toluene, xylene and trimethylbenzene. The soil used in Harper's experiment was silt loam, and the one-dimensional column

geometry including flow parameters were kept identical in 1D-SVE-L. Expeimental approach see Appendix A4.

Figure 3-1 shows the comparison of breakthrough curves of concentration of offgas from the 1D-SVE-L model, Harper's experimental results and numerical simulation by means of the finite difference method. These outcomes indicate that 1D-SVE-L can fit the experimental results better with an extremely decreased value of NSSRD (Normalized Sum of Squared Residual Difference) (Harper, 1999) compared to Harper's model. The simulated results from the 1D-SVE-L model can match successfully the one-dimensional column experimental results and represent the phenomenon of early rising effluent concentration. It was capable of predicting both the initial and final concentrations of offgas more accurately than Harper's (1999) model was able to.

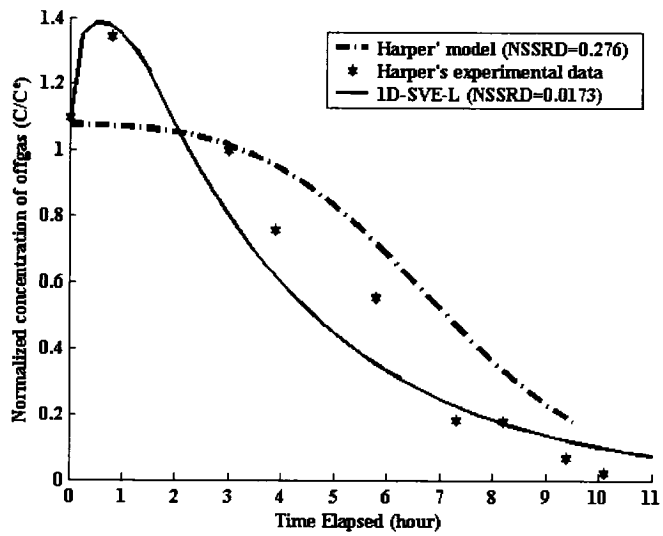

Figure 3-1 Comparison of Experimental and Modeled Results
(C^e refers to the equilibrium concentration of offgas)

It must be stated that the 1D-SVE-L model's governing equation describes the same experimental approach as Harper (1999); experimental outline given in Appendix A4, where different mass transfer coefficients and dispersion coefficients were used. There are two aspects of modification which cause the improved simulation results by 1D-SVE-L. The first modification was the inclusion of dispersion in the transport equation. The dispersion coefficient in 1D-SVE-L was expressed as (Bear, 1972):

$$D = \alpha_L \upsilon + \tau D_m \tag{3.2}$$

Where:

D = dispersion coefficient, L^2/T

α_L = longitudinal dispersivity, L

D_m = diffusion coefficients in free air, L^2/T

υ = seepage velocity, L/T

τ = tortuosity, $\tau = \frac{(\varepsilon)^{10/3}}{\varphi^2}$ (ε = air-filled porosity; φ = porosity of soil)

The second modification was to apply the exponential transient mass transfer coefficient expression denoted in Equation (3.3) replacing the linear one in Equation (3.2) which was proposed by Harper (1999).

$$k_g\alpha = k_g\alpha_{\min} + m(\frac{\theta}{\theta_i}) \tag{3.2}$$

$$k_{ng} = a(\frac{S_n}{S_{n,i}})^b \tag{3.3}$$

Where:

k_{ng} = mass transfer coefficient from NAPL to gas phase, T^{-1}

a = fitting parameters, T^{-1}

b = fitting parameters, dimensionless.

S_n = NAPL saturation

$S_{n,i}$ = NAPL initial saturation

3.3 Testing FEMLAB with a Groundwater Flow Model

The second case tested was groundwater flow, as soil and groundwater contaminations are closely related to each other because contaminated soils are both buffer and source regions for groundwater contamination. Moreover, groundwater contamination modeling needs contaminant concentration information from the soil. Remedial actions for hazardous waste sites and risk assessments also need data for the contaminant concentration in soil (Nair et al., 1990). Considering the close connection between soil and groundwater contamination and their corresponding numerical simulation, the testing of FEMLAB for groundwater modeling is conducted in this and afterwards sections. Also these simulated scenarios are necessary to test the capacity of FEMLAB software in solving coupled flow and transport numerical models.

The most general governing equation of 3D groundwater flow can be derived by applying the principle of mass conservation and Darcy's law (Bear, 1972) and can be written as Equation (3.4) (Fang and Singh, 1994). Hereafter, many cases of groundwater flow in saturated and unsaturated zones may be treated as the corresponding simplified versions of Equation (3.4) with various degrees of complexities of settings and specific initial and boundary conditions.

$$\frac{\partial}{\partial x}(K_{xx}\frac{\partial h}{\partial x})+\frac{\partial}{\partial y}(K_{yy}\frac{\partial h}{\partial y})+\frac{\partial}{\partial z}(K_{zz}\frac{\partial h}{\partial z})+\sum_{i=1}^{n_s}Q_i(t)\delta(x-x_i,y-y_i,z-z_i)=S_s\frac{\partial h}{\partial t} \tag{3.4}$$

Where:

$Q_i(t)$ = i-th point source rate, negative for a sink, L^3/T

K_{xx}, K_{yy}, K_{zz} = hydraulic conductivity in principal coordinate, L/T

δ = Dirac delta function

h = hydraulic head, L

S_s = specific storage coefficient, L^{-1}

For statistical measures of goodness-of-fit for the case studies in this section, the root mean of squared residual errors (RMS) is used (Zheng and Bennett, 2002):

$$RMS = \left[\frac{1}{N} \sum (Cal_i - Obs_i)^2 \right]^{1/2} \tag{3.5}$$

Where:

N = number of calibrated points

i = i-th calibrated points

Cal_i = calculated value

Obs_i = observed value.

The general groundwater flow equation was applied to simulate a two-dimensional steady-state groundwater flow case in a confined aquifer with non-homogeneous and anisotropic porous media and irregular boundaries modeled by Fang and Singh (1994). Figure 3-2 provides a schematic of the case where the direction of groundwater flow is along the x direction (Fang and Singh, 1994). The flow equation is based on a simplified form of Equation (3.4). The parameters used as inputs for the FEMLAB model are listed in Table 3-1 from Fang and Singh (1994).. The typical FEMLAB output colour and contour map of the simulated hydraulic heads are shown in Figures 3-2 and 3-3. The hydraulic heads on the specific locations

on the domain which are solved by the FEMLAB model and Fang and Singh (1994) are listed in Table 3-2. Using data in Table 3-2, the calculated RMS according to Equation (3.5) is 0.416. This indicates a good match between the numerical simulation with FEMLAB and Fang and Singh's (1994) data.

Table 3-1 The Parameters Applied in FEMLAB Groundwater Model

Parameters	Values
Hydraulic conductivity in region I, $k_{xx}=k_{yy}$, m/day	1
Hydraulic conductivity in region II, $k_{xx}=k_{yy}$, m/day	0.1
Head boundary at the western boundary, m	125
Head boundary at the eastern bourndary, m	90
Rate of pumping well, m^3/day	5

Table 3-2 The Comparison of the Simulated Results of Hydraulic Head Values

Node Number	Node Coordinates (Km)	Hydraulic Head (m)	
		FEMLAB model	Fang and Singh (1994)
1	(3,5)	124.990	125.000
2	(8,5)	123.780	123.560
3	(13,5)	108.710	108.890
4	(18,5)	94.000	94.810
5	(5,10)	124.990	125.000
6	(10,10)	121.010	122.030
7	(15,10)	88.590	88.560
8	(20,10)	97.360	97.670
9	(2,17)	124.99	125.000
10	(8.33, 16.33)	123.350	123.530
11	(14.66,16)	106.790	106.42
12	(21,15)	89.293	89.433

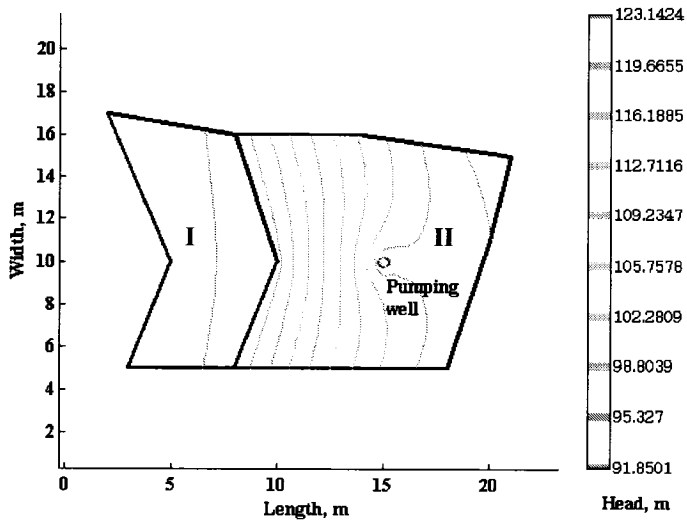

Figure 3-2 The Calculated Contour Map
(Simulating a Confined 2D Heterogeneous Aquifer with a Pumping Well)
(I) --- Sandy Gravel; (II) --- Silty Sand

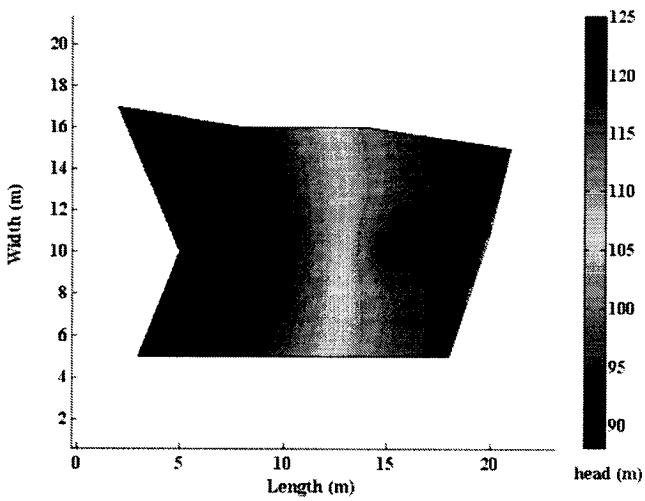

Figure 3-3 The Calculated Colour Map of Hydraulic Head
(Same case as the Figure 3-2)

3.4 Transport of a Contaminant under Steady-State Flow of Groundwater

This tested scenario was based on Rao et al.'s work (2000). The modified governing equations for the groundwater flow and contaminant transport processes are denoted by Equation (3.6), neglecting chemical reaction. The system of the governing transport equations is linked to the governing flow equation through Darcy's velocity. Data on the geological features of the site and flow and transport of contaminant conditions are summarized in Table 3-3. This scenario simulated an unconfined groundwater steady state flow and transient transport of SO_4^{2-} and Cl^- contaminants from a wastewater pond located above the simulated groundwater aquifer. The constant concentration of discharged chemicals in the wastewater is 600 mg/L. The simulated results gave the prediction of migration of chemicals after 1000 days which was not completed by Rao et al. (2000).

$$\begin{cases} S_s \dfrac{\partial h}{\partial t} = \dfrac{\partial h}{\partial x_i}\left(K_{ii} \dfrac{\partial h}{\partial x_j} \right) + Q_s \\ R\dfrac{\partial C}{\partial t} = \dfrac{\partial h}{\partial x_i}\left(D_{ij} \dfrac{\partial C}{\partial x_j} \right) - \dfrac{\partial}{\partial x_i}(\upsilon_i C) + Q\dfrac{\overline{C}}{\varphi} - \lambda\left(C + \dfrac{\rho_b}{\varphi} C_s \right) \end{cases} \qquad (3.6)$$

Where:

K_{ii} = a principal component of hydraulic conductivity tensor, L/T

v_i = interstitial velocity, L/T

Q_s = volumetric flux of water per unit volume, T^{-1}

R = retardation coefficient, dimensionless, defined as $R = 1 + \frac{\rho_b K_d}{\varphi}$

S_s = specific storage of the porous medium, L^{-1}

φ = porosity of porous medium

h = hydraulic head, L

$\overline{C}$ = concentration of contaminant source, M/L^3

C_s = concentration of contaminant sorbed in porous medium, M/M

C = concentration of contaminant dissolved in the groundwater aquifer porous medium, M/L^3

D_{ij} = hydrodynamic dispersion coefficient, L^2/T

λ = chemical reaction constant, T^{-1}

ρ_b= bulk density of porous medium, M/L^3.

Table 3-3 Inputs for 3D Groundwater Flow and Transport of Contaminant Model

Size of domain 2000m * 2000m * 100 m Hydraulic conductivity K = 2.5 m/day Longitudinal dispersivity α_L =100 m, Horizontal dispersivity α_{TH}=10 m Vertical dispersivity α_{TV}= 1 m Porosity φ = 0.2 Recharge =65 mm/year Neglect chemical reaction and adsorption action, that is, λ=0, R=0 Boundary conditions: For the groundwater flow equation, the boundaries are inflow and outflow constant head condition from the west to the east. No flow boundaries were simulated on the north and the south boundaries. For transport equations, all boundaries are no flux. Initial condition: Source concentration is 600 mg/L; all other areas are 400 mg/L uniform background concentrations in the aquifer. The unconfined groundwater table is located at the depth 1.88 m. The water table equivalent potential line is 173 m at the western boundary and 162 m at the east boundary.

In this case, the flow equation, in terms of hydraulic head, is solved prior to solution of the transport equation. Velocity components throughout the region of interest then are calculated by Darcy's law; the transport equation is solved using these velocities as inputs. Hydraulic gradients in the flow area do not change significantly over time. Thus, the flow of groundwater is steady-state. Figure 3-4 shows the predicted hydraulic head steady-state profile. It indicates the experted reasonable result. Figure 3-5 demonstrates the advancement of the solute migration simulated by FEMLAB model at 1,000 days. This is a reasonable output with respect to direction of groundwater flow and the simulated concentration of contaminant. There were no sampled quantitative data or outputs from Rao et al.'s work (2000) that could be used to calibrate the developed model using FEMLAB.

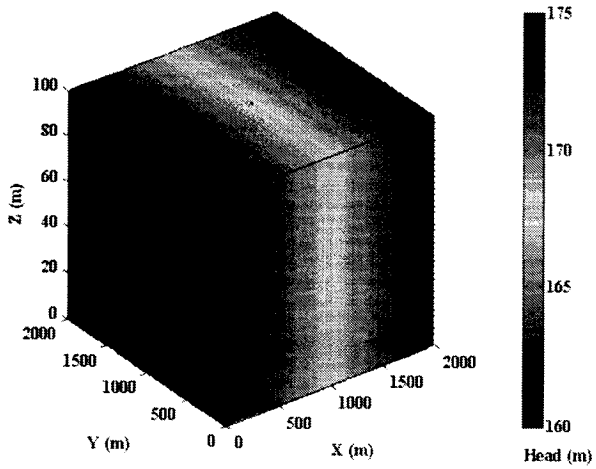

Figure 3-4 The Simulated Profile of the Hydraulic Head (the flow along *x* direction)

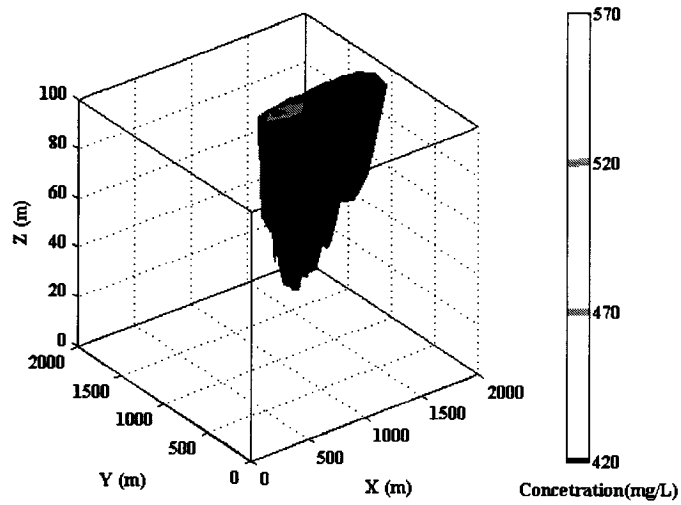

Figure 3-5 The Predicted Distribution of Concentration at 1000 Days

3.5 Density-Driven Flow and Transport in the Unsaturated Zone

Variable density flow issues originate from the concerns of seawater intrusion in a subsurface system, for example (Kolditz et al., 1998). The difference in fluid density in a groundwater system gives rise to the advective flux and velocity-dependent hydrodynamic dispersion (Zheng and Bennett, 2002). Modeling of variable density flow in groundwater systems has been addressed by numerous researchers (Ying and Zheng, 1999). The prediction of the migration of contaminants simultaneously in the saturated and unsaturated zone is an active area of study. However, currently, there have been no calibrated outcomes reported for an advection and dispersion transport equation.

Utilizing the governing equations that were presented by Ying and Zheng (1999), the density-driven flow and transport of contaminants in a variably saturated zone is simulated with FEMLAB. The movement of solute predicted by the transport equation causes significant change in water density; the flow equation, often expressed in terms of pressure of the mobile phase, is solved as a coupled set of governing equations.The coupled approach requires considerably more computational effort than the decoupled approach, but it is necessary for the solution of transport problems in which fluid density varies in response to the solute transport. This causes the cross coupling of highly nonlinear governing equations, which differ from the constant density cases of groundwater flow and contaminant transport. The simulated three-dimensional domain has an area of 10 m x 10 m with a vertical thickness of 2 m; the site is assumed to be homogeneous, isotropic, incompressible and isothermal. The governing equations for flow and transport are described by the following equation system:

$$\begin{cases} \dfrac{\rho}{\rho_w}\varphi\dfrac{dS}{dh_p}\dfrac{\partial h_p}{\partial t} = \nabla\left[K\nabla h_p + \dfrac{\rho}{\rho_w}\nabla z_g\right] + \dfrac{\rho^*}{\rho_0}Q \\ \dfrac{\rho}{\rho_w} = 1 + (\dfrac{\rho}{\rho_w} - \dfrac{1}{\rho_s})C \\ q_d = -K_{ij}\left[\dfrac{\rho}{\rho_w} + \nabla h_p + \nabla z_g\right] \\ \theta\dfrac{\partial C}{\partial t} + \nabla(qC) - \nabla(\theta D_{ij}\nabla C) = \dfrac{\rho^*}{\rho}QC \end{cases} \tag{3.7}$$

Where:

C = mass concentration of chemical, M/L^3

ρ = density of solution at chemical concentration C, M/L^3

ρ_w = referenced density of water at zero chemical concentration, M/L^3

ρ^* = density of either injection water or withdrawn water, M/L^3

ρ_s = density of pure chemical, M/L^3

h_p = soil water pressure head for unsaturated condition, L

S = degree of soil water saturation

q_d = density related to Darcy's velocity, L/T

θ = soil moisture content, L^3/L^3

z_g= elevation head, L

Q= chemical source/sink, M/L^3T

Kolditz et al. (1998) simulated the impact of variable fluid density by using a coupled nonlinear groundwater flow and transport model. In terms of mass concentration, the linearized form of equation of state of bulk fluid density is given by Equation (3.8):

$$\rho = \rho_w[1 + \beta_c C + \beta_h(h_p - h_0)] \tag{3.8}$$

Where:

β_c = volumetric concentration coefficient of expansivity, L^3/M

h_0 = reference pressure head or soil water potential, L.

β_h = coefficient of expansivity from change of hydraulic head, L^{-1}

The coupled flow and transport equations were solved using data in Table 3-4. Figures 3-6 and 3-7 indicate the results drawn as slices at different depths at 1000 days from density-driven flow and no density-driven flow cases. The results show that the density-driven force causes extended migration of chemicals than no density-

driven force. Likewise, Figures 3-8 and 3-9 demonstrate the spreading of contamination from the source by the continuous isosurface of chemical distribution.

Table 3-4 Inputs for the Density-driven Flow and Transport Model
(Ying and Zheng, 1999)

Parameters	Values
Brooks Corey constitutive relation empirical parameter, λ	3.45
Soil porosity, φ	0.52
Saturated hydraulic conductivity, K_s, m/day	0.3
Density of water, ρ_0, kg/m^3	1000
Bulk density of soil, ρ_b, kg/m^3	1650
Density of chemical, ρ_s, kg/m^3	1350
Source flow rate, Q, kg/m^{3}day	0.1
Longitudinal dispersivity, α_L, m	3
Coefficient of expansivity from solute concentration, m^3/kg	0.2

Although no exact calibrations of the simulated results against known data can be presented, reasonable migration and comparisons of the concentrations between the density-driven and the constant density case have been demonstrated. The simulated results show that the difference of concentrations in chemical due to density-driven flow is relatively about 8.2 % higher over the same history period compared to constant density situation without calibration. The results show that such a complex scenario can be modeled successfully with FEMLAB.

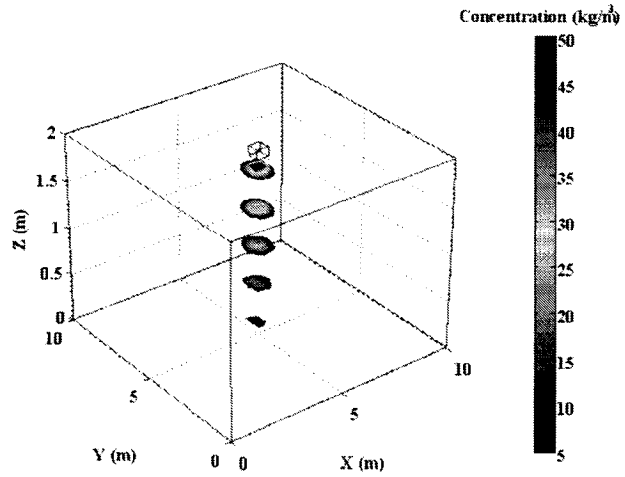

Figure 3-6 Concentration of Chemical for Density-Driven Transport at 1000 Days

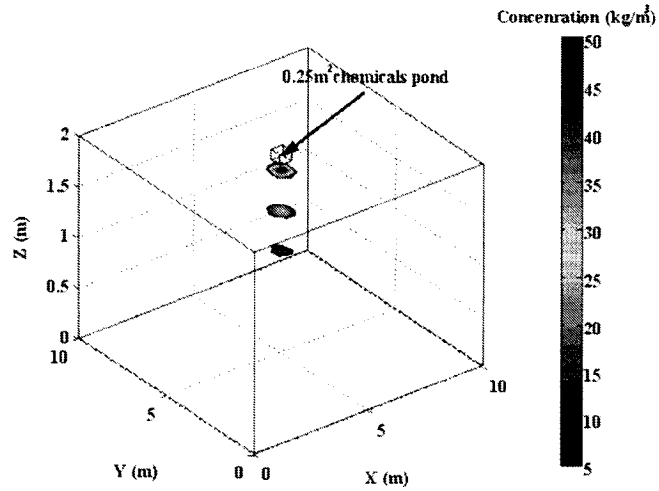

Figure 3-7 Concentration of Chemical for Constant Density Transport at 1000 Days

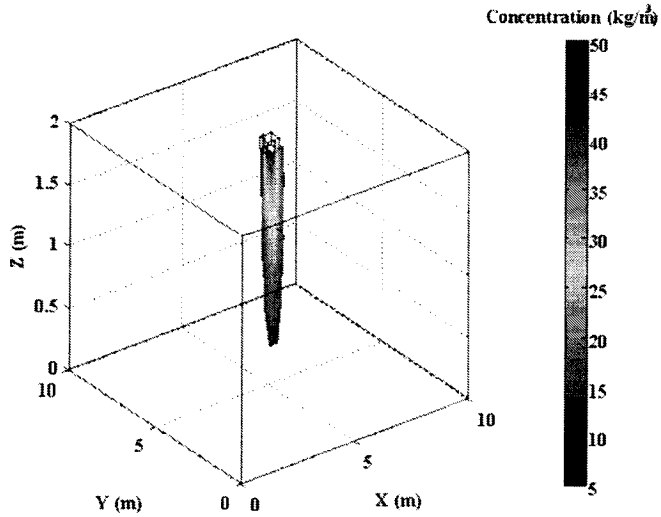

Figure 3-8 Concentration of Chemical for Density-Driven Transport at 1000 Days

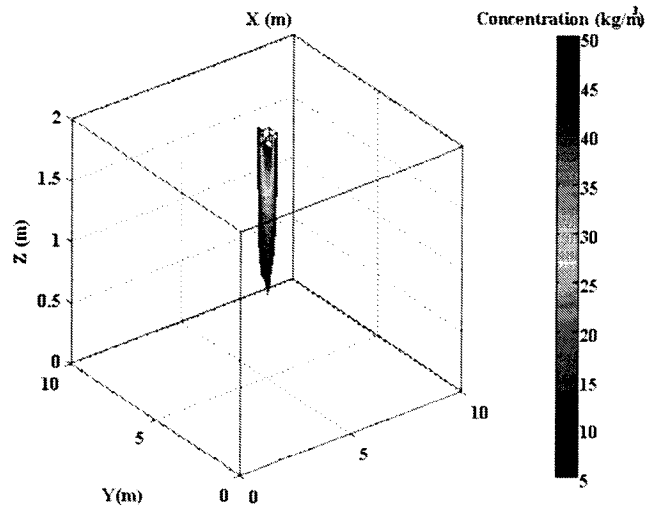

Figure 3-9 Concentration of Chemical for Constant Density Transport at 1000 Days

3.6 Movement of Soil Moisture

Considering the multiphase flow involved in an SVE operation, if movement of the aqueous phase in an SVE site is present, the aqueous phase flow equation for the SVE process is represented by the Richards equation. Therefore, the solution for a two-dimensional *h*-based Richards equation was applied to validate the aqueous phase flow equation which is involved in the proposed SVE model (Abriola et al., 1999). The constitutive relationship between the moisture content and pressure head makes the possible conversion of the θ-based to *h*-based Richards equations. Equation (3.9) is the classical θ-based Richards equation. By using FEMLAB, the tested case is to solve Richards equations in two and three dimensions using the specified hydraulic conductivity and diffusivity functions.

An example of classic finite element solution in two dimensions for unsteady and unsaturated flow cases was reported by Brunch (1975). This scenario was first simulated with FEMLAB and then extended to a three-dimensional domain. The governing partial differential equations are highly nonlinear as expressed by Richards equation due to the moisture content-dependent hydraulic conductivity and diffusivity.

$$\frac{\partial\theta}{\partial t}=\frac{\partial}{\partial x}\left(D(\theta)\frac{\partial\theta}{\partial x}\right)+\frac{\partial}{\partial y}\left(D(\theta)\frac{\partial\theta}{\partial y}\right)+\frac{\partial}{\partial z}\left(D(\theta)\frac{\partial\theta}{\partial z}\right)+\frac{\partial K(\theta)}{\partial z} \tag{3.9}$$

The soil water hydraulic diffusivity is formulated as:

$$D(\theta)=1.25*10^{-3}e^{27.8\theta}\ \text{cm}^2/\text{min} \tag{3.10}$$

The hydraulic conductivity is expressed as:

$$K(\theta) = 6.25 * 10^{-3} (\frac{\theta - 0.04}{0.33 - 0.04})^6 \text{ cm/min} \quad (3.11)$$

Along with the geometry of the simulated domain as shown in Figure 3-10, boundary and initial conditions are described as:

$\theta = 0.33$ along BC;

$\frac{\partial \theta}{\partial x} = 0$ along AB and DE;

$-D(\theta)\frac{\partial \theta}{\partial z} + K(\theta) = 0$ along AE and CD;

$\theta(x, y, z, 0) = 0.1$

The simulated results by Brunch (1975) (2D only) and by using FEMLAB respectively, are shown in Figures 3-10(a) and 3-10(b), which show the simulated front of moisture which migrates into the soil with the water content marked on the moisture contours for two specific times. The simulation results in 2D are calibrated against the results by Brunch (1975). The calculated value of NSSRD is equal to 0.0985. This result shows that the solution obtained using FEMLAB is accurate when compared to the solution by Brunch (1975).

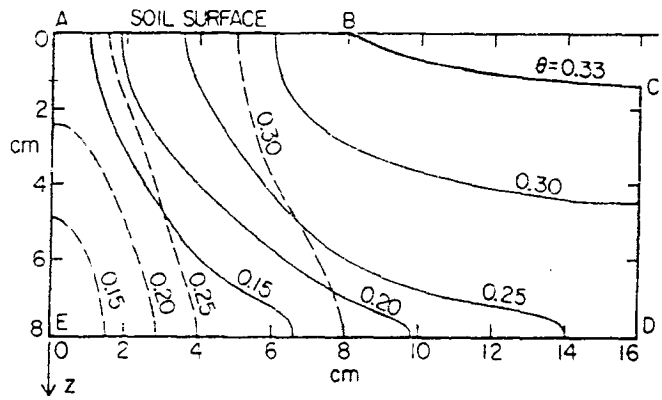

Figure 3-10 (a) 2D Contour of Moisture Front by Brunch (1975)

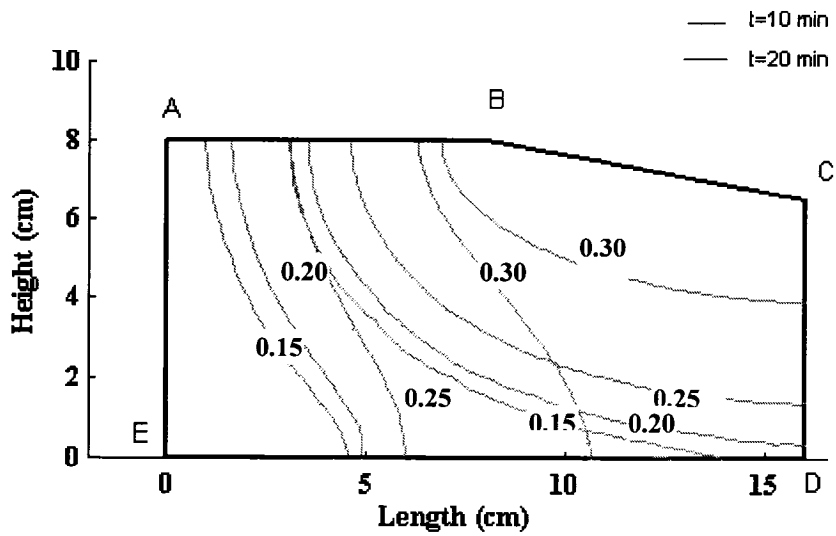

Figure 3-10 (b) **2D Contour of Moisture Front by FEMLAB (NSSRD=0.0985)**

By introducing an additional boundary condition $\frac{\partial \theta}{\partial y} = 0$, the simulation can be extended to the three dimensions. The corresponding three-dimensional distributions of moisture in the extended domain are shown in Figures 3-11(a) and 3-11(b), which demonstrate the migration of the front of moisture in x and y direction slices, respectively.

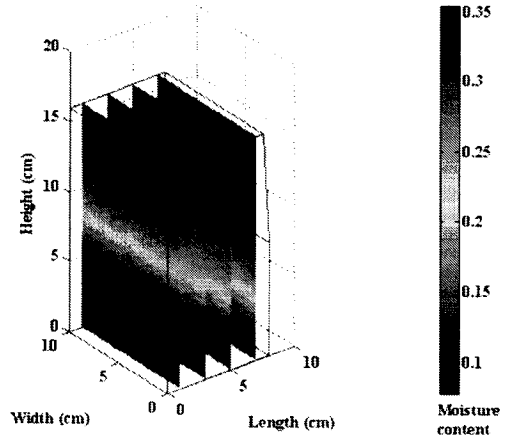

Figure 3-11(a) 3D Moisture Profile (*x*-Direction Slices)

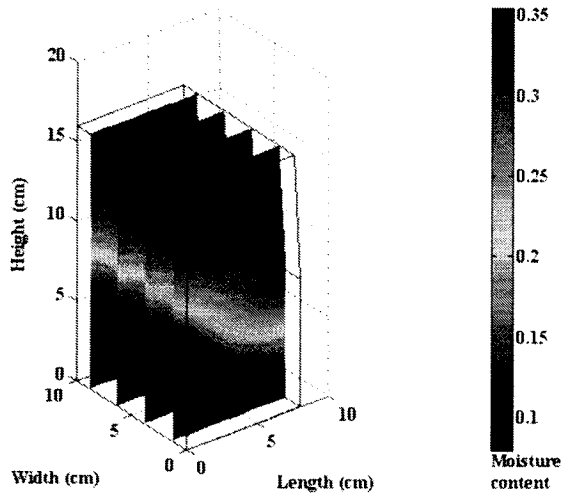

Figure 3-11(b) 3D Moisture Profile (*y*-Direction Slices)

3.7 Summary

The completed numerical simulations for the test cases described in this chapter show the ease and high level of accuracy by which 3D modeling can be done with FEMLAB. Therefore, FEMLAB was selected as the modeling tool for this

research. Several preliminary simulations were completed following the overall procedures outlined in Appendix A.

Choosing the appropriate commercial modeling software from a number of commercial candidate software packages is essential to developing a three-dimensional SVE model. Generally speaking, modeling software for engineering design and research orientation should have the following advantages:

- powerful calculation capability related to solving the multiphysics highly nonlinear PDEs, including prompt technical support and updating;
- general running platform;
- confirmed applied experience in relevant areas; and
- easy to understand visualization and animation functions to demonstrate the modeling results including outputs of all involved dependent variables.

In addition to broad PDE-based modeling studies conducted by the developer of FEMLAB, the outcomes of the preliminary modeling studies completed in this chapter with respect to a one-dimensional SVE model, groundwater models, and soil physics cases have shown that FEMLAB is capable of dealing with PDE-based numerical simulation for a complex 3D SVE model. The success of the typical cases undertaken illustrates the capability of FEMLAB in the advanced finite element method and post-processing function. It can quite adequately be used to describe various typical hydrological processes in the saturated and variably saturated zones.

The completed simulations show that FEMLAB can integrate several cross-coupled controlling processes. Besides the above-mentioned general advantages as a

modeling software, the pertinent advantages in using FEMLAB for SVE modeling can be summarized in the following capacities in:

- treating heterogeneous and anisotropic media representing many geologic formations;
- handling both distributed area and point sources/sinks that are spatially and temporally dependent;
- accepting two types of boundary conditions (i.e., Dirichlet (fixed-head or concentration), specified-flux, Neumann (specified-pressure-head gradient or specified-dispersive flux), and any variables dependent on the spatially- and temporally-independent variables;
- powerful numerical simulation method, such as mesh refinement of finite element, integrator, time-dependent linear solver, controlled relative and absolute error of numerical solution, tracking the process of convergence, and treatment of the nonlinear coefficients;
- post-processing functions for the simulated results, which improves understanding issues related to the saturated and unsaturated zone modeling studies; and
- solving the complex three-dimensional soil vapour extraction model.

The experiences gained from these various testing scenarios will be applied to the proposed 3D SVE model.

CHAPTER 4

DEVELOPING THE MATHEMATICAL MODEL OF SVE

In this chapter, the methodology and procedures used to develop the SVE conceptual model and mathematical model are presented. At first, the theories and essential laws on the fluid flow and transport of contaminants in porous media, partitioning of contaminants between contiguous phases, and the relevant properties are highlighted. Secondly, systematical and detailed descriptions for average SVE field settings and characteristic physico-chemical processes are given. Finally, the most general SVE conceptual model and the corresponding mathematical model including the constitutive relationship and rate-limited mass transfer are illustrated.

4.1 Properties of an SVE System

This section highlights the main features of the soil porous media and the target contaminants (BTEX) of concern in environmental sites. These properties are included in SVE models and significantly influence the simulated results due to their response to various system configurations and/or uncertainty. The performance of an SVE system depends on the properties of the contaminant and the soil, as well as the SVE operational parameters (Nobre and Nobre, 2004). Proper air flow spreading over the site and transport characteristics as well as mass transfer processes determine the success of SVE technology (Suthersan, 1996). A model which can capture these crucial processes can be used to design an SVE system and accurately predict the response for various design options.

4.1.1 Properties of Contaminants

In the present research, the contaminant simulated in the lab-scale model is toluene. For the field-scale model, the contaminants are BTEX (Benzene, Toluene, Ethylbenzene and Xylene), because BTEX is a major group of target contaminants for soil and groundwater remediation (Johnson et al. 1990a; Hayden et al., 1994; Yang et al., 2001; Widdowson et al., 2001). BTEX is the first group of hydrocarbons to volatize from the subsurface, and is highly correlated with the concentration of hydrocarbons in offgas.

As the advancement in SVE experimental and numerical studies has occurred, components in the gas phase may be tested and simulated according to the following three stages of advancement to handle hydrocarbon species in contaminant mixtures:

- pseudo single compound with unique physico-chemical properties the same as the air (Lee et al., 2000);
- multicomponent mixture such as BTEX, which is regarded as limiting SVE target compounds; and
- all components at the concentration higher than their detection limits by the conventional measurement methods, such as gas chromagraphic separation method, in order to explore the continuity of contaminants separated by SVE operation from the discernible volatility of individual compounds.

In order to handle the transport of multicomponent distributed in a soil multiphase system, an SVE mathematical model needs to capture the complexity of the proposed conceptual model and also can be solved numerically by powerful modeling software.

4.1.1.1 Density of a Phase

For a multiphase system, the densities of individual phases affect the performance of an SVE system. For a pure NAPL phase, the density of a component of contaminant mixture is constant while the density of each phase depends on the composition of the liquid. The molar density of NAPL liquid phase ρ_n is denoted by:

$$\rho_n = \sum_{i=1}^{N_c} C_{n,i} \tag{4.1}$$

Where:

ρ_n = molar density of NAPL, mol/L^3

N_c = number of components in the NAPL phase

$C_{n,i}$ = molar concentration of i-th component in NAPL phase, mol/L^3.

Density of vapour depends on both the composition and state of the phase, i.e., the concentration of a single component in the gas phase and the temperature and pressure of the gas phase. Due to the compressibility of gas and variations in the concentration of constituents of a contaminant mixture during an SVE operation, an estimation of the density of the gas phase is important. Also, handling the density of the gas phase causes a more complex numerical simulation than the NAPL and aqueous phase. Considering the complex situation of gas phase present, there are two types of methods to formulate the density of the gas phase in terms of the various simplified assumptions. In the simplest case, the density of the gas phase is treated simply as being equal to the density of air under a specific pressure and temperature. Thus, the gas phase molar density can be estimated using the ideal gas law:

$$\rho_g = \frac{p_g}{RT} \tag{4.2}$$

Where:

ρ_g = molar density of gas phase, mol/L^3

p_g = pressure of gas phase, Pa

R = universal gas constant, 8.3145 J/mol K

T = absolute temperature, K°

Kalurachchi and Parker (1990) introduced an appropriate formulation to update the density of the gas phase ρ_g based simply on the molar concentration of component in the gas phase:

$$\rho_g = \rho_a + C_g(1 - \frac{\rho_a}{\rho_v}) \tag{4.3}$$

Where:

C_g = molar concentration of gas phase, mol/L^3

ρ_a = molar density of air-specific pressure, mol/L^3

ρ_v = reference density of air, mol/L^3

The most complete form of density for a multicomponent gas mixture under a specific pressure and temperature is expressed by Kalurachchi and Parker (1990):

$$\rho_g = \frac{p_g}{RT}\left(\frac{\rho_0 + \sum_{k=1}^{Nc} C_{g,k}}{\frac{\rho_0}{M_a} + \sum_{k=1}^{Nc}\frac{C_{g,k}}{M_k}}\right) \tag{4.4}$$

Where:

ρ_0 = density of fresh air, mol/L^3

M_a = molecular weight of pure air, g/mol

M_k = molecular weight of component k, g/mol

$C_{g,k}$ = concentration of component k in air phase, mol/L^3.

4.1.1.2 Viscosity of Gas Phase

Viscosity of the vapour phase depends on the temperature and composition of the gas phase. The gas viscosity variation due to a pressure gradient can be neglected at low pressure (below 10 atmospheres) (Abriola et al., 1999). In this context, viscosity of the gas phase is considered to be equal to the viscosity of air.

4.1.1.3 Solubility

Solubility is defined as the maximum mass of compound that may be dissolved in water at a specific temperature. Solubility is one of the most important properties of petroleum hydrocarbon contaminants, which affect the fate and transport of organic compounds in the environment (Nyer, 1993) because of partitioning of components in a multiphase system between the aqueous and solid phases. Generally, NAPLs in the vadose zone are sparingly dissolved in the aqueous phase. Solubility can also have an impact on the sorption in contaminated soil, in particular, under the circumstance of groundwater table fluctuation or high water content (Zhou and Blunt, 1997). For an organic contaminant mixture such as gasoline, solubility is a function of the mole fraction of each component in the NAPL mixtures:

$$C_i = X_i \gamma_i C_i^* \tag{4.5}$$

Where:

C_i = equilibrium concentration for compound i in NAPL mixture, mol/L^3

C_i^* = equilibrium concentration for compound i as pure compound, mol/L^3

γ_i = activity coefficient of compound i

X_i = molar fraction of compound i in NAPL mixture.

4.1.1.4 Vapour Pressure

Two important processes in SVE operation are volatilization and gas/water partitioning, which link to the mass transfer from the NAPL phase (if present) and the aqueous phase (if present) to the gas phase. The first step to confirm whether a contaminated site can be remediated by means of SVE technology is to evaluate the volatility of contaminants (DiGiulio, 1992). As the major characteristic of volatility of a contaminant, vapour pressure indicates the tendency of a compound to volatilize into the gaseous phase. Under ideal conditions, NAPL volatilization abides by Raoult's law and gas/water partitioning processes follow Henry's law. Transport of contaminants in vapour phase is favoured by high vapour pressures and high Henry's law constant (Riser, 1998). The equilibrium partitioning relationships among NAPL, aqueous, and vapour phase have been derived by Harper (1999) based on Henry's law and Raoult's law.

4.1.2 Properties of Soil Porous Media

4.1.2.1 Soil Texture and Soil Structure

The major physical and chemical properties of soil which affect transport processes are permeability, porosity, soil structure, and water saturation (Karimi et al., 1987; Yong, 2001). Soil texture refers to the proportions of various particle-size groups in the soil mass, and typically refers to sand, clay and silt (Russell and Ginn, 2004). Soil structure is the shape and size of aggregates in a soil based on its physical and chemical properties (Yong, 2001). Soil structure is very important since (along with soil texture) it affects the porosity of the soil. Soil structure relates to the fabric

of soil plus interparticle forces. Information regarding soil structure may be used to delineate the form and distribution of contaminant in the soil. Also it may affect the transport and retention of contaminant (Sharma and Reddy, 2004). The soil texture triangular diagram, as shown in Figure 4-1, reflects the relative amounts of the three particle-size groups, and is used to depict the texture of soils according to the percentage of sand, clay, and silt.

Soil texture strongly influences the air-permeability. Generally, it is an important indicator which determines whether the contaminated site may be appropriately remediated by an SVE system or not. The more permeable a porous medium, the more appropriate is SVE remediation (Russell and Ginn, 2004). Soil texture influences infiltration and adsorption capacity of the contaminants, which may further affect the removal rate of contaminants. Moreover, contaminant diffusion coefficients are texture-dependent (Hillel, 1990, 1998). As identified in the shaded bottom region in the soil textural triangular diagram in Figure 4-1, the appropriate soil for SVE remediation are loam, sand and silt (Suthersan, 1996).

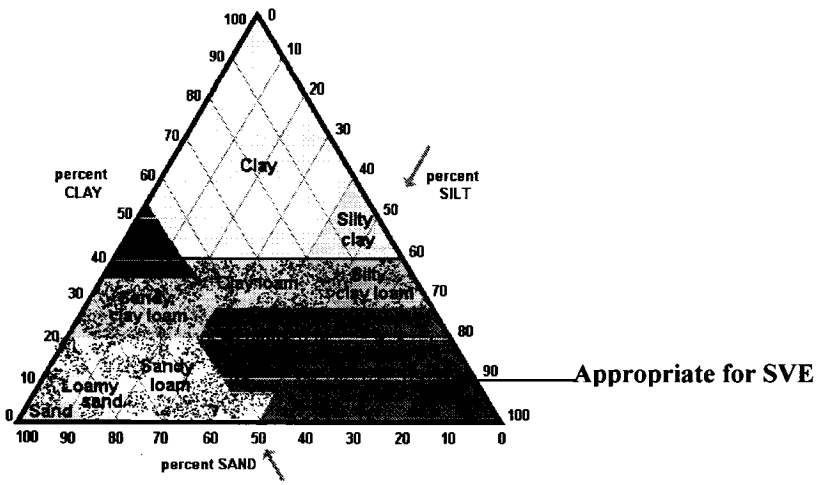

Figure 4-1 Textural Classification of Soils
(Modified from http://www.oneplan.org/Water/soil-triangle.shtml**)**

4.1.2.2 Organic Matter Content

The sorption of organic contaminants in soils is primarily due to sorption on the organic carbon fraction (f_{oc}) (Sharma and Reddy, 2004). Soil organic matter is the active fraction in soil, which severely affects adsorption of organic contaminants (Yong, 2001) and controls the sorptive intake of nonionic organic contaminants from the aqueous phase (Boyd and Sun, 1990). The natural organic matter becomes the partitioning medium for nonionic organic contaminants. Organic matter content in the field can vary anywhere from zero to ten percent. For transport of contaminants during SVE remediation, the organic matter content can affect more than just the velocity of the vapour phase (Boyd and Sun, 1990; Yong, 2001), and is a very sensitive property (Gribb et al., 2002). Organic matter content produces a more sophisticated relationship among the concentration of offgas, mass transfer, and sorbed phase and air phase. In petroleum-contaminated soils, organic carbon associated with the total petroleum hydrocarbon content, TPH (mg/kg), may be present. Residual heavy hydrocarbons can also be effective sorbents for the lighter hydrocarbons (Boyd and Sun, 1990). To account for this effect, Gribb et al. (2002) applied that f_{cs} parameter defined by Equation (4.6) replaces f_{oc}, assuming that the heavy hydrocarbon can be an effective absorbent for the lighter hydrocarbon.

$$f_{cs} = f_{oc} + \frac{TPH}{1.724} \tag{4.6}$$

Where:

1.724 = conversion factor for calculating the organic matter content considering the total petroleum hydrocarbon content

TPH = total petroleum hydrocarbon content, mg/kg

f_{oc} = organic matter content of soil, %

Equation (4.6) does not account for any non-aqueous phase liquid that may be present in heavily contaminated soils. The partitioning coefficient for the contaminant between water and organic carbon, K_{oc} (cm^3/g), which demonstrates the capacity of adsorption of contaminant to soil, strongly depends on a soil's organic carbon content.

4.1.2.3 Water Content

Water content in soil porous media is a critical factor, which seriously impacts one-dimensional SVE column experimental results (Harper et al., 1999, 2003; Gidda, 2003; Zhao and Zytner, 2005). Yoon et al. (2003) elucidated that high water content causes rate-limited diffusion through the water film, and at low water content rate-limited desorption, sorption and vapour phase diffusion are dominant.

The present work treats the influence of soil water content through:

- nonequilibrium mass transfer between aqueous and solid, NAPL and aqueous, and partitioning between aqueous and vapour phases; and
- relative permeability of aqueous phase.

4.1.2.4 Permeability

A key parameter in modeling soil venting systems is the relative air permeability, determined as a function of total liquid saturation. The effectiveness of an SVE operation in removing volatile petroleum hydrocarbon greatly depends on air permeability and diffusivity. These parameters strongly impact the SVE air flow and

mass transfer limitations, which are diffusive controlling processes from a low permeability zone to the higher permeability zone. The air permeability is often assumed as constant during the venting operation because of the lack of information on the variations in permeability over time (Stylianou and DeVantier, 1995). Many researchers have discussed the variations in permeability occurring during SVE operations (Poulsen et al., 1998).

Farhan et al. (2001) developed a model by which the variation in air permeability was predicted during SVE operations. This air permeability model cannot be employed to directly model SVE operations because of its complex deduced processes with unavailability of controlling parameters and unproven application in multiphase flow and transport modeling issues. Permeability is one of the most uncertain parameters in soil-water models (Farquhar et al., 1990). Farhan et al. (2001) estimated the variation in permeability of an SVE soil site to be around 25-125%. Stylianou and DeVantier (1995) proposed a polynominal expression that represents the relationship between relative permeability and total liquid saturation to be used for SVE design replacing the soil-water retention curve-based model. The detailed relationship among relative permeability, saturation and capillary pressure will be addressed in Section 4.3.

4.2 Multiphase Flow in Porous Media and Multicomponent Transport

4.2.1 Extended Darcy's Law in a Multiphase Flow System

The two fundamental components in multiphase flow theory are extended Darcy's law and the above-mentioned constitutive relationships. In 1856, Darcy set out to find an experimental groundwater flow law. Darcy's law is applicable when average velocities of water and gas flow are within the laminar flow range, i.e., *Re* is less than one (Bear, 1972). Darcy's law provides a good approximation for gas flow in sand, silt, clay, and other low-permeability media, where gas slippage (the Klinkenberg effect) is negligible (Massman, 1989; Sleep and Sykes, 1989; Falta et al., 1989, 1992a,b, 1993; Mendoza and Frind, 1990; Shikaze et al., 1994; Helmig, 1997).

Darcy's law has been extrapolated to a multiphase flow system to calculate the Darcy's velocity of each fluid phase. In a multiphase flow system, the permeability of a fluid phase is the product of the intrinsic permeability of a porous medium and the relative permeability of the fluid phase. The seepage velocity of a mobile phase is a function of relative permeability, properties of fluid and porous medium as well as the mobile phase pressure according to the extended Darcy's law. Darcy's velocity and the seepage velocity are represented as Equation (4.7) (Bear, 1972):

$$q_\beta = \varphi S_\beta \upsilon_\beta = -\frac{k_{ij} k_{r\beta}}{\mu}(\nabla p_\beta - \rho_\beta g \nabla z) \tag{4.7}$$

Where:

p_β = pressure of β phase, Pa

q_β =Darcy's velocity of β phase, L/T

v_β = seepage velocity, L/T

φ = porosity of porous medium

S_β = saturation of β phase

ρ_β = density of β phase, M/L^3

k_{ij} = intrinsic permeability of porous medium, L^2

$k_{r\beta}$ = relative permeability of β phase

z = elevation head, L.

4.2.2 Advection and Dispersion

There are potentially four phases in a contaminated soil, i.e., gaseous, NAPL, aqueous and solid. Contaminant movement within these phases depends on the advection and dispersion transport processes, adsorption and desorption, volatilization and water/gas partitioning. Interphase mass transfer processes occur across the gas-NAPL, aqueous-solid, aqueous-vapour and aqueous-NAPL interfaces. This section will introduce the transport of contaminants, and mass transfer processes will be addressed in Section 4.3.

4.2.2.1 Advection

During an SVE operation, fresh air is injected into the subsurface, and the dynamic partitioning relation is kinetically varying due to advection, dispersion transport, and mass transfer (Lingineni and Dhir, 1997). Advection pertains to mass transport due to the flow of the mobile phases in which the mass exists and is carried as SVE operations proceed. Advection is driven by the pressure, gravitational and

density gradients of mobile phases. Advection is the dominant process in SVE operations, and contributes to contaminant migration to a venting well. Generally, dispersion would also occur in the region of the flow domain where advection is present. The advection flux J_α of a contaminant in a mobile phase is expressed as:

$$J_a = q_\beta C_{\beta,k} \tag{4.8}$$

Where:

J_α = advection flux, mol/L^{2}T

q_β = Darcy's velocity of β phase, L/T

$C_{\beta,k}$ = concentration of component k in β phase, mol/L^3

4.2.2.2 Dispersion and Dispersion Coefficient Tensor

It is important to consider dispersion phenomena in SVE modeling in order to improve the accuracy of the simulated results (Cann et al., 2002; Gidda, 2003; Gidda et al., 2006). The variations in local velocity both in magnitude and direction along the tortuous flow paths and, simultaneously, the presence of a pore system and heterogeneity create mechanical dispersion and molecular diffusion, resulting in concentration variations (Schwartz and Zhang, 2003). Hydrodynamic dispersion has an essential influence on the accuracy of a mathematical model. The variations in concentration of contaminants cause the changes in density and viscosity of the NAPL and further affect the flow regime (Bear, 1972). In the present work, diffusion and hydrodynamic dispersion will be incorporated into the developed 3D SVE model.

Molecular diffusion of contaminant in a gas phase in porous media has been studied by extrapolating knowledge obtained about molecular diffusion in air.

Accordingly, the diffusion phenomenon has been extensively incorporated in SVE modeling studies (Harper, 1999; Yoon et al., 2003). Effective diffusion coefficients of gas, based on a Millington and Quirk (1961) model, introduce molecular diffusion theory in free air into the diffusion in porous media by dealing with the tortuosity of porous media, and are expressed as:

$$D_e = D_m \frac{(\varepsilon)^{10/3}}{\varphi^2} \tag{4.9}$$

Where:

D_e = effective diffusion coefficient, L^2/T

D_m = molecular diffusion coefficient in free air, L^2/T

ε = air-filled porosity in porous medium, L^3/L^3

φ = total porosity of soil porous medium, L^3/L^3

An accurate description of gas diffusivity, which is the ratio of gas diffusion in soil and free air, is a prerequisite for predicting in-situ transport and fate of volatile organic chemicals. The proposed model for predicting gas diffusivity for various types of soils (Moldrup et al., 1996, 1997, 1998, 1999) is expressed by Equation (4.10), which is a soil-type-dependent power functional relationship between gas diffusivity and air-filled porosity.

$$\frac{D_e}{D_m} = (\frac{\varepsilon}{\varphi})^{\eta(b)} \tag{4.10}$$

Where:

$\eta(b)$ = empirical expression dependent on the soil type and soil structure.

Ng and Mei's (1996) model considered the feasible diffusion in water-saturated spherical aggregates, and advection and diffusion in air-filled porous media.

This transport model for the first time connected both aqueous and air phase diffusion in the SVE domain because the diffusion in the aqueous phase can affect the diffusion in the soil gas phase. Based on the relationship between the diffusion in aqueous and gas phases coupled with linear insothermal adsorption, the sorption-retardation effective diffusion coefficient of aqueous or gas phases is denoted by Ng and Mei (1996) as:

$$D_e = \frac{\varphi D_m}{K_d(1-\varphi)\rho_b + \varphi} \tag{4.11}$$

Where:

K_d = adsorption coefficient, g/g soil

ρ_b = bulk density of soil, M/L^3.

One of the most poorly developed issues in SVE transport modeling studies is the dispersivity in contaminated soils. Experimentally measuring dispersivity is a difficult task, especially for three-dimensional flow, because it is a challenge to determine both the longitudinal and transversal (vertical and horizontal) dispersivity (Zou and Parr, 1993). The complexity of porous media and the lack of consistent system characteristics preclude a quantitative evaluation of the dispersion coefficient for SVE remediation operation processes. The dispersion coefficient is highly uncertain, but its effect is large for vapour flow and transport of contaminants in the subsurface. Hence, assessing the dispersivity of porous media has theoretical and practical implications for SVE modeling.

Gidda (2003) proposed a reliable experimental procedure to measure statistically the dispersivity of various soils using sulfur hexafluoride (SF_6), an inert

tracer. For Ottawa sand (a uniform soil) and Brookston soil (a complex soil) under the water contents of 0 to 40%, and a controlled flow rate of 0.6 to 20 L/min, the longitudinal dispersivity was reported as 0.006 to 0.024 m in the laboratory.

Scaling up of dispersivity will occur whenever an (n-1) dimensional model is calibrated or used to describe an n-dimensional system (Domenico and Robbins, 1984). Heterogeneity and variability in velocity will increase a dispersion coefficient (Smith and Schwartz, 1980).

Dispersion in the direction perpendicular to the mean direction of flow is referred to as transverse dispersion, while the dispersion parallel to the mean direction of flow is termed longitudinal dispersion. Longitudinal dispersion is 10 times bigger than vertical dispersivity (Schwartz and Zhang, 2003). In the present work, because the SVE venting operation is radially toward the venting well, the relationship between the longitudinal and transversal dispersivity is expressed as:

$$\alpha_L = \alpha_{TH} = 10\alpha_{TV} \tag{4.12}$$

Where:

α_L = longitudinal dispersivity, L

α_{TH} = transversal dispersivity in horizontal direction, L

α_{TV} = transversal dispersivity in vertical direction, L.

The mechanical dispersive and diffusive rates can be combined as a total dispersive flux and expressed as:

$$J_{dis} = J_{mdis} + J_{dif} = -\varphi S(D_{mdis} + \tau D_m)\nabla C = -\varphi SD\nabla C \tag{4.13}$$

Where:

J_{dis} = dispersive flux, mol/L^{2}T

J_{mdis} = mechanical dispersive flux, mol/L^{2}T

J_{dif} = diffusive flux, mol/L^{2}T

C = concentration of compound, mol/L^3

D = dispersion coefficient tensor, L^2/T

D_{mdis} = mechanical dispersion coefficient, L^2/T

The dispersion coefficient tensor "D" is dependent on the advective velocity vectors, diffusion coefficients and dispersivities as formulated in Equation (4.14). In a uniform flow field, only the dispersion coefficient tensor is distributed in the x, y, z principal coordinate directions, with the cross-terms regarded as zero.

$$D = \begin{pmatrix} D_x & D_{xy} & D_{xz} \\ D_{yx} & D_y & D_{yz} \\ D_{zx} & D_{zy} & D_z \end{pmatrix} \tag{4.14}$$

Where:

$$D_x = \alpha_L \frac{\upsilon_x^2}{|\upsilon|} + \alpha_{TH} \frac{\upsilon_y^2}{|\upsilon|} + \alpha_{TV} \frac{\upsilon_z^2}{|\upsilon|} + \tau D_m$$

$$D_y = \alpha_L \frac{\upsilon_y^2}{|\upsilon|} + \alpha_{TH} \frac{\upsilon_x^2}{|\upsilon|} + \alpha_{TV} \frac{\upsilon_z^2}{|\upsilon|} + \tau D_m$$

$$D_z = \alpha_L \frac{\upsilon_z^2}{|\upsilon|} + \alpha_{TV} \frac{\upsilon_y^2}{|\upsilon|} + \alpha_{TV} \frac{\upsilon_x^2}{|\upsilon|} + \tau D_m$$

$$|\upsilon| = \sqrt{\upsilon_x^2 + \upsilon_y^2 + \upsilon_z^2}$$

υ_x υ_y υ_z = component of seepage velocity in a coordinate system.

4.3 The Conceptual Model

A conceptual model demonstrates the understanding of SVE processes and their mutual relations. Developing the pertinent conceptual model for field SVE operation is the first step to conducting modeling studies, as it outlines all the relevant physico-chemical processes affecting SVE. The conceptual model translates real world processes into ones which may be mathematically described (Chien et al., 2004). SVE remediation operation is prevalently regarded as a multiphase flow, multicomponent transport and nonequilibrium mass transfer process in the vadose zone (Looney and Falta, 2000). Therefore, the overall conceptual model will be envisioned in terms of the practical operation situations, flow and transport and mass transfer processes as well as the distribution of NAPL in the subsurface.

4.3.1 The Air Flow Field and Multiphase System

SVE technology takes advantage of the volatility of the petroleum hydrocarbons so that petroleum hydrocarbon contaminants may volatilize from adsorbed, dissolved, and pure NAPL phases in the soil to the vapour phase. The contaminants, which are transferred into the vapour phase will be removed by a venting well and treated aboveground. The configuration of SVE wells and vacuum conditions in these wells contribute to the establishment of the air flow schematic as shown in Figure 4-2. The flow of gas phase is the dominant mechanism during SVE operation.

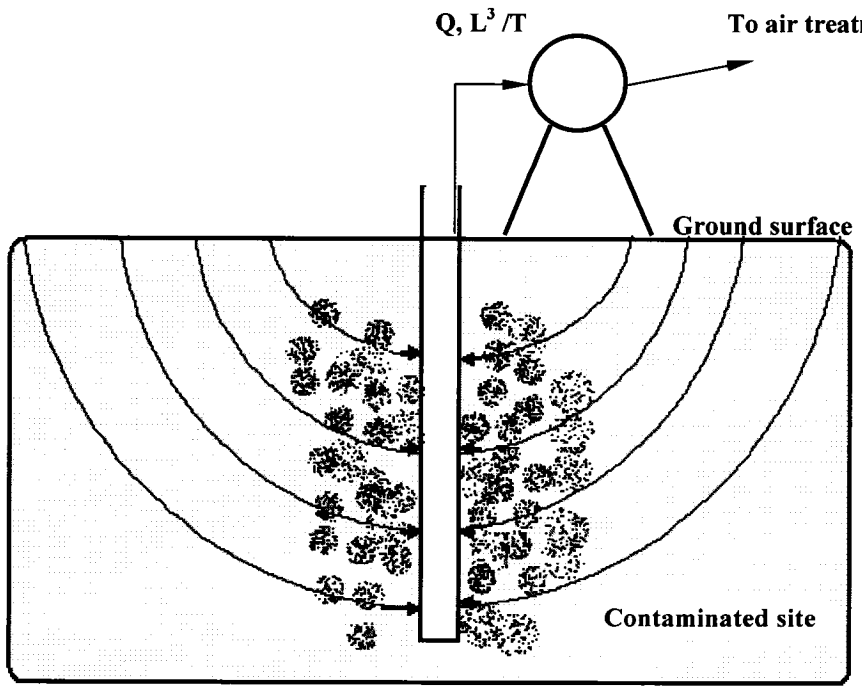

Figure 4-2 Typical SVE System Configuration

The fundamental settings of the contaminated site are considered as a heterogeneous porous medium. Installations of injection or passive wells strongly improve the flow of fresh air. Sealing the ground surface of the contaminated zone overcomes the bypass of air flow around the venting well. Three-dimensional modeling domains allow the modeler to simulate an SVE system under these practical operational conditions and settings.

Figure 4-3 depicts a generic scenario of a combined soil and groundwater remediation site. The presence of other groundwater remediation operations, such as air sparging or the fluctuation of the groundwater table can cause the movement of the moisture front in the vadose zone, which may significantly affect the SVE process.

Figure 4-4 illustrates the typical multiphase flow process diagram that exists in the unsaturated zone.

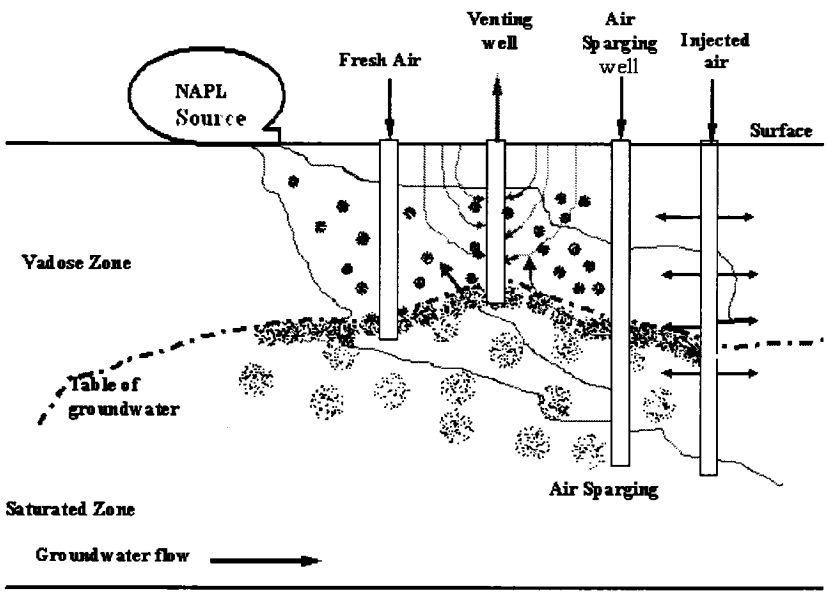

Figure 4-3 Settings of an SVE and Groundwater Remediation Site

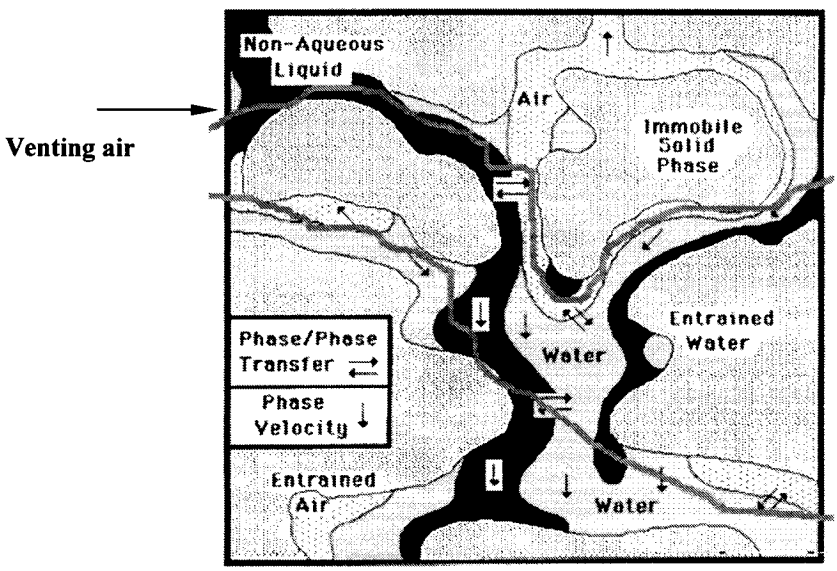

Modified from Aaron A. Jennings
At http://ecivwww.cwru.edu/civil/research/airflow.html, Access Data for Dec. 2003

Figure 4-4 Multiphase Flow Diagram in an SVE Setting

4.3.2 Mass Transport and Mass Transfer Processes

Currently the representative advanced studies on transport and mass transfer processes involved in SVE are the mass transfer processes in one-dimensional column experimental and numerical simulations (Harper, 1999; Yoon et al., 2002; Gidda, 2003) and the three-dimensional model (Zhao and Zytner, 2005). Comprehensive conceptual models have integrated the processes identified in three-phase flow and multicom-ponent compositional transport with nonequilibrium interphase mass transfer.

Most of these one- or two-dimensional models handle individual processes on the distribution and transport of NAPL as well as mass transfer, and their relationships have been described. Figure 4-5 shows simplified SVE settings where only the gas phase is mobile while the NAPL and aqueous phases are immobile. Figure 4-5 also illustrates the possible distribution of the liquid phase and advection-dispersion phenomena in a porous medium. Figure 4-6 depicts the typical mass transfer processes between contiguous phases involved in SVE. Initially, the volatile organic contaminants present in the soil may be adsorbed on the soil solid surface, be dissolved in aqueous phase, occur purely as NAPL, or be free in soil. It is crucial that these processes in the conceptual model be captured accurately by the mathematical model.

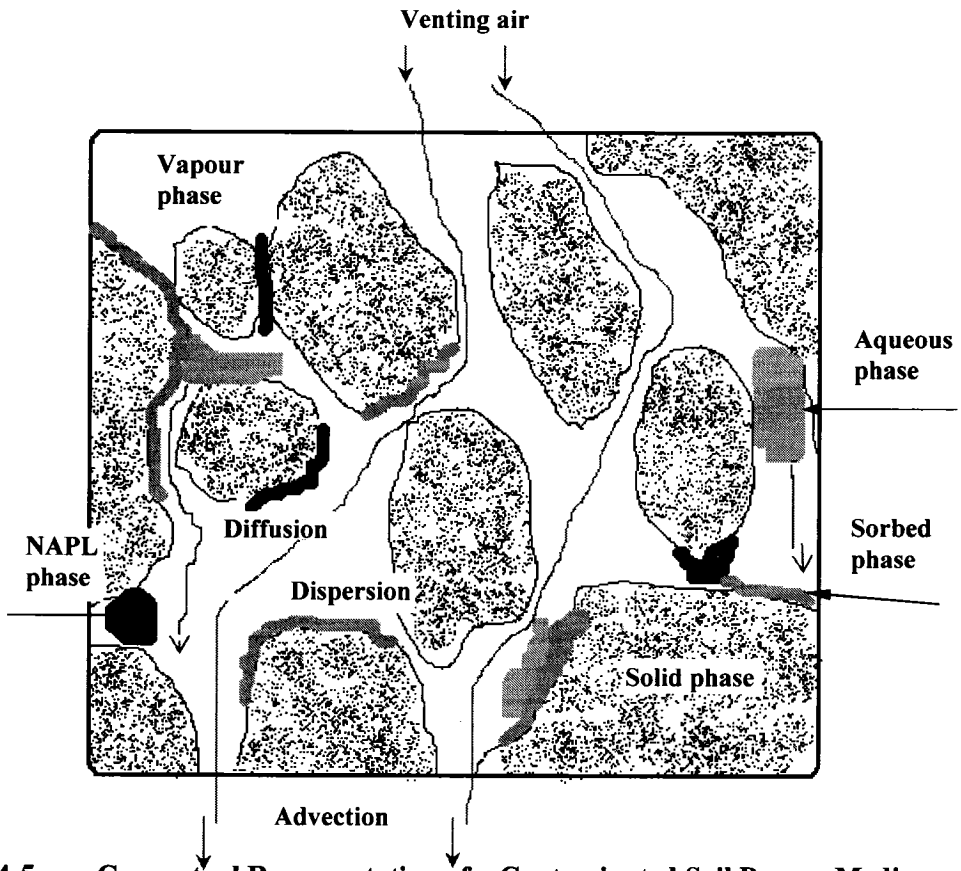

Figure 4-5 Conceptual Representation of a Contaminated Soil Porous Medium with Venting Operation (NAPL and aqueous are immobile phase)

Lenhard et al. (2004) proposed the history-path constitutive relationship based on the conceptual model of the NAPL distributions as subcategories of the entrapped, residual and free parts in the subsurface as shown in Figure 4-7. In order to track NAPL distribution, van Geel and Roy (2002) and van Geel and Sykes (1994a, b) improved the understanding and applications of the constitutive relationships by identifying the impact of residual saturation of NAPL in porous media.

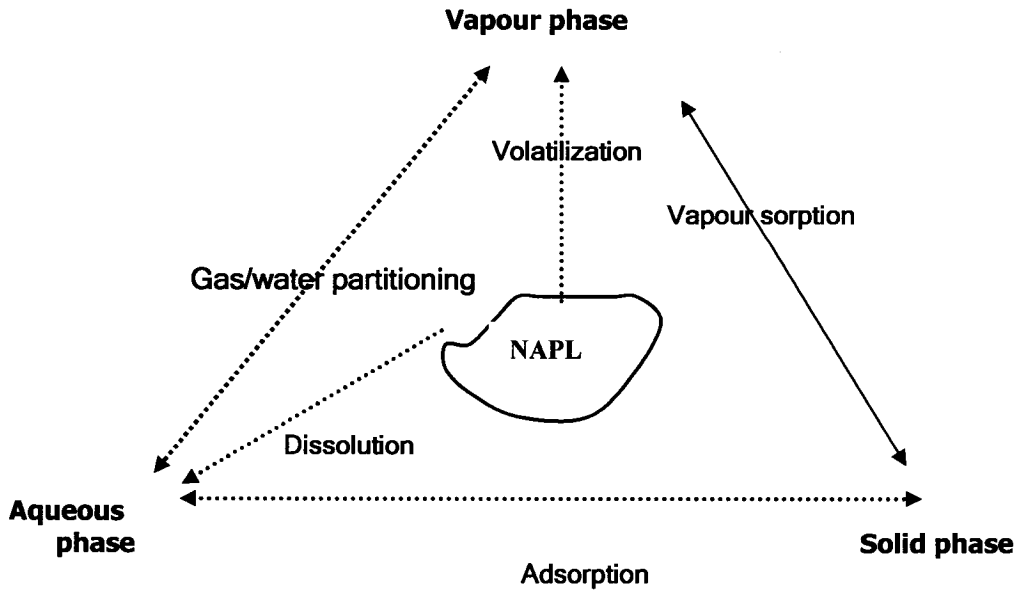

Figure 4-6 Mass Transfer Processes in SVE Operation
Equilibrium process: _____ ; Nonequilibrium processes: .....

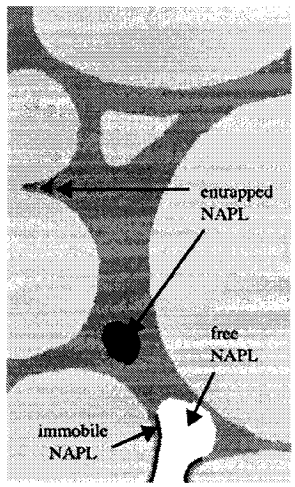

Figure 4-7 Distribution of NAPL in a Porous Medium (Lenhard et al., 2004)

SVE system configurations and site settings including the heterogeneity of porous media can be represented in a three-dimensional modeling domain. A significant implementation of the present work is that these issues can be quantified from the most general conceptual model to the final decision making for cost-

effectively stopping SVE operations. The modeling results will provide improved understanding of important processes that have not yet been captured by previous modeling investigations, especially the coupled multiphase flow and multicomponent transport with nonequilibrium mass transfer processes.

4.4 Basic Simplifying Assumptions

In field situations, all processes involved in SVE operations are acting simultaneously and interdependently. Pertinent understanding and application of the simplifying assumptions for mathematical simulation are necessary to obtain time-efficient accurate solutions for a particular problem.

Prior to modeling an SVE operation in a real world situation, effective assumptions are applied in two aspects: one, to simplify the real processes of SVE operations into a conceptual model, which may be further expressed in a mathematical formulation; another, to obtain the numerical solution of a mathematical model, which is denoted by a system of partial differential equations. Additionally, some implicit assumptions or specific assumptions (e.g., site homogeneity, boundary conditions, absence of layers) that match the realistic site conditions are included. An implicit assumption in calibration and verification exercises is that the model can predict the current events with proper inputs. Therefore, a reasonable validity regarding the calibrated properties can be expected to apply to other cases, at least for those that have similar configurations or characteristics (Vogele, 1996).

For the proposed conceptual models, the numerical behaviour of the model depends on the simplifying assumptions and complexity of the model to handle SVE system configuration and soil heterogeneity. Generally, in this context, modeling of SVE processes is typically based on the following simplifying assumptions:

- water is the preferential wetting fluid, the NAPL phase is the intermediate wetting fluid, the gas phase is the nonwetting phase; wettability decreases in the order of water to NAPL to gas (Weber and DiGiano, 1996).
- solid phase sorption occurs only through the aqueous phase (Faust et al., 1985).
- porous medium is incompressible, and porosity is constant (Bear, 1972).
- Darcy's law is valid in a multiphase system.
- system is isothermal.
- gas phase migration due to evaporation of water is neglected.
- hysteresis in the retention is neglected since environmental engineering processes are always drainage (Weber and DiGiano, 1996).
- density of water and the density of each component in the NAPL mixture are constant.
- gas-liquid interface sorption is neglected.

4.5 Developing the Mathematical Model

Generally, modeling SVE processes involves formulating the conceptual model into a mathematical model and solving the system of partial differential governing equations numerically with a computer code with respect to a real SVE scenario or a simplified one. The system of partial differential equations captures the

characteristics of the physical and chemical processes well established in the above-mentioned conceptual model in SVE operation. Generally, the system of governing equations is of a mathematical model derived from the following laws and theories:

- conservation of mass;
- conservation of energy;
- conservation of momentum;
- Darcy's law and its extended application within multiphase flow;
- equations of state;
- interphase mass transfer; and
- constitutive relationships.

4.5.1 The Continuity Theory and Governing Equations

The classic continuity principle is one of the fundamentals of bridging conceptual and mathematical models. It has been applied extensively in soil physics, petroleum reservoir simulation, groundwater flow and contaminant transport modeling and is often based on a number of necessary simplifying assumptions for various specific situations. By using the continuum approach, the mass accumulation over a certain interval of time in a finite control element or volume can be described as (Bear, 1972; Bear and Bachamat, 1990):

Accumulated mass = the rate of inflow – the rate of outflow (4.15)

On the basis of the continuity principle, the governing equations for multiphase flow and multicomponent transport in vadose zone were elucidated by Bear (1972). The

following content will formulate mathematically the characteristic processes delineated in the above-mentioned SVE conceptual model based on Equation (4.15).

In terms of the continuity principle, as expressed in Equation (4.15), the general form of a continuous partial differential equation for flow is expressed by:

$$-\left[\frac{\partial(q_x\rho)}{\partial x}+\frac{\partial(q_y\rho)}{\partial y}+\frac{\partial(q_z\rho)}{\partial z}\right]\pm Q+E=\frac{\partial(\rho\theta)}{\partial t} \tag{4.16}$$

Where:

q = Darcy's velocity, L/T

ρ = mass density of a phase, M/L^3

θ = volumetric fluid content in porous medium, L^3/L^3

Q = source or sink, mol/L^3T

E = rate of mass transfer, mol/L^3T

Related to the most general conceptual model developed in the previous section, the mathematical model should capture that the multiphase flow of NAPL, water and gas as mobile phases and transport of multicomponent contaminants with nonequi-librium rate-limited interphase mass transfers. The basic three-phase flow equation derived from Equation (4.16) is described as (Bear, 1972):

$$\frac{\partial}{\partial t}(\varphi\rho_\beta S_\beta)=\nabla[\frac{\rho_\beta k_{ij}k_{r\beta}}{\mu_\beta}(\nabla p_\beta-\rho_\beta g\nabla z)]+E_\alpha^\beta+Q_\beta \tag{4.17}$$

Where:

β = a fluid phase: aqueous, pure NAPL, gas phases, i.e., $\beta = a, n, g$

ρ_β = density of β phase, M/L^3

Q_β = source/sink of β phase, mol/L^3T

S_β = saturation of β phase

k_{ij} = intrinsic permeability of porous medium, L^2

$k_{r\beta}$ = relative permeability of β phase

p_β = pressure of β phase, Pa

E_α^β = summation of interphase mass transfer of all components in β phase from contiguous phases, mol/L^{3}T

The mass transfer term E_α^β in Equation (4.17) is the sum of the rate of mass transfer of all components within all contiguous phases and is expressed as:

$$E_\alpha^\beta = \varphi S_\beta \sum_\alpha \sum_k \gamma_{\alpha\beta,k} \tag{4.18}$$

Where:

$\gamma_{\alpha\beta,k}$ = rate of mass transfer of component k between α and β phases, mol/L^{3}T.

Expanding the left side of Equation (4.17) creates the single variable time-derivative terms below:

$$\frac{\partial}{\partial t}(\varphi \rho_\beta S_\beta) = \rho_\beta S_\beta \frac{\partial \varphi}{\partial t} + \varphi S_\beta \frac{\partial \rho_\beta}{\partial t} + \varphi \rho_\beta \frac{\partial S_\beta}{\partial t} \tag{4.19}$$

The first term on the right side of Equation (4.19) represents the change in mass storage due to the matrix compressibility, and it is assumed to be negligible, i.e., $\frac{\partial \varphi}{\partial t} = 0$. The middle term on the right side of Equation (4.19) represents the temporal change in phase density. The changes in saturation and phase density are considered within the whole modeled process, but at a given time step the magnitudes of $\frac{\partial \rho_a}{\partial t}$ for aqueous phase and $\frac{\partial \rho_n}{\partial t}$ for NAPL phase have the negligible effect on the solution of governing equations, so $\frac{\partial \rho_a}{\partial t} = 0$ and $\frac{\partial \rho_n}{\partial t} = 0$.

The density of a compressive gas phase is dependent on the composition and the pressure of the gas phase under isothermal condition. It is necessary to have another equation of state to express the relationship between the density, absolute pressure and temperature. As an alternative, the ideal gas assumption is used; the temporal change of gas density may be extended as Equation (4.20). For multiple gas mixtures, the density of the gas phase also depends on the mole fraction of each component.

$$\varphi S_g \frac{\partial \rho_g}{\partial t} = \varphi S_g \frac{\partial}{\partial t}\left(\frac{M_g p_g}{RT}\right) = \frac{\varphi S_g M_g}{RT}\frac{\partial p_g}{\partial t} \tag{4.20}$$

The last term in the right side of Equation (4.19) refers to the change in phase mass storage due to the change in fluid saturation. For any interface between α and β phases, this term may be extended in terms of the capillary pressure theory of multiphase flow:

$$\varphi\rho_\beta \frac{\partial S_\beta}{\partial t} = \varphi\rho_\beta \frac{\partial S_\beta}{\partial p_c}\frac{\partial p_c}{\partial t} = \varphi\rho_\beta C_p\left(\frac{\partial p_\alpha}{\partial t} - \frac{\partial p_\beta}{\partial t}\right) \tag{4.21}$$

Where:

$$C_p = \frac{\partial S_t}{\partial p_c} = -\frac{\partial S_g}{\partial p_c}.$$

p_c = capillary pressure, Pa.

S_t = total liquid saturation, $S_t = S_n + S_a$.

Capillary pressure in unsaturated soils is a nonlinear function of saturation of wetting phase. Brooks and Corey (1964) and van Genuchten (1980) gave analytical functions between the capillary pressure and the saturation for a two-phase system. The details on the closed relation for a three-phase system will be given in Section

4.4.3. According to the van Genuchten (1980) closed relation, Jury and Horton (2004) deduced the following formulation that describes the relation between the change in the saturation of a phase and the change in capillary pressure:

$$C_p = \frac{\partial S_l}{\partial p_c} = -\frac{\partial S_g}{\partial p_c} = \frac{\alpha(S_l - S_r)(n-1)(-p_c)^{n-1}}{\left[1+\alpha(-p_c)^n\right]^{2-1/n}} \tag{4.22}$$

Where:

α and n = van Genuchten empirical parameters

S_r = residual saturation

The mass balance equation for each phase is expressed by Equations (4.23), (4.24), and (4.25), respectively.

For aqueous phase:

$$\frac{\partial(\varphi S_a \rho_a)}{\partial t} + \nabla(\rho_a q_a) = Q_a + E_n^a - E_{n/a}^g - E_{n/a}^s \tag{4.23}$$

Where:

E_n^a = mass transfer rate of all components into aqueous phase from NAPL phase, M/L^3T

$E_{n/a}^g$ = partitioning between aqueous and vapour phase, M/L^3T

$E_{n/a}^s$ = rate of mass transfer from aqueous phase to solid phase, M/L^3T

For NAPL phase:

$$\frac{\partial(\varphi S_n \rho_n)}{\partial t} + \nabla(\rho_n q_n) = Q_n - E_n^g - E_n^a \tag{4.24}$$

Where:

E_n^g = rate of mass transfer from NAPL to vapour phase, M/L^3T

$E_{n/a}^s$ = rate of mass transfer from aqueous to solid phase, M/L^3T

For gas phase:

$$\frac{\partial(\varphi S_g \rho_g)}{\partial t} + \nabla(\rho_g q_g) = Q^g + E_n^g + E_{n/a}^g \tag{4.25}$$

For the transport process of contaminants and mass transfer, the form of the partial differential equation based on the continuity principle represented in Equation (4.16) is expressed as general formulation:

$$-\left[\frac{\partial(J)}{\partial x} + \frac{\partial(J)}{\partial y} + \frac{\partial(J)}{\partial z}\right] + E = \frac{\partial(\varphi SC)}{\partial t} \tag{4.26}$$

Where:

J = mass flux including the advective and dispersive flux, M/L^2T

C = concentration of a component, M/L^3

E = mass transfer rate of a component into a phase, M/L^3T

Mass transport in the aqueous, gaseous and NAPL phase (if applicable) for each constituent, k, under investigation is assumed to follow the nonlinear advective-dispersive conservation formulation (Bear, 1972). Substituting advective flux in Equations (4.8) and dispersive flux in Equation (4.13) into Equation (4.26) plus mass transfer rate and source/sink, the complete transport equation of a component in a phase becomes:

$$\frac{\partial}{\partial t}(\varphi S_\beta C_{\beta,k}) = \nabla(\varphi S_\beta D_{\beta,k} \nabla C_{\beta,k}) - \nabla(q_\beta C_{\beta,k}) + \varphi S_\beta \sum_\alpha \gamma_{\alpha\beta,k} + Q_{\beta,k} \tag{4.27}$$

Where:

$Q_{\beta,k}$ = source/sink of component k in β phase, mol/L^3T

$C_{\beta,k}$ = molar concentration of species k in β phase, mol/L^3

$D_{\beta,k}$ = dispersion coefficient tensor of component k in β phase, L^2/T

Equations (4.17) and (4.27) comprise the highly nonlinear governing equation system of an average three-dimensional SVE mathematical model, which incorporates coupled multiphase flow and multicomponent transport with rate-limited interphase mass transfer.

In order to close Equations (4.17) and (4.27), additional constitutive relationships, constraint relationships and equations of state are required to describe the coefficients in the flow equation as a function of the primary unknown variables (Helmig, 1999). They are summarized as follows:

Phase saturations must sum to one:

$$S_g + S_n + S_a = 1 \tag{4.28}$$

The sum of molar mass fractions of all species in a phase is one because any fluid phase is completely defined by its components:

$$\sum_{k=1}^{Nc} X_\beta^k = 1 \tag{4.29}$$

4.5.2 The Constitutive Relationships

4.5.2.1 Capillary Pressure

The system of governing equations for describing two or three immiscible fluid phases in soils is created by describing the conservation of mass in each phase coupled with the capillary pressure $p_c(S_n)$, relative permeability k_{ri} (S_n), and mass transfer between contiguous phases. Most of the uncertain effects and processes that influence the retention and distribution of contaminants in the subsurface and further remediation operation performance, such as immiscibility, interfacial tension,

wettability, capillary pressure, and hysteresis presence of microscopic scale fluid-fluid interfaces, fluid viscosity, macroscale heterogeneities, fluid composition, etc., are lumped into the $p_c(S_c)$ relationship between capillary pressure and saturation (Weber and DiGiano, 1996). Capillary action and capillary pressure are of central importance in describing the multiphase flow in porous media (Majia and Gray, 1993).

It is odd that little research has been reported on the relative permeability and capillary pressure measurements for specific multiphase soil/water/NAPL systems and the range of empirical constants of interest, despite these relations being the essential part of multiphase flow theory (Miller et al., 1990; Looney and Falta, 2000; Chien et al., 2004).

4.5.2.2 Constitutive Relationship

Almost all multiphase flow simulations applied empirical parameters to demonstrate the constitutive relationship among the relative permeability of a fluid phase, the saturation of a phase and capillary pressure ($k_{ri} - S_n - p_c$) (Sleep and Sykes, 1989; Rathfelder et al., 2000). The significance of the pertinent representation of real processes on NAPL residual saturation, which is related to constitutive relations in a multiphase flow system, has been proposed by van Geel and Sykes (1994a, b) and van Geel and Roy (2002) and later Lenhard et al. (2004). However, there is still a challenge to introduce these improved constitutive relationships into multiphase flow and multicomponent transport models related to a specific remedial operation because of the lack of appropriate complex models and realistic scenarios.

The physical behaviour and mathematical behaviour of multiphase flow are largely controlled by the relative permeability-saturation-capillary pressure constitutive relationships (Falta, 1989; Fischer et al., 1998). Experimental determination of the capillary pressure curve with the saturation of a phase is a necessary issue. However, no data are currently available to represent the situation for the typical NAPL contaminants and porous media systems. There have been very few studies on how the constitutive relationships may affect the behaviour of multiphase flow and transport models (van Geel, 1999; Lenhard et al., 2004).

Brooks-Corey (1966) and van Genuchten (1980) developed mathematical closed relationships which are suitable for wetting and nonwetting two multiphase flow systems to describe the dependence of relative permeability and capillary pressure on saturation. The explicit functional form is considered to be specific to the combinations of the properties of fluids and porous media and be dependent on the history of the processes, i.e., drainage or imbibition. Many engineering and environmental issues are considered to occur during drainage (Weber and DiGiano, 1996).

Lenhard and Parker (1987) regarded wetting and non-wetting theory for three phase flow systems. The wettability within a three-phase system follows this order: water, NAPL, and air. Thus, in a three-phase fluid system, there are two interfaces present: water-NAPL and NAPL-air. Relative to the gas phase, both the NAPL and aqueous phases are treated as wetting phases. According to the van Genuchten (1980) constitutive relationship, the saturation of the aqueous phase is a function of the water-NAPL capillary pressure, whereas the total liquid saturation is assumed to be a

function of NAPL-air capillary pressure. Respectively, the effective and total saturation and capillary pressure are expressed as:

$$\overline{S_a} = \left[1 + (\alpha p_{cna})^n\right]^{-m} \text{ for } p_{cna} > 0 \quad (4.30)$$

$$\text{and} \quad \overline{S_a} = 1 \quad \text{for } p_{cna} < 0$$

$$\overline{S_t} = \left[1 + (\alpha p_{cgn})^n\right]^{-m} \text{ for } p_{cgn} > 0 \quad (4.31)$$

$$\text{and} \quad \overline{S_t} = 1 \text{ for } p_{cgn} < 0$$

Where:

α = van Genuchten empirical parameter, Pa^{-1}

m = van Genuchten empirical parameter, $m = 1 - \frac{1}{n}$

$p_{cna} = p_n - p_a$, capillary pressure between aqueous and NAPL phase, Pa

$p_{cgn} = p_g - p_n$ capillary pressure between air and NAPL phase, Pa.

For any three-phase system, the effective saturation is calculated by Lenhard and Parker (1987):

$$\overline{S_a} = (S_a - S_{ar})/(1 - S_{ar}) \quad (4.32)$$

Where:

S_{ar} = residual saturation of aqueous phase

$$\overline{S_n} = S_n/(1 - S_a) \quad (4.33)$$

$$\overline{S_g} = S_a/(1 - S_{ar}) \quad (4.34)$$

$$\overline{S_t} = (S_a + S_n - S_{ar})/(1 - S_{ar}) \quad (4.35)$$

Considering the NAPL entrapped by the air phase, Lenhard et al. (2004) defined the apparent total liquid saturation as:

$$\overline{S_t} = \frac{S_g + S_n + S_{ge} - S_{ar}}{1 - S_{ar}} \quad (4.36)$$

$S_{ge} = S_{gea} + S_{gen}$ is the saturation of fluid entrapped by the air phase; it is the sum of the saturation of the aqueous phase occluded by air and the saturation of the NAPL phase occluded by air.

The non-hysteretic three-phase relative permeability for aqueous, NAPL and gas phases is a function of effective and total liquid saturations, and the expressions are denoted by Lenhard and Parker (1987):

$$k_{ra} = \overline{S_a}^{1/2}[1-(1-S_a^{1/m})^m]^2 \tag{4.37}$$

$$k_{rg} = \overline{S_t}^{1/2}(1-S_t^{1/m})^{2m} \tag{4.38}$$

$$k_{rn} = (\overline{S_t} - \overline{S_a})^{1/2}[(1-S_a^{1/m})^m - (1-\overline{S_t}^{1/m})^m]^2 \tag{4.39}$$

Where:

k_{ra} = relative permeability of aqueous phase

k_{rg} = relative permeability of gas phase

k_{rn} = relative permeability of NAPL phase.

4.5.3 Rate of Interphase Mass Transfer

For SVE operations, experimental and numerical investigations have shown that rate-limited mass transfer causes a long tailing effect after a sharp decrease in offgas concentration (Chai and Muira, 2004). Existing models have limited flexibility to include rate-limited mass transfer simultaneously and interdependently in multiphase flow and multicomponent transport processes even though rate-limited mass transfer inevitably hampers the performance of SVE, and causes less than optimal remediation. A number of nonequilibrium one- and two-dimensional

transport models have described rate-limited mass transfer between the NAPL and aqueous, gaseous and sorbed phases using first-order kinetics (Braida and Ong, 1998; Hayden et al., 1994, 1997). The following five main types of mass transfer processes are involved in an SVE operation, which should be included in a complex mathematical model:

- NAPL phase to vapour phase
- aqueous phase to vapour phase
- NAPL phase to aqueous phase
- aqueous phase to solid phase
- gaseous phase to solid phase

The rate of mass transfer between each individual phase pair in the mathematical model, in terms of Equation (2.13), will be addressed respectively.

4.5.3.1 Rate of Mass Transfer from NAPL Phase to Air Phase

Mass transfer between NAPL and gas phase is the basic fundamental process in the presence of NAPL in the subsurface. In terms of the first-order kinetics expression in Equation (2.13), the molar rate of mass transfer per unit volume of the porous medium is given as:

$$\gamma_{ng,k} = \rho_g k_{ng} (x^e_{g,k} - x_{g,k}) \tag{4.40}$$

Where:

$\gamma_{ng,k}$ = rate of mass transfer of component k from α phase to β phase, M/L^3T

ρ_g = density of gas phase, M/L^3

k_{ng} = lumped mass transfer coefficient from NAPL to air phase, T^{-1}

$x_{g,k}$ = molar fraction of component k in vapour phase

$x^e_{g,k}$ = molar fraction of component k in vapour phase in equilibrium with NAPL phase.

4.5.3.2 Rate of Mass Transfer from Aqueous Phase to Vapour Phase

Studies have explored the mass transfer of volatile petroleum hydrocarbons from the residual water to the mobile gas phase (Armstrong et al., 1994; Powers et al., 1992, 1994). In the presence of entrapped NAPL, the controlling mechanism for the contaminant migration is mass transfer to the aqueous phase and vapour phase. Under advection-dominated conditions, laboratory and controlled field experiments have indicated that water-gas mass transfer also may be rate-limited (Gierke et al. 1992). Assuming that the rate of aqueous-gas phase mass transfer is controlled by resistance in the aqueous phase, the analogous expression may be given as:

$$\gamma_{ag,k} = \rho_a k_{ag}(x^e_{a,k} - x_{a,k}) \tag{4.41}$$

Where:

k_{ag} = mass transfer coefficient for the aqueous phase to vapour phase, T^{-1}

$x^e_{a,k}$ = aqueous molar fraction of component i in equilibrium with the vapour phase as estimated using Henry's law

$x_{a,k}$ = molar fraction of NAPL in aqueous phase.

Gidda (2003) formulated the mass transfer coefficient for the aqueous phase to vapour phase mass transfer as a two-parameter expression:

$$k_{ag} = c(C_{a,k})^d \tag{4.42}$$

Where:

$C_{a,k}$ = concentration of component k in aqueous phase, mol/L^3

c, d = mass transfer empirical constants.

4.5.3.3 Rate of Mass Transfer from NAPL Phase to Aqueous Phase

Generally, the petroleum hydrocarbons in SVE candidate sites have very poor solubility, so the mass transfer coefficient between the NAPL and aqueous phase k_{na} is often considered as a constant. For the tested SVE cases, the values of k_{na} are within the reasonable range of 0.1 to 0.01 s^{-1} (Gidda, 2003).

Assuming that the rate of NAPL dissolution is controlled by resistance in the aqueous phase, an analogous linear driving force expression for this process may be written as:

$$\gamma_{na,k} = \rho_a k_{na}(x^e_{a,k} - x_{a,k}) \tag{4.43}$$

Where:

k_{na} = mass transfer coefficient from aqueous to vapour phases, T^{-1}

$x^e_{a,k}$ = aqueous molar fraction of component k in equilibrium with the NAPL phase

$x_{a,k}$ = molar fraction of component k in aqueous phase.

4.5.3.4 Rate of Mass Transfer from Aqueous Phase to Solid Phase

Sorption may occur as vapour sorption on exposed mineral and organic surfaces, vapour sorption at the gas-liquid interface, and soil matrix sorption from the aqueous phase (Rathfelder et al., 1995). Solid phase sorption occurs only through the aqueous phase (Faust et al., 1985). Equilibrium between the dissolved phase and solid phase is described by the linear Freundlich isotherm (McLaren, 1972). If n = 1, the linear isotherm sorption is expressed and the relevant coefficients are denoted in Equations (4.46) through (4.48):

$$C_s = K_d C_a^{1/n} \tag{4.44}$$

$$K_d = K_{oc} f_{oc} \tag{4.45}$$

$$K_{oc} = 0.63 * K_{ow} \tag{4.46}$$

Where:

n = Freundlich empirical parameter

C_s = concentration sorbed on the solid, mol/M soil

C_a = concentration of contaminant in aqueous phase, mol/L^3

K_d = adsorption distribution constant, L^3/M soil.

K_{oc} = octanol–organic carbon distribution coefficient

K_{ow} = octanol-water distribution coefficient.

The most significant process that contributes to the retention of organic components in two-phase aqueous-vapour systems is solid-phase sorption and desorption. Any mechanisms that influence the rate of sorption and desorption from the soil matrix and organic matter will have the potential to substantially decrease the removal of VOC species during SVE operation. The mass transfer between the solid and aqueous phases may be expressed as (Abriola et al., 1999):

$$\gamma_{as,k} = \rho_a k_{as} (x^e_{a,k} - x_{a,k}) \tag{4.47}$$

Where:

$x^e_{a,k}$ = maximum aqueous-phase molar fraction of component k

$x_{a,k}$ = aqueous-phase molar fraction of component k

k_{as} = mass transfer coefficient between aqueous and solid phase.

The rate of mass transfer of component k on the solid phase is expressed in Equation (4.50) (Kaleris, 2002; Hoeg et al., 2004).

$$\gamma_{as,k} = (1-\varphi)\rho_b(\frac{\partial C_{s,k}}{\partial t}) = \varphi S_a k_{as}(C_{a,k} - \frac{C_{s,k}}{K_d}) \quad (4.48)$$

Where:

$C_{s,k}$ = sorption concentration of component on the solid phase, M/M soil

ρ_b = bulk density of soil, M/L^3

K_d = adsorption distribution constant, L^3/M soil.

The rate of mass transfer between sorbed aqueous and solid phase is relatively insignificant in SVE, therefore it is considered as an equilibrium mass transfer or rate-limited mass transfer with constant mass transfer coefficient (Gidda, 2003).

4.5.3.5 The Rate of Mass Transfer from Vapour to Solid Phase

Vapour sorption of volatile organic chemicals (VOC) to soil minerals and organic matter exist (Poulsen et al., 1998a,b; Yoon et al., 2003), especially at low soil-water contents. Very few SVE models have incorporated this effect into modeling. The vapour sorption model has been used in combination with a two-dimensional VOC transport model to evaluate the effect of vapour sorption on TCE transport in the unsaturated zone under both natural conditions and in connection with soil vapour extraction systems. The simulations show that vapour sorption can result in increased cleanup times, especially when using vapour extraction in arid regions. Vapour and solid phase sorption is similar to the sorption between aqueous and solid phases and can be described by the isotherm adsorption formulation as (Yoon et al., 2003):

$$C_{sg} = K_{sg}C_g \quad (4.49)$$

Where:

C_{sg} = gas adsorption concentration on solid phase, mol/M soil

K_{sg} = gas adsorption distribution coefficient, L^3/M soil

C_g = concentration of gas phase, mol/L^3

Combining the sorption of solid from both aqueous and vapour phases considering partitioning between aqueous and vapour phases, the total distribution becomes the sum of aqueous and vapours sorption:

$$K_d^{'} = K_d + K_{sg} \tag{4.50}$$

The value of $K_d^{'}$ is obtained by fitting model output to experimental results; K_{sg} is related to the soil water content and soil properties (Poulsen et al., 1998, 1999). The spatial and temporal variations in water content and cation exchange capacity of soil affect the sorption. Under both vapour and aqueous phases present, the sorption capacity of NAPL on the soil particle surface becomes:

$$C_s = C_{sg} + C_{sa} \tag{4.51}$$

Where:

C_{sg} = adsorption amount from gas phase, mol/M soil

C_{sa} = adsorption amount from aqueous phase, mol/M soil

Unfortunately, due to the lack of relevant data on gas phase adsorption on soil, the numerical simulation with 3D-SVE-L/F numerical models by using FEMLAB did not include solid-vapour phase mass transfer rate.

4.6 Summary of the System of Governing Equations for the Developed 3D SVE model

The complex mathematical models, which formulated the most general SVE processes have been developed. These models completely formulate the conceptual model into the mathematical realization in order to predict the real SVE process. Concisely, the constructed mathematical models have the following features:

- tackle the coupled multiphase flow and multicomponent transport;
- include diffusion, dispersion and constitutive relationships;
- incorporate rate-limited mass transfer processes and introduce transient mass transfer coefficients for volatilization and gas-aqueous partitioning processes, and nonequilibrium constant mass transfer coefficients for dissolution and solid phase adsorption processes.

The system of governing equations of the developed general mathematical model is summarized as follows:

$$\frac{\partial}{\partial t}(\varphi \rho_\beta S_\beta) = \nabla[\frac{\rho_\beta k_{ij} k_{r\beta}}{\mu_\beta}(\nabla p_\beta - \rho_\beta g \nabla z)] + E_\alpha^\beta + Q_\beta \tag{4.52}$$

$$\frac{\partial}{\partial t}(\varphi S_\beta C_{\beta,k}) = \nabla(\varphi S_\beta D_{\beta k} \nabla C_{\beta,k}) - \nabla(q_\beta C_{\beta,k}) + \gamma_{\alpha\beta,k} + Q_{\beta,k} \tag{4.53}$$

$$E_\alpha^\beta = \varphi S_\beta \sum_\alpha \sum_k \gamma_{\alpha\beta,k} \tag{4.54}$$

The closed relations for 3D-SVE-L/F models include:

$$S_w + S_g + S_n = 1 \tag{4.55}$$

$$\sum X_\beta^k = 1 \text{ (k=BTEX, β=solid, aqueous, NAPL and vapour phase)} \tag{4.56}$$

The equation of state of gas phase, which is modified from Sleep and Sykes (1989), was also applied by Jang (2005):

$$\rho_g(p_g,C) = \rho_0 + \lambda_g p_g + \sum_{k=1}^{Nc} C_{g,k}\left(1 - \frac{\rho_0}{\rho_v^k}\right) \tag{4.57}$$

Where:

λ_g = gas phase compressibility, M/L^3 Pa.

ρ_v^k = density of component in vapour phase, mol/L^3

The multiphase flow and multicomponent contaminant transport governing equations under a specific setting of a candidate SVE site were set up in FEMLAB to demonstrate mathematically the performance of an SVE operation. The partial differential equations together with additional constraint relations plus simplifying assumptions and initial and boundary conditions, can be solved in three-dimensional space and time for lab-scale and field-scale scenarios.

CHAPTER 5

Numerical Simulation of the 3D-SVE-L/F models

In this chapter, the general SVE mathematical model developed in Chapter 4 is specified for lab-scale and field-scale SVE simulations. For both lab-scale and field-scale models, the following aspects of the methodology of 3D SVE modeling studies are addressed. At first, the physical properties of lab and field SVE modeling scenarios and the relevant conceptual models are demonstrated including the geometry of the simulated domains. Secondly, the system of governing equations of the mathematical models and the corresponding input parameters as well as boundary and initial conditions are illustrated. The mathematical models are numerically solved using FEMLAB and then are calibrated against lab-scale experimental and actual field SVE sampling data by adjusting two empirical mass transfer parameters. Furthermore, the time-variant mass transfer coefficients are determined by corresponding calibrations. Thirdly, the stability of FEMLAB numerical schemes for the spatial and temporal discretization used is analyzed. Finally, by running the calibrated model, the distribution of pressure, gas saturation levels and concentration of contaminants are examined so that the accuracy of the modeling studies can be illustrated.

5.1 Modeling the Lab-scale SVE Operation

5.1.1 SVE Experiments in a Lab-Scale Reactor

In this section, simulated lab-scale SVE scenarios are based on a series of lab SVE experiments completed by Duggal (2005). These experiments were conducted under various air flow rates for two types of soils (Ottawa sand and Elora silt). The conceptual SVE model is envisioned according to appropriate flow, transport and mass transfer processes in a multiphase system. The mathematical model based on this experimental setting is entitled the 3D-SVE-L model.

The lab-scale model illustrates the performance of experiments conducted in settings where a screened venting well at a controlled flow rate penetrates through the cylindrical reactor containing contaminated soil mixed with toluene in advance. Both top and bottom ends of this cylindrical reactor have an impermeable seal. The lateral fine-screened metal wall is open to the atmosphere and supports soil away from the wall. The geometry of this reactor is shown in Figure 5-1. The design parameters are summarized in Table 5-1.

The radial seepage velocity in the reactor is produced by the screened venting well. During the venting process, advection and dispersion mass transport occur in the mobile gas phase, and volatilization, dissolution, adsorption and partitioning between aqueous and vapour phases are present due to the presence of the residual immobile NAPL phase. All mass transfer processes are assumed to be rate-limited.

Table 5-1 Design Parameters of the Lab-Scale Reactor

Radius of Venting Well, r_w, m	Radius of Reactor, r, m	Height of Reactor, h, m
0.025	0.23	1.00

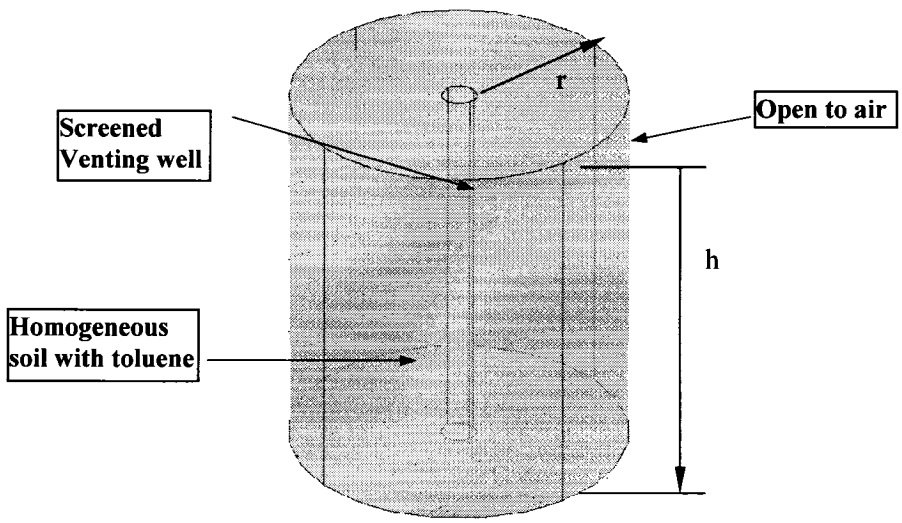

Figure 5-1 The Sketch of a Lab-Scale Reactor Designed and Utilized by Duggal (2005)

5.1.2 The 3D-SVE-L Mathematical Model

The multiphase flow and multicomponent transport model developed in Section 4.6 is configured into the above-established underlying conceptual model of an SVE operation in a reactor (Figure 5-1) after applying simplifying assumptions. This conceptual model is similar to the classic application of the Richards equation as a specialized multiphase flow where the movement of soil moisture is reasonably handled as a specific case of multiphase flow. The corresponding single gas phase active flow based on multiphase flow theory has been used to deal with SVE operation (Looney and Falta, 2000). Accordingly, the 3D-SVE-L model handles

single gas phase as active flow with NAPL and aqueous phases being treated as immobile phases. Hence, mass transfer processes occur only between NAPL and air, aqueous and air phases and aqueous and solid phases. The system of governing equations of the 3D-SVE-L model is summarized below.

The vapour phase flow and transport of component equations are given by:

$$\frac{\partial}{\partial t}(\varphi S_g \rho_g) = \nabla[\frac{\rho_g k_{ii}}{\mu_g}(\nabla p_g - \rho_g g \nabla z)] + \varphi S_g k_{ng}(C_g^e - C_g) + \varphi S_g k_{ag}(C_g - HC_a) \quad (5.1)$$

$$\frac{\partial}{\partial t}(\varphi S_g C_g) = \nabla(\varphi S_g D \nabla C_g) - \nabla(q_g C_g) + \varphi S_g k_{ng}(C_g^e - C_g) + \varphi S_g k_{ag}(C_g - HC_a) \quad (5.2)$$

The NAPL phase mass balance governing equation is denoted by:

$$\frac{\partial}{\partial t}(\varphi S_n \rho_n) = -\varphi S_g k_{ng}(C_g^e - C_g) - \varphi S_a k_{an}(C_a^e - C_a) \quad (5.3)$$

The aqueous phase mass balance governing equation is expressed by:

$$\frac{\partial}{\partial t}(\varphi S_a \rho_a) = -\varphi S_g k_{ag}(C_g - HC_a) - \varphi S_a k_{as}(C_a^e - C_a) + \varphi S_a k_{na}(C_a^e - C_a) \quad (5.4)$$

The system of governing Equations (5.1) through (5.4), including the closed relationships given in Section 4.5, will be numerically solved using FEMLAB by combining the following initial and boundary conditions as well as the relevant inputs.

5.1.3 Boundary and Initial Conditions and Inputs

Boundary conditions for governing equations can be specified as either constant Type I (Dirichlet boundary condition) or specified flux Type II (Neumann

boundary condition). Both Type I and Type II cannot be specified simultaneously over the same period of time, but can be switched from one to another in different periods of time. In this section the boundary conditions are illustrated respectively, for mass balance of phase and transport equations. For each governing equation, the boundary conditions assigned at the venting well, outside boundaries of the simulated domain of the contaminated site, and at the surface of the reactor are illustrated.

5.1.3.1 The Relation between Venting Pressure and Flow Rate

The maximum negative pressure, which is the difference between vapour pressure and ambient pressure in the extraction well, is approximately proportional to the possible blower capacity (Chai and Miura, 2004). Based on the principle of simplistic steady state radial flow for compressible gas, Equation (5.5) demonstrates the relationships among the venting flow rate, permeability and the specific absolute pressures at the venting well which are assigned as boundary conditions for the numerical model (Johnson et al., 1990a).

$$k_{ii} = \frac{\mu_g Q_w}{\pi p_W H} * \frac{\ln\left(\frac{r_w}{r_1}\right)}{1-\left(\frac{p_{atm}}{p_w}\right)^2} \tag{5.5}$$

Where:

k_{ii} = intrinsic permeability of porous media, L^2

Q_w= flow rate of venting well, L^3/T

p_W = venting absolute pressures on the venting well, Pa

p_{atm} = atmospheric pressure, Pa

r_W = radius of venting well, L

r_I = radius of influence of venting well, L

H_w = height of the screened well through contamination region, L

5.1.3.2 Boundary Conditions

The pressure boundary conditions of the flowing phase are assigned in the following manner:

- boundary condition at the venting well:

For phase flow equations, when assigning an air flow pressure to a venting or injection well, a Dirichlet condition (Type I) is used. Specific exerted vacuum pressure results in a constant-head Dirichlet boundary condition for radial pressure in the vicinity of the screened venting well. During the lab-scale SVE operation completed by Duggal (2005), the airflow rate is controlled; in this context the corresponding absolute pressure at the venting well is calculated by the Equation (5.5).

- boundary condition at the outside of the contaminated site:

The region of the site beyond the radius of influence of a venting well that connects to the atmosphere; therefore, the boundary conditions are assigned as atmospheric pressure, i.e., Type I specific pressure boundary conditions.

- boundary condition at the top and bottom ends of the reactor:

Both the top and bottom of the reactor are completely impermeable, so they

are assigned as no flux, i.e., Type II $\frac{\partial p}{\partial z} = 0$.

The boundary conditions of governing equations of immobile phases at the venting well and ground surface are assigned as no flux, that is, $\frac{\partial S_n}{\partial x_j} = 0$, $\frac{\partial S_a}{\partial x_j} = 0$. Boundary conditions at the outside of the domain have not been affected by contamination, hence, NAPL saturation S_n is set equal to zero, and the aqueous phase saturation of soil inside the reactor S_a is equal to the initial measured saturation of the aqueous phase without contamination.

The boundary conditions of the concentration of contaminants in the transport equations of the NAPL, aqueous and vapour phases are assigned as, respectively:

- boundary condition at the venting well and the ends of reactor:

All transport equation boundary conditions were assigned as Type II zero dispersive flux boundary conditions at the screened part of the venting well, i.e., $\frac{\partial C}{\partial x_j} = 0$. The non-screened interval of well casing is impermeable and is represented by a Type II no flow boundary condition for flow, and zero concentration and saturation are assigned for transport equations (Nobre and Nobre, 2004).

- boundary at the outside of the contaminated site:

Because the region beyond the influence zone of the remediated site is considered as an uncontaminated zone, the boundary condition outside of the contaminated zone is assigned Type I, which is zero concentration. All the boundary conditions for the 3D-SVE-L model are illustrated in Figure 5-2.

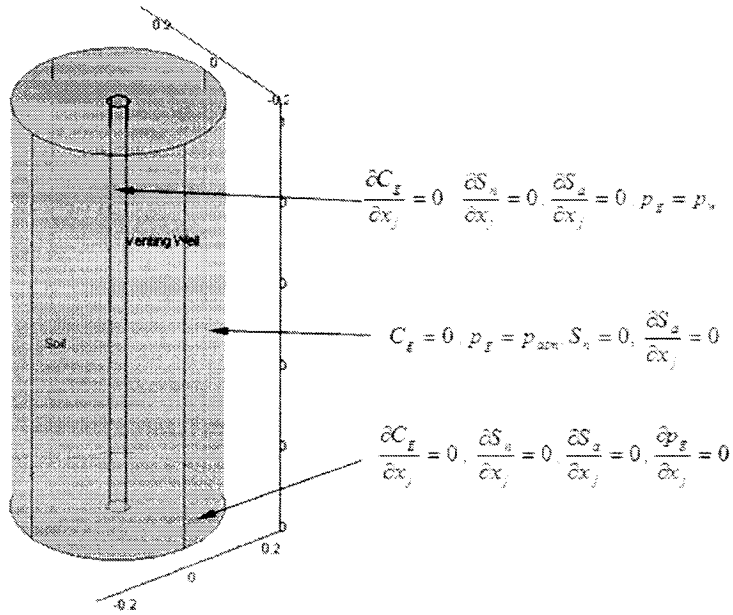

Figure 5-2 Schematic of Boundary Conditions for the 3D-SVE-L Model

5.1.3.3 Initial Conditions

For the 3D-SVE-L model, the initial conditions for the gas flow equations are $p(x, y, z, 0) = p_{atm}$; saturation of NAPL $S_n(x, y, x, 0)$, saturation of aqueous phase $S_a(x, y, z, 0)$, and concentration of contaminant $C(x, y, z, 0)$ refer to each experiment's initial condition data. The initial conditions in all phases for either SVE model simulations or lab-scale reactor experiments are established by the equilibrium relations. The initial condition data for the 10 sets of lab experiments are listed in Table 5-2.

Table 5-2 Initial Conditions for the 3D-SVE-L numerical model

Case №	SVE Experiments									
	Elora Silt					Ottawa Sand				
	1	2	3	4	5	6	7	8	9	10
Concentration of toluene in soil gas phase*, mol/m^3	1.408	1.007	0.804	0.446	0.417	1.213	1.211	1.206	1.105	1.401
Saturation of initial NAPL*	0.027	0.021	0.020	0.016	0.011	0.025	0.025	0.025	0.024	0.027
Molar density of toluene***, mol/m^3	$9.4085*10^3$									
Solubility of toluene***, mol/m^3	5.752									

* Duggal's (2005) experimental design data;

** Reference (*ASTM standard E1739-1995);

*** Calculated by Equation 5.1 and air flow rate measured by Duggal (2005)'s experiments.

5.1.3.4 The Input Parameters of the 3D-SVE-L model

Obtaining the numerical solutions of the 3D-SVE-L model demands many parameters as inputs. Inputs include properties of the contaminated soil porous media, empirical parameters, and the physical and chemical properties of toluene. The input parameters for the 3D-SVE-L model are given in Table 5-3.

Table 5-3 Inputs for Numerical Simulation of the 3D-SVE-L Model

Input parameters	Value	Remarks
Intrinsic permeability of Elora silt, k_{se}, m^2	6.05e-12	Duggal, 2005
Intrinsic permeability of Ottawa sand, k_{so}, m^2	1.98e-12	Duggal, 2005
Elora silt bulk density, ρ_{be}, kg/m^3	1151.5	Duggal, 2005
Ottawa sand bulk density, ρ_{bo}, kg/m^3	1158	Duggal, 2005
Octanol-water partitioning coefficient, L/kg, $log\ K_{oc}$	2.13	Mirsal, 2004
Vapour pressure, Pa	3800	Mirsal, 2004
Water solubility, kg/m^3	0.515	Mirsal, 2004
Density of toluene, ρ_n, kg/m^3	866.9	Mirsal, 2004
Dimensionless Henry's law constant	0.26	Mirsal, 2004
Porosity of Elora silt, φ_e	0.40	Duggal, 2005
Porosity of Ottawa sand, φ_o	0.53	Duggal, 2005
Longitudinal dispersivity, a_L, m	0.0037*	Assumed
Diffusion coefficient in air, m^2/sec	8.5e-6	Mirsal, 2004
Density of air, ρ_{air}, kg/m^3	1.229e-3	Mirsal, 2004
Dynamic viscosity of air, μ, kg/msec	1.75e-5	Mirsal, 2004
Residual soil water saturation, S_a	0.001	Duggal, 2005
Van Genutchen empirical constant, α, m^{-1}	1	Thomson et al., 1997
Van Genutchen empirical constant, n	2	Thomson et al., 1997
Gas phase compressibility, λ_g, $kg/m^3\ Pa$	$1.2*10^{-5}$	Thomson et al., 1997
Number of finite element mesh	976	FEMLAB
Time step, Δt, hours	1	FEMLAB

Note: *Longitudinal dispersivity is based on the recommended range given in Gidda's (2003) experiments and statistical calculations.

5.1.4 The Calibration of the 3D-SVE-L Model and Goodness of Fit

5.1.4.1 Calibration of a Model

Calibration of the constructed model is required to determine whether the elements of actual systems can adequately be described by the model (Farquhar et al., 1990). Calibration is completed by successively running the numerical model and adjusting the chosen fitting parameters to achieve an acceptable correlation between the sampled data set and the modeled outputs (Schwartz and Zhang, 2003).

In this study, the outputs of the 3D-SVE-L model are typically depicted by the breakthrough curves of offgas concentration, which are plotted as the concentration of contaminants in the offgas versus the elapsed time of SVE operation.Visual comparison of simulated and experimental results is based on the semi-log coordinate system. Using logarithmic scale system can improve considerably the resolution of the concentration readings over a large range (10^{0} to10^{-7} mol/m^{3}) of the magnitude of the concentration of contaminant for average SVE settings. This wide range represents a typical range of contaminant concentration between the initial concentration of the contaminants in the subsurface and the concentration of the tailing cleanup target of SVE operation for both simulated and experimental results. Initially, calibration is done manually by visual trial-and-error. Based on the manual fit, the parameters are adjusted.

There are no hard-and-fast rules on how to determine the adjustable parameters for any given modeling scenarios (Aziz and Settari, 1979) to improve the best fit. The general rule of calibration is to modify the parameters that have the largest uncertainty and also have the largest influence on the sensitivity of the numerical solutions of the constructed models. This includes parameters that cannot be measured directly, but are obtained by the calibration of a model, such as the mass transfer coefficients. Other non-adjustable parameters integrated in the mathematical model are considered as fixed values because they are measurable, have relatively low or medium uncertainty, or do not greatly affect the results.

Additionally, which and how many parameters are chosen simultaneously as adjustable parameters during the calibration depends on the complexity of the constructed model and the power of the chosen computer code. Computational software must run quickly enough to give results within an acceptable program execution time. Also, the model should incorporate significantly complex processes including information on the actual SVE settings. The parameters such as mass transfer coefficients, intrinsic permeability, and dispersivity, porosity of soil, bulk density, and moisture content may be selected as adjustable parameters. Vogele et al. (1996) and Barnes and White (2006) undertook an approach to calibrate their models by adjusting the initial concentration and intrinsic permeability (two parameters) due to their evaluated high uncertainty.

5.1.4.2 Goodness of Fit

The goodness-of-fit can be assessed quantitatively by the NSSRD index after the trial visual best fit has been attained. NSSRD is expressed in log form in order to

prevent the round-off error calculation problems around asymptotic zero concentrations occurring during the SVE tailing stage, but also to raise the resolution for the measurement of the quality of the fit. The NSSRD expression in Equation (5.9) was first proposed and applied by Harper (1999). Later Gidda (2003) and Zhao and Zytner (2004, 2005) used this NSSRD expression to systematically quantify the goodness of fit of the relevant calibrations.

$$NSSRD = \frac{1}{N}\sum_{i=1}^{N}\left\{\frac{\log(C_{g,i})_{\exp} - \log(C_{g,i})_{\mathrm{mod}}}{\log(C_{g,i})_{\exp}}\right\}^2 \tag{5.9}$$

Where:

N = number of sampled points in predicted and experimental data used to calibrate the model

i = i-th sampled point for experimental and predicted data

$(C_{g,i})_{exp}$ = i-th concentrations of offgas from the experimental data, mol/L^3

$(C_{g,i})_{mod}$ = i-th predicted concentrations of offgas from the model, mol/L^3.

The best-fit status will be determined by the minimized NSSRD value in this work. If unsatisfactory matching with the known data occurs, the corresponding adjustable parameters will be systematically varied to attain the least NSSRD. It is important to state that the adjustable parameters should not be tuned outside of the reasonable range of experimentally determined values reported in the literature, if applicable.

5.1.4.3 Calibration of the 3D-SVE-L Model

As above-mentioned, the nonequlibrium phase pairs include NAPL to vapour, aqueous to vapour, NAPL to aqueous and aqueous to solid phases. The mass transfer

rates between these four phase pairs are updated during the SVE process. The incorporated mass transfer coefficients in the 3D-SVE-L/F models for all nonequilibrium phase pairs are summarized in Table 5-4.

Table 5-4 Mass Transfer Coefficients Applied in the 3D-SVE-L/F Model

Nonequilibrium Phase Pairs	Expressions or Values, h^{-1}	Remarks
NAPL to vapour	$k_{ng} = a\left(\frac{S_n}{S_{n,i}}\right)^b$	*"a"*, *"b"* are adjustable parameters
Aqueous to vapour	$k_{ag} = c(C_a)^d$ $c = 0.001$, d=1.9	*"c"*, *"d"* values are same as Gidda (2003)
Aqueous to solid	$k_{as} = 3.6$	Same as Gidda (2003)
NAPL to aqueous	$k_{na} = 36$	Same as Gidda (2003)

In the present work, the simulated results of the 3D-SVE-L model are calibrated by adjusting the two empirical parameters formulated in the NAPL-vapour interphase mass transfer coefficient expression. There are two reasons for this choice: (1) it is the dominant mechanism according to the principle of SVE technology, which benefits significantly from the volatilization of petroleum hydrocarbon contaminants; and (2) experimentally and theoretically, mass transfer between the NAPL and vapour phase has been demonstrated to have a critical influence on performance of SVE (Harper, 1999; Gidda, 2003).

Compared to the rate of mass transfer between NAPL and vapour phase, the rate of mass transfer between aqueous to vapour phase is less because the solubility of hydrocarbon contaminants is low. Hence, the empirical parameters *"c"* and *"d"*, which are within the aqueous and vapour phase mass transfer coefficient expression, are treated as constants. The multivariable regression method sensitivity analysis of

the 3D-SVE-L/F models presented in Chapter 6 will confirm this issue. The mass transfer coefficients of aqueous to solid and NAPL to aqueous phase pairs are constant in the 3D-SVE-L model due to their mass transfer rates being much less than the mass transfer of NAPL to vapour phase.

Ten cases of experimental data were matched by the 3D-SVE-L model in order to calibrate the model and demonstrate that the 3D-SVE-L model can describe the SVE experiments with appropriate inputs. Consider as an example to demonstrate the calibration procedure of the case 4 as depicted in Figure 5-3. Starting at the elapsed time t = 0, the early stage is matched by adjusting the magnitude of *"a"* until a best fit at the early stage and an approximate fit at the tailing stage approach. Once the value of *"a"* was determined, different *"b"* values were tested. Figure 5-3 illustrates how a ± 0.005 variation in the values of parameter "b" affected the fitting of the model at the tailing stages. The final visual best fit is quantitatively confirmed when the least NSSRD, 0.0735, is reached. The NSSRD values associated with tested *"b"* values are listed in Table 5-5. The results show that the numerical simulation of the 3D-SVE-L model can fit experimental Case 4 well by adjusting two empirical parameters of NAPL to the vapour phase mass transfer coefficient. The calibrations for the remaining cases go through a similar process.

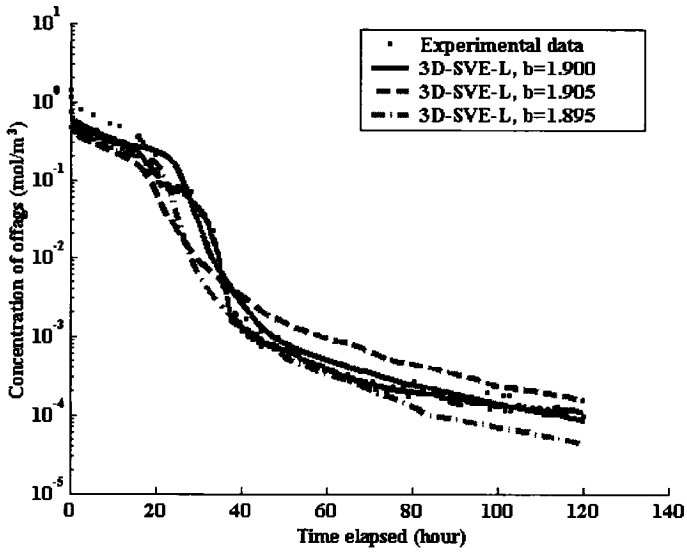

Figure 5-3 Breakthrough Curves for Case 4 and the Approach to Best Fit Using 3 Values of Parameter b (Elora Silt, a= 42.9 h^{-1})

Table 5-5 Variations of NSSRD Values during Calibration*

Calibration Process by adjusting "b" (a= 42.89 h^{-1})	NSSRD	Calibration Process by adjusting "a" (b=1.90)	NSSRD
b=1.905	0.289	45.50	0.0903
b=1.900	0.0735	42.89	0.0735
b=1.895	0.291	35.10	0.1208

* Keep the value of "a" constant, which has been determined in initial fitting.

Table 5-6 gives final empirical mass transfer parameters as well as the mass transfer coefficients and the corresponding NSSRD values for the best fit of all experiments. All experimental and simulated breakthrough curves for these completed experimental cases are illustrated in Figures 5-4 through 5-13. As judged by the fitting status in Table 5-6, seven out of ten cases can be matched to approach

the best fit. The performance of these best-matched cases is consistent with the characteristics of SVE. As depicted in all figures, there are three stages present during an average SVE operation: early gentle decrease of concentration in the offgas, followed by a transition stage of a rapid decrease in concentration, and finally a tailing stage. Theoretically these three stages represent the advection and dispersion mass transport and mass transfer dominant controlled mechanisms during SVE operation. In conclusion, adjusting two empirical mass transfer parameters for NAPL to vapour phase can allow the 3D-SVE-L model to successfully match the various characteristic experimental results of lab-scale SVE operation. Mass transfer between aqueous and solid phase and between NAPL and aqueous phase can be reasonably represented by constant mass transfer coefficients due to the air dry experimental conditions.

Inversely, three cases listed in Table 5-6 behave with some error and have not attained the satisfactory matching quality by the visual fitting as shown in Figure 5-6 through 8. The main reasons are that these experiments have not been conducted ideally. Their removal rate is around 70% (Duggal, 2005) which is much lower than other cases with the removal rate of above 99.9%. Because these experiments have not attained a significant removal rate and show inappropriate operation, the behaviour of these experiments cannot be predicted by the 3D-SVE-L model with the relevant inputs.

Table 5-6 The numerically determined mass transfer coefficients and NSSRD

№	Soil type	Flow rate (L/min)	Mass transfer Empirical parameters		Mass transfer coefficient ($hour^{-1}$)				NSSRD	Fitting Status
					k_{ng}		k_{ag}			
			a (h^{-1})	b	Initial	Final	Initial	Final		
1	Elora silt	9.70	32.32	1.70	32.32	0.148	$1.2*10^{-4}$	$3.2*10^{-6}$	0.215	Very good
2	Elora silt	33.0	18.54	1.95	18.54	0.063	$1.3*10^{-4}$	$4.1*10^{-6}$	0.0021	Best
3	Elora silt	30.6	47.78	1.81	47.78	0.727	$1.3*10^{-4}$	$3.6*10^{-6}$	0.528	Good
4	Elora silt	30.3	42.89	1.90	42.89	0.076	$1.0*10^{-4}$	$8*10^{-7}$	0.0735	Best
5	Elora Silt	20.9	59.23	1.80	59.23	0.443	$8.0*10^{-5}$	$1*10^{-6}$	0.082	Best
6	Ottawa sand	1.5	6.11	1.95	6.11	0.016	$1.3*10^{-4}$	$1.2*10^{-6}$	1.389	Poor
7	Ottawa sand	5.4	11.27	1.80	11.27	0.603	$1.4*10^{-4}$	$2*10^{-7}$	1.169	Poor
8	Ottawa sand	10.6	12.01	1.80	12.01	1.50	$4*10^{-5}$	$6.2*10^{-6}$	0.985	Very poor
9	Ottawa sand	20.9	4.52	1.85	4.52	0.250	$10*10^{-4}$	$2.1*10^{-6}$	0.161	Best
10	Ottawa sand	11.1	43.09	1.70	43.09	0.107	$1.4*10^{-4}$	$3.4*10^{-6}$	0.983	Best

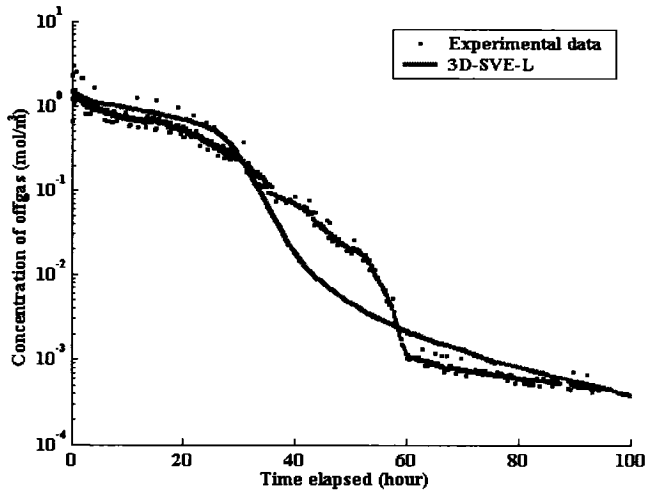

Figure 5-4 Matched Breakthrough Curves for Case 1 (Elora silt, NSSRD=0.215)

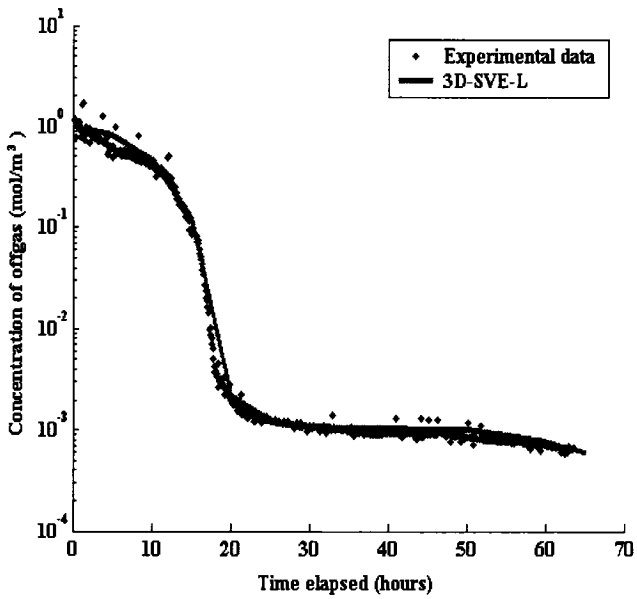

Figure 5-5 Matched Breakthrough Curves for Case 2 (Elora silt, NSSRD= 0.0021)

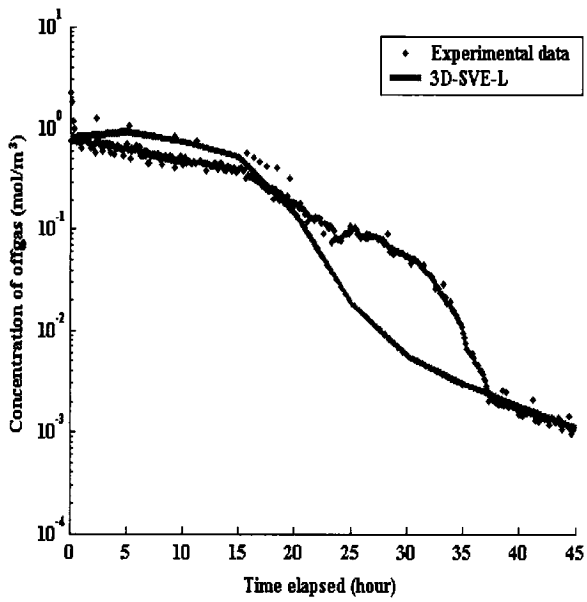

Figure 5-6 Matched Breakthrough Curves for Case 3 (Elora silt, NSSRD= 0.528)

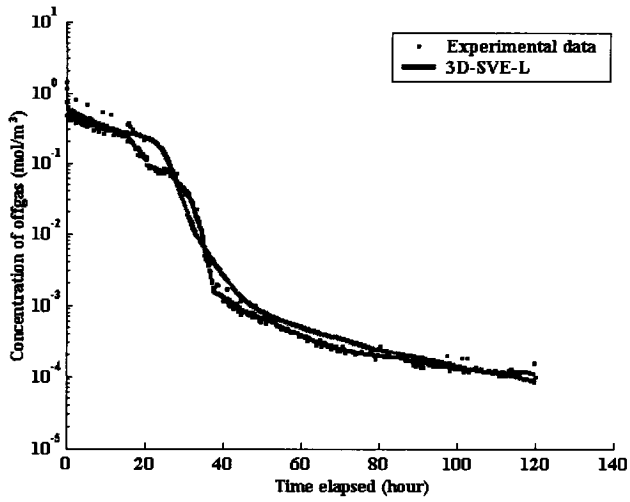

Figure 5-7 Matched Breakthrough Curves for Case 4 (Elora silt, NSSRD=0.0735)

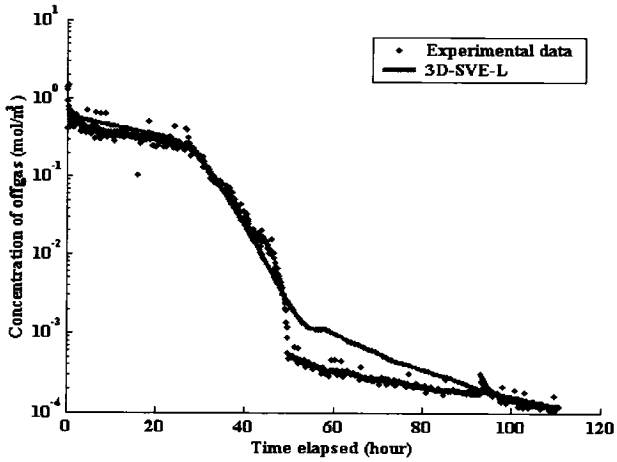

Figure 5-8 Matched Breakthrough Curves for Case 5 (Elora silt, NSSRD=0.082)

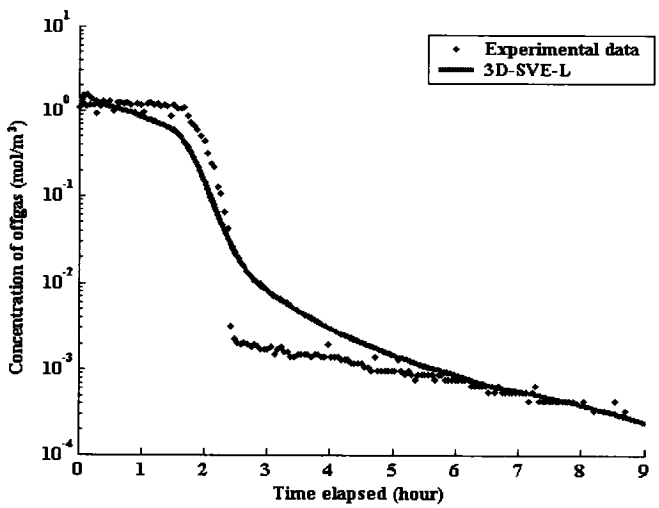

Figure 5-9 Matched Breakthrough Curves for Case 6 (Ottawa sand, NSSRD=1.389)

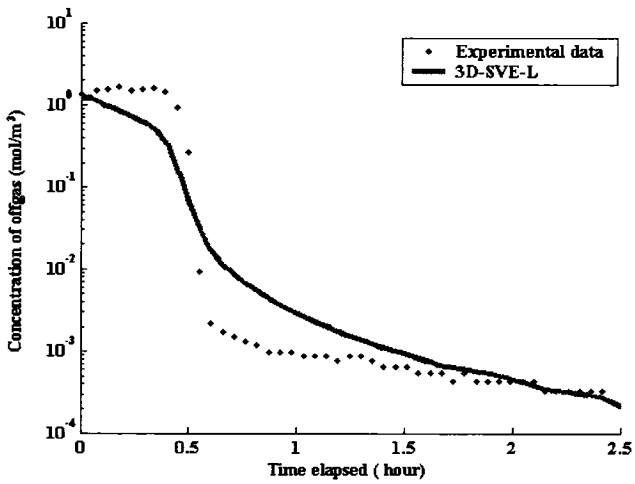

Figure 5-10 Matched Breakthrough Curves for Case 7 (Ottawa sand, NSSRD=1.169)

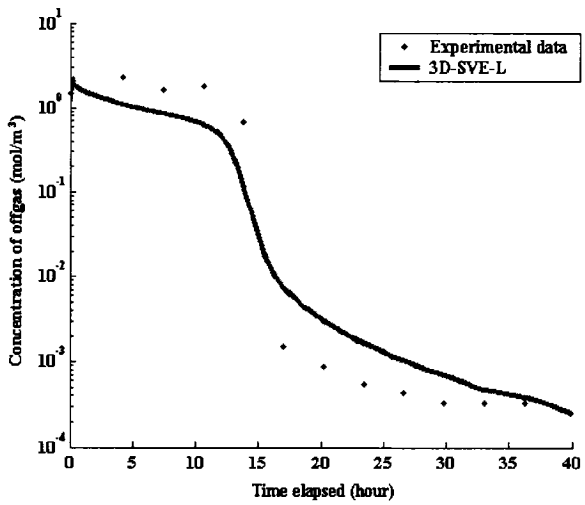

Figure 5-11 Matched Breakthrough Curves for Case 8 (Ottawa sand, NSSRD=0.985)

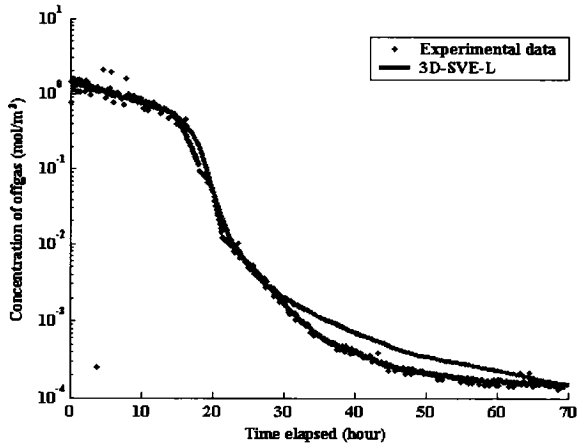

Figure 5-12 Matched Breakthrough Curves for Case 9 (Ottawa sand, NSSRD=0.161)

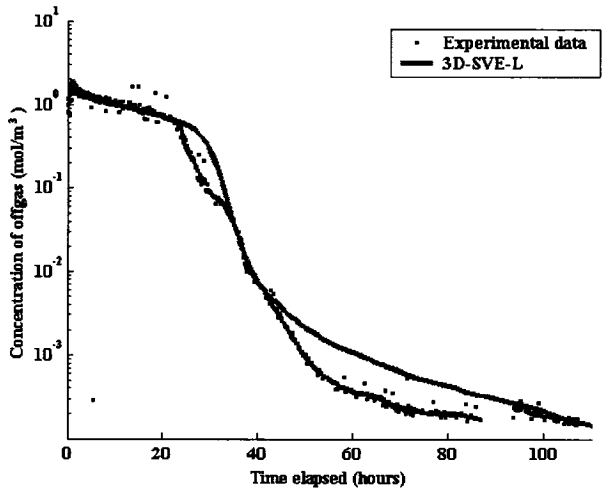

Figure 5-13 Matched Breakthrough Curves for Case 10 (Ottawa sand, NSSRD=0.983)

Thus far, the NAPL-vapour and aqueous-vapour mass transfer coefficients have been determined by calibrating the 3D-SVE-L model. In order to identify the typical features of the 3D-SVE- model, a review of the current existing representative mass transfer coefficients reported in the literature and modeling settings are listed in Table 5-7.

Table 5-7 Time-Variant Mass Transfer Coefficients and the Calibrated Settings

Case	Mass transfer coefficients, h^{-1}		Predicted tailing effect?	Features of the models	Referance
	NAPL-vapour k_{ng}	Aqueous-vapour k_{ag}			
1*	Lumped 95-225	Equilibrium	Yes	1D multiphase multicomponent transport model	Harper, 1999 Harper et al., 2003
2*	Isolated 10^{-2}-10^{2}	10^{-4}~10^{-2}	Yes	1D multiphase and single component transport	Gidda, 2003
3*	Lumped 9~12	Equilibrium	No	1Dmultiphase and single component transport	Yoon, 2002
4**	Isolated 4^{-3}~541	4^{-3}~7	No	2D multiphase flow and single component transport	Rathfelder et al., 2000

* One-dimensional 0.2 m experimental column, mass transfer coefficients are time-variant.
** No mass transfer was obtained by the relevant calibrations for a model, rather from different mass transfer processes based on the literature. Therefore, the mass transfer coefficients cannot be compared to differentiate the degree of the rate of mass transfer of the integrated phase pairs in a single SVE setttings.

A comparison with other one-dimensional SVE models incorporating the transient mass transfer coefficients, as summarized in Table 5-7, shows the 3D-SVE-L model is able to represent the physical processes occurring in the lab reactor. The complex combination of SVE processes is adequately reflected by the 3D-SVE-L model. The outputs of the 3D-SVE-F model match the performance of actual lab-scale SVE experiments very well from the initial stage to the tailing stage. A review of the range of mass transfer coefficients k_{ng} of NAPL to vapour phase for the lab-scale experimental cases in this study show that initial values of k_{ng} ranged from 5 to 60 h^{-1} which is within the range given in Table 5-7. The mass transfer coefficients k_{ng} for all cases at the tailing stage are less than 1 h^{-1}. The magnitude of the mass transfer coefficients do fall within the typical range obtained by other researchers as summarized in Table 5-7. The wide range of mass transfer coefficients indicates the

typical time-variant nonequilibrium features present during SVE processes. Comparing this with literature results of $4.16*10^{-3}$-541 h^{-1} (Poulsen et al., 1996; Rathfelder et al., 2000) shows that for the calibrated 3D-SVE-L model at the initial stage of SVE the determined mass transfer coefficients fall into this range.

The mass transfer coefficients for aqueous to vapour phase mass transfer also are tracked, and the values of k_{ag} are approximately 10^{-4} h^{-1} at the initial stage and 10^{-6} h^{-1} at the tailing stage. Unfortunately at the tailing stage, there are no comparable results reported for the data of mass transfer coefficients from numerical simulation based on the three-dimensional SVE settings. The transient mass transfer coefficients determined by the 3D-SVE-L model are reasonable to represent the performance of the complete initial and tailing stages of SVE operation in a lab-scale reactor.

The current range of mass transfer coefficients of NAPL to vapour mainly originated from relatively simple one- or two-dimensional models, so that the essential elements rather than the mass transfer coefficients, which significantly affect the outputs of the model, inappropriately have been neglected due to an oversimplified model and the relevant assumptions.

5.1.5 Numerical Outputs of the Calibrated 3D-SVE-L Model

The reasonable and accurate numerical solutions for the primary unknowns which refer to the concentration of component, saturation of a phase and pressure of vapour phase involved in the governing equations are crucial to indicate the predictive capacity of the 3D-SVE-L model. In this section the numerical simulation of the calibrated 3D-SVE-L model for the unknown primary variables (pressure of

vapour phase, saturation of vapour phase in the soil and concentration of toluene) are demonstrated and examined in terms of the expected consequences. Insights into improving future experimental work and accuracy of the constructed model are developed based on the modeling studies, especially when limited sampled data are available for calibration. It is essential to demonstrate how the numerical solutions of the primary unknowns directly affect the accuracy of predicting empirical mass transfer parameters and behaviour of the model.

5.1.5.1 Distribution of Vapour Pressure

The pressure gradient around a venting well and the profile of the pressure field have significant implications for the SVE remediation, as venting pressure is one of the most sensitive factors in the success of SVE (Rathfelder et al., 1991). Based on the physical structure of the lab-scale cylindrical reactor, the distribution of vacuum pressure in the vicinity of the venting well should be radially symmetrical and gradually increase throughout the soil, and should extend to the fine screened outside wall of the reactor. Figure 5-14(a) shows the cylindrical shaped isosurface of pressure profile around the venting well and reflects quantitatively the expected outcomes of the pressure field through a radial venting operation. Figure 5-14(b) indicates the pressure variations along the radial distance from venting well to the outside of the reactor. In the vertical direction, the pressure is identical because of the impermeable boundary conditions on the top and bottom ends of the reactor. The outside boundary of the reactor is open to air which is at atmospheric pressure. The predicted profile of the pressure distribution is helpful for calibrating the flow equation if pressure-monitoring data are available during the venting process.

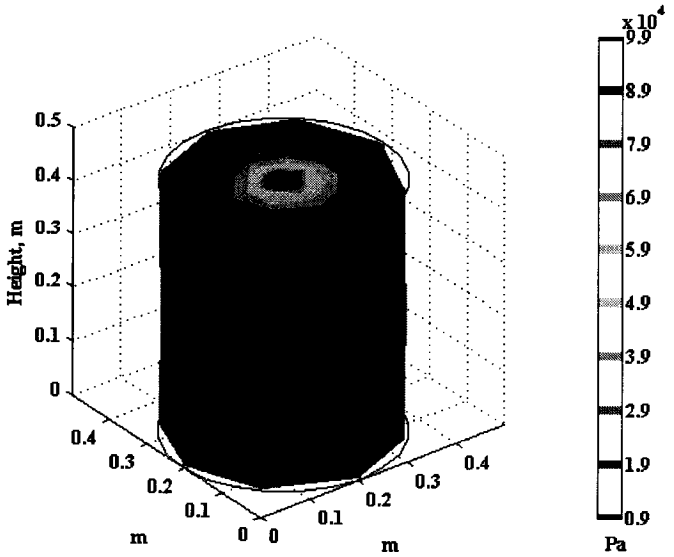

Figure 5-14(a) The Profile of Pressure at t=120 hour for Case 4

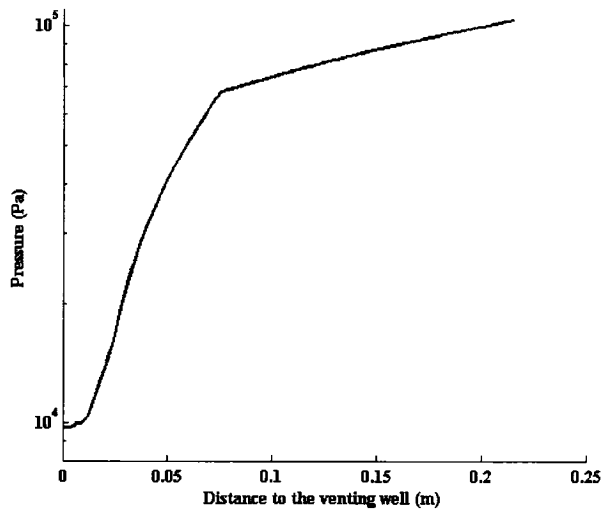

Figure 5-14(b) The Radial Pressure Variation at t=120 hour for Case 4

In order to survey the temporal variation in pressure, which depends on the radial distance away from the venting well, the outputs are tracked at two locations of radius 0.01 m and 0.17 m as shown in Figures 5-15 and 5-16. The results of the pressure estimates at the two different locations indicate that the relative mass

transfer causes the profile of the time-variant venting pressure. What is important is that the initial pressures at these two locations are identical and equal to atmospheric pressure. Apparently, fixed boundary conditions at the venting well and at the outside wall of the reactor cause a steady-state pressure gradient; however, the time-variant rate of mass transfer and density-driven flow also cause the pressures of vapour phase to be time-dependent. The small variation in pressure versus time can be barely detected and denoted by conventional logarithmic coordinate within the range of the magnitude of venting pressure and atmospheric pressure. The comparison of the variation in pressure at radii 0.01 and 0.17 m indicates that the mass transfer is significant because the accumulation towards the venting well occurs. Pressure changes during the elapsed time are equal to 40 Pa at r = 0.01 m and 1 pa at r = 0.17 m over the course of 120 hours; the different changes indicate the rate of mass transfer is quite different at the two locations. Near the well, the variation in pressure is greater because of the migration of contaminants toward the venting well where an increase in concentration and saturation of the contaminant toluene occurs. This finding indicates that the time-variant behaviour of the coupled flow and transport model should be stressed in order to improve the accuracy of any SVE model.

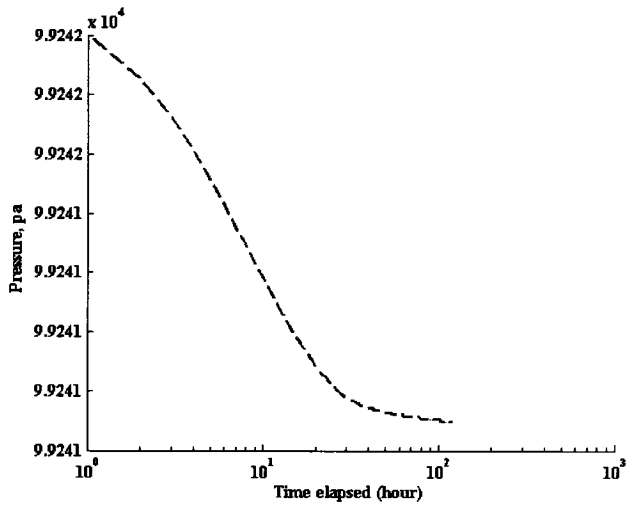

Figure 5-15 Time-Variant Pressure at the Radius of 0.17 m away from Venting Well (1 Pa pressure drop during 120 hours)

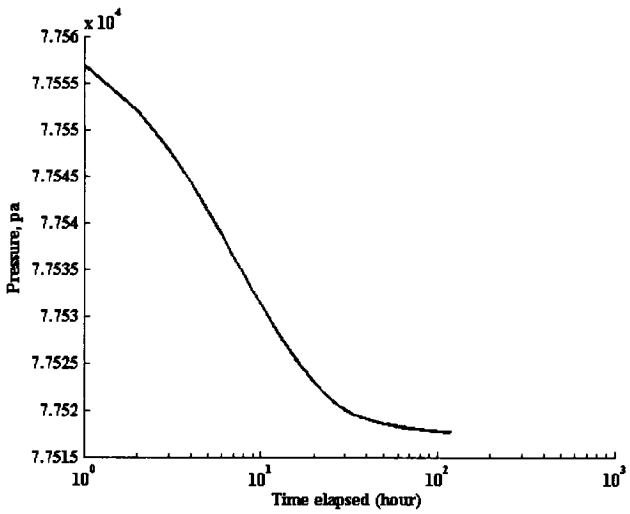

Figure 5-16 Time-Variant Pressure at the Radius of 0.01 m away from venting well (40 Pa pressure drop during 120 hours)

5.1.5.2 Variations of Saturation and Concentration of Toluene

Modeling studies can quantitatively and visually explore the time-variant profile of the saturation and concentration of toluene throughout the entire site. Figure 5-17 shows the distribution of saturation of vapour phase around the venting well in the lab reactor at t = 99 hours. It depicts that the saturation and concentration

of toluene in the soil vapour phase becomes larger when approaching the venting well, because of the migration and the gradual accumulation of toluene contaminant toward the venting well. Figure 5-18 indicates the variation in saturation of vapour phase versus time at two different radial distances of radii 0.023 m and 0.075 m away from the venting well. Vapour migration toward the venting well and the phase conversion from NAPL to vapour phase significantly contribute to the early increase in toluene offgas concentration. The initial uniform saturation of NAPL becomes the accumulative distribution when approaching the venting well; the vapour phase saturation farther from the well initially reduces faster than that closer to the venting well. However, the distribution of the vapour phase becomes asymptotic uniformly over the entire site when SVE approaches the tailing stage. The overlap of saturation curves at the tailing stage is shown in Figure 5-18.

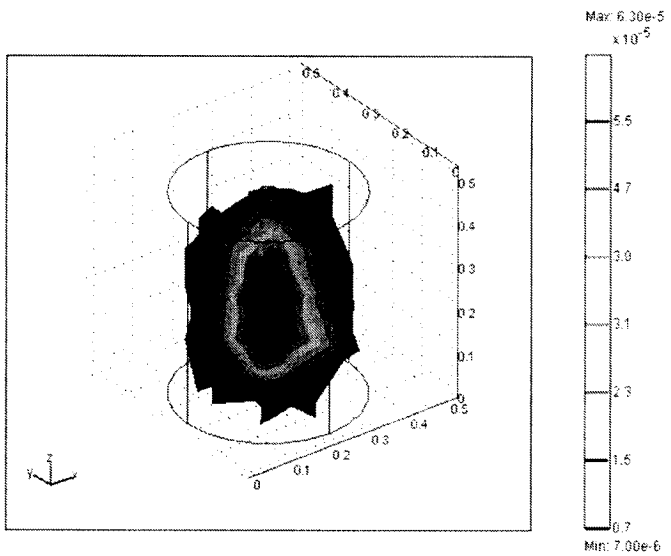

Figure 5-17 Profile of Saturation of Toluene in the Lab Reactor at t=99 Hours

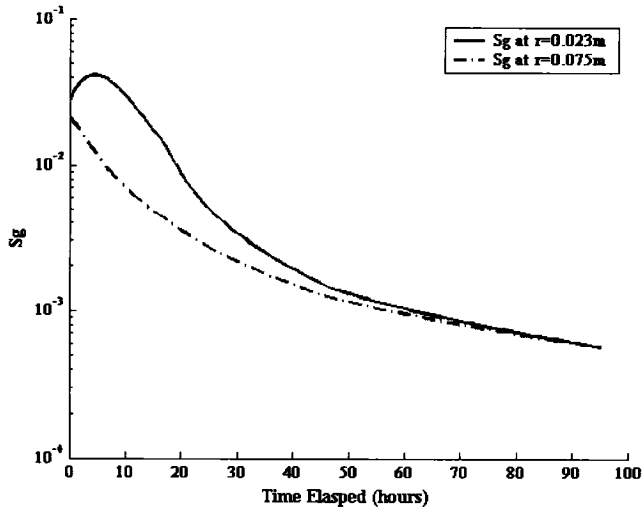

Figure 5-18 Variation in Saturation of Toluene in Soil Vapour Phase

During SVE operation, the contaminant is expected to migrate towards the venting well by advection and dispersion and the resulting mass transfer; then it is pumped to the surface. Eventually, major concerns are the concentrations of offgas and contaminants remaining in the soil throughout the site. Theoretically, the concentration of toluene can be predicted by 3D-SVE-modeling investigations. The predicted concentration of toluene in the soil vapour phase along the radial distance from venting well to the outside of the reactor versus the elapsed time is shown in Figure 5-19, which illustrates the decreasing toluene concentration along a radial direction away from the venting well. This shows the simultaneous migration and accumulation of toluene contaminant towards the venting well. This result can provide helpful information when the residual toluene concentration is monitored for the whole site. Calibration of the complex three-dimensional model for the concentration of toluene in the soil vapour phase may be conducted if the soil vapour

phase data from the lab-scale experiment were available. Unfortunately, the concentration of toluene in soil vapour inside the reactor was not sampled in Duggal's (2005) experiment.

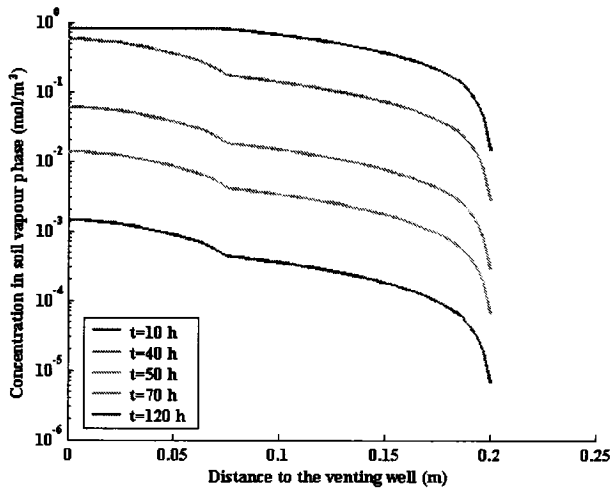

Figure 5-19 Concentration of Toluene in Soil Vapour Phase versus time for Case 4

Based on the above analysis, the 3D-SVE-L model provides reasonable pressure, saturation, and concentration behaviours throughout the entire site as time passes. Therefore, the model can predict and monitor the status of remediation throughout a site. Ideally, the modeled results could be compared to sampled data to aid in the decision process. The modeling results can also provide considerable insight into the design of more advanced experimental procedures and the improvement of the understanding of the dominant mechanisms.

5.1.6 Stability and Convergence Analysis for 3D-SVE-L Numerical Model

In this section, the sensitivity of the numerical simulation of the 3D-SVE-L model for the number of finite elements in the mesh and the time step will be examined in order to ensure a stable and convergent solution. Stability and convergence analysis for the numerical schemes of the complex 3D-SVE-L model are also checked in this section.

In this work, stability and convergence were examined through a series of solutions based on the refined size of mesh and time steps with FEMLAB. Under attainable relative error of 10^{-6}-10^{-9} with FEMLAB, a non-oscillatory smooth solution obtained using FEMLAB is considered if the numerical model remains stable and converges, and the solutions are acceptable (Istok, 1989).

In order to examine the stability of the FEMLAB for the developed 3D-SVE-L model, a series of numerical simulations are obtained by refining the space and time steps. The results are listed in Tables 5-8 and 5-9. Analysis shows that stability for a complex three-dimensional model can be obtained by refining the proper range of size of finite elements, even though the degree of mesh refinement is very limited for the complicated three-dimensional model. Generally, the finite element mesh determined by refining the initial coarse mesh three times can produce an accurate solution with satisfactory relative error (Rao, 2005).

Table 5-8 3D-SVE-L Model Stability Affected by the Time Discretization*

Time step (hours)	Concentration of offgas (mol/m^3)	
	t=100 hours	t=10 hours
10	1.811e-4	0.756
1	1.811e-4	0.756
0.1	1.811e-4	0.756
0.01	1.811e-4	0.756

*The outputs are from Case 4, and the number of the mesh is 1358.

Table 5-9 3D-SVE-L Model Stability Affected by the Mesh Refinement*

Number of finite element mesh	Concentration of offgas (mol/m^3)	
	t=100 hours	t=10 hours
906	1.7908e-4	0.7563
1352	1.811e-4	0.7562
2006	1.811e-4	0.7565
2500	1.811e-4	0.7565

* The outputs are from Case 4, and time step is 1 hour.

The results in Tables 5-8 and 5-9 show that one refinement to time step and mesh of finite elements causes the stable solution. The finer mesh of elements and time step causes the computation load and longer execution time. It is appropriate to use a time step of 1 hour and number of finite element mesh of 1352 to undertake the numerical simulation.

5.1.7 Impact of the Typical Dominant Parameters

5.1.7.1 Impact of Intrinsic Permeability of Porous Media

The quantitative analysis for the impact of the intrinsic permeability of soil porous media on the behaviour of offgas concentration is completed by running the calibrated 3D-SVE-L model. The intrinsic permeability of the contaminated soil site is one of the critical factors in evaluating whether the contaminated site may be remediated by SVE or not, and the success of the corresponding SVE remediation. Vogele (1996) reported that a magnitude of 10^{-14} m^2 for soil permeability is the lowest limit at which a site can be remediated by SVE technology. Conceptually, the higher the intrinsic permeability of soil porous media under the same flow rate, the faster the concentration of offgas decreases because the higher Darcy's velocity can cause a substantial amount of advective flux. Figure 5-20 shows the effect the intrinsic permeability has on the breakthrough curves from the 3D-SVE-L model during the whole time span of an SVE operation for case 4. The greater permeability causes the lower concentration of offgas at the same elapsed time. This consequence implies that the advective transport process dominates the SVE operation, and the 3D-SVE-L model behaves reasonably in response to changing the soil permeability as an input parameter.

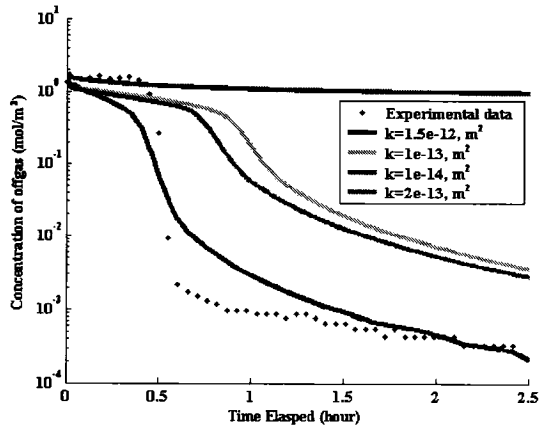

Figure 5-20 Effect of Intrinsic Permeability on Offgas Concentration

5.1.7.2 Impact of the Empirical Mass Transfer Parameters "*a*" and "*b*"

Since mass transfer coefficients can be obtained by the calibration of a model, the knowledge of how an empirical mass transfer parameter affects the outputs of the developed model is an important issue. It is critical to explore the appropriate way to adjust the magnitude of the adjustable parameters. As shown in Figure 5-21, the empirical mass transfer parameter "*a*" imposes a discernable influence on the behaviour of the 3D-SVE-L model.

A natural question arises from the fitting processes by adjusting more than one parameter, that is, whether the uniqueness of the magnitude of each adjustable parameter for best fit is present or not. The presence of uniqueness can be explained by means of the mathematical expression NAPL to vapour phase mass transfer coefficients. In this study, empirical parameter *"a"* produces a modification over the SVE operation time for the ratio of the current saturation (S_n) of the NAPL and the initial saturation ($S_{n,i}$) as a multiplier. But empirical parameter *"b"* is placed on the

position of the exponent of the ratio of $S_n/S_{n,i}$. Therefore, parameter *"b"* has the more intensive influence than parameter *"a"*. Obviously, at the very early stage of an SVE operation, the change in the saturation of NAPL phase is very little; as such, *"b"* value provides insignificant impact, and *"a"* has more influence on the behaviour of the model than *"b"*. Inversely, at the tailing stage as the ratio $S_n/S_{n,i}$ asymptotically approaches zero, and both *"a"* and *"b"* can modify the mass transfer coefficient; moreover, the impact of *"b"* as an exponent is more significant than that of "a" as a multiplier. Therefore, during the calibration process, empirical parameter *"a"* controls the whole SVE process of the early and tailing stages and *"b"* strongly controls the tailing process. The individual features of *"a"* and *"b"* in the mathematical formulation of the mass transfer coefficient determine the uniqueness of the empirical parameters when the final best fit is achieved. It can be concluded that the two-parameter expression is suitable for the realistic situation of an actual SVE operation with tailing effects through the 3D-SVE-L model.

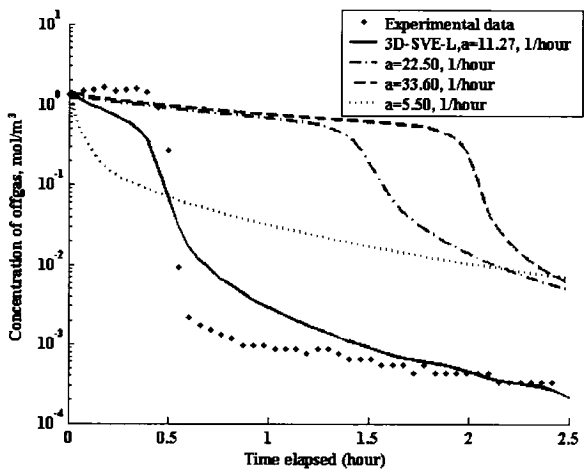

Figure 5-21 Effect of "a" on the Offgas Concentration

5.1.7.3 Impact of Water Content

Soil water content is a very complex issue, which can affect the SVE process in mass transport and mass transfer. The 3D-SVE-L model was calibrated against the known experimental data sampled under air dry soil conditions (water content 0.5-3%). However, the developed model can be used to investigate the impact of increasing water content. The predicted impact of soil water content on the concentration of offgas based on the 3D-SVE-L model is demonstrated in Figure 5-22. An increase of 7% water content from 3 to 10 % causes an increase of 17.66% in concentration of offgas during the tailing stage. The soil water content more obviously affects the behaviours of the tailing stage because more rate-limited mass transfer may occur between the aqueous phase and solid phases.

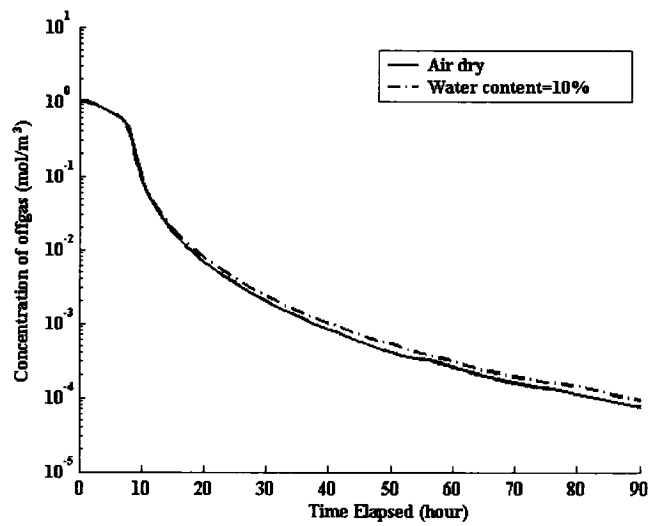

Figure 5-22 Impacts of Water Content on the Concentration of Offgas

5.2 Modeling Field-Scale SVE Operation

In this section, the general three-dimensional mathematical model developed in Chapter 4 is applied to an actual field SVE operation conducted by CRA in 1997. However, because of confidentiality, the detailed system configurations including geological data of the site and layouts of monitoring, venting, passive and inject wells have been described only in a simplified manner. Accordingly, the modeling domain, initial and boundary conditions, calibration and the outputs of the simulated variables are demonstrated; the effects of operation conditions on the concentration of offgas are examined by running the calibrated 3D-SVE-F model. One of the most important issues is to determine the mass transfer coefficients for the field-scale SVE model. No research has as yet provided the details of mass transfer coefficients based on field-scale settings and modeled results.

5.2.1 The Physical Properties of Field-Scale SVE Site

The field SVE scenario used in this study is a gasoline station remediation case conducted by CRA in 1997. More than 20 monitoring wells were installed on the site in order to survey the site remediation. For this work, a region having the dimensions of 10 m length by 10 m width by 5 m depth with an ROI (Radius of Influence) of the chosen well more than 5 m. The isolated domain consists of isotropic and homogeneous silty sand determided from the monitoring well with one venting well centered in the region as shown in Figure 5-23. The concentration of contaminants in the soil, groundwater, soil vapour, effluent vapour of SVE venting

well, and total hydrocarbon content of offgas were monitored over time from different monitoring wells. The single venting well setting is chosen in order to develop the 3D-SVE-F model and implement the calibration against the sampled concentration of offgas in the simulated single venting well system.

The corresponding conceptual model for this SVE remediation operation was proposed as follows. A screened venting well is controlled as a specific vacuum pressure on the contaminated silty sand zone, and causes the injected air to flow radially throughout the contaminated soil, and then vapour is carried through the venting well. During SVE operation, the residual contaminant BTEX mixture is removed by advection and dispersion transport in vapour phase with rate-limited mass transfer between contiguous phases and then is carried away from the subsurface up to ground surface where the vapour is treated. Nonequilibrium mass transfers were considered between NAPL to vapour phase, NAPL to aqueous phase, aqueous to vapour phase, and aqueous to solid phase.

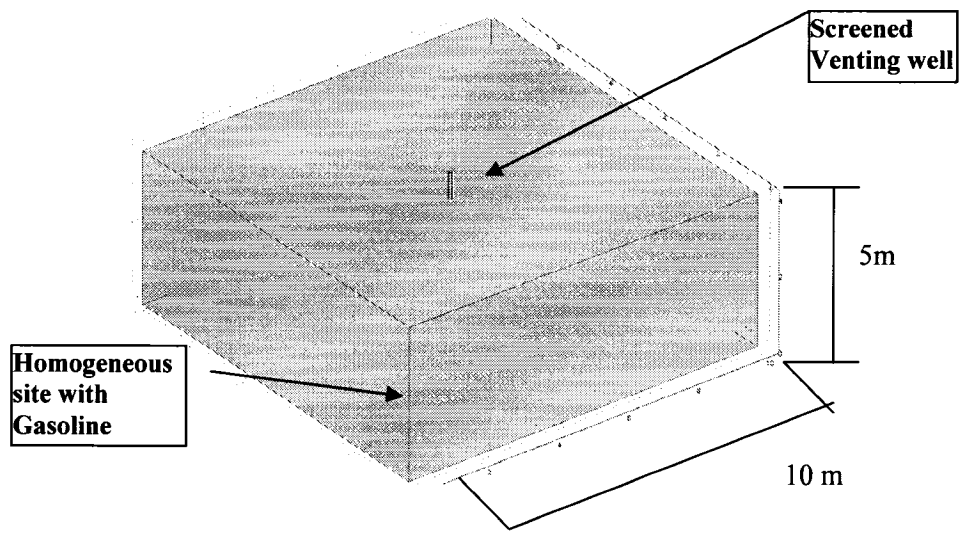

Figure 5-23 Schematic of the Simulated SVE Site Remediated by CRA in 1997

5.2.2 The 3D-SVE-F Mathematical Model

For the SVE operation undertaken by CRA in 1997, the developed model considered only the vapour phase to be mobile, with the aqueous and residual NAPL phases being considered immobile at residual saturation. As a reasonable and necessary assumption to tackle flow in the vadose zone, lab-scale experiments and field SVE are handled as single gas phase active flow (Looney and Falta, 2000). Van Dijke et al. (1995) used the mixed form of the Richards equation for both water and air phases to describe an interactive movement of the fluids in a porous medium. Based on the conceptual model in the preceding section with simplifying assumptions, the system of governing equations of the 3D-SVE-F model is described below.

The NAPL phase flow governing equation is reduced as:

$$\frac{\partial(\varphi\rho_n S_n)}{\partial t} = -E_{na}^{g} - E_{ng}^{g} = -\varphi S_g \sum_{k=1}^{Nc} k_{ng}(C_{g,k}^{e} - C_{g,k}) - \varphi S_a \sum_{k=1}^{Nc} k_{na}(C_{a,k}^{e} - C_{a,k}) \quad (5.7)$$

$$\rho_n = \sum_{k=1}^{Nc} C_{n,k} \quad (5.8)$$

The transport governing equation is given by:

$$\frac{\partial}{\partial t}(\varphi S_n C_{n,k}) = -k_{na}\varphi S_a(C_{a,k}^{e} - C_{a,k}) - \varphi S_g k_{ng}(C_{g,k}^{e} - C_{g,k}) \quad (5.9)$$

Where:

$C_{n,k}$ = concentration of component k in NAPL phase

N_c = number of components, here refers to BTEX

The vapour phase governing equation is given by:

$$\frac{\partial}{\partial t}\left(\varphi S_g \rho_g\right) = \nabla\left(\frac{\rho_g k_{ij} k_{rg}}{\mu}(\nabla p_g - \rho_g g \nabla z)\right) + E_{\alpha}^{g} \quad (5.8)$$

Where:

E_α^g = rate of mass transfer into vapour phase, M/L^{3}T

Mass transfer for vapour phase is given by:

$$E_\alpha^g = \varphi S_g \sum_{k=1}^{Nc} \left[k_{ng}(C_{g,k}^e - C_{g,k}) + k_{ag}(C_{g,k} - H_k C_{a,k}) \right] \tag{5.9}$$

Where:

H_k = dimensionless Henry's law constant of component k

Transport governing equation of component k is denoted by:

$$\begin{aligned} &\frac{\partial}{\partial t}(\varphi S_g C_{g,k}) = \nabla(\varphi S_g D_k \nabla C_{g,k}) - \nabla(q_g C_{g,k}) \\ &+ \varphi S_g k_{ng}(C_{g,k}^e - C_{g,k}) + \varphi S_g k_{ag}(C_{g,k} - H_k C_{a,k}) \end{aligned} \tag{5.10}$$

The aqueous phase balance governing equation is simplified for the mass transfer processes by considering sorption on solid phase, NAPL dissolution, and partitioning between aqueous and vapour phases:

$$\begin{aligned} &\frac{\partial(\varphi S_a \rho_a)}{\partial t} = E_n^a - E_{n/a}^g - E_{n/a}^s \\ &= \varphi S_a \sum_{k=1}^{Nc} k_{na}(C_{a,k}^e - C_{a,k}) - \varphi S_g \sum_{k=1}^{Nc} k_{ag}(C_{g,k} - H_k C_{a,k}) - \varphi S_a \sum_{k=1}^{Nc} k_{as}(C_{a,k}^e - C_{a,k}) \end{aligned} \tag{5.11}$$

Transport equation for component k in aqueous phase is given by:

$$\frac{\partial}{\partial t}(\varphi S_a C_{a,k}) = \varphi S_a k_{na}(C_{a,k}^e - C_{a,k}) + \varphi S_g k_{ag}(C_{g,k} - H_k C_{a,k}) \tag{5.12}$$

This system of governing equations of SVE mathematical model consisting of Equations (5.7) through (5.12) including the closed relations and equations of state of a phase will be solved numerically using FEMLAB; the following initial and

boundary conditions and input parameters collected during the actual measurements by CRA in 1997 are applied in the numerical simulation.

5.2.3 Boundary and Initial Conditions and Inputs

The fundamental principles for the flow and transport equation are similar to the boundary conditions introduced in Section 5.1.3 for the lab-scale model. The following three types of boundaries should be assigned:

- boundary conditions at the outside of the simulated contaminated zone, which are via natural leakage to the atmosphere;
- boundary conditions at a venting well, where the controlled vacuum pressure is induced;
- boundary conditions at the ground surface and the bottom of the site.

There are two alternatives to treat the ground surface of the site. The vapour phase boundaries on the surface may be in the range from completely impermeable to vapour transport (e.g., when the ground is covered) to very permeable (e.g., when the ground is uncovered, open to the air). If open to air, i.e., uncovered, the ground surface of the site connects to the atmosphere; using a Type I boundary condition, the pressure at the ground surface is equal to atmospheric pressure. If the covered surface exists, the surface boundary condition is assigned as a no-flow boundary condition, i.e., Type II $\frac{\partial p}{\partial x_j} = 0, x_j = x, y, z$. x_j refers to *x, y, z* principal coordinate directions. The

bottom soil zone is assumed to be impermeable; hence it is treated the same as a covered surface, i.e., no-flow boundary condition $\frac{\partial p}{\partial z} = 0$.

Boundary conditions of immobile phase mass balance equations at the venting well and the ground surface are assigned as no flux, that is, $\frac{\partial S_n}{\partial x_j} = 0$, $\frac{\partial S_a}{\partial x_j} = 0$. Boundary conditions at the outside of the domain have not been affected by contamination, hence, NAPL saturation S_n is equal to zero, and the aqueous phase saturation of soil porous media S_a is equal to the initial measured saturation of the aqueous phase in soil without contamination.

For the transport equations for the individual component k in phase β, the outside boundary conditions of the domain are assigned as specific concentration of zero, $C_{\beta,k} = 0$; other boundary conditions are considered as zero flux, $\frac{\partial C_{\beta,k}}{\partial x_j} = 0$, ($x_j$ refer to x, y, z). The details on the assigned boundary conditions are illustrated in Figure 5-24, which gives the specific expression and values for the pressure of vapour phase, concentration of the contaminant component, saturation for NAPL and saturation of aqueous phase.

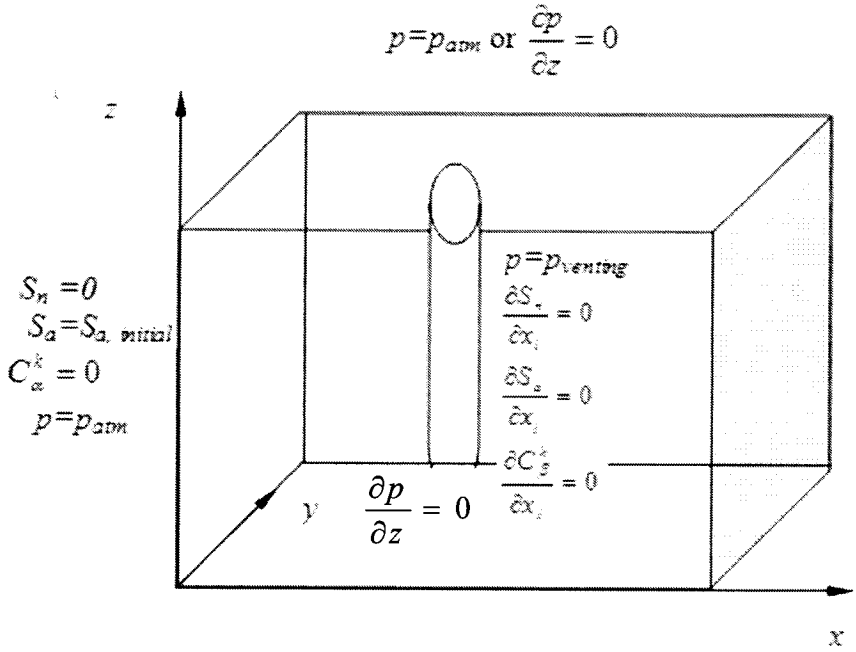

Figure 5-24 Schematic of Boundary Conditions for the Flow and Transport Equations for the Field Site

5.2.3.2 The Inputs for the 3D-SVE-F Model

Generally, there are two different groups of parameters considered, which are site/contaminant parameters and SVE operation design parameters (Nobre and Nobre, 2004):

- data from the field SVE operation such as site borehole sampling data, site historical data, properties of the contaminated soil, and other measurable data; and
- empirical parameters, data on the physical and chemical properties of BTEX from literature.

The chemical properties of BTEX are given in Table 5-10 and the operation condition data and the properties of the soil porous media are given in Table 5-11.

Table 5-10 Properties of BTEX

Properties	Benzene	Toluene	Ethyl benzene	m-Xylene
Water solubility, kg/m^3	1.7	0.515	0.152	0.125
Molecular weight, g/mol	78	92	106	106
Diffusion coefficient, m^2 /sec	$8.91*10^{-6}$	$8.5*10^{-6}$	$7.6*10^{-6}$	$7.2*10^{-6}$
Liquid density, kg/m^3	878.7	866.9	867.0	864.2
Dimensionless Henry's Law constant (air/aqueous partition coefficient)	0.22	0.26	0.32	0.29
Saturated vapour pressure, Pa	12700	3800	1270	880
Octane-water partitioning coefficient, $log\ K_{oc}$, L/kg	1.58	2.13	1.93	2.38

* ASTM standard E1739-1995

Table 5-11 Inputs for the Numerical Simulations of the 3D-SVE-F model

Parameter, symbol, unit	Value	Sources
Aqueous phase saturation, S_a	0.1	CRA, 1997
Molecular weight of air, M_{air}	0.0293	Mirsal, 2004
Intrinsic permeability, k_{ij}, m^2	$1.2*10^{-12}$	CRA, 1997
Dynamic viscosity of air, μ, kg/m^2sec	1.75e-5	Mirsal, 2004
Venting flow rate, scfm*	1000	CRA, 1997
Longitudinal dispersivity, a_L, m	0.6	Assumed
Organic carbon content, f_{oc}, %	0.02	CRA, 1997
Porosity, φ	0.517	CRA, 1997
NAPL initial saturation, S_{ni}	0.002	CRA, 1997
Soil bulk density, ρ_b, kg/m^3	2160	CRA, 1997
Mass transfer empirical parameter, c	0.001	Gidda, 2003
Mass transfer empirical parameter, d	2	Gidda, 2003
Aqueous solid phase mass transfer coefficient, k_{as}, sec^{-1}	3.6	Gidda, 2003
NAPL to aqueous phase mass transfer coefficient, k_{na}, sec^{-1}	36	Gidda, 2003
Temperatures, K	230	CRA, 1997
Barometric pressure, Pa	101325	Mirsal, 2004
Surface conditions	covered	CRA, 1997
Radius of venting well, m	0.05	CRA, 1997
Residual soil water content, S_a	0.001	CRA, 1997
Van Genutchen empirical constant, α, m^{-1}	1	Thomson et al., 1997
Van Genutchen empirical constant, n, m^{-1}	2	Thomson et al., 1997
Vapour phase compressibility, λ_g, , kg/m^3Pa	$1.2*10^{-5}$	Thomson et al., 1997
Number of finite element mesh	1356	
Time step, days	1	

* scfm standard cubic feet per minute.

5.2.4 Calibrations of the 3D-SVE-F Model

Calibration of the 3D-SVE-F model was conducted by matching the simulated and experimental breakthrough curves of the benzene vapour concentration of offgas. In this context, the concentration of benzene in offgas is calibrated for the quaternary component model. The non-calibrated breakthrough curves for the rest three components are demonstrated.

Initially, the considered nonequilibrium mass transfer processes and the relevant mass transfer coefficient expressions and values are the same as those summarized in Table 5-4 except the BTEX components. They are obtained from the preceding lab-scale modeling studies and the calibration against the known experimental results reported in Duggal's work (2005). Accordingly, the mass transfer coefficients "k_{ng}" of NAPL to vapour phase and "k_{ag}" of aqueous to vapour phase are transient expressions, whereas mass transfer coefficients of NAPL to aqueous k_{na} and aqueous to solid phase "k_{as} "are considered as constant and not adjustable parameters.

The initial values of the empirical mass transfer parameters for the field-scale 3D-SVE-F model are the average magnitude of the lab-scale empirical mass transfer parameters summarized in Table 5-12. As illustrated in Figure 5-25, a series of trial values of the empirical mass transfer parameter "a" were incorporated into the 3D-SVE-F model, and the corresponding range of concentrations of offgas at the tailing stage were obtained. As presented in Table 5-12, the predicted concentration of offgas approaches the final target of the known sampled data of SVE operation as the

magnitude of the empirical mass transfer parameter "*a*" decreases. This tendency shows that fitting field SVE sample data requires a lower value of the fitting parameter "*a*" that is less than 0.001 as shown in Table 5-12 compared to the lab-scale cases.

Table 5-12 The Response of 3D-SVE-F Model to Empirical Mass Transfer Parameter "*a*"

	Empirical mass transfer parameter "a", day^{-1}				
	1	0.1	0.01	0.005	0.001
The predicted benzene concentration of offgas at tailing stage, mol/m^3	10^{-10}-10^{-9}	10^{-9}-10^{-7}	10^{-8}-10^{-6}	10^{-7}-10^{-6}	10^{-7}-10^{-6}

Taking the minimum tested empirical parameter "a" of 10^{-3} day^{-1} in Table 5-12 as input and running the field-scale 3D-SVE-F model, the predicted breakthrough curves do not fit the known sampled data well, as shown in Figure 5-25. The results demonstrate that the performance of the field SVE system could not be represented by the lab-scale empirical mass transfer parameters. Obviously, this extrapolation from lab-scale into field-scale introduces significant error. Accordingly, it is important to explore the range of empirical mass transfer parameters, which are appropriate for the field-scale model.

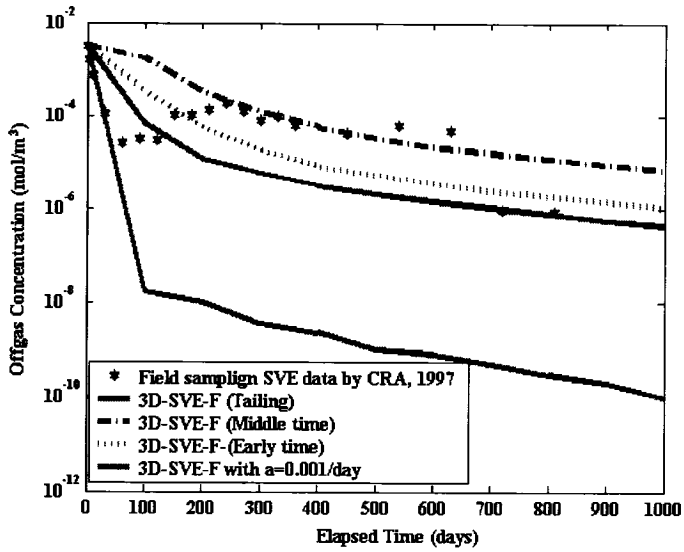

Figure 5-25 Trial to Determine Field-Scale Empirical Mass Transfer Parameters

Because of the limited availability of the SVE operational history and site geological data, the tailing information is difficult to interpret in terms of data sampled in the real SVE field operation as shown in Figure 5-25. The sampled data sets during SVE remediation operation often have poor continuity. Often unpredictable circums-tances around SVE operation may occur, such that once an SVE operation starts, some other operation may be present, such as excavation, or installing a passive well. These additional disturbances may cause the escape of contaminants or migration along other routes. Therefore, the abrupt reduction of offgas concentration in the venting well may occur. However, the overall tailing concentration in Figure 5-25 is credible because the operation and sampling at the tailing stage occurred for hundreds of days.

Other abnormal activities also could cause decreases in vapour concentration such as water table fluctuations, mass transfer resistance and poor diffusion due to

drying and leaks occurring in the venting system. Therefore, the calibration of the 3D-SVE-F model will follow three possible tendencies from the field data, which are matched according to the early time, medium-time and tailing stage concentrations of offgas. Early time refers to the trend seen in Figure 5-26 for the first 600 days, tailing refers to the time in Figure 5-26 for complete data set, while middle is between both. In this context, the field data could not be fitted as one experimental set due to the discontinuity seen in the data. No reasons were provided by CRA for the observed discontinuity. Nevertheless, confidence is expressed in the fitting that was done.

Three possible trends are considered when calibrating the 3D-SVE-F model to the present field sampling data shown in Figure 5-25. The characteristic breakthrough curve gained using a minimum amount of fitting parameters has been matched as shown in Figure 5-26. The best fit for these three possible tendencies of the concentration of offgas and the individual fitting parameters are summarized in Table 5-13. The consequences of matching the field data show that modifying the two mass transfer parameters describing k_{ng} appropriately simulate the performances of field operations. The prolonged long tailing effect, which follows the sharp decline in concentration of the effluent vapour, has been seen by others (Barnes and McWhorter, 2000a, b); also, the sampled data from the site remediated by CRA in 1997 displayed the tailing effects. However, there has been little work reported about the performance of the SVE tailing effect with the aid of a three-dimensional comprehensive model (Barnes and White, 2006).

Table 5-13 The Determined Mass Transfer Coefficients of the 3D-SVE-F Model

Status of fitting	Empirical parameter		k_{ng} h^{-1}		k_{ag} h^{-1}		NSSRD
	a h^{-1}	*b*	Initial time	Final time	Initial time	Final time	
Tailing	4.17e-4	1.80	4.17e-4	6.02e-6	2.16e-6	1.02e-9	0.348
Middle time	3.38e-4	1.90	3.38e-4	7.67e-6	2.16e-6	2.67e-9	2.89
Early time	3.76e-4	1.95	3.76e-4	9.01e-6	2.16e-6	9.01e-9	0.643

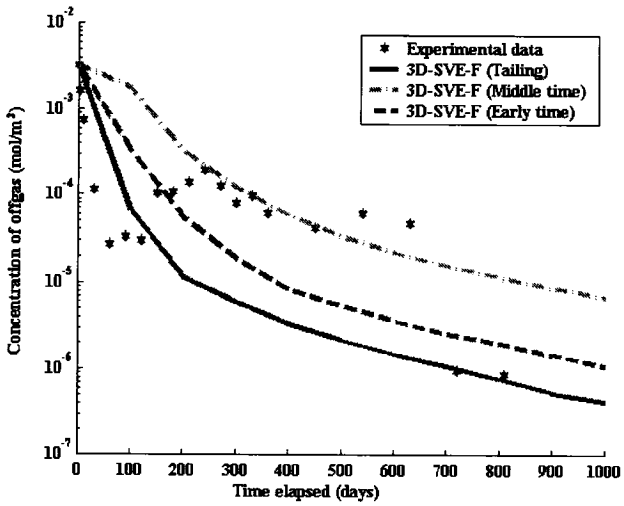

Figure 5-26 Matched Results for Field SVE Operation by CRA in 1997

The mass transfer coefficients of NAPL to vapour phase for the field-scale 3D-SVE-F model fall into the order of $3*10^{-4}$ $hour^{-1}$ at the initial stage of SVE operation and $9*10^{-6}$ $hour^{-1}$ at the tailing stage. The results show that mass transfer coefficients must be considered as transient expressions. The mass transfer coefficients of aqueous to vapour phase for three matched breakthrough curves are the same at the initial point because the initial concentration of contaminants is identical in the aqueous phase, but different at the tailing stage, as shown in Figure 5-

26. The mass transfer coefficients for the aqueous and vapour phases also vary in the range of 10^{-6} to 10^{-9} hour^{-1}. The essential difference between these curves as shown in Figure 5-26 is in the tailing stage.

Figure 5-27 shows that varying the magnitude of "a" value affects the concentration of offgas within the entire SVE operation. At the early stage of SVE operations, the concentration of offgas decreases as the magnitude of "a" decreases. However, at the tailing stage, the effect of "a" parameter has an inverse impact compared to at the initial stage. That is, the greater the value of "a", the lower the concentration of offgas. The effect of "b" parameter strongly controls the tailing behaviour as shown in Figure 5-28. The greater the "b" value, the lower the concentration of offgas. The impacts of "a" and "b" on the concentration of offgas estimated by the 3D-SVE-F model are similar to that of the 3D-SVE-L model.

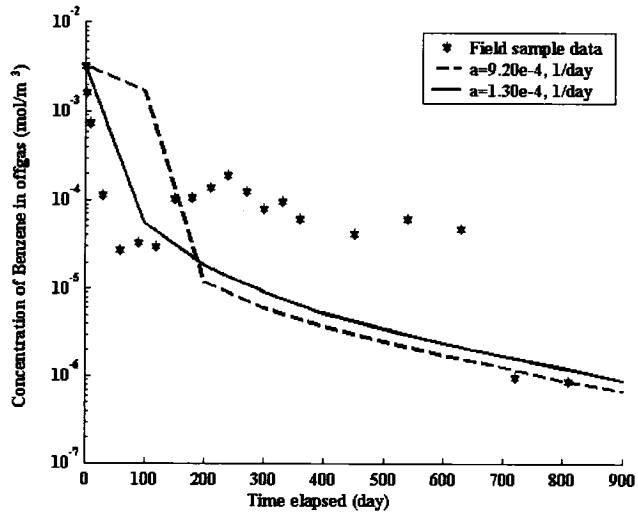

Figure 5-27 Influence of Empirical Parameter "a" (b=1.9) on Breakthrough Curves

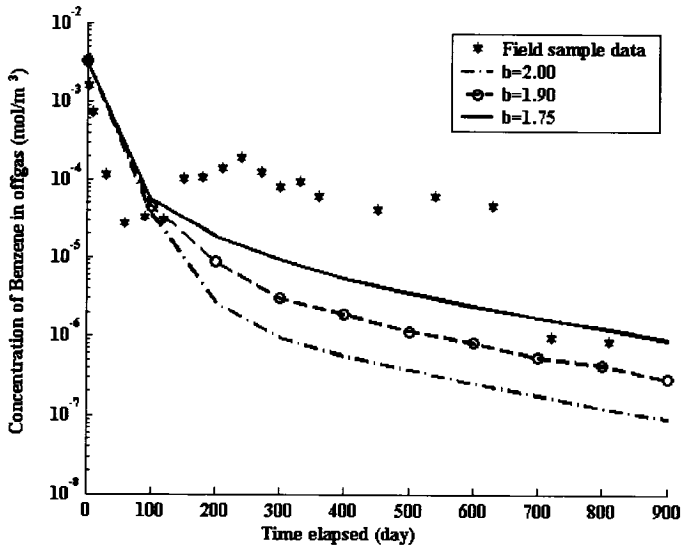

Figure 5-28 Influence of Empirical Parameter "b" on Breakthrough Curves ($a= 4.17*10^{-4}\ h^{-1}$)

Figure 5-29a shows the breakthrough curves of all BTEX compounds, which represent the outputs of the quaternary BTEX components from the simulation of the calibrated 3D-SVE-F model. These reasonable offgas concentration and the variations in mass transfer coefficients for BTEX compounds were based on calibrating the 3D-SVE-F model against the benzene data. The breakthrough curves from the sampled data of BTEX by CRA as shown in Figure 5-29b and the predicted breakthrough curves by the 3D-SVE-F models have consistent tendency.

This research attempts to explore the capability of the mathematical model capture the essential processes involved in an actual SVE setting rather than work out a relationship between lab-scale and field-scale models. For example, what caused the difference in "a" values between lab and field setting? There were differences like homogenous soil in the lab compared to non-homogenous in the field, dry soil in

the lab and wet soil in the lab. These factors and others can contribute to the differences noted, and are part of the scale-up factor. The examination of scale up factor is an important issue that needs to be considered. However, investigation into the actual scale –up factor was beyond of the scope of this research topic.

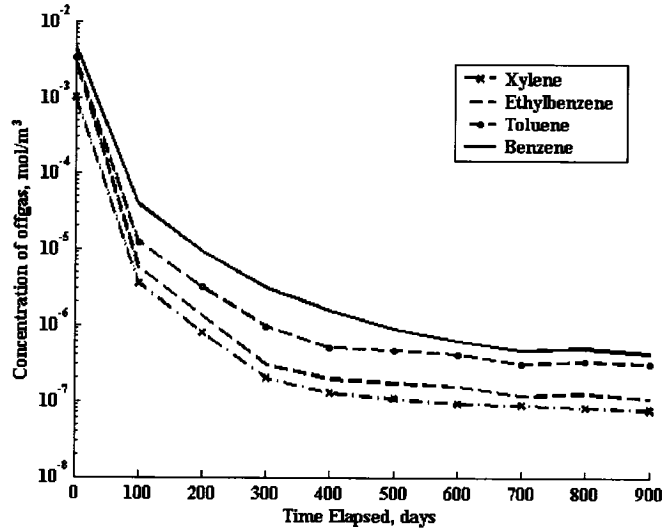

Figure 5-29(a) Breakthrough Curves of BTEX from the Calibrated 3D-SVE-F Model

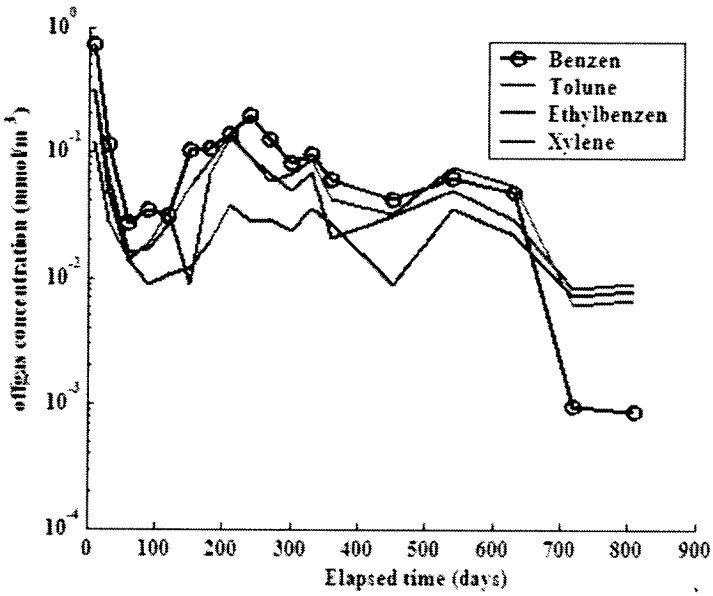

Figure 5-29(b) Breakthrough Curves of BTEX from the sampled data by CRA

5.2.5 The Behaviour of the 3D- SVE- F Model

This section demonstrates the outputs of the simulated primary unknowns in the governing equations by means of the calibrated field-scale 3D-SVE-F model, such as the pressure field, saturation of a vapour phase, and concentration of benzene in soil vapour phase and offgas. The expected outcomes and the accuracy and realism of the numerical solutions for these primary unknowns are essential to confirm the precision of the empirical mass transfer parameters through calibration of the 3D-SVE-F model. Additionally, the pressure of a mobile phase and the concentration of contaminants in an SVE system also may be sampled and analyzed in order to improve the accuracy of numerical simulation and predictions for similar settings.

Predicting the concentration of contaminants in the offgas and the soil vapour phase might provide assistant information on the progress of remediation. In a field SVE operation, the distribution of the pressure around a venting well may be used to delineate the radius of influence (ROI) of the well with a controlled venting pressure. The ROI and spacing of wells can be estimated in terms of the pressure profile. Therefore, the fundamentals of the initial design of SVE configuration can be obtained in terms of the predicted pressure field by the 3D-SVE-F model. Meanwhile, the consequences of the design can be predicted such as closure time, pressure field and the distribution of contaminants.

Vacuum extraction wells produce a reduced pressure zone; the size of the reduced volume depends on the following elements (DiGiulio, 1992):

- applied vacuum pressure and surface treatment;

- venting geometry (e.g., depth to water table);
- soil heterogeneity; and
- permeability.

The impacts of these elements on the behaviours of the 3D-SVE-F model will be demonstrated in this section and next chapter respectively.

Laboratory-determined parameters using the simple models cannot directly represent field-scale processes because a lab experiment and simple model never incorporate enough information related to the physico-chemical processes, geometry of domain, layout issues and operational conditions in SVE field-scale settings. However, these elements are essential for the design of well spacing, number of wells, location of wells and radius of influence (ROI). Ultimately, the efficiency of an SVE operation dramatically relies on the profile of the pressure field. The parameter estimations on the pressure field directly influence the accuracy of the contaminant transport simulation.

A natural impermeable stratum above the contaminated soil or an artificial surface seal is needed to impede vertical air flow in a conventional SVE operation. Here, the characteristic pressure field was examined by means of the 3D-SVE-F model. Uncovered and covered surface situations affect the pressure pattern throughout the site; hence it has an impact on the velocity field and the profile of contaminant migration toward the venting well. For covered ground surface settings, the isosurface profile of the pressure field should be a cylindrical spread around the venting well with identically vertical distribution as shown in Figure 5-30. The

isosurface viewed from the bottom side is the same as the view from the top side because identical no-flow boundary conditions are assigned to both sides.

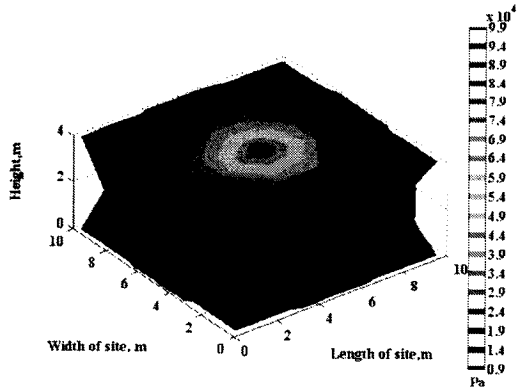

Figure 5-30 The Isosurface of Pressure Field with Covered Surface

For an uncovered ground surface, the top and bottom side pressure profiles are shown, respectively, in Figures 5-31 and 5-32. For uncovered ground surface, Figure 5-31 shows the upper projection of the pressure isosurface profile. Accordingly, the pressure at the uncovered surface is equal to atmospheric pressure. However, the pressure field viewed at the bottom side has a no-flow boundary, so the isosurface of pressure as shown in Figure 5-32 is the same as the settings of the covered surface case as shown in Figure 5-30.

Streamlines are drawn as the tangent value to the direction of radial velocity, which represents a path flow field along with vapour phase travel in a specific time period. The streamline and slice images of the simulated pressure fields, as shown in Figures 5-33 through 5-36, indicate the far sweep zone with a covered surface and the leakage shortcut of vapour flow with an uncovered surface. In SVE operations, establishing horizontal air flow in the vadose zone is favourable.

A cylindrical isosurface pressure profile shows the radial uniform distribution with a covered surface. Additionally, Figure 5-33 illustrates the vertically identical pressure distribution because of the identical top and bottom boundary conditions. A cone-shaped pressure field appears in the uncovered situation as shown in Figure 5-35, which causes the reduced radius of influence.

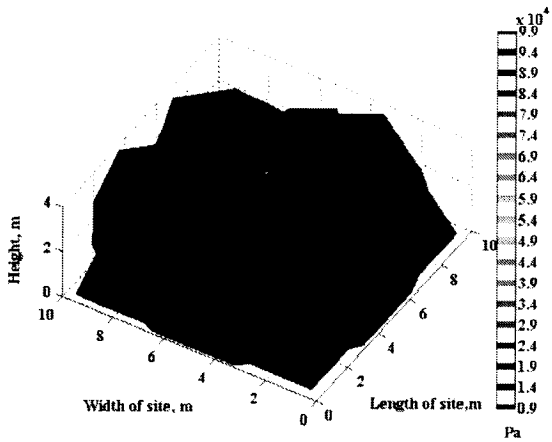

Figure 5-31 The Isosurface of Pressure Field with Uncovered Surface (top side view)

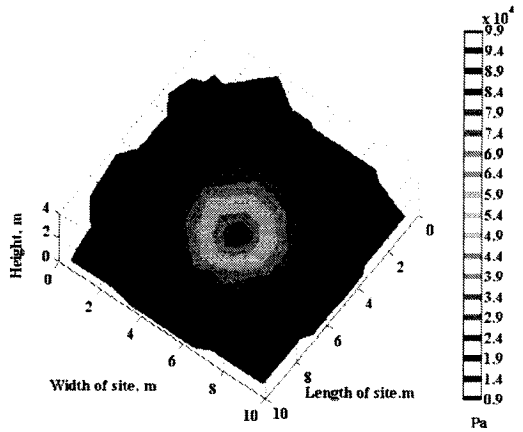

Figure 5-32 The isosurface of Pressure Field with Uncovered Surface (bottom side view

(Bottom projection similar to the pressure distribution with covered surface)

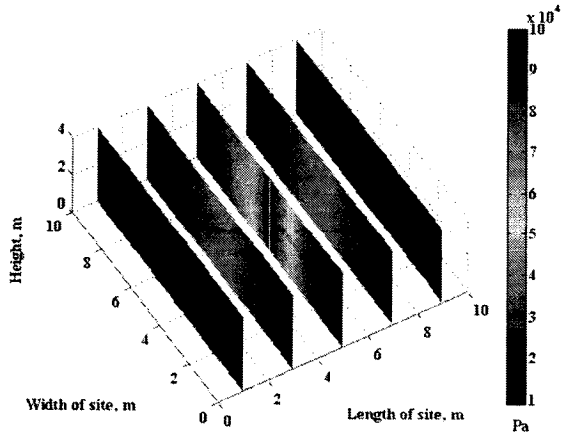

Figure 5-33 Slices of Pressure Field with Covered Surface Site

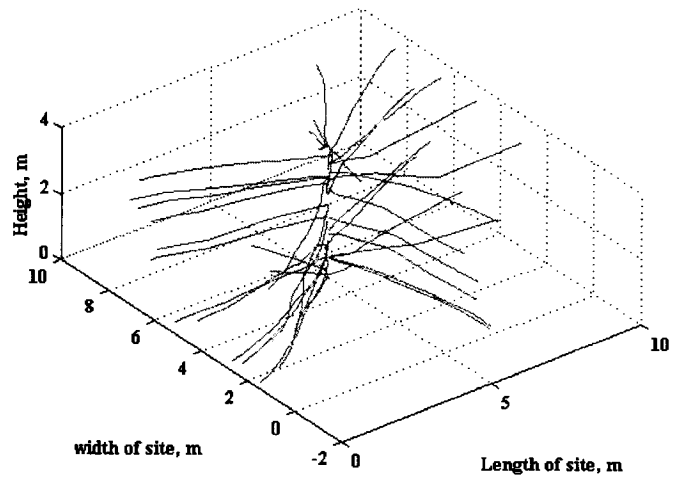

Figure 5-34 Streamlines of Pressure Field with Covered Surface Site
(streamlines have 30 start points)

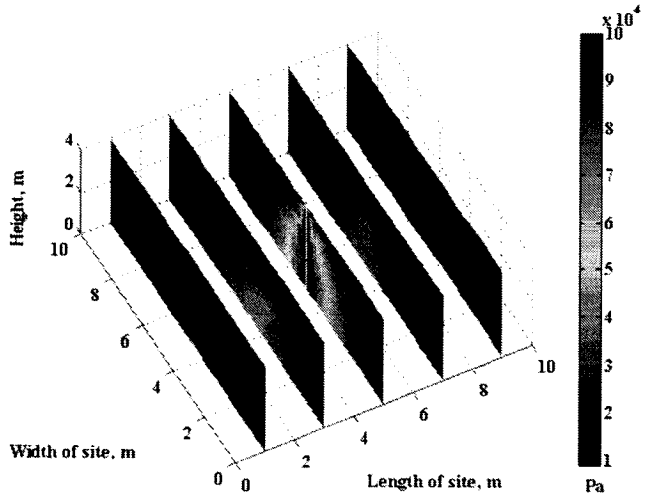

Figure 5-35 Slices of Pressure Field with Uncovered Surface Site

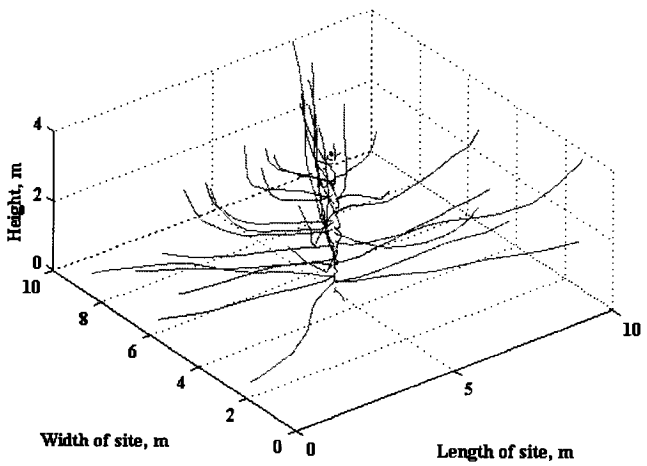

Figure 5-36 Streamlines of Pressure Field with Uncovered Surface Site
(streamlines have 30 start points)

As shown in the preceding figures, having a covered surface is very helpful in improving the mass removal effectively because of a more extensive ROI. The streamlines of pressure are shown in Figure 5-34 under the covered-surface condition; the uncovered surface leakages emerge near the venting well as shown in Figure 5-36.

One of the most important factors in determining the duration of SVE is the extent of air flow in the subsurface (Massman and Farrier, 1992; Massman and Madden, 1994). Obviously, a covered surface can cause more effective remediation than an uncovered surface. Comparisons of the breakthrough curve indicate that the covered treatment causes a greater removal rate, as shown in Figure 5-37.

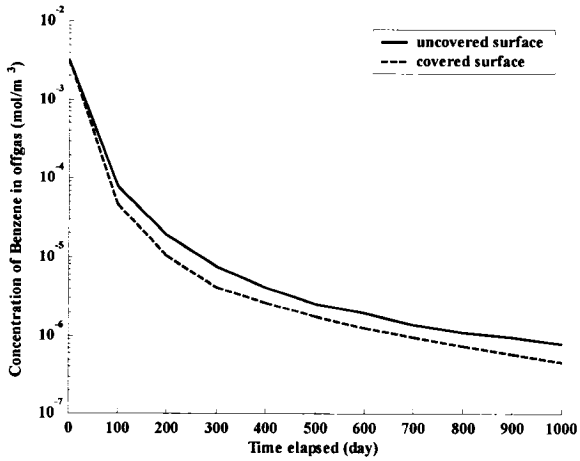

Figure 5-37 Concentration of Offgas by Covered and Uncovered Surfaces

Although the ROI may be used to confirm the number of venting wells needed, it does not imply that the site can be cleaned up under the estimated ROI range (Beckett and Huntley, 1994). The reasonable theoretically estimated pressure profile is the prerequisite for further predicting of the concentration of contaminants throughout a site as time passes. Based on the predicted pressure, the coupled 3D-SVE-F model has the ability to predict the concentration of contaminants and the impact of pressure.

As a controlled condition of SVE operation, the magnitude of the venting vacuum pressure also affects the efficiency of SVE operation as shown in Figure 5-39.

The higher the vacuum pressure, the faster the remediation and the lower concentration of offgas. Increasing the venting pressure can also impact the concentration of offgas and the soil vapour over an entire site as shown in Figures 5-38 and 5-39.

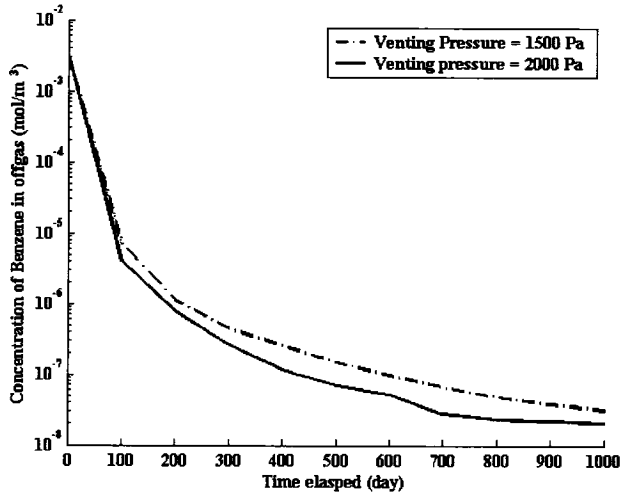

Figure 5-38 The Impact of Venting Pressure on Offgas Concentration

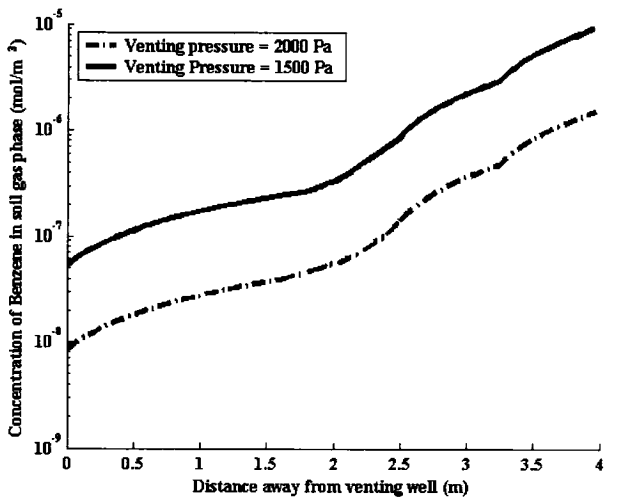

Figure 5-39 The Impact of Venting Pressure on the Concentration of Soil Vapour Phase

As an essential feature, the permeability of site soil and its variations have a significant impact on the removal rate of contaminants. The higher permeability will create a higher seepage velocity, thus lowering the concentration of offgas as shown in Figure 5-40.

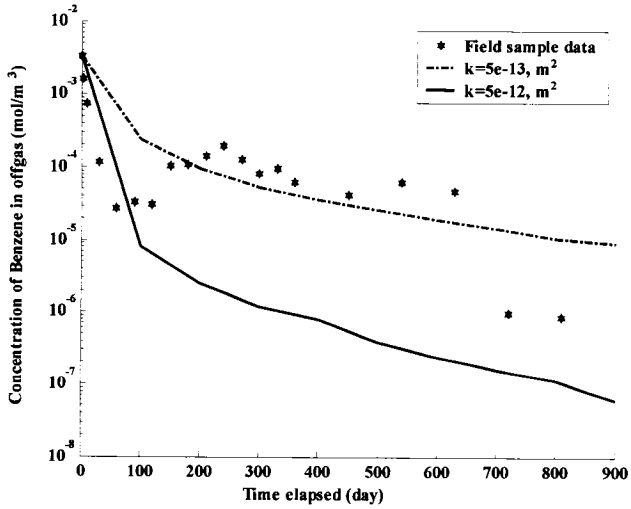

Figure 5-40 The Effect of Soil Intrinsic Permeability on Offgas Concentration

5.2.6 Stability and Convergence Analysis for 3D-SVE-F Numerical Model

Compared to the lab-scale case, the 3D-SVE-F model has a more daunting computational load. It is important to explore the stability and convergence of the numerical simulation of the 3D-SVE-F model and determine the optimized number of finite elements and time step. The selected size of finite element mesh should fall into the range of number where minimal variations occur during the refining of the spatial and temporal discretization. The data listed in Tables 5-14 and 5-15 indicate that stable solutions are available over a wide range of time steps by the low number of

mesh refinements using FEMLAB. FEMLAB can handle actual SVE modeling simulation as a predicting and monitoring tool with stable spatial and temporal discretization.

Table 5-14 3D-SVE-F Model Stability on the Time Discretization

Time step (days)	The concentration of offgas (mol/m^3)	
	t=400 days	t=900 days
10	3.294e-5	1.0077e-6
2	3.294e-5	1.077e-6
1	3.294e-5	1.077e-6
0.5	3.264e-5	1.077e-6

* the number of finite element in mesh 2657

Table 5-15 3D-SVE-F Model Stability on the Mesh Refinement

Number of finite element mesh	The concentration of offgas, mol/m^3	
	t=400 days	t=900 days
1102	3.294e-6	1.077e-6
2615	3.300e-6	1.092e-6
3217	3.321e-6	1.109e-6
3456	No solution	No solution

* time step is equal to 1 day.

As shown in Tables 5-15 and 5-16, FEMLAB produces a highly consistent solution for a wide range of time steps. In order to obtain both the accurate solution and fast program execution time, choosing the time step of one day is appropriate. The number of finite element mesh of 2615 is chosen as reasonable to conduct the numerical simulation for the 3D-SVE-F model.

CHAPTER 6

APPLICATION OF 3D-SVE-L/F MODELS

Throughout the preceding discussion, numerical simulations for lab and field SVE by the 3D-SVE-L/F models have been completed the model was calibrated to lab-scale and field-scale experiments with the relevant inputs. In this chapter, the 3D-SVE-L/F models are examined further with respect to:

1) SVE operation in a hypothetical heterogeneous site simulation

2) Sensitivity of 3D-SVE-L/F models

3) Predicting the closure time of lab-scale and field-scale cases

4) Design protocol.

6.1 Modeling in a Heterogeneous Domain

In addition to rate-limited mass transfer, which causes non-ideal nonequilibrium performance of SVE (Abriola et al., 1999), prolonged tailing effects originate from two main reasons:

- nonuniform distribution of contaminant mixtures in subsurface and local lower permeability in the subsurface (Johnson et al., 1990a, b);
- air bypasses the residual and saturated zone (Ho and Udell, 1992).

Currently, little modeling effort on tailing effects has been reported in research literature, particularly with three-dimensional medium heterogeneities and nonequi-librium mass transfer. Exploring the implications of nonequilibrium

interphase mass transfer of two-dimensional and three-dimensional models requires the analysis of the effluent gas concentration from the field-scale investigation with significant heterogeneity (Powers et al., 1992). Air permeability can vary greatly over the entire site in the range of 100- to 10,000-fold, depending on the soil types (Baehr and Hult, 1991). With the aid of the 3D-SVE-F model, the present work can study the impact of porous medium heterogeneity on the long tailing effect.

An ideal three-layer soil porous medium is hypothetically simulated to investigate the impacts of the heterogeneous permeability as shown in Figure 6-1. The permeability with the top layer and bottom layers is equal to $3*10^{-12}$ m, which is the same as the homogeneous domain simulated in Section 5.2. The middle layer has a permeability 10^2 higher than top and bottom layers, i.e., $3*10^{-10}$ m. All other inputs are the same as the previously modeled CRA SVE scenario in Section 5.2. The SVE model for this heterogeneous domain is entitled 3D-SVE-FH model.

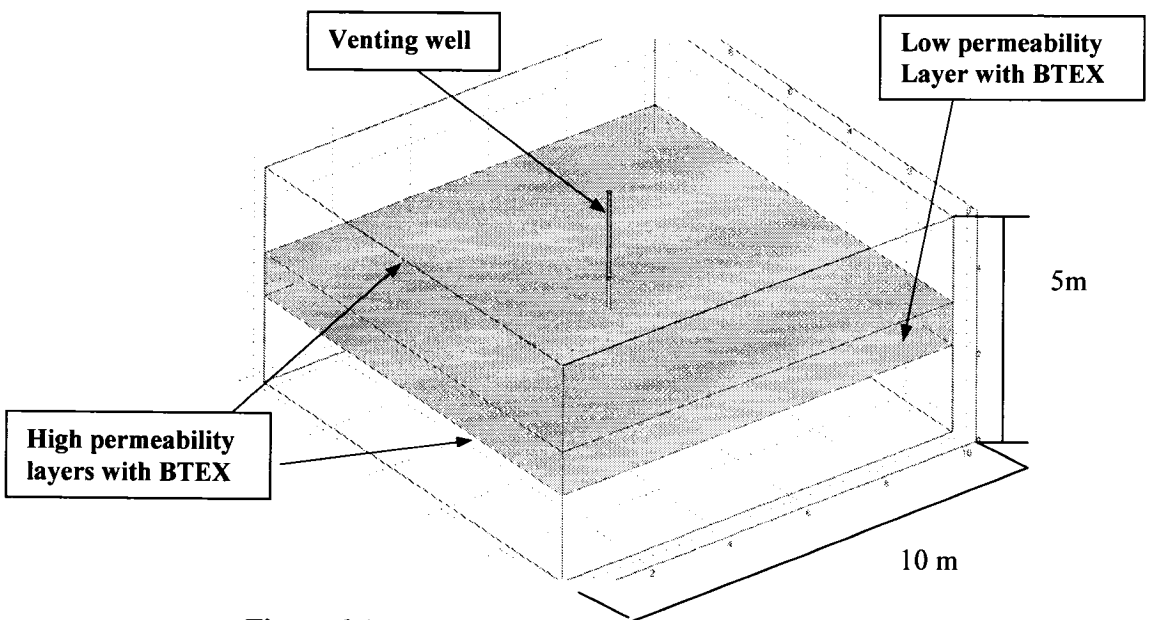

Figure 6-1 The Hypothetical Heterogeneous SVE Site

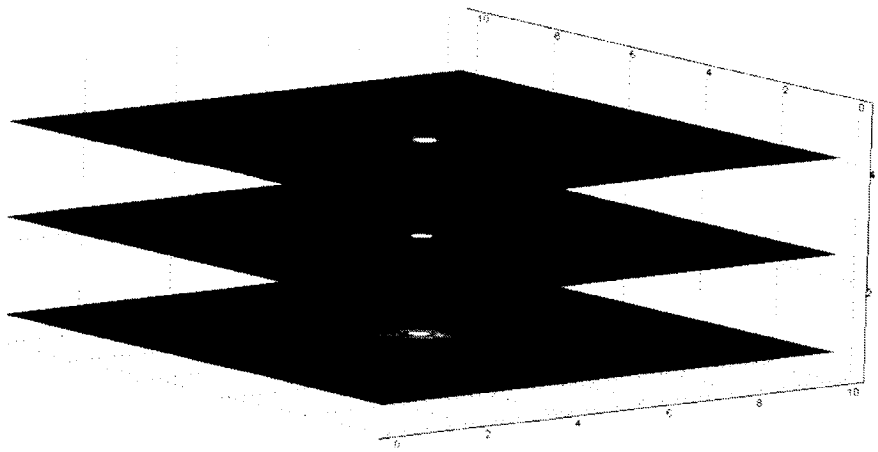

Figure 6-2 The Profile of Concentrations Distributed in Different Zones

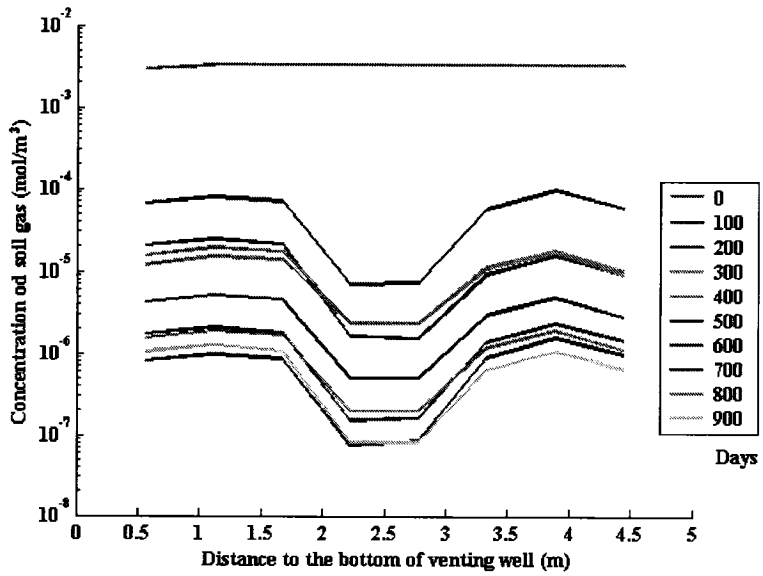

Figure 6-3 The Concentration of Benzene in Soil Vapour versus Time along vertical line 0.05 m radially away from venting well

The distribution of benzene contaminant in three layers in the vicinity of the venting well at 900 days is shown in Figure 6-2. The apparent higher concentration of contaminants in soil vapour phase is in the region where the permeability is lower.

Figure 6-3 shows the distribution of the concentration of benzene in soil vapour phase versus time along the line connected from two point coordinates (5, 5.5, 0) and (5, 5.5, 5) in the simulated domain and 0.5 m away from the venting well, parallel to the venting well. During a certain elapsed time, the simulated results show that benzene in the soil vapour phase is distributed mainly in the low permeability zone at the tailing stage. This indicates that the contaminants in soil vapour phase in the higher permeability vadose zone have been easily removed by advection-dispersion transport with higher seepage velocity and rate of mass transfer. However, the contaminants distributed in the lower permeability vadose zone still remain in the soil vapour phase due to the lower seepage velocity. The contaminants in the low permeability zone further diffuse into the adjacent layers, contributing to tailing effects. If the venting well is shut down, and then reopened, the concentration of offgas will rebound because of the diffusion. This result implies the importance with respect to exploring the variations in permeability over the soil site and conducting a thorough site investigation before SVE operations.

6.2 Sensitivity Analysis by Multivariable Regression Method

Once an adequate numerical model has been obtained, sensitivity analysis must be completed as an integral part of modeling studies. Doing so will bring improvement in the input parameters and the control processes involved. This section elaborates on the procedure for the multivariable regression method and implements sensitivity analysis of the 3D-SVE-L/F models. With multivariable regression method,

modelers are able to identify the combined influence of multiple dominant parameters on the performance of an SVE system. In this context the empirical mass transfer parameters, intrinsic permeability, and dispersivity were chosen to conduct the sensitivity analysis.

6.2.1 Introduction to Sensitivity Analysis of an SVE Model

In a vadose zone numerical simulation, all parameters incorporated in the developed mathematical model may not play an isolated role under given circumstances. Complicated cross-mutual actions may be present. Very few researchers have explored the issues of sensitivity of an SVE model for parameters (Rathfelder et al., 1991); fewer studies have dealt with the multiple parameter sensitivity analysis simultaneously. The conventional method for sensitivity analysis of a hydrological model is only an expedient approach for contamination in the vadose zone like SVE remediation operation. Especially, sensitivity analysis of SVE models is not common.

In conventional sensitivity analyses, one parameter is changed at a time, while keeping all other parameters as constants at fixed base values (Kaleris, 2002). The base values and the range of the possible uncertainty, which depends on site or remediation operation conditions, are set up for all the parameters considered uncertain (Mendoza and Frind, 1990b; Gribb, 2002). By using the conventional method, Rathfelder et al. (1991) and Poulsen et al. (1996) investigated the effects of multiple parameter variations on SVE efficiency.

In fact, modeling results may depend on more than one independent parameter simultaneously. Multivariable regression analyses can be used to establish the relationship among the parameters involved in a multiphase flow and transport of multicomponent model (Fanchi, 2001). Even if one is interested in the effect of only one variable involved in a model, it usually is wise to include other variables influencing the outputs of the models (McBean and Rovers, 2001). The principle of multivariable regression method has been applied in a wide variety of industries to analyze multiple element influences (Wonnacott and Wonnacott, 1981). Relative to the conventional sensitivity analysis method dealing with multiple controlling parameters, the use of multivariable regression to deal with the sensitivity issues of the SVE model has distinct advantages in that it:

- executes sensitivity analysis by a mathematical method;
- considers the uncertainty of the multiple controlling parameters simultaneously;
- reduces stochastic error and therefore reduces the residual variance and causes confidence intervals to be more precise;
- eliminates bias that might occur if the variable is neglected that might influence the response of a model substantially; and
- reflects the interaction among the predictors because the association of predictors is estimated. The greater the number of variables that would affect the responses that are included, the more precise is the response to the variations in the simulated results depending on the predictors (Fanchi, 2001).

6.2.2 Sensitivity Analysis by Multivariable Regression Method

6.2.2.1 Multivariable Linear Regression Method

All integrated controlling parameters that may affect the sensitivity of the 3D-SVE-L/F models are called predictors. If the p sampling values of a controlling parameter and n parameter predictors are incorporated into a multivariable parameter regression model, the sample matrix of the predictor X is expressed as:

$$X = \begin{vmatrix} 1 & x_{11} & x_{12} \ldots\ldots & x_{1p} \\ 1 & x_{21} & x_{22} \ldots\ldots & x_{2p} \\ & & \ldots\ldots & \\ 1 & x_{n1} & x_{n2} \ldots\ldots & x_{np} \end{vmatrix} \quad (n=1.....N;\ p=1.....P) \qquad (6.1)$$

Where:

n = number of parameters considered in sensitivity analysis

p = number of samples for a parameter in sensitivity analysis.

The simulated results for the 3D-SVE-L/F models for the predictors are called regressors. In this context, the regressor is expressed as the matrix of offgas concentrations as follows:

$$C_g = \begin{bmatrix} y_1 \\ y_2 \\ \ldots \\ y_N \end{bmatrix} \qquad (6.2)$$

Where:

C_g = concentration of component in vapour phase, mol/L^3

y = the simulated results for n-th series of sampling values, mol/L^3

In order to overcome the round-off error introduced by the big difference in the magnitude of the related parameters during the statistical procedure of multivariable regression, the standardized variables for a series of samples for a parameter are defined as:

$$\delta_{n,p} = \frac{X_{n,p} - \overline{X_n}}{\sigma_n} \tag{6.3}$$

Where:

$\delta_{n,p}$ = standardized variables of the i-th sample of the n-th parameter

$X_{n,p}$ = i-th sampled value of the n-th parameter, $p=1...P$

$\overline{X}_n$ = mean of all samples of the n-th parameter

σ_n = variance of a series of samples of the n-th parameter involved in sensitivity analysis.

The physical meaning of the standardized variable in Equation (6.3) represents the deviation of a parameter per unit variance of the parameter samplings. According to the definition by Wonnacott and Wonnacott (1981), the sample variance of the predictors, which are associated with the inputs for the 3D-SVE-L/F models is expressed as:

$$\sigma_n = \frac{1}{n}\sum_{p=1}^{P}(\delta_{n,p} - \overline{\delta}_n)^2 \tag{6.4}$$

Where:

$\overline{\delta_n}$ = average of the samples of the n-th parameter.

Generally, the sensitivity formulation of a model is constructed by applying the following procedure:

- obtain the simulated results by running the numerical models for the predictor sample matrix X defined in Equation (6.1);

- calculate the multivariable regression equation.

Therefore, the sensitivity of the 3D-SVE-L/F models is the response to the change in unit variance of a series of samples, which is an index to explore the possible range of changes in a controlling parameter. The final sensitivity model responds not only to the change in the values of multiple parameters, but also to the possible range of the values concerned and interrelation between these parameters.

According to the rationale of a multivariable linear regression (Younger, 1979), the relationship between the standardized variables in Equation (6.3) and the response from the simulated results is denoted in terms of the multivariable linear regression equation:

$$C_g = \alpha_0 + \alpha_1\delta_1 + ...\alpha_j\delta_j .....\alpha_n\delta_n + e \tag{6.5}$$

$$\alpha_j = \frac{\partial C_g}{\partial \Delta \delta_X} \tag{6.6}$$

Where:

e = error of linear multivariable method

δ = standardized variable

α_0 = constant in linear multivariable regression equation

α_j = linear regression coefficients of the variable j.

Equation (6.5) can be expressed as the matrix of coefficients of the multivariable linear regression Equation (6.5):

$$C_g = \alpha\delta_n + e \tag{6.7}$$

Where:

$$\boldsymbol{\alpha} = \begin{bmatrix} \alpha_0 \\ \alpha_1 \\ \cdots \\ \alpha_j \\ \cdots \\ \alpha_n \end{bmatrix}$$ matrix of the constant and coefficients which compose the linear regression equation

$\boldsymbol{\delta_n}$ = standardized variables for parameter samples defined in Equation (6.3), also called regressors.

The coefficients in Equations (6.5) or (6.7) mean that the change of offgas concentration results from an increase in unit δ_n while other variables are held constant. Conservative interpretation for the estimates of the linear regression coefficients by the magnitude and the sign of the estimates of the coefficients in the linear regression equation has been addressed clearly (Wonnacott and Wonnacott, 1981). The sign of the parameter estimates indicate the direction, i.e., increase or decrease, of the relations between the predictors and responses.

6.2.2.2 Significance and Standard Error of Estimates

The standard error of estimates may be estimated by the variance described in the form of a matrix. The variance of the coefficients in the multivariable regression equation is expressed as:

$$\text{var}(\alpha) = s^2(\delta_n^T \delta_n)^{-1} \tag{6.8}$$

Where:

var(α) = variance of the coefficients

s = standard error of estimate

δ_n^T = transfer matrix of δ_n.

The residual variance of the response estimated is expressed by:

$$s_e^2 = \frac{1}{p-n-1}\sum_{p=1}^{P}(C_{g,p} - \hat{C}_g)^2 \tag{6.9}$$

Where:

$C_{g,i}$ = predicted i-th concentration of offgas from 3D-SVE-L model, mol/L^3

$\hat{C}_g$ = average value of concentration of offgas, mol/L^3

$df = p-n-1$, is defined as the freedom of regression estimates.

The standard error of estimate from multivariable regression can be used to formulate the maximum and minimum estimates under a confidence interval for a given series of controlling parameters. The confidence interval is expressed as 100*(1-α) %. The distribution of *"α"* relates to the significant level of the multivariable linear regression. Significance levels show how likely it is that a result is due to chance. Highly significant estimates mean that these estimates are very probably true if confidence interval is 95% (Younger, 1979).

For a confidence interval of mean response and individual response, $t_{0.05}$ for the corresponding *df* value is obtained by the *t*-distribution table in Wonnacott and Wonnacott (1981). The true value is estimated by the multivariable linear Equation (6.5), and then the general form of a 95% confidence interval considering the regression error. The actual output will fall into the range which is expressed as:

$$C_g^e = C_g \pm t_{0.025} s_e \sqrt{1 + x_0 (X^T X)^{-1} x_0} \tag{6.11}$$

Where:

C_g^e = estimate of concentration of offgas with 95% confidence interval, mol/L^3

C_g = the predicted concentration of offgas by sensitivity model, mol/L^3

$$x_0 = \begin{vmatrix} \delta_1 \\ \cdot \\ \cdot \\ \delta_i \\ \cdot \\ \delta_m \end{vmatrix}, i=1\ldots m \text{ (the number of the multiple variables estimated)}$$

Considering confidence intervals and the standard error of the estimated coefficients, the values of the estimated coefficients in the resultant multivariable linear regression equation are expressed as:

$$\alpha_i = \hat{\alpha}_i \pm t_\alpha \, \mathrm{var}(\sigma)_{\alpha,j} \; (i=1\ldots p) \tag{6.12}$$

Where:

$\hat{\alpha}_i$ = estimate of coefficient

α_i = possible maximum and minimum values by considering the standard errors

$\mathrm{var}(\sigma)_{\alpha,i}$ = variance for the estimate of $\hat{\alpha}_i$

t_α = considered confidence interval from student distribution.

6.2.3 The Sensitivity Analysis for the Calibrated 3D-SVE-L Model

Using the above-summarized multivariable linear regression method, the consequences for sensitivity analyses of the 3D-SVE-L model were illustrated in this section. The intrinsic permeability of soil, dispersivity and two empirical mass transfer parameters "a" and "b" are chosen to engage the sensitivity analysis of the 3D-SVE-L model. Soil permeability is the most sensitive during the venting

operation (Rathfelder et al., 1991), and of all soil physical parameters, it has the greatest variation. There is very little knowledge of dispersivity in the SVE field. But the dispersion process has a considerable effect on the removal rate of contamination. Based on the one-dimensional column experiment and mathematical modeling investigation, Cann et al. (2002) and Gidda et al. (2006) proved the importance of the appropriate dispersivity for SVE modeling consequences. On the other hand, Armstrong et al. (1994) determined that a lab-scale model is insensitive to dispersivity. Mass transfer coefficients which consist essentially of the empirical parameters can be obtained only by calibrating a model. In summary, these four properties were considered because all four parameters have been demonstrated to significantly influence the performance of SVE operation, respectively, by others.

The data set used to calculate the sensitivity model is listed in Appendix. Tables B1 and B2. Table 6-1 gives the range of the parameter values handled.

Table 6-1 The Range of Estimated Parameter Values for Sensitivity Analysis of the 3D-SVE-L Model

Parameters	Range of values	Remarks
Intrinsic permeability, k, m^2	$6*10^{-10}$-$4*10^{-13}$	Typical range for SVE site
Longitudinal dispersivity, α_L, m	0.037-0.1	Gidda et al., 2003; Rathfelder et al., 2000
Empirical mass transfer parameter, a, $hour^{-1}$	10-40	Determined by the 3D-SVE-L model
Empirical Mass transfer parameter, b	1.6-2.0	Determined by the 3D-SVE-L model

After applying the constructed sensitivity approach and a series of data as noted above for a 50 hour elapsed time, the sensitivity equation of the calibrated 3D-

SVE-L model for the four parameters is given by the following linear regression equation:

$$C_{50} = 0.0672 - 0.0213\delta_k - 1.98\delta_{\alpha L} - 0.12\delta_a - 3.02\delta_b \qquad (6.13)$$

Where:

C_{50} = concentration of offgas at t=50 hour time elapsed, mol/L^3

δ_i = standardized parameters of the linear regression equation for variables defined in Equation (6.3), *i* refers to the considered parameters, i.e., intrinsic permeability *k*, longitudinal dispersivity α_L, empirical mass transfer parameters *a* and *b*, respectively.

The resulting minimum and maximum estimated standard error of regression coefficient and the residual variance of the predicted results from the sensitivity linear regression model are listed in Tables B3 and B4 in the Appendix. Figure 6-4 illustrates the multivariable linear regression sensitivity results for the 3D-SVE-L model. The figure shows the constants, the four coefficients and their minimum and maximum values under a 95 % confidence interval. These results demonstrate that the estimates for the regression coefficients are highly significant.

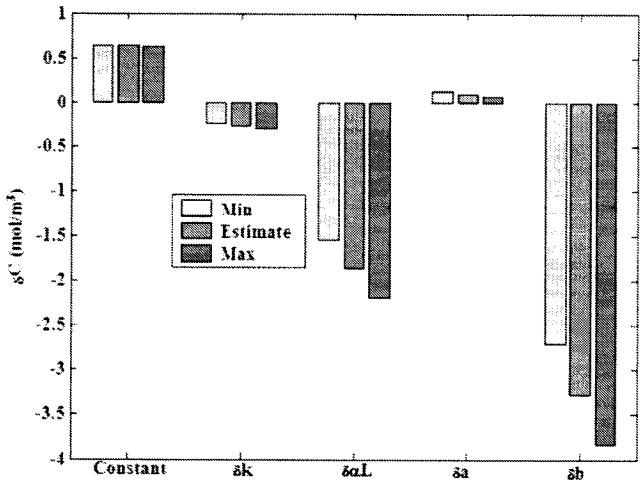

Figure 6-4 95% Confidence Interval Coefficients of Regression for the 3D-SVE-L Model (t=50 Hours)

In terms of sensitivity model Equation (6.13) of the 3D-SVE-L model, the most sensitive parameter for the concentration of offgas "C_{50}" is empirical mass transfer parameter "b" which is the exponent of the NAPL saturation in the mass transfer coefficient. The second one is dispersivity, while the third is the permeability and the least sensitive is the other empirical mass transfer parameter "a". This sequence shows that relative significance of empirical mass transfer parameters and system parameters involved in the 3D-SVE-L model. A review of the literature (Gidda, 2003) has shown the dominant mass transfer process in SVE is volatilization from NAPL to vapour phase. Since the lab experiment was conducted only in air dry condition, it was decided that aqueous to vapour phase mass transfer has the minimal importance. The sensitivity analysis of a one-dimensional SVE transport model determined that the mass transfer from the NAPL to aqueous phase and longitudinal dispersivity are insensitive in the range of studied values (Rathfelder et al., 1991).

Therefore no sensitivity testing for empirical mass transfer parameters "c" and "d" was done for the 3D-SVE-L model.

While the modeling results indicate a lower sensitivity for permeability and dispersion than one of the empirical mass transfer parameters, it is desirable to collect more consistent and intensive data during site characterization and evaluate the impacts of permeability and dispersivity properties. The mass transfer coefficient is most sensitive, which implies that the knowledge of mass transfer and the relevant mechanism is critical for improving the predictive capacity and accuracy of models.

6.2.4 Sensitivity Analysis of the Calibrated 3D-SVE-F Model

The behaviours of the 3D-SVE-L/F models reasonably and quantitatively describe the performance of the lab and field SVE remediation operations. In particular, the calibrations of the field-scale model precisely match the non-ideal characteristics due to integrating the characteristic rate-limited mass transfer. A sensitivity analysis provides the insights into the impact of the uncertainty of parameters and their likely variations on the behaviour of the 3D-SVE-F model. A well-informed selection of parameters for all SVE systems available is necessary to consider the possible variation of intrinsic permeability, porosity, dispersivity, organic carbon content, distributions of contaminants and heterogeneity of porous media. For the 3D-SVE-F model, four parameters, intrinsic permeability, dispersivity, and two empirical mass transfer parameters "a" and "b" were chosen to conduct the

sensitivity analysis. The entire dataset of these relative parameter samples to be used to calculate the sensitivity linear regression equation is listed in Appendix B5. The ranges of the relevant parameters are summarized in Table 6-2. The sensitivity multivariable regression linear equation for these four parameters is calculated as:

$$C_{100} = 0.824 - 1.734\delta_k + 0.526\delta_{\alpha L} - 1.892\delta_a + 2.132\delta_b \qquad (6.14)$$

Where:

C_{100} = predicted concentration of offgas at t= 100 days elapses time by multivariable linear regression sensitivity model, mol/L^3

δ = estimated coefficients of the linear regression equation for variables defined in Equation (6.5); the considered parameters are k, α_L, a and respectively.

For the smaller than 95% confidence interval, the estimates of the coefficients and constant composing the sensitivity regression equation keep similar trends as lab-scale sensitivity results as shown in Figure 6-5. It is seen that the multivariable linear regression sensitivity estimate is highly significant. The consistencies of the minimum and maximum estimates indicate that it is very appropriate to develop the sensitivity model for the 3D SVE model by the multivariable linear regression method. The estimates are highly significant. In terms of the coefficients given in Equation (6.14) and visually shown in Figure 6-4, the order of sensitivity of parameters is empirical mass transfer parameter "b", "a", permeability and dispersivity.

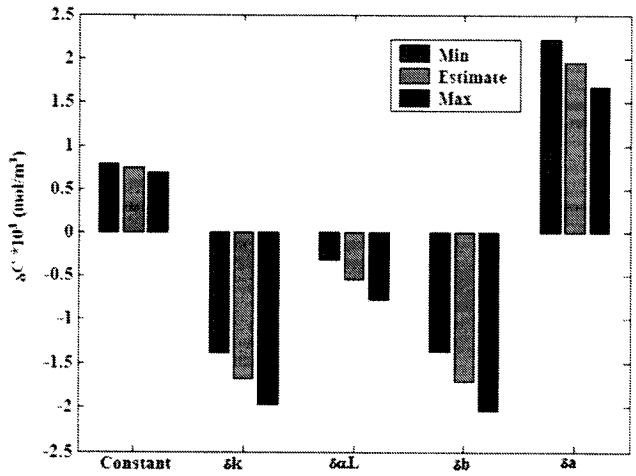

Figure 6-5 95% Confidence Interval Coefficients and Constant of Regression Equation for 3D-SVE-F (t=100 days)

In order to compare the significance of the different interphase mass transfer processes considered possibly present in SVE operation to the simulated results, the multivariable regression sensitivity analysis was extended to introduce two additional empirical mass transfer parameters *"c"* and *"d"*, which are formulated in the mass transfer coefficient expression for aqueous to vapour phase (see Table 5-4). This is due to the higher water content in the field SVE that may be present as compared to the lab studies. The examined ranges of these six parameters are listed in Table 6-2.

Table 6-2 The Range of Estimated Parameters Values for Sensitivity Analysis of the 3D-SVE-F Model

Parameters	Range of values	Remarks
Permeability, k, L^2	1.0^{-10} - $6*10^{-13}$	Vogele, 1996
Empirical Mass transfer parameter "a"	10^{-3} - 10^{-4}	Present work
Empirical Mass transfer parameter "b"	1.6 - 2.0	Present work
Empirical Mass transfer parameter "c"	0.001- 0.1	Gidda, 2003
Empirical Mass transfer parameter "d"	1.6 - 2.0	Gidda, 2003
Dispersivity, α_L, m	0.36 - 0.75	Rathfelder et al., 2000

This six-parameter multivariable linear regression sensitivity model is denoted by Equation (6.15) and the corresponding constant and estimates of coefficients, including the minimum and maximum estimates of constant and coefficients under a 95% confidence interval, which are shown in Figure 6-6. The most sensitive parameter is the empirical parameter "b" in NAPL-vapour mass transfer coefficient. The order of decreasing sensitivity for the other considered parameters is empirical mass transfer parameter *"a"* contained in NAPL-vapour phase mass transfer coefficient, intrinsic permeability and dispersivity. The least sensitive parameters are the empirical parameters *"c"* and *"d"*. Therefore, it is reasonable that empirical mass transfer parameters for aqueous-vapour phases are treated as constants during calibrations of the 3D-SVE-F model. This consequence also supports the reason not to pursue sensitivity studies for "*c*" and "*d*" in lab-scale cases.

$$C_{400} = 0.0676 - 0.059\delta_k - 0.044\delta_{\alpha L} + 0.05171\delta_a + 0.146\delta_b - 0.00021\delta_c + 0.0287\delta_d \quad (6.15)$$

Where:

C_{400} = predicted concentration of offgas at t= 400 days elapsed time by multivariable linear regression sensitivity model, mol/L^3

δ = estimated coefficients of the linear regression equation for variables defined in Equation (6.3); the considered parameters are *k*, a_L, *a*, *b*, *c* and *d*, respectively.

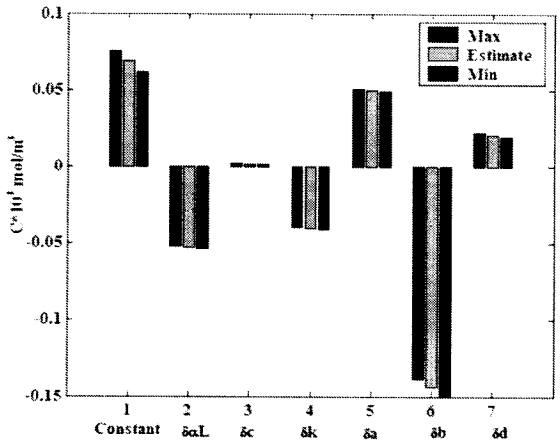

Figure 6-6 95% Confidence Interval Coefficients and Constant of Regression Equation for 3D-SVE-F Model (t=400 Days)

In summary, for the 3D-SVE-L/F models, the most sensitive parameters are the NAPL-vapour phase mass transfer coefficients. Therefore, the importance of studying mass transfer processes in SVE operation will play an essential role in accurately predicting the behaviour of SVE, especially when accurately matching the tailing stage.

The sensitivity of vapour extraction efficiency and contaminant migration to system parameters depends theoretically on well vacuum, NAPL-air mass transfer rate, permeability, and heterogeneities in soil (Poulsen et al., 1996, 1999). However, there have been no quantitative analyses to prove that these behaviours are reasonable for application to an SVE field operation. Certainly, it is unavoidable that the various inconsistent or biased conclusions have been drawn by the models of many different levels of complexity, which originated from various simplified scenarios in the conceptual models and the corresponding mathematical models. The pertinent conclusions come from the comprehensive field-scale 3D-SVE-F model because it

may handle more processes of SVE systems and simulate the real performance of SVE including the numerical simulation.

6.3 Prediction of the Closure Time of SVE

Closure time refers to the duration of operation for an SVE system to remediate a contaminated site to a safe level. The determination of closure time is directly related to the life-cycle cost of an SVE operation. The concentration of effluent vapour typically declines sharply by an asymptotic approach to zero or extended tailing performance (Digiulio, 1992). The decision-making process related to the closure time is important because tailing strongly affects cost effectiveness and the final cleanup level to which the contaminant is removed. The effective way would be to track tailing by the mathematical prediction, properly shut down SVE and then switch SVE operation to another cost-effective remediation option to achieve site closure. For example, as shown in Figure 6-7, a typical field SVE remediation operation breakthrough curve, apparently, the SVE operation during the tailing stage of 20-100 day elapsed time is not cost-effective because the cleanup level is not improved remarkably. If the concentration of offgas could be predicted by modeling studies and then analyzed to examine when the ideal time is to stop, there could be a substantial life-cycle cost saving for this SVE operation.

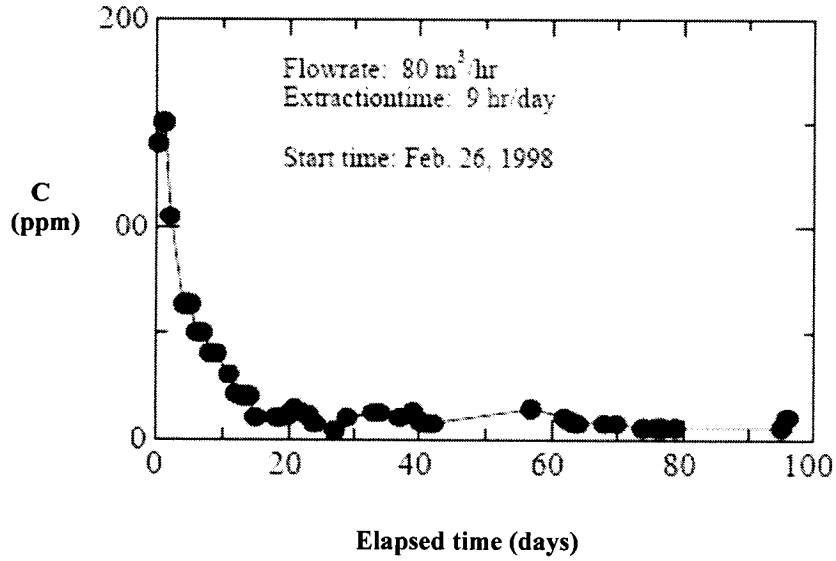

Figure 6-7 The Breakthrough Curve of Offgas Concentration of an SVE Rmediation (Chai and Miura, 2004)

As SVE proceeds, the personnel and equipment overhead will increase and have a major impact on cost. An accurate prediction for the closure time to adequately stop SVE is required. Currently there are very few discussions on SVE closure time in the literature (Barnes and White, 2006). On the basis of the accurately modeled results from the 3D-SVE-L/F models illustrated in the preceding chapters, a procedure is proposed in the present work. Firstly, it is proposed that the relative slope *"R"* of the breakthrough curve of the offgas concentration versus operation time be related to the removal degree in order to describe the performance of SVE tailing effects. Mathematically the definition of *"R"* is described by:

$$R = -\frac{C_{i+1} - C_i}{t_{i+1} - t_i} * \frac{1}{C_1} * 100\% \tag{6.16}$$

Where:

R = relative slope of the modeled breakthrough curve, T^{-1}

C_{i+1} = concentration of offgas at the t_{i+1} elapsed time, mol/L^3

C_i = concentration of offgas at the t_i elapsed time, mol/L^3

C_i = initial concentration of contaminant in the subsurface, mol/L^3

t = elapsed time of SVE operation, T.

The relative slope R of the breakthrough curves predicted by the 3D-SVE-L/F models are given in Appendix C as MATLAB files. Accordingly, the following modification of *"R"* is proposed considering the total elapsed time:

$$E = \frac{R}{t} \tag{6.17}$$

Where:

E = relative slope of breakthrough curve weighted by the operation time elapsed, T^{-2}.

The *"E"* index in Equation (6.17) estimates total relative efficiency of an SVE remediation operation over time. Normally, the tendency of index *"E"* is to decrease as the SVE operation proceeds. Take as an example, a lab-scale case where the simulated breakthrough curves demonstrate the procedure to track tailing progress by the variations of *"E"* during the overall SVE operation. As shown in Figures 6-8 one of the typical remediation cases is demonstrated by the experimental breakthrough curve, the predicted breakthrough curve by the calibrated 3D-SVE-L model and the distribution of E values and Δt. Figure 6-8(a) shows the actual experimental and simulated breakthrough curves; correspondingly, the curve of the *"E"* over elapsed time is drawn as shown in Figure 6-8(b) based on the simulated breakthrough curves.

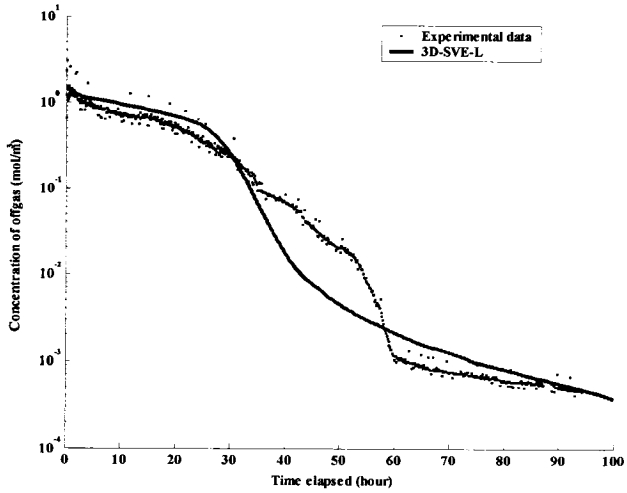

Figure 6-8 (a) Breakthrough Curves of Case 1

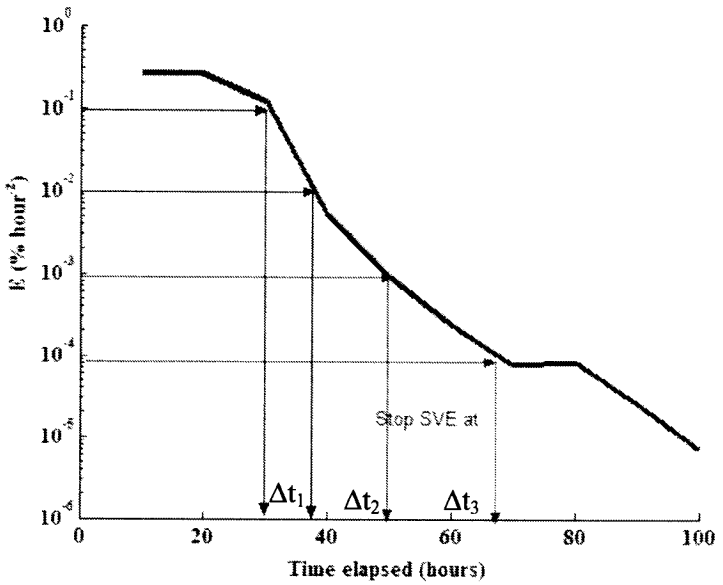

Figure 6-8 (b) The Operation Weighted Relative Slope of the Simulated Breakthrough Curve versus Elapsed Time for Case 1, Elora Silt ($\Delta t_1 < \Delta t_2 < \Delta t_3$)

The characteristic curves as shown in Figure 6-8 demonstrate that there are typically three stages in an SVE process:

- nonequilibrium terminal sharp decline stage,

- transition stage, and
- non-zero asymptotic stages.

Obviously, these three substages of the tailing stage can be represented by the ranges of *"E"* values and the corresponding time intervals:

1) $\Delta E = 10^{-1}$-10^{-2} % (terminal sharp decline stage) initial phase conversion rate of advection and dispersion, the early reduction of the relative slope of the breakthrough curve is insignificant,

2) $\Delta E = 10^{-2}$-10^{-3} % (transition stage) change from sharply decreasing area to non-zero asymptotic stage, which reflects the principal features of decontamination by SVE remediation technology. Stop time should be considered at the end of this stage,

3) $\Delta E = 10^{-3}$-10^{-4} % (non-zero asymptotic stage) a further 10-fold reduction of *"E"* value indicates a relatively long period of operation time but has little impact on the offgas concentration. During this stage, SVE operation is totally deficient. SVE should be shut down or switched to other effective remediation such as boiventing in order to reach the cleanup target of the site.

The intervals of the elapsed time corresponding to each equal specific decreasing fold of *"ΔE"* values, which characterize the progress of the tailing stage are represented by the elapsed time interval Δt_1, Δt_2, Δt_3, respectively. The next step is how to determine the proper closure time.

All calculated *"E"* values and breakthrough curves of the simulated cases in this work are referred to in Appendix D. The eight cases are chosen to determine the closure times in terms of *"ΔE"* values and the corresponding time intervals. Two of

ten simulated cases listed in Table 5-7 have not been examined for closure time because they have the relative short operation time of only two and nine hours. Reviewing all simulated cases by the 3D-SVE-L model, the following tendencies, which indicate the relationships among Δt_1, Δt_2, and Δt_3 are representative:

(i) $\Delta t_1 \leq \Delta t_2 < \Delta t_3$: this indicates that further SVE operation cannot significantly improve the level of cleaning;

(ii) $\Delta t_1 > \Delta t_2 < \Delta t_3$: is a typical SVE process, with early slow reduction, sharp decrease, and then approaching the tailing stage.

Accordingly, it is proposed that the *CTI* (critical time index) is related to the ratios of $\Delta t_2/\Delta t_1$ and $\Delta t_3/\Delta t_2$, and has significant implication for the tailing progress. Generally, for two continuous time steps, *CTI* is defined as:

$$CTI = \frac{\Delta t_{i+1}}{\Delta t_i} \tag{6.18}$$

When the *CTI* reaches the certain critical value and *"ΔE"* falls into the magnitude of 10^{-1} -10^{-4} %, the time to reach *CTI* is the time to stop the SVE operation for a specific case. *CTI* means within tailing stage if ideal *E* interval and the corresponding *CTI* are approached, at this time SVE can be stopped. Generally, that *CTI* is more than or equal to 1 already indicates the later time step already cause the delay resulted from tailing, in order to assure the tailing start as much as using the benefit of SVE operation might cause the cleaning up. Based on the survey of the simulated lab-scale cases (see Figures marked with *"ΔE"* and Δt in Appendix D), for any situation of SVE, when *"ΔE"* ranges from 10^{-3}- 10^{-4} %, it was determined that the average *CTI* = 2.1. But experimental cases 3 and 5 in Table 6-3, which have *CTI* is equal to 1.6,

because they do not experience the tailing stage. Table 6-3 gives the tabulated results of the analysis for all lab cases and the resulting predicted times that the laboratory experiments should have stopped. The effectiveness of *CTI* will be demonstrated by first using the laboratory data to calculate and verify the *CTI*. The results from examining *CTI* will then be applied to the field case to test the hypothesis.

Table 6-3 gives the predicted closure time for all the lab cases closure time. It is seen that the closure time for all predicted cases are significantly are short than the actual run times. This confirms that all lab cases could have been shut down earlier from tailing properties.

Table 6-3 The Prediction of the Closure Time to Stop SVE Operations

Case***	Lab-scale models (hours)								Field-scale Case model (days)
	Case 1	Case 2	Case 3	Case 4	Case 5	Case 8	Case 9	Case 10	
Δt_1 (E=0.1~0.01‰)	5	3	5	6	6	2.5	3	10	110
Δt_2 (E=0.01~0.001‰)	9	3	8	10	8	5	6	5	330
Δt_3 (E=0.001~0.0001‰)	18	9	NA	20	13	NA	12	14	∞
$\Delta t_2/\Delta t_1$	1.8	1.9	1.6	1.7	1.3	2.0	2	0.5	2.1
$CTI=\Delta t_{i+1}/\Delta t_i$**	2	3	1.6	2	1.6	2.0	2	2.8	∞
The predicted time to stop SVE operation	66	27	44*	67	71	25	43	64	330*2.1= 693

Note: * there was not tailing effect to be approached;
** The average of CTI for all lab-scale cases is 2.1 ± 0.6.
*** The number of the cases are consistent with the numbered cases in Table 5-7
NA—Not applicable

Based on the analysis for the closure time index by virtue of the lab-scale numerical and experimental data, the critical range of the "*E*" value falls into 10^{-1}~10^{-4} % with tailing stage. To test the validity of this criterion for field case, the *CTI* for field-scale SVE operation was examined in terms of the range of E from 3D-SVE-F model. As outlined in Section 5.2 there were three possible fitting curves from the known field SVE remediation operated by CRA 1997. As such, the analysis will proceed according to all three fits. The corresponding breakthrough curves which are used to check "*E*" value are illustrated in Figure 6-9. Figure 6-9 shows the results of the analysis for the three types of field situations. It is seen that for all three situations the average time to close the operation was 330*2.1= 693 days. However, according to the data provided, it was seen that the site still operated for more than 960 days. This meant that the site ran approximately 267 days longer than it should have, with ineffective treatment.

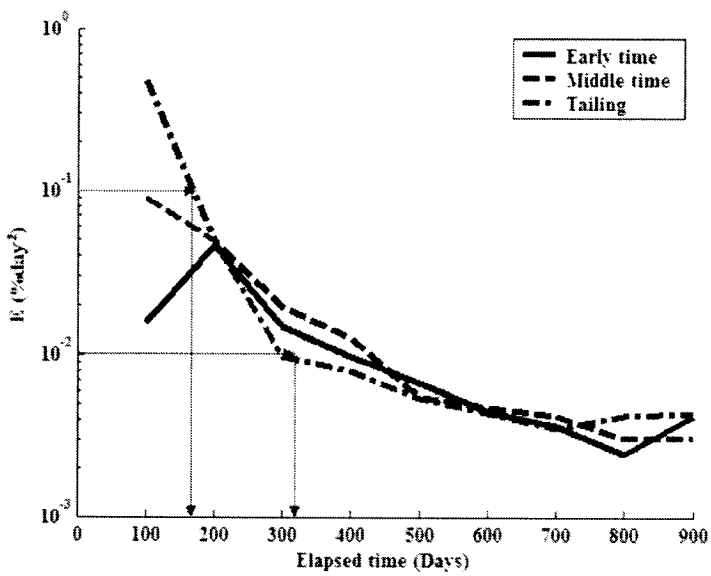

Figure 6-9 The Relative Slope of Breakthrough Curve verse Time for Field-Scale SVE Operation

The analysis for the behaviour of the tailing stage based on *CTI* shows the reasonable evaluation of closure time can bring at least two-thirds equipment using and overhead expense savings. Additionally, even though three field–scale trends have been predicted, they have same predicted closure time but real different cleaning up degree. This facts support the viewpoint that the removal rate of contaminant can not be considered the index to accurately stop SVE. Tailing effects as a discernable processes results from the poor progress of removal of contaminant not only the absolute concentration before reaching the target of cleanup. In other words, even though still higher is the level of concentration of contaminants, the mass transfer limitation appears intensive, even though the concentration is not low enough to reach the cleanup target, the SVE operation should be stopped. The *CTI* discussed here can also be used to see if it makes sense to stop and start the SVE process during the system. During shutdown, there will be rebound of the concentration of contaminant, allowing a higher mass to be extracted.

The procedure to estimate the closure time can be summarized as follows:

- run the 3D-SVE-L/F models and obtain the breakthrough curve of offgas concentrations;
- calculate the elapsed time weighted relative slope of the breakthrough curve "*E*";
- Determine the appropriate time intervals "Δt" and the corresponding "*E*" value,
- Apply CTI of 2.1 to determine the corresponding closure time.

6.4 The Guidelines of SVE System Design by Modeling

The implementation of the 3D-SVE-L/F models in this thesis has provided many insights into the capability of a complex three-dimensional model, governing mechanism of SVE systems and the predictable performance of SVE operation. FEMLAB multiphysics modeling software meets the requirements of complex SVE modeling tasks and allows for improved understanding of the simulated scenarios through powerful pre- and post-processing and computational capacities. Using the 3D-SVE-F model, SVE process modeling in three dimensions with the appropriate input parameters of SVE associated with design configuration (number, locations and spacing of wells, operation conditions) may be implemented. How the 3D-SVE-F model can be used to assist an SVE system design will be discussed in this section.

SVE system design refers to the determination of the number and location of extraction wells and corresponding extraction rates (Johnson et al., 1990a, b; Sun et al., 1996; Sun and Yeh, 1996, 1998). Success of SVE remediation strongly depends on the design of the SVE system (USEPA, 2004). Using a comprehensive numerical simulation tool to design may significantly increase the ability to optimize SVE remediation operations. One of the indispensable and most cost-effective tools is to predict the response of a system by modeling. Because of the lack of the prevalence of modeling practices present for the response of an SVE design current designs of SVE systems depend on the empirical guidelines, experience, or the trial-and-error method. Few reports have shown how an SVE model can be used for field-scale SVE

remediation (Bradner and Murdoch, 2005; Barnes and White, 2006) based on the closure time and final cleanup degree criteria to identify the preferred alternative from various SVE design options.

The completed 3D-SVE-F model can be used to conduct various stages of SVE design tasks. An optimal design can be evaluated in both aspects of maximizing contaminant mass removal design and the most time-efficient design. The developed 3D-SVE-F model has the capability to do this.

Fundamentally, the main three aspects of the model are related to:

- evaluating the performance of SVE physico-chemical processes in a quantitative format and the critical influence elements;
- predicting the closure time and cleanup degree for a specific SVE system design; and
- assisting in SVE system design: optimizing the design candidates or examining effects of site parameter spatial and temporal variations.

To fully describe an SVE system, designers need to identify:

(1) specific numerical values for parameters that characterize the relevant processes;

(2) conceptual model and the corresponding mathematical model including powerful computer code for numerical simulations;

(3) simulating parameters, geometry of regions including the simulated heterogeneity, and initial and boundary conditions.

Figure 6-10 gives an overall systematical flowchart. This chart represents the procedure of predicting an SVE process based on the 3D SVE model responses for an

SVE system configuration, the expected operational conditions, and all known conditions and parameters. The recommended protocol related to the technical chart, Figure 6-10, is outlined as follows:

- implement site characterization based on the broad data sources;
- determine the conceptual model and plan the initial design;
- collect the design parameters. There are two different groups of parameters:

  (a) site/contaminant parameters, such as the geometry of a modeled site, geological information, boundary and initial conditions, modeled domain parameters, physico-chemical properties of contaminants and soils, empirical mass transfer parameters

  (b) design parameters for SVE system configuration and operational conditions;
- set up the 3D-SVE-F model and run according to site data;
- predict closure time and final degree of cleanup and examine with the standards or criteria for the expected SVE operations; and
- once system is set up and running, model can be calibrated for refinement.

If the design requirements are met, confirm the current design. If not acceptable for the system design, further modify for the SVE configuration, repeating the above steps up to the point at which a reasonable closure time and a relevant cleanup degree can be attained.

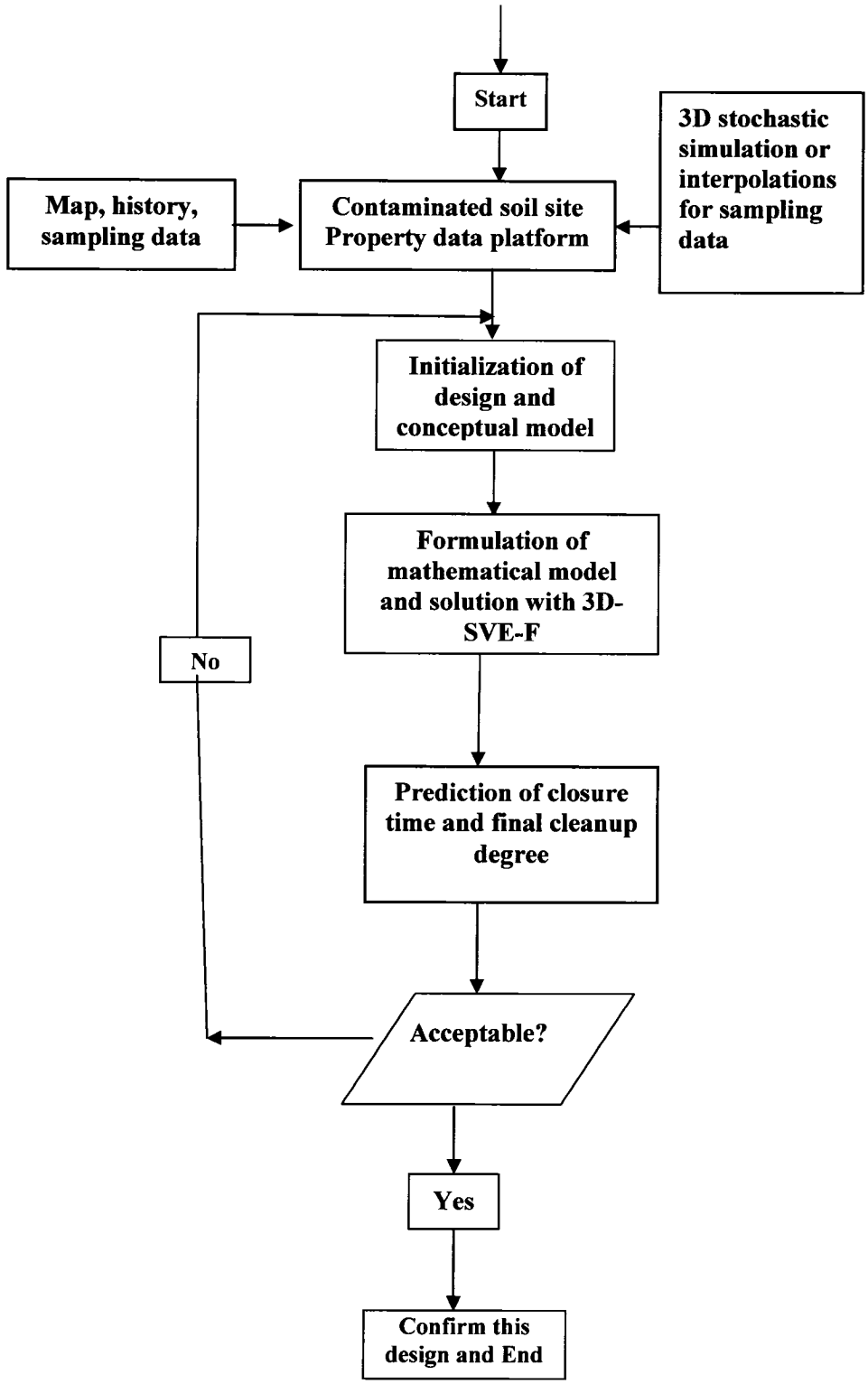

Figure 6-10 An Integrated Flowchart of Designing an SVE Remediation by Modeling

CHAPTER 7

CONCLUSIONS AND RECOMMENDATIONS

This dissertation has provided the methodology and insights into how the developed 3D-SVE-L/F models can be utilized to quantitatively predict and monitor the response to the expected performance of an SVE operation. The 3D-SVE-F model can also be used as an assisting engineering design tool. The completed work has extended the theoretical and numerical studies of the characteristic flow and transport as well as mass transfer processes involved in SVE remediation. Moreover, it has provided a quantitative evaluation for the effects of permeability, dispersivity and mass transfer coefficients on the behaviours of 3D-SVE-L/F models as well. This chapter will depict the essential conclusions drawn out of the overall research work and propose recommendations regarding future studies.

7.1 Conclusions

Specifically, the conclusions drawn can be summarized as follows:

- A complex and comprehensive 3D modeling study is a realistic cost-effective tool to simulate an SVE operation. The geometry of the SVE system and the corresponding operational conditions can be captured with the numerical simulation to develop the SVE design and prediction tool.

- 3D-SVE-F model successfully deals with multiphase flow and multicomponent transport with nonequilibrium rate of mass transfer and accounts for the real site conditions.
- 3D-SVE-L/F models successfully were calibrated to diverse performance of lab-scale experiment and field-scale SVE operation, and mass transfer coefficients have been determined.
- Sensitivity analysis for the complex 3D-SVE-L/F models can be conducted through multivariable linear regression method. With a 95% confidence interval, the order of sensitivity of 3D-SVE-L/F models for the multiple parameters from the most sensitive to least sensitive is the empirical mass transfer parameters "b," for NAPL to vapour phase then permeability of porous medium and dispersivity, "a". The parameters "c" and "d" for aqueous to vapour phase are insensitive.
- Predicting the closure time of various specific cases based on the slope of effluent vapour breakthrough curve, and the weighted relative slope of breakthrough curve to stop SVE falls into in the range of 10^{-3}-10^{-4}%. The corresponding *CTI* (critical time index) 2.1 can be applied to determine the time of SVE operation. Further research should be done to check the validity of $CTI = 2.1$.
- *CTI* and final cleanup degree over entire site can be considered as criteria to compare alternative SVE designs.

7.2 Recommendations

Based on the affirmative consequences of the 3D-SVE-F model as an advanced design and predictive tool, it is possible to tackle more complicated field SVE operations and designs. To improve the modeling results to attain more accurate prediction of SVE operation, further study is needed to include the theoretical and experimental investigations as well as numerical simulation with FEMLAB. Calibration and validation of the constructed model by broad field operation data sets from the various characteristic scenarios are necessary as well.

With respect to theoretical and experimental work on the soil and contaminants, more work should cover the following aspects:

- measuring the features of specific interaction between contaminants and porous media in multiple phase flow and transport, such as experimental measurement for the relative permeability, capillary pressures, and empirical parameters in the relevant constitutive relations, and the effect of constitutive relationship on the behaviours of 3D-SVE-L/F models;
- refining generic characteristics of mass transfer coefficients from possible rate-limited processes in diverse field-scale models to match well the performance of SVE;
- determining the dispersivity of the different types of soils and the influence elements.

With respect to numerical modeling with FEMLAB multiphysics modeling software, the future work should be designed to:

- improve the capability of the model to simulate more complex SVE configurations, such as multiple types of well systems;
- embrace the operation conditions and more complex soil structure and textures and well screening, and mimic the continually and/or intermittently changed flow rate and the exerted venting pressures;
- demonstrate how to introduce the site characterization data into the model's initial condition because MATLAB and FEMLAB can manage the data of site characterization from multiple data sources including the direct utilization of a GPR (Ground Penetrate Radar) data set and other data set of measurable properties of contaminated sites;
- introduce stochastic variations in permeability, moisture content, and contaminant concentrations and try to determine how these variations may influence the results of model simulation;
- develop a more extensive capability to simulate heterogeneous soil and multi-well SVE system configurations;
- further generalize the approach to determining the group compound or compound selection with 3D modeling and SVE remediation to improve the accuracy of multicomponent modeling;
- verify the calibrated 3D SVE model through more data sets from field-scale remediation operations.

References

Abriola, L. M. and Pinder, G. F., 1985. A multiphase approach to the modeling of porous media contamination by organic compounds, 1. Equation development. Water Resources Research. **21**(1): 11–18.

Abriola, L. M., 1987. Modeling contaminant transport in the subsurface: An interdisciplinary challenge, Reviews of Geophysics, 25(2):125-134.

Abriola, L. M., J. R. Lang, and K. Rathfelder, 1997. Michigan soil vapour extraction remediation (MISER) model: A computer program to model soil vapor extraction and bioventing of organic chemicals in unsaturated geological material. USEPA, Cincinnati, Ohio, EPA/600/R-097/099. (NTIS: PB98-115355INZ, 264 pp.)

Abriola, L. M., K. D. Pennell, W. J. Weber, J. R. Lang, and M. D. Wilkins, 1999. Persistence and interphase mass transfer of liquid organic contaminants in the unsaturated zone, Experimental Observations and Mathematical Modeling, published in Vadose zone hydrology: cutting across disciplines, Oxford University Press, INC., ISBN: 0-19-510990-2.

Adeel, Z, J. W. Mercer, and C. R. Faust, 2001. Models of multiphase flow and transport of contaminants, published in ground water contamination by organic pollutants: analysis and remediation, ASCE press, ISBN: 07844-0527-1, pp 1-39.

Adenekan, A. E., T. W. Patzek, and K. Prucess, 1993. Modeling of multiphase transport of multicomponent organic contaminants and heat in the subsurface: numerical model formulation, Water Resources Research, 29(11): 3727-3740.

Aelion, C. M., J. N. Shaw, M. A. Widdowson, and H. W. Reeves, 1996. The use of

simplified methods for monitoring petroleum–contaminated groundwater and soil vapour, Journal of Soil Contamination, 5(3):225-241.

Allen, III M. B, G. A. Behie, and J. A. Trangenstein, 1988. Multiphase flow in porous media: Mechanics, mathematics, and numeric, Springer – Verlag, ISBN: 0-387-96731- 1.

Anwar, F., M. Bettahar and U. Matsubayashi, 2000. A method for determining air–water interfacial area in variably saturated porous media. Journal of Contaminant Hydrology, 43(2), 129– 146.

Armstrong, Amit, 1998. A finite difference approach for mathematical simulation of soil vapor extraction from unsaturated zone, PhD thesis, Texas Tech University.

Armstrong, J. E., E. O. Frind, and R. D. McClellan, 1994. Nonequilibrium mass transfer between the vapour, aqueous, and solid phases in unsaturated soils during vapour extraction, Water Resources Research, 30(2): 355-368.

Aziz, K. and A. Settari, 1979. Petroleum reservoir simulation, Applied Science Publishers Ltd., London, ISBN: 085334-787-5.

Baehr, A. L., 1987. Selective transport of hydrocarbons in the unsaturated zone due to aqueous and vapour phase partitioning, Water Resources Research, 23(10): 1926-1938.

Baehr, A. L. and M. F. Hult, 1991. Evaluation of unsaturated zone air permeability through pneumatic tests, Water Resources Research, 27(10): 2605-17.

Baehr, A. L., G. E. Hoag and M. C. Marley, 1989. Removing volatile contaminants

from the unsaturated zone by inducing advective air-phase transport, Journal of Contaminant Hydrology, 4(1): 1-26.

Ball, R. and S. Wolf, 1990. Design considerations for soil cleanup by soil vapour extraction, Environmental Progress, 9(3): 187-189.

Barnes, D. L., 2003. Estimation of operation time for soil vapour extraction systems, Journal of Environmental Engineering, 129(9): 873-878.

Barnes, D. L. and D. B. McWhorter, 2000a. Uncertainty in predicting the rate of mass removal created by soil vapor extraction systems, Groundwater, 38(2): 209-226.

Barnes, D. L. and D. B. McWhorter, 2000b. Design of soil vapour extraction systems under conditions of uncertainty, Journal of Soil Contamination, 9(1): 13-29.

Barnes, D. L. and T. C. White, 2006. Application of a simple decision model for soil vapor extraction system operation, Ground Water Monitoring and Remediation, 26(4): 107-114.

Bear, J., 1972. Dynamics of fluids in porous media. New York: American Elsevier. ISBN: 0486656756.

Bear, J. and Y. Bachamat, 1990. Theory and applications of transport in porous media, Introduction to modeling of transport phenomena in porous media, Kluwer Academic Publishers, ISBN: 0-7923-0167-6.

Beckett G. D. and D. Huntley, 1994, Characterization of flow parameters controlling soil vapour extraction, Groundwater, 32(2): 239-247.

Benitez J., 2002. Principles and modern applications of mass transfer operations, John Wiley & Sons, Inc. ISBN: 0-471-20344-0.

Benson, D. A., P. Huntley, and P. C. Johnson, 1993. Modeling vapour extraction and general transport in the presence of NAPL mixtures and nonideal conditions, Ground Water, 31(3): 437-45.

Boyd, S. A. and S. Sun, 1990. Residual petroleum and polychlorobiphenyl oils as sorptive phases for organic contaminants in soils, Environmental Science and Technology, 24 (1): 142–144.

Bradford, S. A., T. J. Phelan and L. M. Abriola, 2000. Dissolution of residual tetrachloroethylene in fractional wettability porous media: correlation development and application, Journal of Contaminant Hydrology, 45(1): 35-61.

Bradner, Graham C. and Lawrence C. Murdoch, 2005. Effects of skin and hydraulic fractures on SVE well, Journal of Contaminant Hydrology, 77 (3): 271-297

Braida, W. J. and S. K. Ong, 1998. Air sparging: air-water mass transfer coefficients. Water Resources Research, 34 (12): 3245-3253.

Brooks, R. H. and A.T. Corey, 1966. Properties of porous media affecting fluid flow, Journal of Irrigation Drainage, Div. Am. Soc. Civ. Eng. 92(2): 61-88.

Brooks, R. H., and A. T. Corey, 1964. Hydraulic properties of porous media, Hydrol. Paper, Volume 3, (1964): Colorado St. Univ., Fort Collins, CO.

Brunch, John C., 1975. Finite element solutions for unsteady and unsaturated flow in porous media, Davis, Calif.: University of California, Contribution (California Water Resources Center): no. 151.

Brush, David J., 1994. Multiphase flow in porous media, Masters thesis, University of Waterloo, Ontario Canada.

Brusseau, M. L., and P. S. C. Rao, 1989. Sorption nonideality during organic contaminant transport in porous media, CRC Critical Reviews in Environmental Control, 19(1): 33-99.

Brusseau, M. L., 1991. Transport of organic chemicals by gas advection in structured or heterogeneous porous media: Development of a model and application to column experiments, Water Resources Research, 27(12): 3189-99.

Campagnolo, J. F. and A. Akgerman, 1995. Modeling of soil vapour extraction (SVE) system- Part I, Waste Management, 15(5, 6):379-389.

Cann, D. P., T. Gidda, W. H. Stiver, and R. G. Zytner, 2002. Estimate of air flow dispersion and dispersivity for five soils of varying sand, silt and clay fractions, An International Perspective on Environmental Engineering, 2002 Joint CSCE/EWRI of ASCE International Conference, on July 21-July 24, Niagara Falls, ON, Canada, ISBN: 0-88955-532-X.

Carey, Graham F., 1995. Finite element modeling of environmental problems surface and subsurface flow and transport, John Wiley and Sons, ISBN: 0 471 95662 7.

Chai J. C. and N. Miura, 2004. Field vapour extraction test and long-term monitoring at a PCE contaminated site, Journal of Hazardous Materials, 110(1-3): 85-92.

Chao K. P., S. K. Ong and A. Protopapas, 1998. Water-to-air mass transfer of VOCs: laboratory-scale air sparging system, Journal of Environmental Engineering, 124 (11): 1054-1060.

Chen, X. H., and D. C. Gosselin, 1998. Numerical simulation of radial gas flow: effects of soil anisotropy, well placement and surface seal, Journal of Hydrologic Engineering, 3(1): 52-61.

Chen, Zhangxin, Guan Qin, and Richard E. Ewing, 2000. Analysis of a compositional model for fluid flow in porous media, SIAM Journal of Applied Mathematics, 60(3): 747-777.

Chien, Calvin C., Miguel A. Medina Jr., George D. Pinder, Danny D. Reible, Brent E. Sleep and Chunmiao Zheng, 2004. Contaminated ground water and sediment modeling for management and remediation, Leiws Publishers, ISBN: 0-56670-667-X.

Cho, J. S., 1993. A three-dimensional air flow model for soil venting: superposition of analytical functions, Journal of Hazardous Materials, 35(1): 31-51.

Cho, J. S., and D. C. DiGiulio, 1992. Pneumatic pumping test for soil vacuum extraction, Environmental Progress, 11(3): 228-33.

Coffin, D., and L. Glasgow, 1992. Effective gas flow arrangements in soil venting, Water Air & Soil Pollution, 62(3-4): 303-24.

Corapcioglu, Yavuz M., 1991, Compositional multiphase flow models, in: Advances in porous media, Vol. 1, ISBN: 044488909-4, pp 1-59.

Delshad, M., G. A. Pope, K. Sepehrnoor, 1996. A compositional simulation for modeling surfactant enhanced aquifer remediation, 1: Formulation, Journal of Contaminant Hydrology, 23 (4): 303-327.

DiGiulio, D.C.,1992. Evaluation of soil venting application. EPA Ground Water Issue, EPA/540/S-92/004, Environmental Protection Agency (EPA): Washington,D. C.

DiGiulio, D. C. and Ravi Varaham, 2001. Development of recommendations and methods to support assessment of soil venting performance and closure, EPA/600/R-01/700.

Domenico, P. A. and G. A. Robbins, 1984. A dispersion scale effect in model calibrations and field experiments, Journal of Hydrology, 70(1): 123-132.

Dortch, Mark S., Christian J. McGrath, John J. Nitao, Mark A. Widdowson, and Steve Yabusaki, 2001. Strategic Environmental Research and Development Program, Development of simulators for in-situ remediation evaluation, design, and operations: final report, US Army Corps of Engineers, Engineer's Research and Development Center, Environmental Laboratory, ERDC/EL TR-01-03.

Duggal, Avin, 2005. An experimental design and study of soil vapour extraction in a lab scale radial column, Mater Degree Thesis, University of Guelph

El-Beshry, M. Z., J. S. Gierke and P. B. Bedient, 2001. Practical modeling of SVE performance at a jet-fuel spill site, Journal of Environmental Engineering, 127(7): 630-638.

Farhan, S M., H. Thomas and J. Budiman, 2001. Interaction of soil air permeability and soil vapour extraction, Journal of Environmental Engineering, 127(1): 32-37.

Faisal, Anwar A. H. M., Truong Hong Tien, Yasushi Inoue, and Fusetsu Takagi, 2003. Mass transfer correlation for nonaqueous phase liquid volatilization in porous media, Environmental Science and Technology, 37(7): 1277-1283.

Falta, R. W., I. Javandel, K. Pruess and P. A. Witherspoon, 1989. Density-driven flow of gas in the saturated zone due to the evaporation of volatile organic compounds, Water Resources Research, 25(10): 2159-2169.

Falta, R. W., K. Pruess, I. Javandel, and P. A. Witherspoon, 1992a. Numerical modeling of steam injection for the removal of nonaqueous phase liquids from the subsurface, 1. Numerical formulation, Water Resources Research, 28(2): 422-449.

Falta, R. W., K. Pruess, I. Javandel, and P. A. Witherspoon, 1992b. Numerical modeling of steam injection for the removal of nonaqueous phase liquids from the subsurface, 2. Code validation and application, Water Resources Research, 28(2): 451-465.

Falta, R.W., K. Pruess, and D. A. Chesnut, 1993. Modeling advective contaminant transport during soil vapour extraction, Ground Water, 31(6): 1011-20.

Fanchi, John R., 2001. Principles of applied reservoir simulation, second edition, Gulf Professional Publishing, ISBN: 0-88415-372-X.

Fang Xin Yu and Vijay P. Singh, 1994. Modeling 3D groundwater flow by modeled finite element method, Journal of Irrigation and Drainage Engineering, 120(5): 892-909.

Farquhar, G. J., E. A. McBean, and R. G. Pearson, 1990. Assessing the impact of hazardous immiscible liquid in soil, ISBN: 0-7729-5246-9.

Faust, Charles R., 1985. Transport of immiscible fluids within and below the unsaturated zone: A numerical model, Water Resources Research, 21(4): 587-596.

FEMLAB, 2006. At website http://www.comsol.com.

Fischer, U., R. Schulin, M. Keller, and F. Stauffer, 1996. Experimental and numerical investigation of soil vapor extraction, Water Resources. Research. 32(12): 3413-3427.

Fischer, U., C. Hinz, R. Schulin and F. Stauffer, 1998. Assessment of nonequilibrium in gas-water mass transfer during advective gas-phase transport in soils, Journal of Contaminant Hydrology, 33(2):133-148.

Freeze, Alan R. and John A. Cherry, 1979. Groundwater, Published by Prentice Hall, ISBN: 0133653129.

Frind E.O., 1982. Simulation of long-term transient density-dependent transport in groundwater, Advances in Water Resources, 5(1): 73-88.

Gamlie, L. A., and A. S. Abdul, 1993. Numerical investigations of optimal well spacing and the effect of screen length and surface sealing on gas flow toward an extraction well, Journal of Contaminant Hydrology, 12(2): 171-91.

Gidda, T., 2003. Mass transfer process in the soil vapour extraction of gasoline from unsaturated soils, PhD thesis, University of Guelph.
Gidda, T, D. Cann, W. H. Stiver and R. G. Zytner, 2006. Airflow dispersion in unsaturated soil, Journal of Contaminant Hydrology, 82(1-2):118-132

Gierke, J. S., N. J. Hutzler, and J. C. Crittenden, 1990. Modeling the movement of volatile organic chemicals in columns of unsaturated soil, Water Resources Research, 26(7): 1529-47.

Gierke, J. S., N. J. Hutzler and D. B. McKenzie, 1992. Vapour transport in unsaturated soil columns: Implications for vapour extraction, Water Resources Research, 28(2): 323-35.

Goltz, M. N., and M. E. Oxley, 1994. An analytical solution to equations describing rate-limited soil vapour extraction of contaminants in the vadose zone, Water Resources Research, 30(10): 2691-8.

Gomez-Lahoz, C., J. M. Rodriguez-Maroto, and D. J. Wilson. 1991. Soil clean-up by in-situ aeration: VI. Effects of variable permeability. Sep. Sci. Technol, 26:133-163.

Gribb, Molly M., K. J. Bene and A. Shrader, 2002. Sensitivity analysis of a soil leachability model for petroleum fate and transport in the vadose zone, Advances in Environmental Research, 7(1): 59-72.

Harper, M. B., 1999. An experimental and numerical modeling investigation of soil vapour extraction in a silt loam soil, PhD thesis, University of Guelph.

Harper, M, W. H. Stiver and R. G. Zytner 1998. Influence of water content on SVE in a silt loam soil, Journal of Environmental Engineering, 124 (11): 1047-1053.

Harper, M. B., W. H. Stiver and R. G. Zytner, 2003. Nonequilibrium nonaqueous phase liquid mass transfer model for soil vapour extraction systems, Journal of Environmental Engineering, 129(8): 745-754.

Hayden, N. J., T. C. Voice, M. D. Annable and R. B. Wallace, 1994. Change in gasoline constituent mass transfer during soil venting. Journal of Environmental Engineering, 120 (6): 1598-1614.

Hayden, N. J., T. C. Voice and R. Wallace, 1997. Residual gasoline saturation in unsaturated soil with and without organic matter, Journal of Contaminant Hydrology, 25(2): 271-281.

Helmig, R., 1997. Multiphase flow and transport processes in the subsurface: a contribution to the modeling of hydro systems (Environmental Engineering): Springer, ISBN: 3-540-62703-0.

Hillel, D., 1990. Movement and retention of organics in soil: a review and a critique of modeling, in petroleum contaminated soils, Vol. 1 Remediation techniques environmental fate and risk assessment, edited by Paul T. Kostecji and Edward J. Calabrece, Lewis Publishers, ISBN:0-87371-135-1.

Hillel, D. 1998. Environmental soil physics, Academic Press, ISBN 012348525-8.

Hinsenveld, Arendt F., W. J. van den Brink, 1990. Modeling of SVE remedial action duration, Contaminated Soil '90, Vol. II, Kluwer Academic Publishers, ISBN:0-7923-1058-6.

Ho, C. K. and K.S. Udell, 1992. An experimental investigation of air venting of volatile liquid hydrocarbon mixtures from homogeneous and heterogeneous porous media, Journal of Contaminant Hydrology, 11(2): 291-316.

Hoeg, S., H. F. Schöler and J. Warnatz, 2004. Assessment of interfacial mass transfer in water-unsaturated soils during vapour extraction, Journal of Contaminant Hydrology, 74(1-4): 163-195.

Hoffman, G. D., D. R. Gan, L. M. Abriola and K. D. Pennell, 1993. Rate limited processes that affect the performance of soil vapour extraction, Proc. of the 14th Annual Superfund Con., Washington D. C., 960-67.

Holzbecher, E. O. 1998. Modeling density-driven flow in porous media: principles, numerics, software, Springer-Verlag, ISBN: 3-540-63677-3.

Huang, J. Q and M. N. Goltz, 1999. Solutions to equations incorporating the effect of rate-limited contaminant mass transfer on vadose zone remediation by soil vapour extraction, Water Resources Research, 35(3): 879-883.

Hutzler, N. F., B. E. Murphy and J. S. Gierke, 1989. State of Technology Review of Soil Vapour Extraction Systems, U.S.\ EPA, EPA/600/2-89/024.

Huyakorn, P. S., S. Panday, and Y. S. Wu, 1994. A three-dimensional multiphase

flow model for assessing NAPL contamination in porous and fractured media: 1. Formulation, Journal of Contaminant Hydrology, 16(1):109-130.

Hyman, M. and R. R. Dupont, 2001. Groundwater and soil remediation: Process design and cost estimating of proven technologies. ASCE press, ISBN: 07844-0427-5, pp 333-366.

Istok, J., 1989. Groundwater modeling by the finite element method, Washington, D. C.: American Geophysical Union.

Jang, Wongyong, 2005. Unsteady multiphase flow modeling of in-situ sparging system in a variably saturated subsurface environment, PhD thesis, Georgia Institute of Technology.

Jennings, Aaron A. and Prithviraj Patil, 2002. Feasibility modeling of passive soil vapour extraction, Journal of Environmental Engineering Science, 1(2):157-172.

Johnson, P. C., C. C. Stanley, M. W. Kemblowski, D. L. Byers and J. D. Colthart, 1990a. A practical approach to the design, operation and monitoring of in situ soil-venting systems, Groundwater Monitoring Review, 10(2): 159-78.

Johnson, P. C., M. W. Kemblowski, and J. D. Colthart, 1990b. Quantitative analysis for the cleanup of hydrocarbon-contaminated soils by in-situ soil venting, Ground Water, 28(3): 413-429.

Jordan, D. L., J. W. Mercer, and R. M. Cohen, 1995. Review of mathematical modeling for evaluating soil vapour extraction systems, Environmental Protection Agency, Rep. No. EPA/540/R-95/513.

Joss, C. J., and A. L. Baehr, 1995. Documentation of AIR3D, an adaption of the

groundwater flow code MODFLOW to simulate three-dimensional air flow in the unsaturated zone. USGS, open-file, pp.94–533.

Jury, William A. and Robert Horton, 2004. Soil Physics, sixth edition, John Wiley & Son Inc. New Jersey, ISBN: 0-471-05965-X.

Kalurachchi, J. J. and J. C. Parker, 1990. Modeling multicomponent organic chemical transport in three-phase porous media, Journal. of Contaminant Transport, **5(3)**: 349-357.

Kaleris, V., 2002. Influence of rate limited sorption on the clean up time in layered soil by vapour extraction, Journal of Contaminant Hydrology, 55(1): 1-27.

Kaleris, V. and J. Croise, 1997. Estimation of cleanup time for continuous and pulsed soil vapour extraction, Journal of Hydrology, 194(3): 330-356.

Kaleris, V. and J. Croisé, 1999. Estimation of cleanup time in layered soils by vapour extraction, Journal of Contaminant Hydrology, 36(2): 105-129

Karapanagioti, H. K., P. Gaganis, and V. N. Burganos, 2003. Modeling attenuation of volatile organic mixture in the unsaturated zone: Codes and usage, Environmental Modeling & Software, 18(4): 329-337.

Karimi, Ali A., W. J. Farmer, and M. M. Cliatch, 1987. Vapour-phase diffusion of benzene in soil, Journal of Environmental Quality, 16(1): 38-43.

Kim, Am Tam, 1994. Mass transfer kinetics during soil vapour extraction of dissolved and sorbed phase volatile organic contaminants: Laboratory and

mathematical modeling studying, PhD thesis, University of Waterloo, ISBN: 0-315-94780-2.

Kolditz, O., R. Rainer, G. D. Hans-Jorg, and Z. Werner, 1998. Coupled ground water flow and transport: 1. Verification of variable density flow and transport models, Advances in Water Resources, 21(1): 27-46.

Lee, H., I. T. Yeom, K. H. Ahn and J. Khim, 2000. A simplified model approach for mass transfer of a complex liquid mixture during soil venting, Environmental Technology, 21(11): 1301-1308.

Lenhard, R. J. and J. C. Parker, 1987. A model for hysteretic constitutive relations governing multiphase flow: 2. Permeability-saturation relations. Water Resources Research, 23(11): 2197-2206.

Lenhard R. J., M. Oostrom and M. D. White, 1995. Modeling fluid flow and transport in variably saturated porous media with the STOMP simulator. 2. Verification and validation exercises, Advances in Water Resources, 18(6):365-373.

Lenhard R. J., M. Oostrom and J. H. Dane, 2004. A constitutive model for air–NAPL–water flow in the vadose zone accounting for immobile, non-occluded (residual) NAPL in strongly water-wet porous media, Journal of Contaminant Hydrology, 71(1-4): 261-282.

Lingineni, S. and V.K. Dhir, 1997. Controlling transport processes during NAPL removal by soil venting. Advances in Water Resources, 20(2-3): 157-169.

Looney, B. B. and R. W. Falta, 2000. Vadose zone science and technology solutions, Battelle Press, ISBN: 1-57477-085-3.

McBean, E. A. and F. A. Rovers, 2001. Statistical procedures for analysis of environmental monitoring data and risk assessment, ISBN: 0-13-675018.

Majid, S., Gray William G., 1993. Thermodynamic basis of capillary pressure in porous media, Water Resources Research, 29(10): 3389-3405.

Massman, J. W., 1989. Applying groundwater flow models in vapour extraction system design, Journal of Environmental Engineering, 115(1): 129-149.

Massman, J. W. and D. F. Farrier, 1992. Effects of atmospheric pressures on gas transport in the vadose zone, Water Resources Research, 28(3): 777-91.

Massman, J. W. and M. Madden, 1994. Estimating air conductivity and porosity from vadose-zone pumping tests, Journal of Environmental Engineering, 120(2): 313-28.

McLaren, D., 1972. Organic chemicals in the soil environment, Vol. 1. Marcel Dekker Inc., New York, ISBN: 0-8247-1256-0.

Mendoza, C. A., and E. O. Frind, 1990a. Advective-dispersive transport of dense organic vapours in unsaturated zone, 1. Model development, Water Resources Research, 26(3): 379–387.

Mendoza, C. A. and E. O. Frind, 1990b. Advective-dispersive transport of dense organic vapors in the unsaturated zone 2. Sensitivity analysis. Water Resources Research, 26(3): 388-398.

Miller, C. T., G. Christakos, P. T. Imhoff, J. F. McBride, J. A. Pedit and J. Trangenstein, 1998. Multiphase flow and transport modeling in heterogeneous porous media: challenges and approaches, Advances in Water Resources, 21(2): 77-120.

Miller, C. T., M. M. Poirier-Mcneill and A. S. Mayer 1990. Dissolution of trapped nonaqueous phase liquids: mass transfer characteristics, Water Resources Research, 26(11): 2783-2796.

Mills, A. F., 2001. Mass Transfer, Prentice Hall Inc., ISBN: 0-13-032829-4.

Mirsal, Ibrahim A., 2004. Soil pollution, origin, monitoring & remediation, Springer-Verlag, ISBN: 3-540-40143-1.

Mohr, D. H. and P. H. Merz, 1995. Application of a 2D air flow model to soil vapour extraction and bioventing case studies, Ground Water, 33(3): 433-444.

Moldrup, P., C. W. Kruse, D. E. Rolston and T. Yamaguchi, 1996. Modeling diffusion and reaction in soils: III. Predicting gas diffusivity from the Campbell soil-water retention model, Soil Science, 161(6): 366-375.

Moldrup, P., Poulsen, T. G., Schjonning, P., Olesen, T., Yamaguchi, T., 1998. Gas permeability in undisturbed soils: measurements and predictive models, Soil Science, 163(3): 180-19.

Moldrup, P., T. Olesen, D. E. Rolston, and T. Yamaguchi, 1997. Modeling diffusion and reaction in soils: VII. Predicting gas and ion diffusivity in undisturbed and sieved soils, Soil Science, 162(9): 632-640.

Moldrup, P., T. Olesen, T. Yamaguchi, P. Schjonning, D. E. Rolston, 1999. Modeling diffusion and reaction in soils: IX. the Buckingham-Burdine-Campbell equation for gas diffusivity in undisturbed soil, Soil Science, 164(8): 542-551.

Nair, S., D. Longwell and C. Seigneur, 1990. Simulation of chemical transport in unsaturated soil, Journal of Environmental Engineering, 116(2): 214-235.

Ng, C. O. and C. C. Mei, 1996. Aggregate diffusion model applied to soil vapour extraction in unidirectional and radial flows, Water Resources Research, 32(5):1289-1297.

Nobre, M. and R. C. M. Nobre, 2004. Soil vapour extraction of chlorinated solvent in industrial site in Brazil, Journal of Hazardous Materials, 110(1): 119-127.

Nyer, Evan K, 1993. Practical techniques for ground water and soil remediation, Lewis Publishers, ISBN: 0-87371-735-7.

Ong, S. K., T. B. Culver, L. W. Lion and C. A. Shoemaker, 1992. Effects of soil moisture and physical-chemical properties or organic pollutants on vapour-phase transport in the vadose zone, Journal of Contaminant. Hydrology, 11: 273-90.

Panday, S., Y. S. Wu, and P. S. Huyakorn, 1994. A three-dimensional multiphase flow model for assessing NAPL contamination in porous and fractured media: 2. Porous medium simulation, Journal of Contaminant Hydrology, 16(2): 131-156.

Panday, S., Y. S. Wu, P. S. Huyakorn, S. C. Wade, Z. A. Saleem, 1997. A composite constituents, Journal of Contaminant Hydrology, 25(1-2): 39-62.

Parker, J. C., Lenhard, R. J., 1987. A model for hysteretic constitutive relations governing multiphase flow: 1. Saturation–pressure relations. Water Resources Research, 23(11): 2187– 2196.

Peaceman, D. W. 1977. Fundamentals of Numerical Reservoir Simulation, Elsevier Scientific Publishing Company, ISBN: 0444415785.

Pedersen, T. A. and J. T. Curtis, 1991. Soil vapour extraction technology-reference handbook, U.S. EPA, EPA/540/2-91/003.

Poulsen, T. G., J. W. Massmann, and P. Moldrup. 1996. Effects of vapour extraction on contaminant flux to atmosphere and ground water, Journal of Environmental Engineering, 122(7): 700-706.

Poulsen, T. G., P. Moldrup, T. Yamaguchi, J. W. Massmann and J. Å. Hansen, 1998. VOC vapour sorption in soil: Soil type dependent model and implications for vapour extraction, Journal of Environmental Engineering, 124(2): 146:155.

Poulsen T. G., P. Moldrup, P. Schjønning, J. W. Massmann and J. Å. Hansen, 1998. Gas permeability and diffusivity in undisturbed soil: SVE implications, Journal of Environmental Engineering, 124(10): 979-986.

Poulsen, T. G., P. Moldrup, P. Schjønning, J. W. Massmann and J. Å. Hansen, 1999. Predicting soil-water and soil-air transport properties and their effects on soil-vapour extraction efficiency, Ground Water Monitoring Review, 21(6): 61-70.

Powers, S. E., L. M. Abriola and W. J. Weber, Jr., 1992. An experimental investigation of nonaqueous phase liquid dissolution in saturated subsurface systems: Steady state mass transfer rate, Water Resources Research, 28(10): 2691-2705.

Powers, S.E. Abriola, L.M. ; Weber, W.J. Jr, 1994. An experimental investigation of nonaqueous phase liquid dissolution in saturated subsurface systems: Transient mass transfer rates, Water Resources Research, Journal Volume: 30(2): 321-332

Rao, P. S. C., R. E. Jessup, D. E. Rolston, J. M. Davidson, and D. P. Kilcrease, 1980. Experimental and mathematical description of nonadsorbed solute transfer by diffusion in spherical aggregates, American Journal of Soil Science Society, 44(6): 684-688.

Rao, P. S. C., R. E. Jessup, T. M. Addiscott, 1982. Experimental and theoretical

aspects of the solute diffusion in spherical and nonspherical aggregates, Soil Science, 133(6): 342-349.

Rao, Gurunadha V. V. S., R. L. Dhar, T. Jayachand, C. S. Khoker, 2000. Mass transport modeling for assessment of groundwater contamination around Mathura oil refinery, Mathura, Uttar Pradesh, India, Environmental Geology, 39(10): 1138-1146.

Rao, S. S., 2005. The finite element method in engineering, Elsevier Butterworth-Heinermann, ISBN: 0-7506-7828-3.

Rathfelder, K, J. R. Lang and L. M. Abriola, 1995. Soil vapour extraction and bioventing: Applications, limitations, and future research directions, Rev. Geophys. Vol. 33 Suppl.

Rathfelder, K. M, J. R. Lang and L. M. Abriola, 2000. A numerical model (MISER) for the stimulation of coupled physical, chemical and biological processes in soil vapour extraction and bioventing system, Journal of Contaminant Hydrology, 43(3-4): 239-270.

Rathfelder, W. W. G. Yeh and D. Mackay, 1991. Mathematical simulation of soil vapour extraction systems: Model development and numerical examples, Journal of Contaminant Hydrology, 8(2): 263-297.

Reeves, H. W. and L. M. Abriola, 1994. An iterative compositional model for subsurface multiphase flow, Journal of Contaminant Hydrology, 15(4):249-276.

Riser, Roberts Eve, 1998. Remediation of petroleum contaminated soil: Biological, physical and chemical processes, Lewis Publishers, ISBN: 0-87371-858-5.

Rolle, Kurt C., 2000. Heat and mass transfer, Prentice-Hall, Inc., ISBN: 0-13-919309.

Rossabi, J, 1997. TNX soil vapour extraction multiphase model summary, at website http://sti.srs.gov/fulltext/tr2000291/tr2000291.html, accessed WSRC-TR-2000-00291

Russell, B. J. and J. S. Ginn, 2004. Practical handbook of soil, vadose zone and groundwater contamination assessment, prevention and remediation, Lewis Publishers, ISBN: 1-56670-610-6.

Sawyer, C. S. and M. Kamakoti, 1998. Optimal flow rates and well locations for soil vapour extraction design, Journal of Contaminant Hydrology, 32(1): 63-76.

Schaefer, C. E., R. R. Arands and D. S. Kosson, 1999. Measurement of pore connectivity to describe diffusion through a nonaqueous phase in unsaturated soils, Journal of Contaminant Hydrology, 40(2): 221-238.

Schnoor J. L., 1996. Environmental modeling-fate and transport of pollutants in water, air, and soil, A Wiley-Interscience Publication, John Wiley & Sons, Inc., ISBN: 0-471-12436-2.

Schulenberg , J. W. and H. W. Reeves, 2002. Axi-symmetric simulation of soil vapour extraction influenced by soil fracturing, Journal of Contaminant Hydrology, 57(2): 189–222.

Schwartz, F. W and Hubao Zhang, 2003. Fundamentals of ground water, John Wiley & Sons, INC., ISBN: 0-471-13785-5.

Sepehr, M. and Z. A. Samani, 1993. In situ soil remediation using vapour extraction well, development and testing of a three–dimensional model, Ground Water, 31(3): 425-436.

Sharma, Hari D. and Krishna R. Reddy, 2004. Geoenvironmental engineering: Site remediation, waste containment, and emerging waste management technologies, ISBN: 0-471-21599-6.
Sherwood, T. K., R. L. Pigford and C. R. Wilke, 1975. Mass transfer, McGraw-Hill: New York.

Shan, C., R. W. Falta, and I. Javandel, 1992. Analytical solutions for steady state gas flow to a soil vapour extraction well, Water Resources Research, 28(4): 1105-20.

Shikaze, Steven G., Edward A. Sudicky and Carl A. Mendoza, 1994. Simulation of dense vapor migration in discretely fractured geologic media, Water Resources Research, 30(7): 1993-2010.

Sleep, B. E. and J. F. Sykes, 1989. Modeling the transport of volatile organics in variably saturated media, Water Resources Research, 25(1): 81-92.

Sleep, B. E., and J. F. Sykes, 1993. Compositional simulation of groundwater contamination by organic compounds, 1. Model development and verification, Water Resources Research, 29(6): 1697-708.

Smith, L. and F. W. Schwartz. 1980. Mass transport, 1. A stochastic analysis of macroscopic dispersion, Water Resources Research, 16(2): 303-313.
Stylianou, C., and B. A. DeVantier. 1995. Relative air permeability as function of saturation in soil venting, Journal of Environmental Engineering, 121(4): 337-347.

Sun, Yung-Hsin, Marshall W. Davert, and William W.-G. Yeh, 1996. Soil vapour extraction system design by combinatorial optimization, Water Resources Research, 32(6): 1863-1873.

Sun, Yung-Hsin, William W.-G. Yeh, 1998. Location and schedule optimization of soil vapour extraction system design, Journal of Water Resource Planning and Mana-

gement, 124(1): 47-58.

Suthersan, S. S., 1996. Remediation engineering: Design concepts, Lewis Publishers Inc., ISBN: 1566701376, pp 27- 67.

Szatkowski, A., P. T. Imhoff, and C. T. Miller, 1995. Development of a correlation for aqueous-vapour phase mass transfer in porous media, Journal of Contaminant Hydrology, 18(1): 85-106.

Taylor, R. and R. Krishna, 1993. Multicomponent mass transfer, Wiley Series in Chemical Engineering, ISBN: 0-471-57417-1.

Thiez, P. A., G. Pottecher, and J. M. Come, 1996. Validation of a general 3-D numerical model for simulating organic pollutants migration and application to site remediation, SPE 35851.

Thomson, N. R., J. F. Sykes, and D. Van Vliet, 1997. A numerical investigation into factors affecting gas and aqueous phase plumes in the subsurface, Journal of Contaminant Hydrology, 28(1-2): 39-70.

Thomson, N.R and R.L. Johnson, 2000. Air distribution during in situ air sparging: an overview of mathematical modeling, Journal of Hazardous Materials, 72(2-3): 265-282.

Travis, C. C., and J. M. Macinnis, 1992. Vapour extraction of organics from subsurface soils--Is it effective?, Environmental Science Technology, 26(10): 1885-7.

USACE, 2001a. Commissioning, and demonstration for soil vapour extraction (SVE) system.

USACE, 2001b. Operation maintenance and process monitoring for soil vapour extraction (SVE) system, USACE-UFGS-1830A.

US EPA, 1998. US EPA Office of Underground Storage Tanks, 1998. Map of Status of ASTM RBCA Training in the UST Program, Website: http://www.epa.gov/swerust1/rbdm/rbcamap.htm, accessed 2/5/01.

USEPA Army Corps of Engineers, 2002. Engineering and design for soil vapour extraction, EM 1110-1-4001.

USEPA, 2004. Underground Storage Tanks, at: www.epa.gov/OUST/test2.htm.

USACE, 2004, at http://www.environmental.usace.army.mil/info/technical/geotech/sve/sve.html

van der Ham, A. G. J., and H. J. H. Brouwers, 1998. Modeling and experimental investigation of transient, nonequilibrium mass transfer during steam stripping of a nonaqueous phase liquid in unsaturated porous media, Water Resources Research, 34(1): 47-54.

van Dijke, M. I. J., C. J. van Duun, S. E. A. T. M. van der Zee, 1995. Multiphase flow modeling of air sparaging, Adv. Water Res., 18(3): 319-333.

van Geel, P. J. and Sykes, J. F., 1994a. Laboratory and model simulations of a LNAPL spill in a variably-saturated sand, 1. Laboratory experiment and image analysis techniques, Journal of Contaminant Hydrology, 17(1): 1-25.

van Geel, P. J. and Sykes, J. F., 1994b. Laboratory and model simulations of a LNAPL spill in a variably-saturated sand, 2. Comparison of laboratory and model

results, Journal of Contaminant Hydrology, 17(1): 27-53.

van Geel, P. J., and S. D. Roy, 2002. A proposed model to include a residual NAPL saturation in a hysteretic capillary pressure–saturation relationship, Journal of Contaminant Hydrology, 58(1): 79– 110.

van Genuchten, M. T., 1980. A closed-form equation for predicting the hydraulic conductivity of unsaturated soils, Soil Science Society of America Journal, 44(8): 892-898.

van Genuchten, M. T., 1999. Recent advances in vadose zone flow and transport modeling in vadose zone hydrology, ISBN: 0-19-510990-2.

Vogele, T. J., A. Kulresthra, J. J. Nitao, and K. Lee, 1996. Simulation of soil vapour extraction at Building 518 Lawrence Livermore National Laboratory Livermore site, University of California, UCRL-AR-124995.

Wagner, C. 1998. Numerical methods for diffusion-reaction-transport processes in unsaturated porous media, Computing Visualization in Science, 1(1): 97-104.

Weber, W. J., Jr., and F. A. DiGiano, 1996. Process dynamics in environmental systems, Wiley, New York, ISBN: 0-471-01711-6.

Wheeler, M. F., 1988. Numerical simulation in oil recovery in the IMA, Volumes in mathematics and its applications, Volume 11, Springer-Verlag, ISBN: 0-387-96653-6.

White M. D., M. Oostrom and R. J. Lenhard, 1995. Modeling fluid flow and transport in variably saturated porous media with the STOMP simulator, 1. Nonvolatile three-phase model description, Advances in Water Resources, 18(6): 353-364.

Widdowson, Mark A., Orrick R. Haney, Howard W. Reeves, C. Majorie Aelion, and Richard P. Ray, 1997. Multilevel soil-vapour extraction test for heterogeneous soil, Journal of Environmental Engineering, 123(2): 160-168.

Wilkins, M. D., L. M. Abriola and K. D. Pennell, 1995. An experimental investigation of rate-limited nonaqueous phase liquid volatilization in unsaturated porous media: Steady state mass transfer. Water Resources Research, 31(9): 2159-2172.

Wilson, D. J., 1995. Modeling of in-situ technology for the treatment of contaminated soils: Soil vapour extraction, sparging and bioventing, Technical Publications, ISBN: 1-56676-234-0.

Wilson, D. J., A. N. Clarke, and J. H. Clarke, 1988. Soil clean up by in-situ aeration. I. Mathematical modeling, Separation Sci. and Tech., 23(10-11): 991-1037.

Wise, Donald L., Debra J. Trantolo, Edward J. Cichon, Hilary I. Inyang and Ulrich Scottmeister, 2000. Remediation engineering of contaminated soils, Marcel Dekker, Inc., New York, ISBN: 0-8247-0332-4.

Wonnacott, Thomas H., and Ronald J. Wonnacott, 1981. Regression: A second course in statistics, John Wiley & Sons, ISBN: 0-471-95974-X.

Yang, Y. J, T. M. Gates and S. Edwards, 1999. SVE design: Mass transfer limitation due to molecular diffusion, Journal of Environmental Engineering, 125(9): 852-860.

Yang, Ji-Won, Hyun-Jeong Cho, Gwan-Young Choi and Sang-Hyun Lee, 2001. Cost effective monitoring for soil vapour extraction (SVE) system, A simplified modeling and gas sensor test, Environmental Monitoring and Assessment, 70(2):201-210.

Ying, Ouyang and Chunmiao Zheng, 1999. Density-driven transport of dissolved chemicals through unsaturated soil, Soil Science, 164(6): 376-391.

Yong, Raymond N., 2001. Geoenvironmental engineering: Contaminated soil, pollutant fate and mitigation, ISBN: 08493-8289-0, CRC Press.

Yoon, Hongkyu, Joong Hoon Kim, Howard M. Lijestr, and Jeehyeong Khim, 2002. Effect of water content on transient nonequilibrium NAPL-gas mass transfer during soil vapour extraction, Journal of Contaminant Hydrology, 54(1): 1-18.

Yoon, Hongkyu, Alberta J. Valocchi, and Charles J. Werth, 2003. Modeling the influence of water content on soil vapour extraction, Vadose Zone Journal, 2(3): 368-381.

Younger, Mary Sue, 1979. Handbook for linear regression, Duxbury Press, ISBN: 0-87872-1878.

Zhao, Lian and Richard G. Zytner, 2004. The application of FEMLAB in modeling soil vapour extraction, Proceedings of the World Engineers' Convention 2004, Environment Protection and Disaster Mitigation, Vol. D, China Science and Technology Press, Beijing, ISBN: 7-5-46-39290-X, pp 115-119.

Zhao, Lian and Richard G. Zytner, 2005. Impact of mass transfer on soil vapour extraction, CSCE 2005, Toronto, Ontario, Canada on Jun 3-6.

Zheng, Chunmiao and Gordon D. Bennett, 2002. Applied contaminant transport modeling, second edition, Wiley Inter science, John Wiley & Sons, Inc, ISBN: 0-471 -38477-1.

Zhou, D. and M. Blunt, 1997. Effect of spreading coefficient on the distribution of light non-aqueous phase liquid in the subsurface, Journal of Contamination Hydrology, 25(1): 1-19.

Zou, S., and A. Parr. 1993. Estimation of dispersion parameters for two dimensional plumes, Ground Water, 31:389-392.

Appendix

PART A *PPLICATION OF FEMLAB MODELING SOFTWARE*

A1 Initialization of a Model

The installation of FEMLAB with MATLAB is strongly recommended because some of the final simulated results need to be edited by means of MATLAB functions in order to implement more varied formats of the simulated outputs and improve the understanding of the modeled results. Additionally, the necessary digital information to assist modeling, such as site characterization, collection of representative soil sample analysis data for soil gas and soil solid contaminant concentration, field measurement for operation conditions, known data analysis and management also can be manipulated under the MATLAB platform. The computational modeling tasks are very conveniently and flexibly implemented when carried out in MATLAB. These include calibrating against experimental data or the outputs from other model results, investigating the effects of various factors on the simulated results, and undertaking sensitivity analyses.

Prior to modeling the designated SVE scenario, the general instructions and clues for the constructed model can be written down in the model properties windows as shown in Figure A1. In the window of the model navigator, all built-in models, according to typical physical processes, are listed in an optional menu. For this work, only the PDE modes can be chosen. The PDE modes allow users to

construct various specific nonlinear coefficients, the rate of mass transfer, source/sink terms along with the advection and dispersion flux items in mathematical models. Further, the general PDE form in PDE modes and subsequent time-dependent forms are chosen.

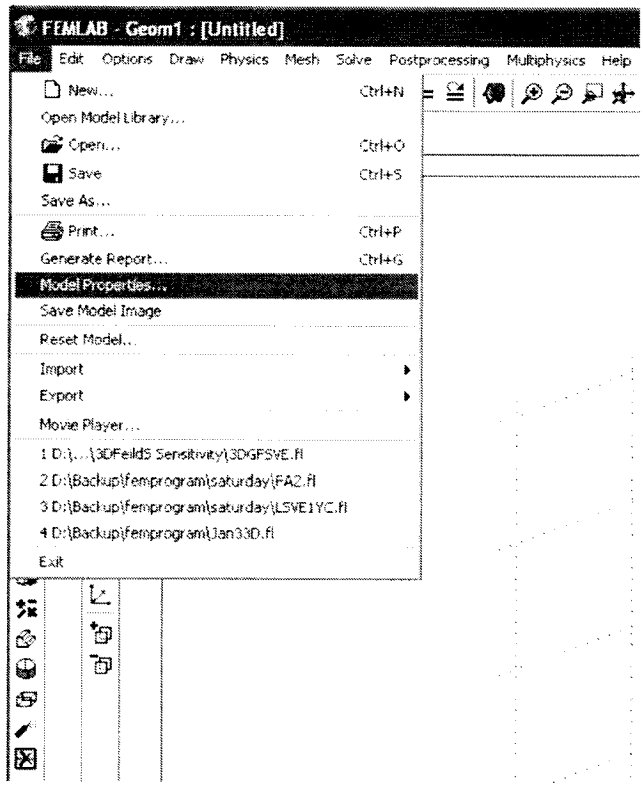

Figure A1 Model Properties

A series of options in the menu of the built-in models are shown in Figure A2. The primary variables in PDEs of a model are input into the dependent variables window. Also, the types of element can be chosen in these windows. Generally, the linear element is defaulted. FEMLAB Version 3.1 defaults to the quadratic element.

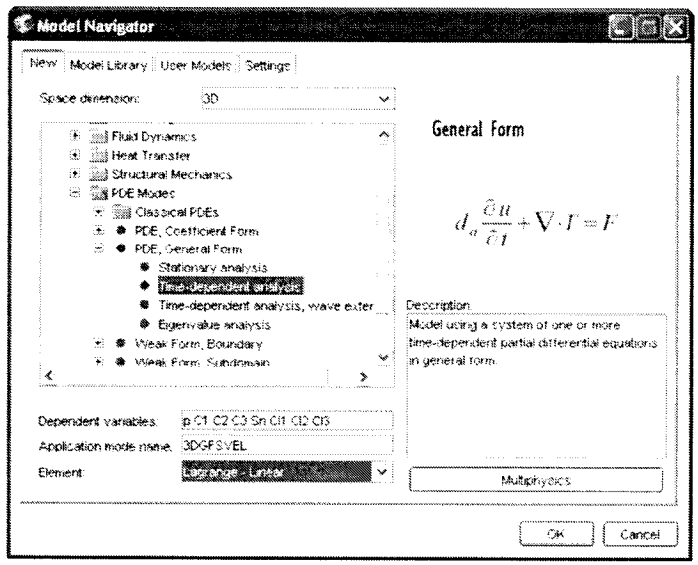

Figure A2 The Description of Initialization of a Model

A2 Setting up Models with FEMLAB

A2.1 Domain Geometry

Under FEMLAB drawing functions, any 3D geometry can be drawn. The single primary 3D geometry can be drawn by means of shortcut icons of specific primary geometries. They can also be combined using the drawing functions of FEMLAB to get the more complex domain geometries through union, difference, or intersection of the drawn primary geometries. More complex geometries of the simulated domains may also be directed in various working planes. This capability to produce diverse geometries allows modelers to set up simple hypothetical heterogeneous sites and add operational equipment.

A2.2 Finite Element Scheme and Interpolation (Shape) Functions

The finite element scheme constitutes weighted residuals and variation methods (Zaradny, 1993). FEMLAB uses the Galerkin finite element scheme, one of the classic weighted residual methods, which is a widely applied finite element method and employs identical weight and base functions. In a general time-dependent problem, three spatial and one time-independent parameter will be involved. Usually, a finite element method is used to formulate the solution in physical space, whereas the time derivative can be approximated by finite difference method such that higher order finite difference equivalence obtains the solution over a period of time.

The finite element method approximates the behaviour of a continuum by discretizing the domain into a finite number of elements. Each element is connected to its neighbour nodes. The field variables are assigned to each node and described by the degrees of freedom. The values of the field primary unknown variables in mathematical model governing equation systems in each element are assumed to be simple functions of these nodal values denoted as:

$$\{u\} = \{N\}\{d\} \tag{A1}$$

Where:

$\{u\}$ = vector of field variable

$\{N\}$ = interpolation (shape) function

$\{d\}$ = vector of nodal points.

Approximation (shape) function $\{N\}$ should not only satisfy the boundary conditions of the given problem but also should make the description of geometry

and material parameters by means of the discretized elements. A shape function is a function that is defined over a single element and is one at a single nodal point and zero at all others. The solution of a numerical model is the linear combination of shape functions. If suitable shape functions are used in the solution procedures, the accuracy of the approximation solution of a numerical method will be improved (Rao, 2005).

There are various types of interpolation functions that can be chosen in FEMLAB, including Lagrange and Hermite interpolation. For classic Lagrange interpolation, shape functions are obtained by fitting a curve for the field variables of a problem without concerning its derivatives. In Lagrange-type elements, the solution for a field variable being approximated is continuous between elements. However, its derivatives are not necessarily continuous. Thus, only second-order partial differential equations can be approximated by Lagrange-type interpolation functions. In many cases, where higher order differential equations might be encountered, Hermite interpolation functions should be applied. There exist shape functions of many different orders such as linear, quadratic, etc. Linear shape functions are used typically in later 3D SVE numerical simulations. The classic multiple order from linear to quartic Lagrange interpolation functions and Hermite interpolation cubic and quartic are covered with FEMLAB. With FEMLAB the type of element and the corresponding shape function can be chosen as shown in Figure A3.

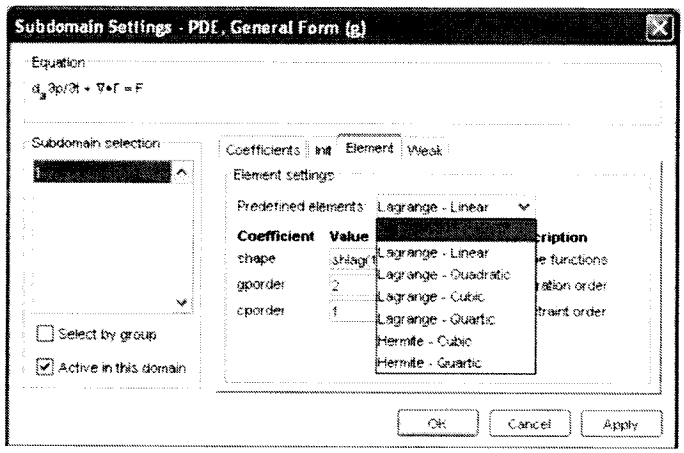

Figure A3 The Options of Shape Functions

A2.3 Input Constants and Expressions

Under the option menu in FEMLAB's main modeling window, there are constants and expression input functions, respectively (Figure A4). The known data and expressions are input separately. The constant is shown in Figure A5 while the expressions are shown in Figure A6. In fact, in the expressions dialogue window, all functional expression can be tracked in spatial and time domains.

A2.4 Setting up the Mathematical Formulations of PDEs

Two essential procedures in modeling are to establish the governing PDEs and the relevant initial and boundary conditions, which are implemented using the physics menu as shown in Figure A7. First, subdomain settings item is chosen as shown in Figure A8. The general principle is to set up a PDE that decomposes derivatives of dependent variables and source/sink terms. Therefore, for any specific

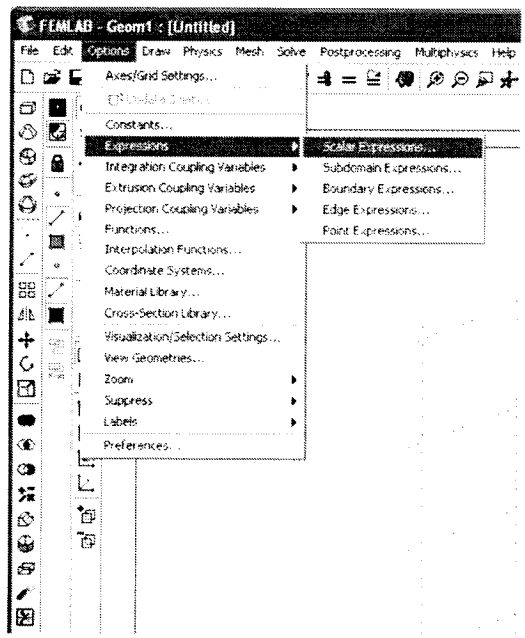

Figure A4 Input of Constants and Expressional Functions

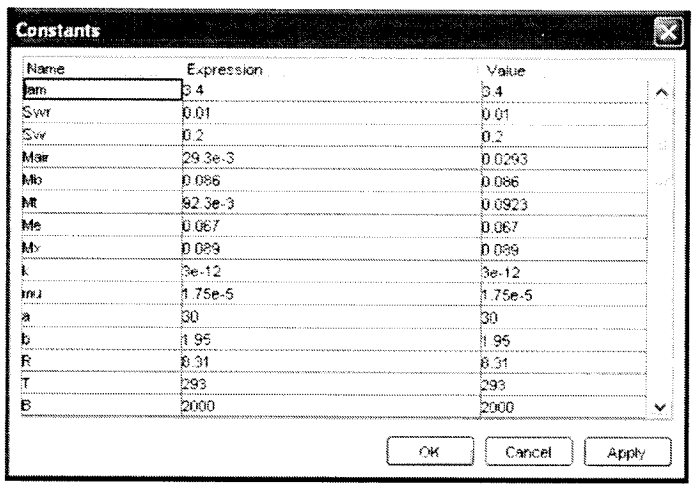

Figure A5 Input of Known Constants

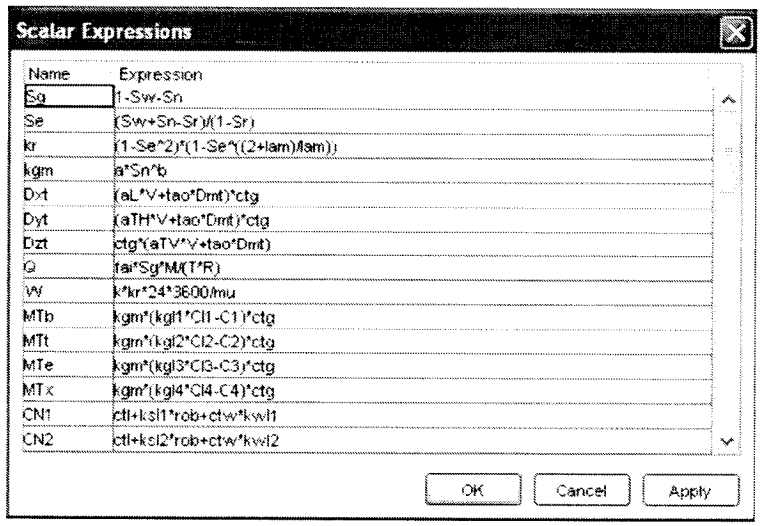

Figure A6 Input of Expressions

PDEs, only according to the mass accumulation term over time, spatial first- and second-order coefficients attached to the above-mentioned items are input into the dialogue windows of the following coefficients:

"d_a", the coefficient of time accumulative term;

"Γ", the coefficient for spatial derivative terms;

"F", source/ sink term; and

"Init", initial conditions.

Accordingly, the setup of a PDE is grounded in the various derivatives for the dependent variable in the PDE. For the cross-coupled multiple dependent primary unknown PDE, there are several unknown dependent variables; thus other variable derivatives should be set up in the "weak" item indicated in Figure A8.

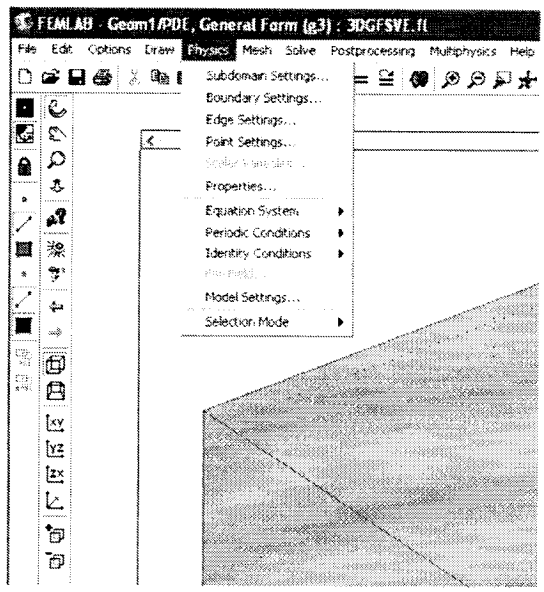

Figure A7 Subdomain and Boundary Settings

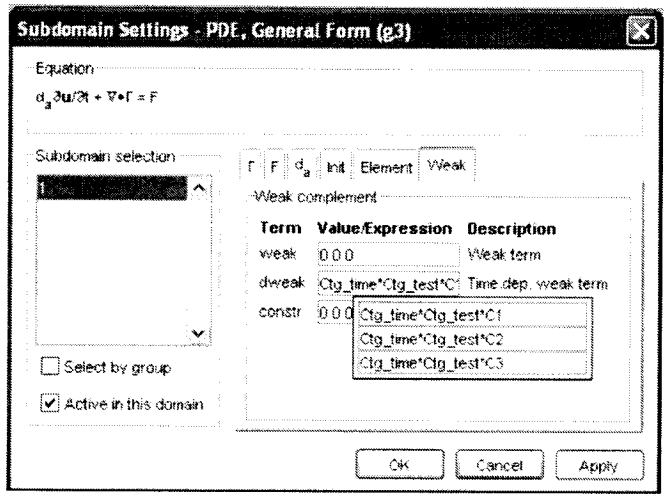

Figure A8 Set up Weak Items for Any Dependent Variable Derivatives

A2.5 Discretization of Space and Time Domain

The shapes, size, and number of the elements have to be chosen carefully such that the original body of a domain is simulated as closely as possible without increasing the computational effort needed. The choice of the type of the element is

indicated by the geometry of the body and the number of independent coordinates necessary to describe the system (Rao, 2005). The types of elements depend on the discretized domain; finite elements with straight sides are linear elements, and those with curved sides are higher order. FEMLAB has been developed for automatic mesh generating for the efficient idealization of complex domains with minimal interface for a given geometry.

Any increase in the number of elements means more accurate results for any given problem. But there will be a certain number of elements beyond which the accuracy cannot be improved by any significant amount. Usually, no more than two or three time mesh refinements are required (Rao, 2005). The sequence of approximate solution will be obtained as the element is reduced successively. This final solution will converge to the exact solution if the interpolation polynomial is satisfactory for the field variable, and interpolation at the dominant boundary has continuity (Rao, 2005).

The sizes of elements influence the convergence of the solution directly and hence it has to be chosen with care. If the size of the elements is small, the final solutions are expected to be more accurate. However, the use of a smaller size of element means more computational time and larger computational load. FEMLAB adapts the different size of elements in the different regions of a simulated domain. The number of nodes in a finite element mesh cannot be determined in advance; the only way to determine the precision of a solution obtained by the finite element method is to repeat the calculation with a finer mesh to see if the results change significantly (Istok, 1989).

FEMLAB deals with time discretization as an implicit scheme with backward differentiation formulas. By setting the degree of the interpolation polynomial used in the discrete-time stepping method, the five orders can be selected (5 by default) as shown in Figure A9. The smaller the order value, the more stable the numerical scheme. Generally, the proper time step is important for the calculation of the flow field and the transport of contaminants. Small time increments should be specific when there are changes in source/sink or time-dependent boundary conditions. Within the length of the simulated period of time, a sixth time increment without significant changes in sink/source and system boundary conditions should be appropriate. The smaller the initial time increment, the greater is the precision (Walton, 1989).

Accounting for the burden of a finite element numerical scheme computation, it is desirable to minimize the number of time steps by employing large time steps. Nonetheless, the sizes of time steps which are critical for obtaining useful results depend on the size and shape of the elements in the mesh and other property parameters of the simulated system. The inappropriate size of time steps may cause the numerical solution to violate reality, instability as well as oscillation (Istok, 1989). Oscillation means that the numerical solution from one step to the next is alternatively above and below the true solution. Instability occurs when the difference between the true solution and the numerical solution becomes great in a few time steps. Fortunately, for some SSOR (Symmetric Successive Over-Relaxation algorithm) linear schemes, when ω (relaxation coefficient) is less than 0.5, the numerical solution will be unconditionally stable.

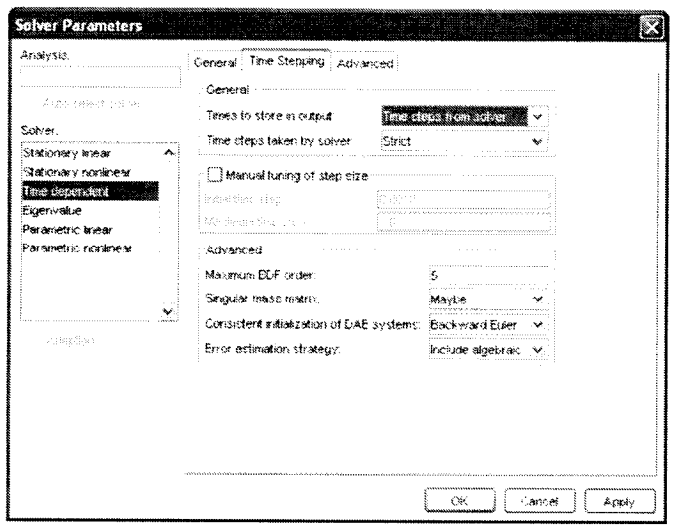

Figure A9 Time-Step Parameters

The size of mesh is controlled by mesh parameters in the Mesh menu shown in Figure A10. Mesh size has a decisive connection with accuracy and stability. For 3D simulation, the general predefined mesh option should be "extremely coarse" so that the initial solution may be obtained as soon as possible.

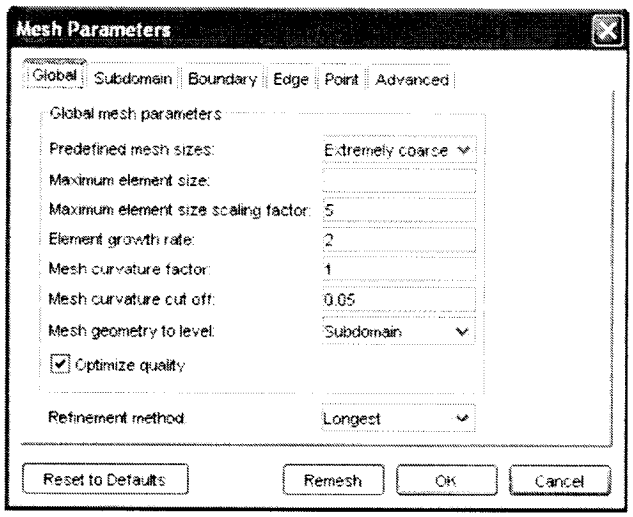

Figure A10 Mesh Optimizations

The seven specific mesh size options can be directly selected by the "Predefined mesh size," which are "Extra fine," "Finer," "Fine," "Normal," "Coarse,"

"Extra coarse," and "Extreme Coarse" mesh. For 3D geometry and a complicated mathematical model, it is difficult to implement the broad refined range of the sizes of element mesh. Also, any specific size of mesh can be generated by setting the specific parameters as shown in Figure A10. In order to obtain the refined meshes of finite elements, the following specific parameters can be assigned as specific values:

- maximum element size, which determines the maximum size of element along with the maximum axial parallel distance;
- element growth rate by which a small size of elements in a region and a large size of elements in a region are generated;
- mesh curvature factor which determines the size of boundary compared to the curvature of the geometric boundary;
- mesh curvature cut-off, which presents the generation of many elements around small curved parts of the geometry.

A2.6 Solving PDEs

Open solver parameters in the solve menu and choose the time-dependent option from the solver list as shown in Figure A11. The time step, absolute and relative error, and various iterative or direct solvers may be chosen to achieve the accurate and quick-solving strategies. First, the absolute and relative error should be set up in advance. There is no accuracy at all when the magnitude of a solution is less than the absolute tolerance. The default relative error is 10^{-6}. Possible various options of iterative methods include incomplete LU, geometric Multigrain, SSOR (Symmetric Successive Over-Relaxation algorithm), SSOR vector, and Jacob.

For the chosen linear solver, the parameters assigned are shown in Figure A12. For a complex 3D simulation, the NSSOR scheme generally is chosen due to its fast convergence and accurate results.

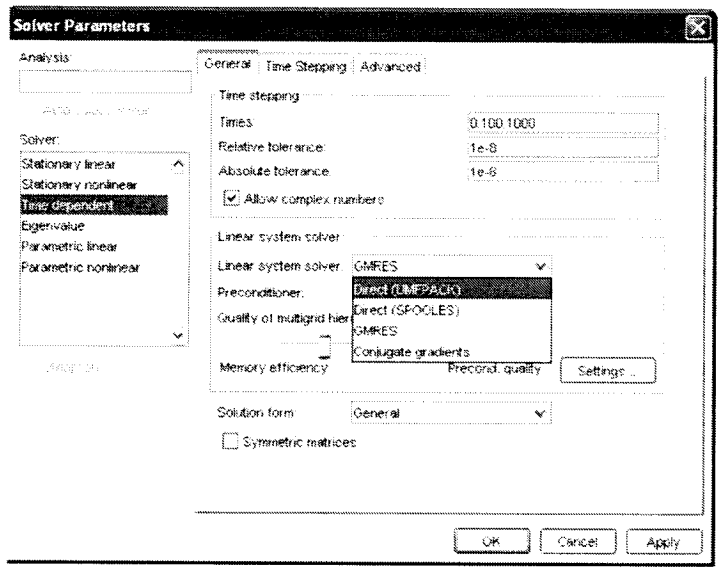

Figure A11 Solver Parameters

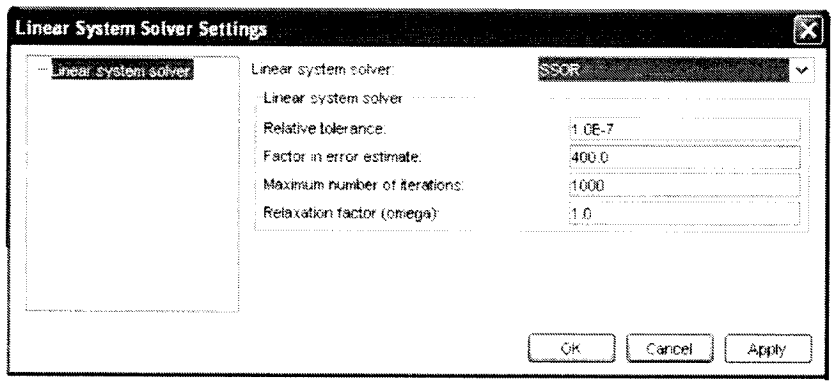

Figure A12 The Linear System Solver Parameters

FEMLAB software has very powerful and diverse post-processing functions for the visualization and animation of the simulated results for any involved variables in the model governing equation system. Figure A13 shows the complete options in the post-processing menu. These options may be set up before running a program. If doing so, the expected images will be displayed as defaults in the main windows.

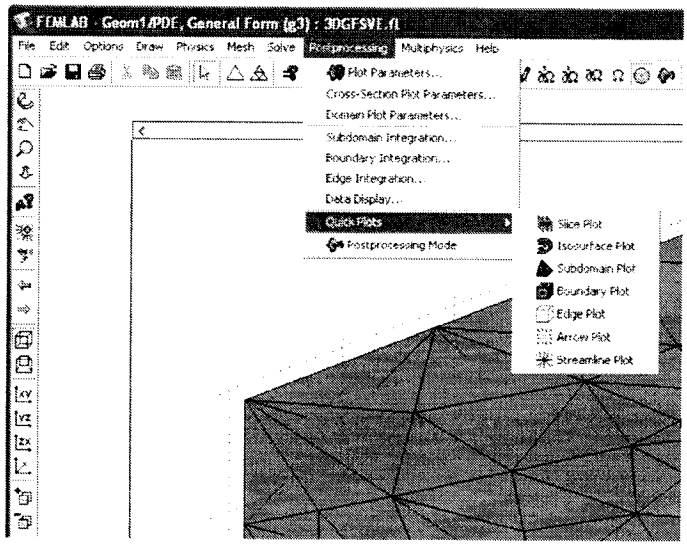

Figure A13 Post-processing for the Simulated Results

To look for the outputs of any variables involved in the numerically solved FEMLAB model, go to **plot parameters** under which the outputs of the dependent variables over the whole simulated domain at a specific time are displayed, or **cross-section plot parameters** under which the simulated results for the specific points or area along a line or a plane in the simulated domain over time are present. The outputs of the required variables versus three-dimensional domain and time can be performed by the movie animation function of FEMLAB. Based on these diverse functions of the post-processing of the simulated results, the desired outputs of the simulated results at any locations in the simulated domain and at any period of the simulated time can be obtained. These outputs optionally can be drawn in MATLAB or FEMLAB graphic user interface windows. But the data management and editing of the resultant drawings for the outputs of the simulated variables have to be undertaken with the MATLAB interface.

There are two basic ways to improve the accuracy of a numerical simulation: the first one is to refine the finite element meshes and time step; another is to adjust criteria for the absolute and relative tolerance error for a solution and choose a different solver in "solve function menu."

In order to reduce the running time, the larger size of meshes is chosen under enough accuracy. Figure A14 illustrates a comparison of solutions from two greatly different time steps, while Figure A15 shows the consequence of refinement of finite elements for 3D-SVE-L model. These results show that FEMLAB has very high accuracy for time and space discretization. This advantage assures that the numerical simulation of field-scale SVE has enough accuracy during the time span of field SVE operation. Refining the size of finite elements by two times still provides a stable solution without computer memory overload.

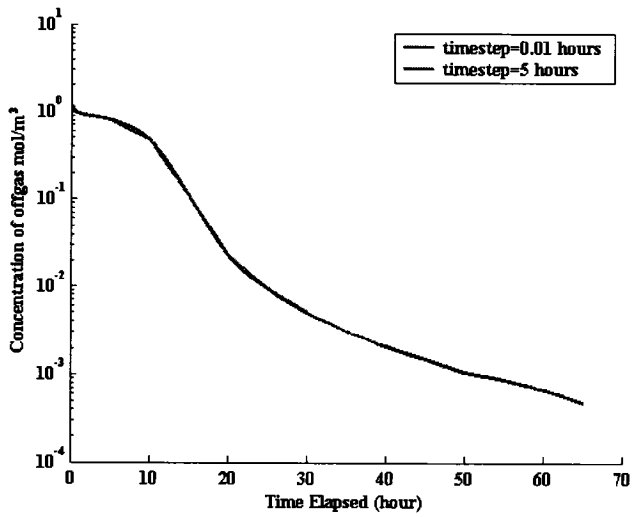

Figure A14 Comparison of Solutions from Different Time Steps

(a) Soil vapor extraction test

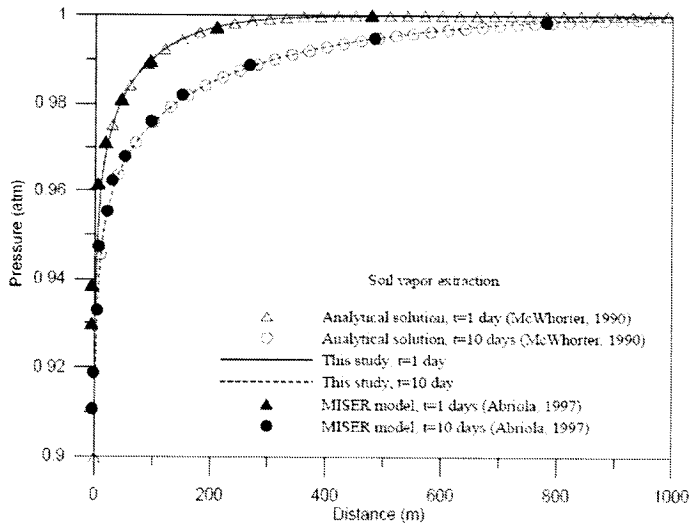

(b) Gas injection test

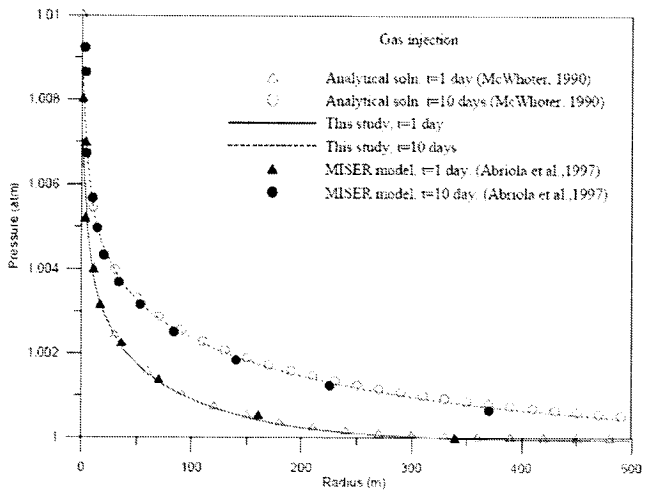

Figure A15 Comparisons of Analytical Solutions and Numerical Results of Two Models (MISER and TechFlow^{MP}) at Gas Extraction/Injection Tests (Cited from Jang (2005))

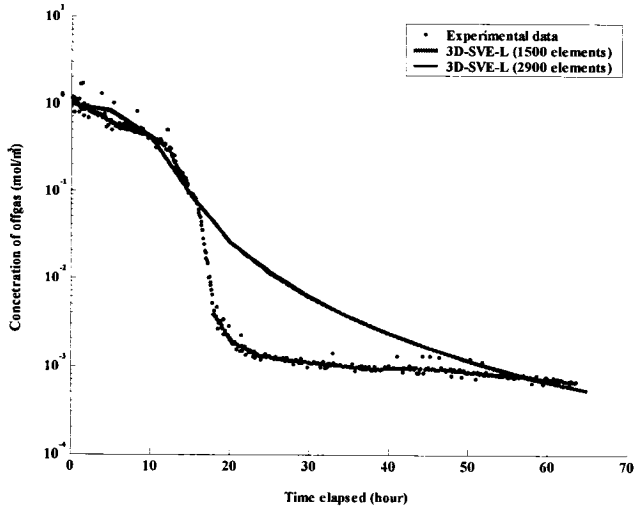

Figure A15 The Impact of Refinement of Element Mesh

In order to review all the details on the modeling processes for a specific case, FEMLAB provides a convenient "report generator" function by which the overall process of modeling is recorded as a final report of the completed project. All input parameters and expressions involved in the model governing equation system and the entire numerical schemes are recorded sequentially in the final report.

A3 Calibration of the Numerical Model against Known Data

After the mathematical model is solved numerically, the simulated results should be calibrated against known results. The convenient data sharing between MATLAB and FEMLAB interactive interfaces makes the combined application more powerful for carrying out the calibration and sensitivity analysis for the modeled results. All known experimental data or data from other simulations which can be used to calibrate the developed model are saved as MATLAB files in advance. In the post-processing menu, the expected dependent variable will be compared against the

modeled value. It is convenient to make a trial visual comparison of the output of FEMLAB modeled results and the known data. For example, in order to calibrate the developed 3D SVE model in this context, the breakthrough curve of offgas concentration is drawn on the same coordinate system as the MATLAB curves of known data. By adjusting the fitting parameters, the updated simulated results are obtained. The match to the known data curves is repeated until visually satisfactory fitting is achieved. The graphics editor can also extract the data from this curve to calculate the final NSSRD (normalized sum of squared residual difference between the calibrated data and the modeled output) in order to confirm the final calibration and quantitatively assess the goodness-of-fit.

A4 The Harper's experimental approach

Harper (1998) completed 1-D column tests with a quaternary component multiphase SVE experiment. The experimental and modeling conditons have been tested using FEMLAB. The following experimental overview is excerpted from Harper et al. (2003).

The soil investigated was a disturbed silt loam soil consisting of 34 wt% sand, 50 wt% silt, and 16 wt% clay. The silt loam had an organic matter content of 2.5 wt %. Venting experiments were performed at three water contents; air dry about 2.7 wt %. The composition of the quaternary contaminant was 42.5 wt% hexane, 25 wt% toluene, 25 wt% m-xylene, and 7.5 wt% trimethylbenzene. Single runs with toluene only were also completed. Following the mixing of the NAPL, water, and soil, the

soil was placed in three lifts in the column to attain a soil bulk density of 1,300 kg/m^3. The columns were made of glass at 200 mm long with a 59 mm outside diameter. The columns were capped with aluminum end plates connected to a diaphragm vacuum pump, which drew humidified atmospheric air.

Venting runs were immediately started, with a combination of manual and on-line sampling used to obtain vapor samples. Manual samples were obtained by inserting a 10 mL gas tight syringe through the septa attached to the sampling port at the top of the column. These vapor samples were injected immediately into an HP 5890 series gas chromatograph equipped with a flame ionization detector for analysis. Manual sampling continued until the vapor concentrations were below the upper detection limit of the photoionization detector of approximately 7.5 g/m^3.

The complete mathematical model FEMLAB file is attached in the Disc with this thesis.

A5 Simulated Case: Duggal 's Experimental Approach

Duggal (2005) designed a SVE reactor and completed a series of SVE experiments. As shown in Figure A16, this SVE system includes with one sreened venting well which creates the radial flow of fesh air through the contaminated soil. The outside of the reactor is connected to atomasphere. The flow rate of each experiment is controlled by the air pump. The concentration of effluent gas is maeasured by online HP 5890 series gas chromatograph.

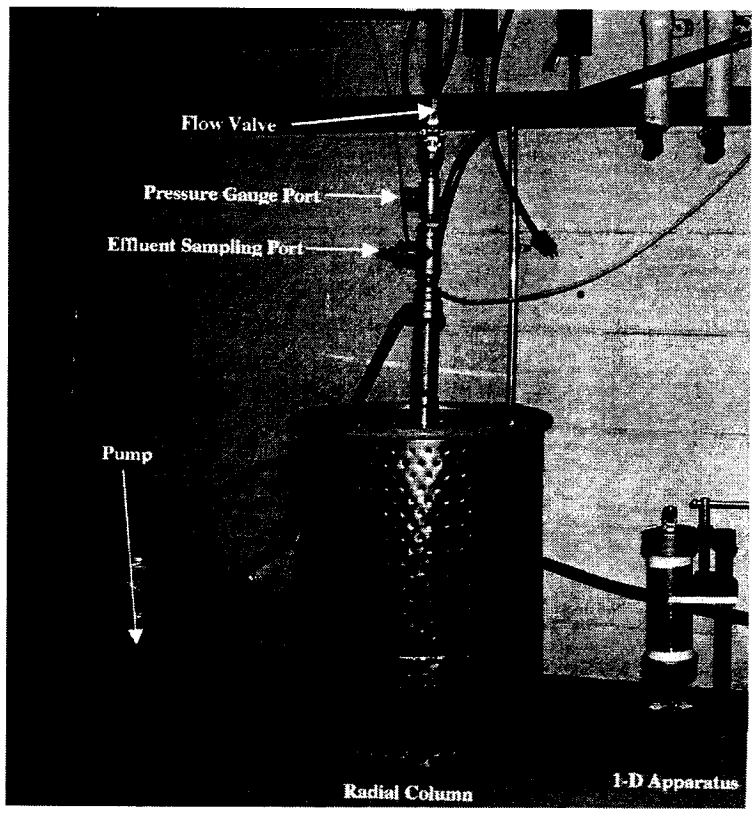

Figure A16 Lab-scale SVE reactor by Duggal (2005)

Part B Experimental and Simulated Breakthrough Curves And Sensitivity analysis

B1 Data Used in the 3D-SVE-L Model

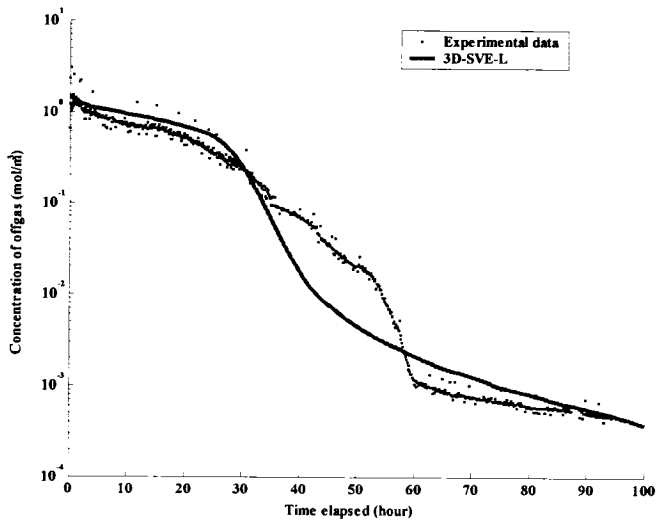

Figure B1 **Fitted Results for Case 1 (Elora silt, NSSRD=0.215)**

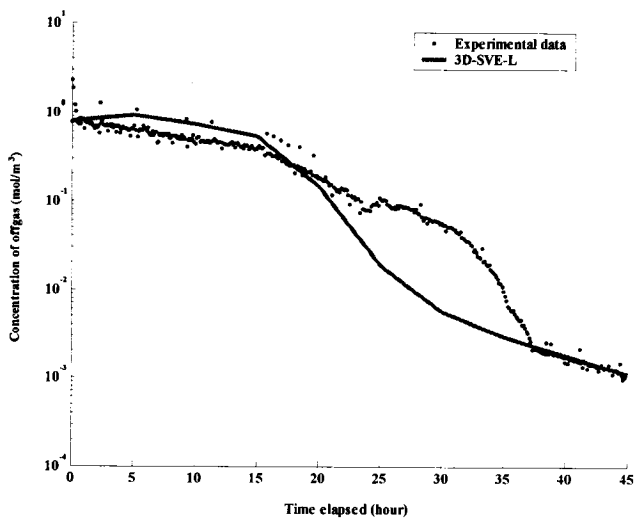

Figure B2 **Fitted Results for Case 2 (Elora silt, NSSRD=1.336)**

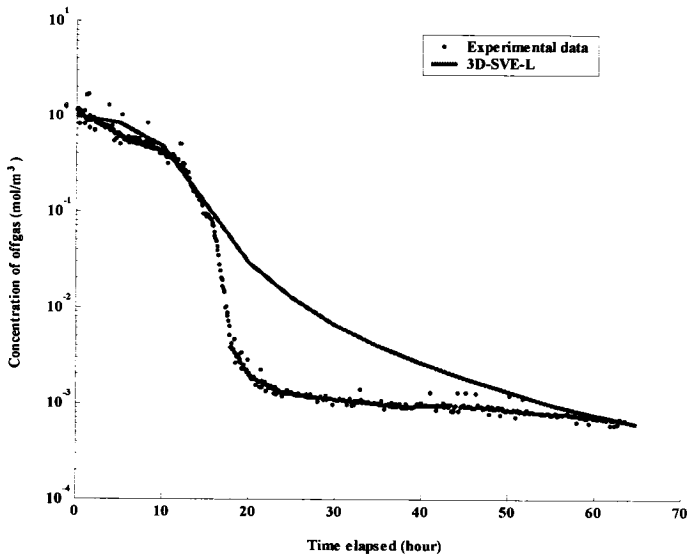

Figure B3 **Best Fitting Results for Case 3 (Elora silt, NSSRD=0.528)**

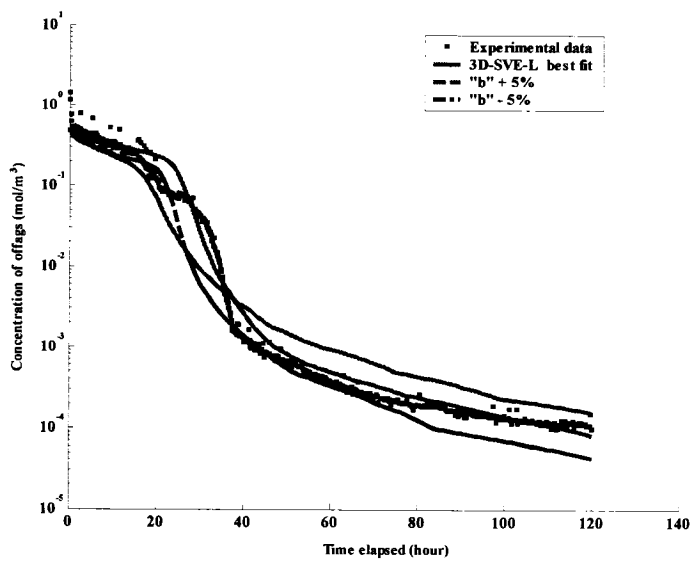

Figure B4 **Best Fitting Results for Case 4 (Elora silt, NSSRD=0.0735) and the Approach to Best Fitting**

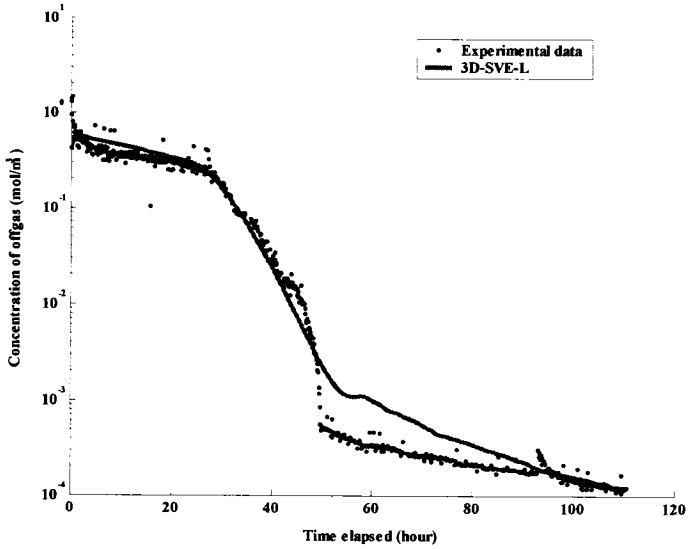

Figure B5 **Best Fitting Results for Case 5 (Elora silt, NSSRD=0.082)**

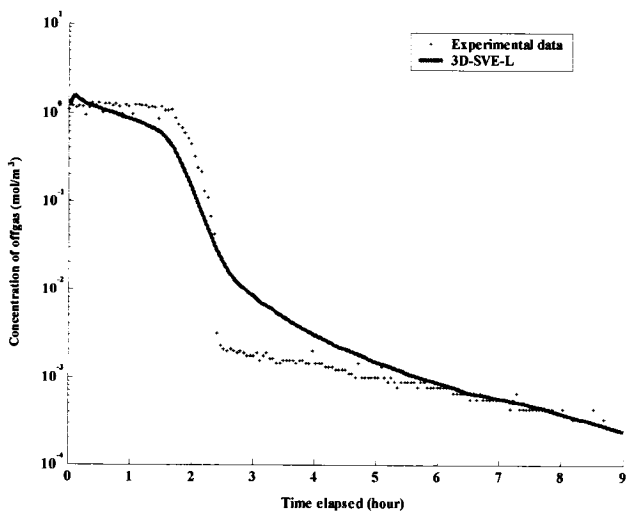

Figure B6 **Best Fitting Results for Case 6 (Elora silt, NSSRD=0.76)**

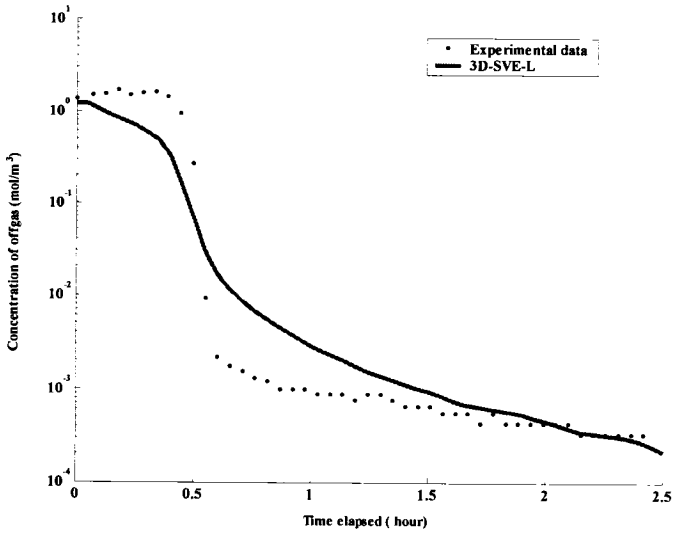

Figure B7 **Best Fitting Results for Case 7 (Ottawa sand, NSSRD=1.38)**

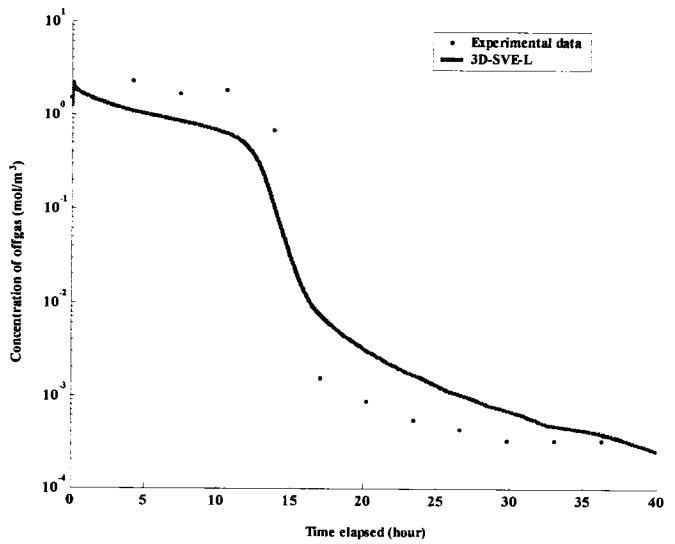

Figure B8 **Best Fitting Results for Case 8 (Ottawa sand, NSSRD=0.98)**

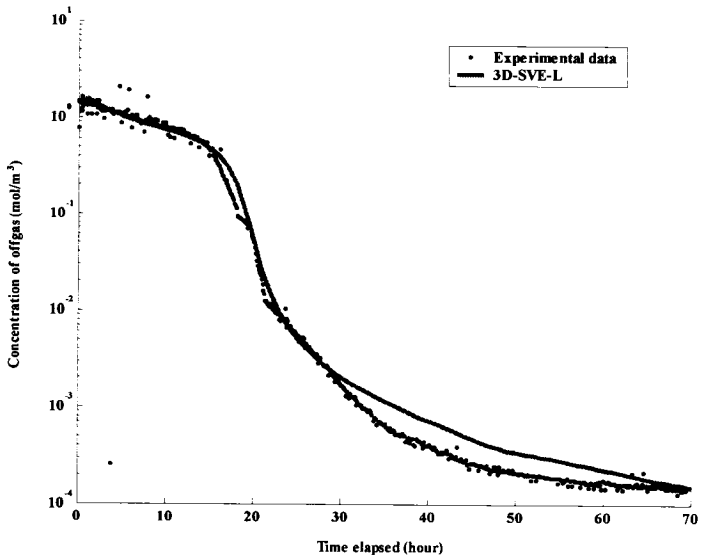

Figure B9 **Best Fitting Results for Case 9 (Ottawa sand, NSSRD=0.163)**

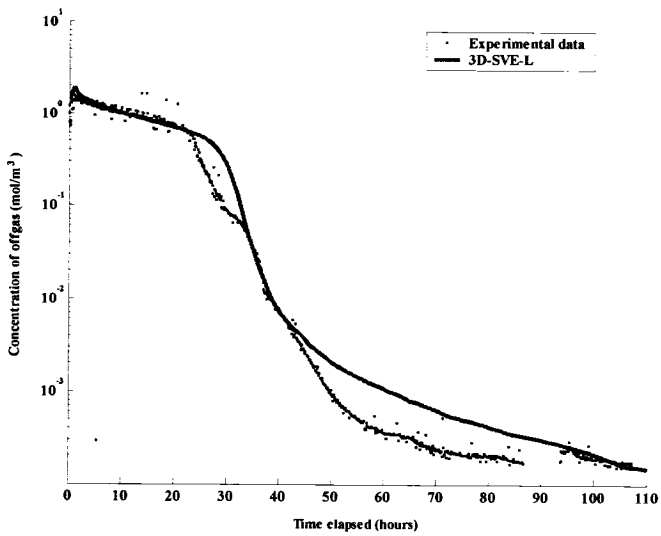

Figure B10 **Best Fitting Results for Case 10 (Ottawa sand, NSSRD=0.938)**

B2 Data for Sensitivity Analysis of 3D-SVE-L/F Models and The Results of Multivariable Regression

Table B1 Data used to calculate the multiple regression sensitivity model for 3D-SVE-L

№	Concentration of offgas at t time (mol/m^3)				Controlling parameters			
	t=10 hours	t=30 hours	t=60 hours	t=100 hours	k (m^2)	α_L (m)	a (h^{-1})	b
1	0.76631	0.38674	0.0022891	0.00038925	6e-10	0.0370	12	1.70
2	0.82146	0.69121	0.42579	0.036385	3e-10	0.0365	19	1.75
3	1.0114	0.71411	0.033437	3.4739e-3	3e-13	0.045	24	1.80
4	0.90501	0.67765	0.081302	0.01063	5e-11	0.040	48	2.00
5	1.0586	0.73421	0.014722	1.2328e-3	2e-12	0.0525	39	1.60
6	0.96849	0.61865	0.0022622	3.3793e-3	4e-11	0.0485	31	1.85

Table B2 The estimated values of coefficients in regression equation for 3D-SVE-L and residual variant

Coefficients in Regression equations for	t=5 hours	t=20 hours	t=50 hours	t=100 hours
Constant	0.92188	0.63709	0.093300	0.009472
δk	-0.034369	-0.263096	-0.52824	-0.045005
$\delta \alpha_L$	0.508129	-1.86766	-5.83854	-0.495624
δa	-0.020833	-0.096575	-0.377933	-0.032205
δb	0.001225	3.2749	9.13539	0.75318
Residual variant of regression equations	8.234e-4	2.977e-4	7.610e-5	6.960e-5

Table B3 Data used to calculate the sensitivity model for 3D-SVE-F

№	Concentration of offgas at t time, (μmol/m^3)				Controlling parameters			
	t=100 days	t=200 days	t=400 days	t=800 days	k (m^2)	α_L (m)	a (h^{-1})	b
1	7.0287	1.1321	1.4976e-1	3.7969e-2	3e-11	0.20	1e-3	1.80
2	4.8240	1.239	1.3194e-1	3.66928e-2	1e-10	0.46	3e-4	1.90
3	2.7443	6.5738e-1	1.0317e-1	2.139e-2	3e-13	0.36	4e-4	1.70
4	11.833	2.4546	2.07086e-1	5.2803e-2	1e-12	0.70	5e-4	1.60
5	9.6075	2.4557	3.1562e-1	1.0297e-1	6e-10	0.95	7e-4	2.00

Table B4 The Regression Equation for 3D-SVE-F and Residual Variant

Coefficients of Regression equations	Concentration, mol/m^3			
	t=100 days	t=200 days	t=400 days	T=800 days
Constant	7.4428e-5	2.3536e-5	7.5616e-6	1.5054e-6
k	-1.1269e-4	-2.8813e-5	-1.1572e-5	-3.2661e-6
α_L	-1.6913e-4	-3.1956e-5	-1.4584e-5	-3.3398e-6
a	-1.21549e-4	-2.8796e05	-1.2100e-5	-3.0350e-6
b	2.2078e-4	5.873e-4	2.3484e-4	.1352e-5
Residual variant of regression equations	1.648e-11	5.219e-13	6.6167e-13	6.2655e-15
Max. errors of regression equations	4.1957e-6	7.4662e-7	8.406e-7	8.1803e-8

Table B5 The Errors of Coefficient of Regression Equation for 3D-SVE-F Model

Coefficient errors of Regression equations for	Standard errors of coefficients, mol/m^3			
	t=100 days	t=200 days	t=400 days	T=800 days
Constant	1.6574e-6	2.945e-7	3.321e-7	3.2315e-8
k	6.664e-6	1.118e-6	1.332e-6	1.296e-7
α_L	2.296e-5	4.086e-6	4.600e-6	4.4771e-7
a	8.199e-6	1.459e-6	1.643e-6	1.5986e-7
b	1.021e-4	1.1818e-5	2.0464e-5	1.9914e-6

Table B6 The Errors of Coefficient of Regression Equation for 3D-SVE-F and the 95% Confidence Interval

Coefficients of Regression equations	Coefficients and distribution					
	t=100 days			t=200 days		
	Estimate*	Max**	Min***	Estimate	Max	Min
Constant	0.7443	0.7868	0.6959	0.2335	0.2400	0.2267
k	-1.1297	-0.9355	-1.3238	-0.2881	-0.2536	-0.3226
α_L	-1.6913	-1.0208	-2.3619	-0.3196	-0.2002	-0.4389
a	-1.2155	-0.9761	-1.4549	-0.2880	-0.2453	-0.3306
b	22.079	25.061	19.096	5.8734	6.4041	5.3427

*** The estimated values of coefficients in regression equations;**
**** 95% confidence interval possible maximum values;**
***** 95% confidence interval possible minimum values.**

Continued Table B6

Coefficients of Regression equations	Coefficients and distribution					
	t=400 days			T=800 days		
	Estimate	Max	Min	Estimate	Max	Min
Constant	0.07515	0.08485	0.0654	0.0151	0.0160	0.0141
k	-0.1157	-0.0768	-0.1162	-0.03326	-0.0280	-0.1546
α_L	-0.1458	-0.0115	-0.2801	-0.3398	-0.0209	-0.2801
a	-0.1210	-0.0730	-0.1689	-0.03036	-0.0257	-0.1689
b	2.3484	2.946	1.7508	0.5135	0.57175	1.7509

Part C Developed Model Software CD disc

FEMLAB and MATLAB files, which are programs of the developed models and data set applied in sensitivity analysis and calibration, are attached on the disc in this thesis.

C1 Data MATLAB File

MATLAB programs contain data and calculus programs:

- Calibration against Duggal's (2005) and Harper's (1999) experimental data and CRA SVE field sampling data and the calculated NSSRD;
- Sensitivity analysis data set which comes from the simulated results from 3D-SVE-L and 3D-SVE-F.

C2 Model FEMLAB Files

The program includes the best fitting program and series simulation for various fitting parameters for sensitivity analysis.

C 2.1 1D-SVE-L

This is a one-dimensional transport model and it is calibrated into the experimental data and simulated results done by Harper (1999).

C 2.2 3D-SVE-L

This is a series of model files which are calibrated into the 10 sets of experimental results with a lab-scale reactor completed by Duggal (2005).

C2.4 3D-SVE-F

This is a model file which is calibrated into the results of a real field SVE remediation operation conducted by CRA Inc. in 1997.

C2.5 3D-SVE-FHE

This program is a model which simulates the hypothetical heterogeneous site SVE operation in field scale.

C3 A Series of FEMLAB Model Files Sensitivity Analysis

C3.1 3D-SVE-L series

C3.2 3D-SVE-F series

Part D Data and Breakthrouhg Curves Used to Predict Closure Time

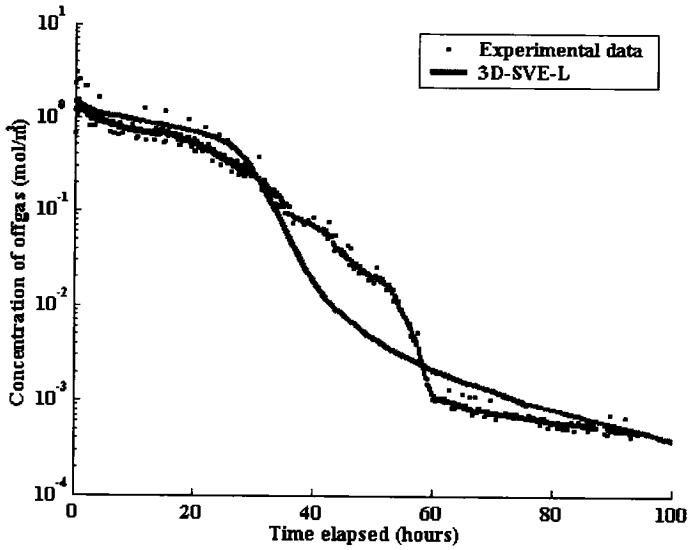

Figure D1a **Matched Breakthrough Curves for Case 1 (Elora silt, NSSRD=0.215)**

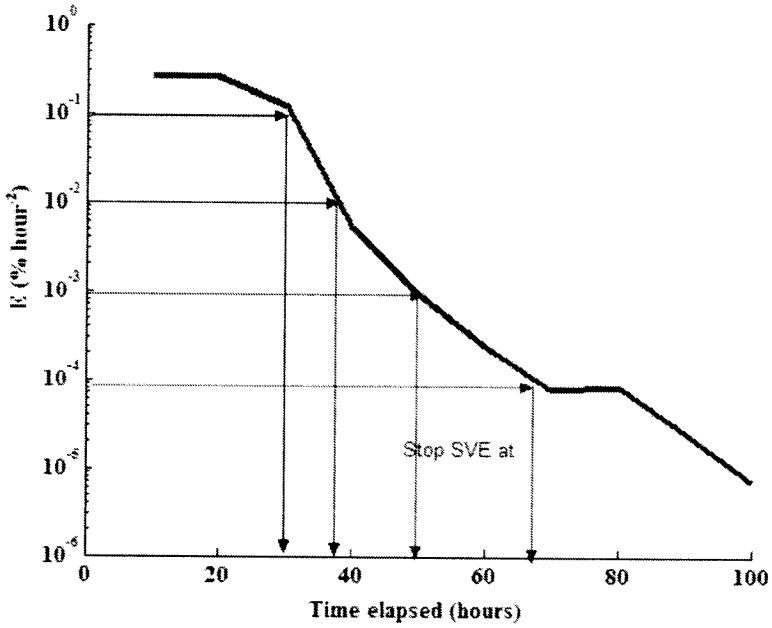

Figure D1b **The Relative Slope of Breakthrough Curve over Time for Case 1, $\Delta t_1 > \Delta t_2 < \Delta t_3$**

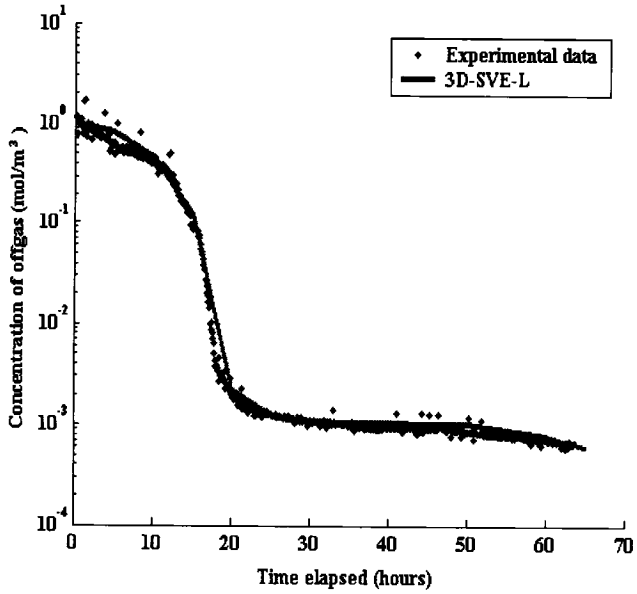

Figure D2a Matched Breakthrough Curves of Case 2 (Elora Silt, NSSRD=0.0021)

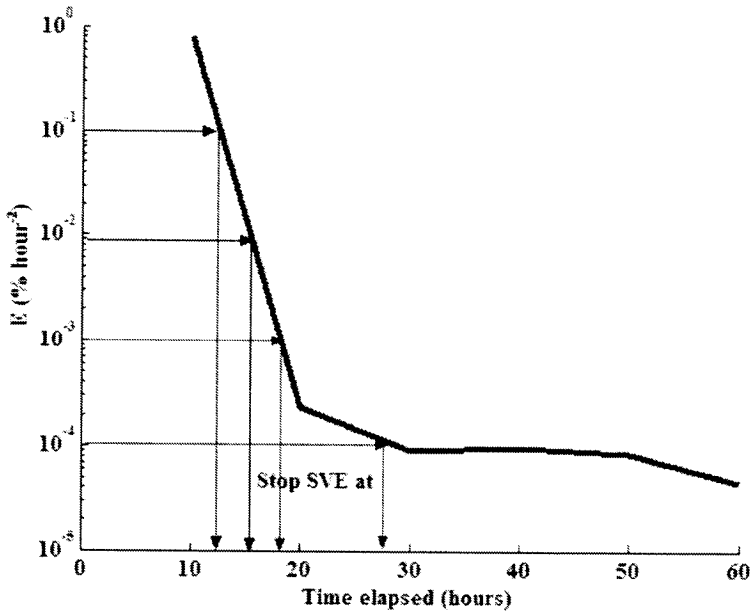

Figure D2b The Relative Slope of Breakthrough Curve over Time for Case 2, $\Delta t_1 < \Delta t_2 < \Delta t_3$

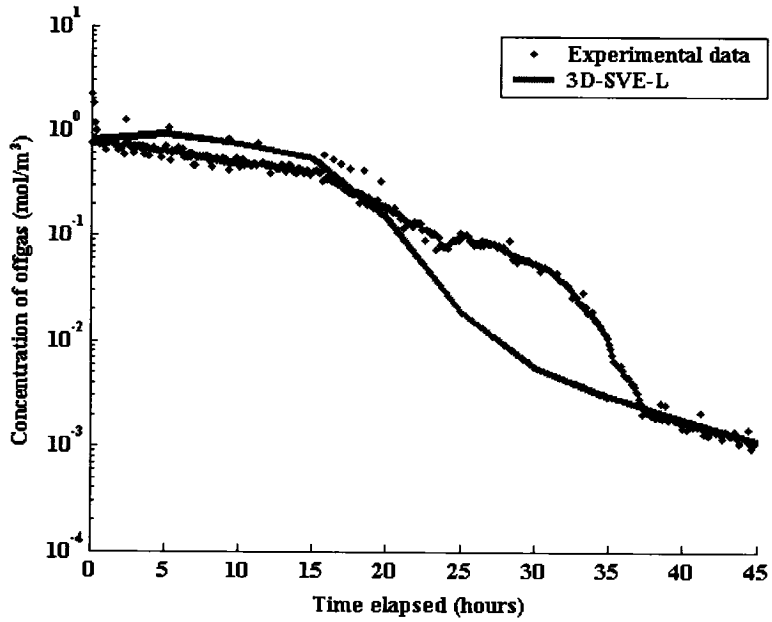

Figure D3a **Matched Breakthrough Curves of Case 3 (Elora Silt, NSSRD=0.528)**

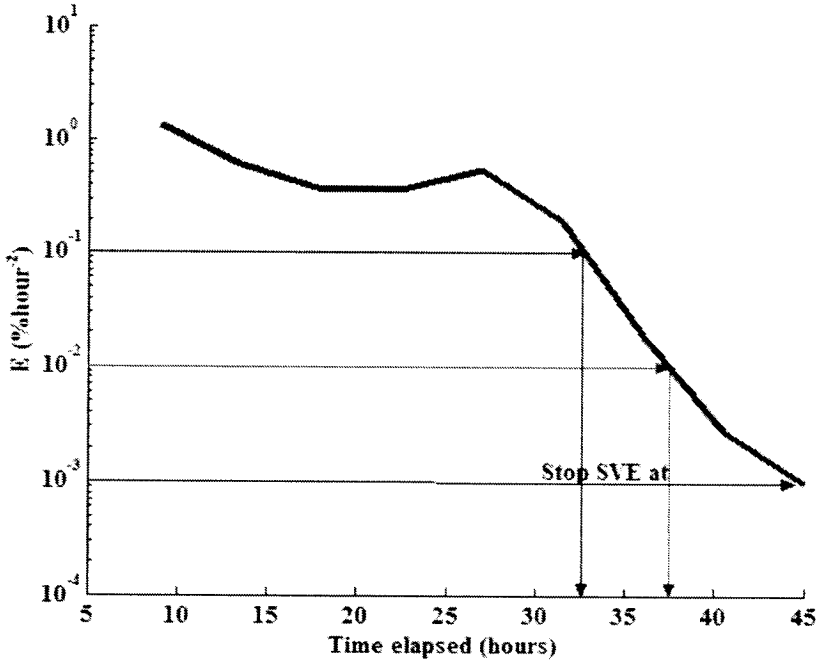

Figure D3b **The Relative Slope of Breakthrough Curve over Time for Case 3, $\Delta t_1 > \Delta t_2 < \Delta t_3$**

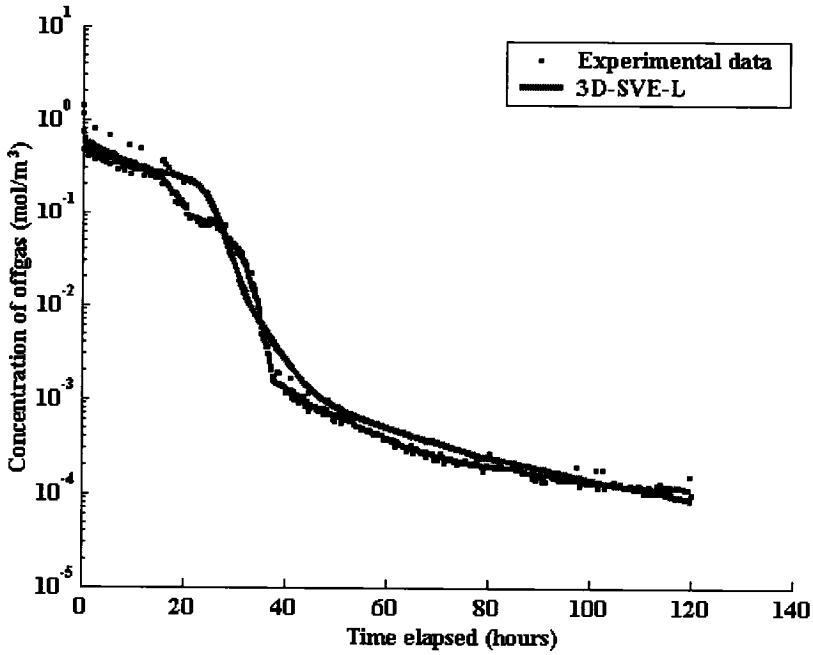

Figure D4a **Matched Breakthrough Curves of Case 3 (Elora silt, NSSRD= 0.0735)**

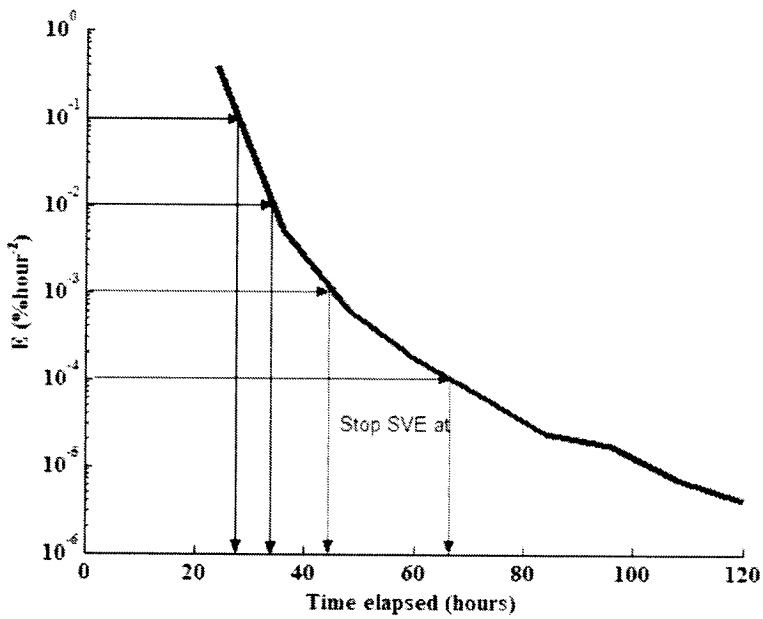

Figure D4b **The Relative Slope of Breakthrough Curve over Time for Case 4, $\Delta t_1 < \Delta t_2 < \Delta t_3$**

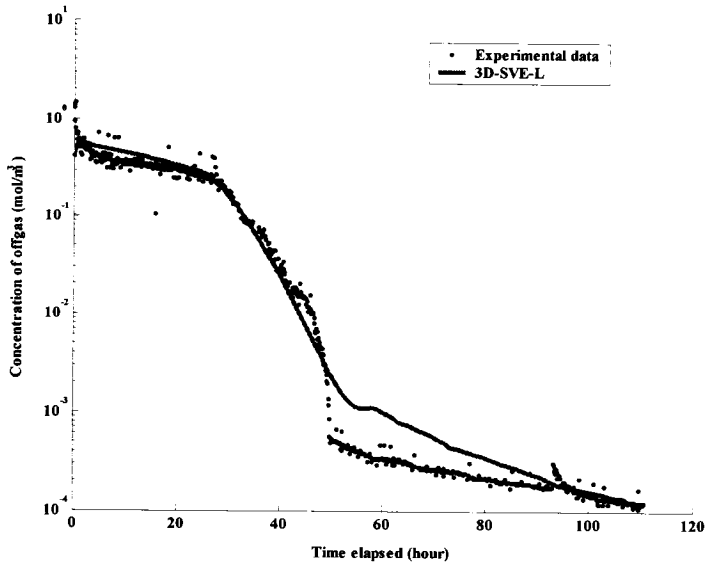

Figure D5a **Matched Breakthrough Curves of Case 5 (Elora Silt, NSSRD= 0.985)**

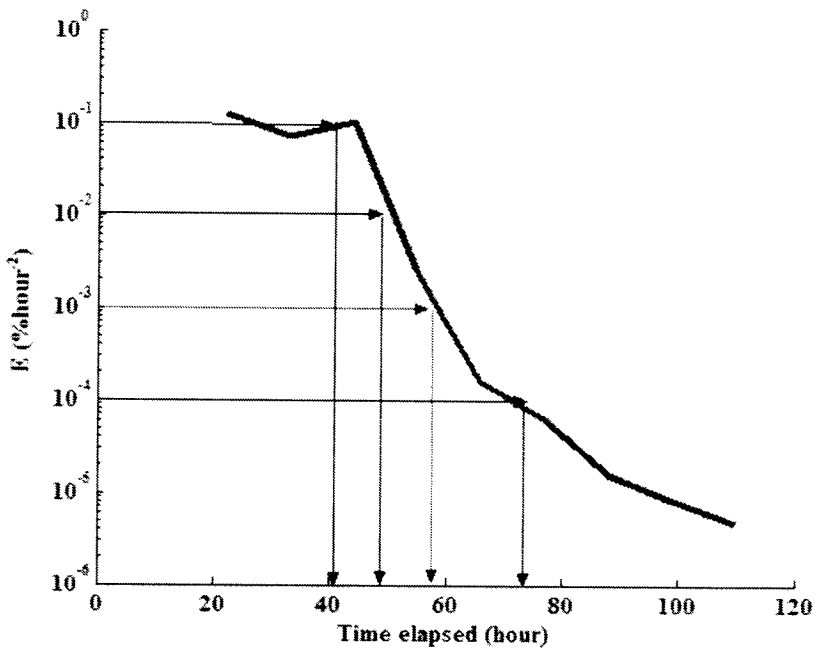

Figure D5b **The Relative Slope of Breakthrough Curve over Time for Case 5, $\Delta t_1 < \Delta t_2 < \Delta t_3$**

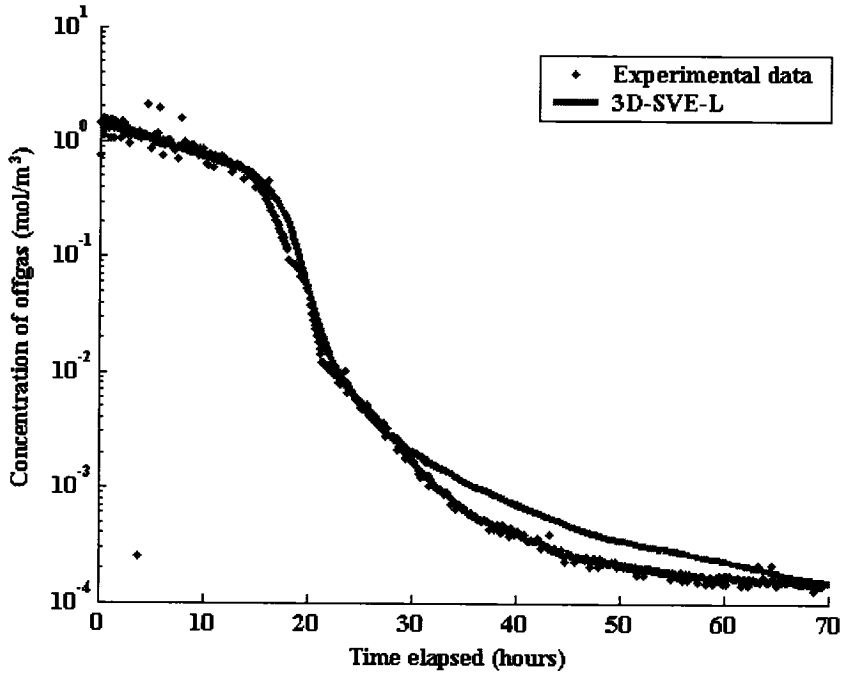

Figure D6a **Matched Breakthrough Curves of Case 9 (Ottawa Sand, NSSRD= 0.161)**

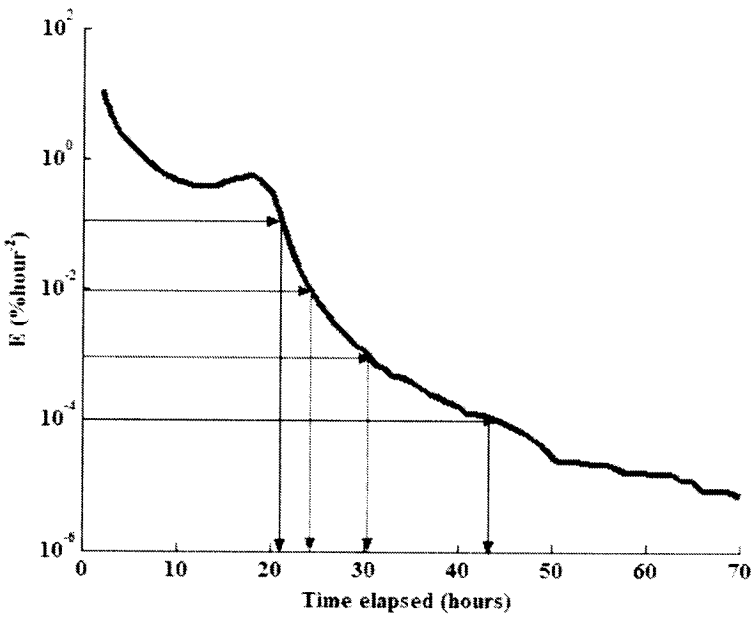

Figure D6b **The Relative Slope of Breakthrough Curve over Time for Case 6, $\Delta t_1 < \Delta t_2 < \Delta t_3$**

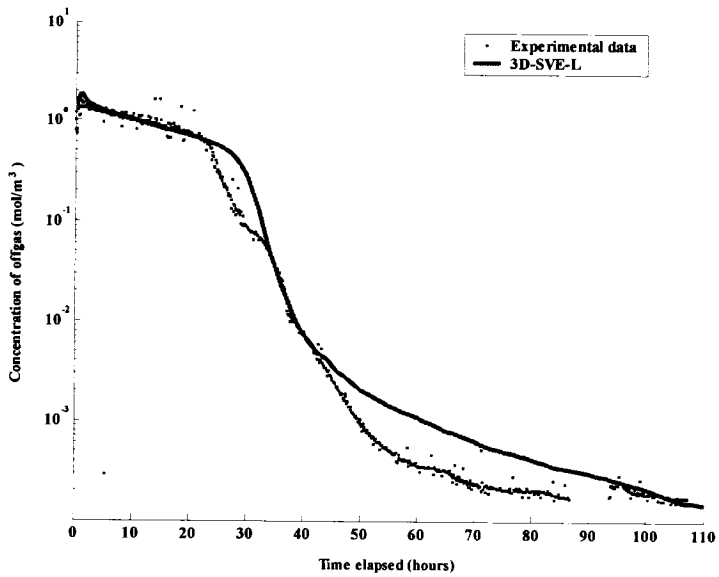

Figure D7a **Matched Breakthrough Curves of Case 10 (Ottawa Sand, NSSRD= 0.983)**

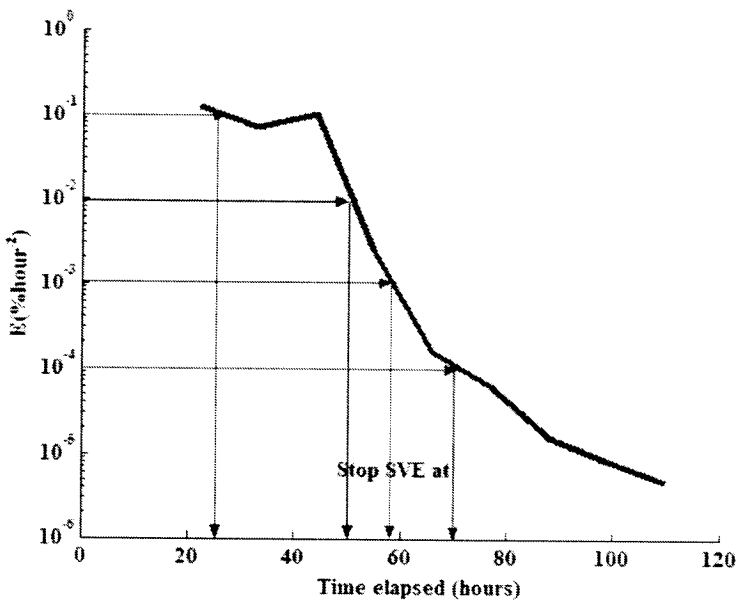

Figure D7b **The Relative Slope of Breakthrough Curve over Time for Case 10, $\Delta t_1 > \Delta t_2 < \Delta t_3$**

Table D1 The Predicted Concentration of Benzene in Offgas versus Time

Operation time, day	C_{off}, mol/m^3		
	Top fitting	Middle fitting	Tail fitting
0	0.0032634	0.0032634	0.0032634
100	0.0012619	0.00032596	6.7384e-5
200	0.00022626	5.5028e-5	1.1539e-5
300	9.0679e-5	1.8586e-5	5.8768e-6
400	4.5914e-5	8.222e-6	3.2782e-6
500	2.7402e-5	5.3133e-6	2.1239e-6
600	1.88766e-5	3.5842e-6	1.4744e-6
700	1.3778e-5	2.524e-6	1.0876e-6
800	1.1041e-5	1.9321e-6	7.6508e-7
900	7.7624e-5	1.4724e-6	5.3063e-7

Table D2 The Predicted Slope of Breakthrough Curve of Benzene in Offgas versus Time

Time, Days	Relative slope of breakthrough curve, R, day^{-1}, %		
	Top fitting	Middle fitting	Tail fitting
100	1.59	9.01	47.43
200	4.58	4.92	4.84
300	1.49	1.96	0.96
400	0.97	1.26	0.79
500	0.68	0.55	0.54
600	0.451	0.48	0.44
700	0.37	0.42	0.36
800	0.25	0.31	0.42
900	0.42	0.31	0.44

Table D3 The Calculated Relative Slope of Breakthrough Curve of Benzene in Offgas versus Time

Time, days	Operation time weighted slope of breakthrough curve, E, day^{-2},%		
	Top fitting	Middle fitting	Tail fitting
100	1.59e-2	9.01e-2	0.47
200	2.29e-2	2.46e-2	2.41e-2
300	4.98e-2	6.54e-3	3.21e-3
400	2.43e-3	3.15e-3	1.98e-3
500	1.35e-3	1.09e-3	1.09e-3
600	7.53e-3	8.00e-4	7.34e-4
700	5.28e-4	6.00e-4	5.08e-4
800	3.09e-4	3.83e-4	5.27e-4
900	2.09e-4	3.46e-4	4.09e-4